MSc. Thesis

Design and validation of a Small and Light robotic arm for Laparoscopic surgery

Alessia De Biasi

Technische Universiteit Delft

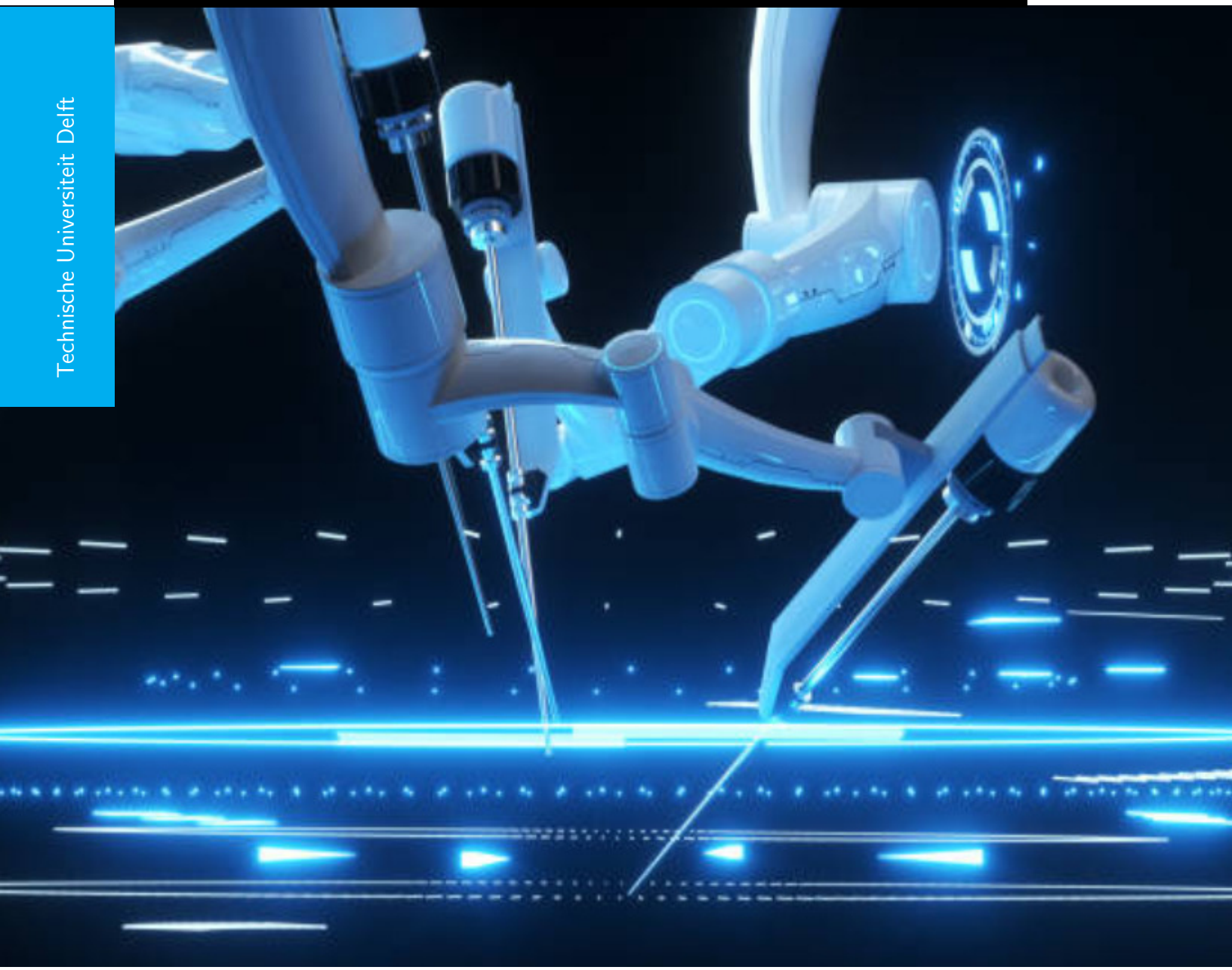

TU Delft Delft University of Technology

Design and validation of a small and light robotic arm for laparoscopic surgery

A thesis submitted to Technische Universiteit Delft in partial fulfillment of the requirements for the degree of

Master of Science in Mechanical Engineering, BioMechanical Design, BioInspired Technologies

Alessia De Biasi
13 September 2022

Supervisors:

Dr. Ir. Tim Horeman

Ir. Tomas Lenssen

Abstract

Minimally invasive surgery (MIS) has developed greatly in the world of surgery in recent years. The use of robotic systems in this field has increased in the past decades. In this procedure, the surgeon requires excellent dexterity and precision. On the other hand, the patient requires safety and minimum incisions during the procedure. These have been the driving forces for the development of robotic systems for laparoscopic surgery. However, existing successful robotic systems have some common drawbacks: high cost, excessive complexity, heavy weight, and large size.

In this work, we focus on the design methodology for developing a robotic arm for minimally invasive surgery that meets all the requirements of the procedure. The aim of this project is to progress towards a next generation surgical robotic arm that reduces the weight and size of the system. Based on a comprehensive study of laparoscopic surgery, the design goals and requirements were defined.

The design is based on a novel division of the surgery into two sub-operations: a global passive positioning and a local active laparoscopic motion. This permits to reduce the overall size of the robotic arm and to develop specific functional mechanisms. The first mechanism allows the alignment of the incision point with the centre of rotation. It is light and intuitive to set up. The second mechanism is responsible for the active surgical movement and is inspired by the spherical linkage.

A complete kinematic analysis and optimization is performed to optimize the geometrical parameters of the mechanisms. The optimization is defined as a multifunctional optimization problem with the aggregation of objective functions, that increase compactness, reduce size, and avoid singularities. In addition, a workspace validation is presented. Motors, sensors, materials, and cross-sectional areas of all parts are selected and tested so that all requirements are satisfied.

Finally, a first prototype of the alignment mechanism is built and an experiment is conducted to prove the ease of setting up the robotic arm. The results demonstrate the ease of setting up the system and the simplicity of the steps for alignment. It also shows that the alignment mechanism is intuitive to use without extensive training.

The proposed robotic arm is suitable for appendectomy, cholecystectomy, and inguinal hernia surgery and has several advantages: It is smaller and lighter than commercially available robotic arms, weighing less than 3 kg and measuring 318 mm x 241.4 mm x 35 mm and 385 mm x 178 mm x 101 mm, and it is portable, as specified in the European standards. This modular design with a division into an alignment mechanism and a surgical mechanism has reduced the size of the overall system and its complexity.

Keywords: laparoscopic surgery, surgical robotic arm, spherical linkage, remote center of motion mechanism (RCM), alignment mechanism

Acknowledgements

This thesis represents the end of my studies in Mechanical Engineering at Delft University of Technology. It has been a great experience and I would like to thank the people that helped me during the project.

First, I would like to thank my supervisor Tim Horeman for the opportunity he provided to work on such an interesting project. I would also like to thank Tomas Lenssen for his support. The feedback he provided really helped me get through the most difficult stages of the thesis.

Secondly, I would like to thank my brother, Vincenzo, and my parents, Anna Maria and Giuseppe, for always being supportive and helping me when possible. Thanks to all the friends I met along the way during my time at the TU Delft, and to the ones that supported me from Rome and Torino. A special thanks to Shreyas, my partner in crime, for all the support and strength he always gives me.

E per finire, un grazie speciale ai miei nonni, e in particolare a nonno Peppe, che anche se oggi non puoi essere qui, so che sei il mio fan numero uno, e questo traguardo lo devo un po' anche a te.

Grazie.

Alessia De Biasi
Delft, September 2022

Contents

1 Introduction **1**
- 1.1 Lead actors in MIS . . . 2
- 1.2 Laparoscopic procedure . . . 2
- 1.3 Trends in Minimally invasive surgery . . . 6
  - 1.3.1 Minimally invasive robotic surgery (MIRS) . . . 6
  - 1.3.2 Reduction in size of the MIRS robotic systems . . . 7

2 Project definition **10**
- 2.1 Problem Analysis . . . 10
- 2.2 Goal of this thesis . . . 11
- 2.3 Environment definition . . . 11
- 2.4 System definition . . . 11
- 2.5 Early decisions . . . 12
- 2.6 Approach and outline . . . 13

3 Specifications **15**
- 3.1 Design goals . . . 15
- 3.2 Design Requirements . . . 15
  - 3.2.1 Mechanical requirements . . . 15
  - 3.2.2 Mechatronical requirements . . . 18
  - 3.2.3 Material requirements . . . 18
  - 3.2.4 Interface requirements . . . 18

4 Conceptual Design **19**
- 4.1 Material design . . . 19
  - 4.1.1 Sterilize robotic arm . . . 19
- 4.2 Interface design . . . 19
  - 4.2.1 Instrument and ground connections . . . 19
- 4.3 Mechanical design . . . 20
  - 4.3.1 Align the RC with the incision point . . . 20
  - 4.3.2 Maintenance of position in place passively . . . 25
  - 4.3.3 Motion . . . 27

5 Concept generation **30**
- 5.1 Four concept designs . . . 30
  - 5.1.1 Concept design 1: The seven-bar mechanism . . . 30
  - 5.1.2 Concept design 2: The cubic design . . . 31
  - 5.1.3 Concept design 3: The "L" mechanism . . . 32
- 5.2 Mechanical design: dependent and independent DOFs . . . 32
  - 5.2.1 Concept solution 4: The double arced mechanism . . . 33
  - 5.2.2 Concept solution 5: The double rings . . . 36

6 Concept selection **37**
- 6.1 Evaluation criteria . . . 37
- 6.2 Harris profile . . . 37
  - 6.2.1 EC1: Minimize size . . . 38
  - 6.2.2 EC2: Optimize weight . . . 38
  - 6.2.3 EC3: Minimize hard-to-sterilize areas . . . 38
  - 6.2.4 EC7: Maximize standard manufacturable parts . . . 38
  - 6.2.5 EC5: Minimize maintenance time and cost . . . 38
  - 6.2.6 EC4: Maximize easiness of set up of the robotic arm . . . 39
  - 6.2.7 EC6: Maximize easiness of control of the robotic arm . . . 39
- 6.3 Final selection . . . 39
  - 6.3.1 Alignment design on the trocar . . . 40
- 6.4 Final selection . . . 40

7 Dimensional design **41**
7.1 Definition of reference frames and nomenclature . . . 41
7.2 Design of the global alignment mechanism . . . 41
7.3 Design of the RCM mechanism . . . 45
7.3.1 Forward kinematics . . . 45
7.3.2 Jacobian matrix . . . 46
7.3.3 Inverse kinematics . . . 47
7.4 Optimization of the RCM design dimensions . . . 47
7.5 Final geometrical design of the RCM mechanism . . . 49
7.6 Final geometrical design of the alignment mechanism . . . 50

8 Analysis of the mechanical design **53**
8.1 Visualize the forward kinematics . . . 53
8.2 Verification of workspace positioning . . . 54
8.3 Procedures analysis . . . 55
8.3.1 Gallbladder removal . . . 55
8.3.2 Appendectomy . . . 55
8.3.3 Inguinal hernia surgery . . . 55
8.4 Proof alignment of workspace . . . 57
8.4.1 Stage 1: Alignment of the RC of the RCM mechanism with the incision point . . . 57
8.4.2 Stage 2: Alignment of the workspace of the robotic arm with the one of the surgery 58
8.4.3 Results . . . 58

9 Background on mechatronical components and material **61**
9.1 Actuators and transmission system . . . 61
9.1.1 Linear system for linear translation . . . 61
9.1.2 Actuators for rotational DOFs . . . 62
9.2 Backdrivability . . . 64
9.3 Position Feedback . . . 66
9.4 Material and Manufacturing processes . . . 68

10 Mechatronical and Material design **72**
10.1 Sizing of actuators, transmission systems and material selection . . . 72
10.1.1 Motor selection for the translational DOF . . . 72
10.1.2 Motor selection for rotational DOFs . . . 72
10.1.3 Transmission selection . . . 73
10.1.4 Cross section area of the beams: Comparison of three different designs . . . 73
10.1.5 Final selection of cross section and selection of material . . . 78
10.1.6 Design of connectors . . . 82
10.1.7 Finalizing the dimensions of the arced beams . . . 89
10.2 Torque calculation for selecting the right rotational motor . . . 93
10.2.1 Resized rotational motors . . . 94
10.3 Final design of the RCM mechanism . . . 96

11 Design of the global alignment mechanism **98**
11.1 Connection between the global alignment and the RCM mechanism . . . 98
11.2 Mechanical design of the alignment mechanism . . . 99
11.2.1 Design of Part 1: Clamp and connecting beam . . . 100
11.2.2 Design of Part 2: Beam a and J_a2 . . . 101
11.2.3 Design of Part 5: Beam b and J_a4 . . . 102
11.2.4 Design of Part 3: Beam c, beam d, beam e . . . 103
11.2.5 Design of Part 4: J_a3 . . . 105
11.3 Final design of the alignment mechanism . . . 108
11.4 Failure analysis of the structure . . . 110
11.5 Position of lasers: indicators for the alignment . . . 114
11.6 Design of position Feedback . . . 115

12 Final design **117**
12.1 Redesign of connection RCM mechanism to alignment mechanism . . . 117
12.1.1 Connection Mechanism Design . . . 117
12.2 Manufacturing processes . . . 119
12.2.1 Beam 1 and beam 2 of RCM mechanism . . . 121
12.2.2 Beam b of alignment mechanism . . . 121
12.2.3 Beam c of the alignment mechanism . . . 121
12.2.4 Beam d of the alignment mechanism . . . 122

13 Validation of the ease of set up: alignment of the incision point with the center of rotation **123**
13.1 Hypotheses . . . 125
13.2 Independent tested variables . . . 125
13.3 Method . . . 126
13.3.1 Results . . . 127
13.3.2 Discussion and conclusion on the experiment . . . 130

14 Discussion **132**
14.1 Limitations of the study and future works . . . 132
14.1.1 Performing a wider range of procedures . . . 132
14.1.2 Design of a control system: selection of sensors . . . 133
14.1.3 Material Study . . . 133
14.1.4 Transmission and motor study: Backdrivability . . . 133
14.1.5 Sterility . . . 133
14.1.6 Plan for instrument insertion and workspace alignment . . . 133

15 Conclusion **134**

16 Appendix A **143**

17 Appendix B **145**
17.1 Attendance to a laparoscopic surgery . . . 145

18 Appendix C **147**
18.1 System for rotational motion . . . 147

19 Appendix D **148**
19.1 Forward Kinematics RCM mechanism . . . 148
19.2 Jacobian matrix RCM mechamism . . . 148
19.3 Inverse kinematics . . . 149

20 Appendix E **150**

21 Appendix F **156**

22 Appendix G **159**

23 Appendix H **162**

24 Appendix I **174**

25 Appendix J **176**

26 Appendix K **178**

27 Appendix L **179**

28 Appendix M **180**
28.1 Procedure for alignment of the mechanism: steps for the experiment . . . 180

List of Figures

1 Graph depicting the number of documents indexed per year in a Scopus search containing the words "minimally invasive surgery" . . . 1
2 Laparoscopic surgery [107] . . . 3
3 Total 4 DOFs in a laparoscopic robotic system . . . 3
4 Workspace of a laparoscopic surgery inside the abdominal cavity . . . 4
5 Gallbladder removal: laparoscopy set up [4] . . . 4
6 Appendectomy: laparoscopy set up [3] . . . 5
7 diameter, length and thickness of appendix on CT [144] . . . 5
8 Inguinal hernia surgery: laparoscopy set up [19] . . . 5
9 Graph depicting the number of documents indexed per year in a Scopus search containing the words "minimally invasive robotic surgery" . . . 6
10 comparison between master-slave systems performed by Kumar and Revi in 2019 [107] . . . 8
11 Graph of volume with respect of year of manufacturing of the MIS robotic systems . . . 8
12 Graph of comparison between categorized papers in size and total papers with respect to the year of publication . . . 9
13 Flange for connecting the instrument's actuator . . . 12
14 Trocar with its components [143] . . . 13
15 Work flow of surgery, concentrating on the trocar [143] . . . 13
16 total DOFs of the robot arm . . . 16
17 Workspace of the tip and of the instrument(yellow) and the instrument (red) . . . 17
18 Grippers . . . 20
19 Some alignment mechanisms 3 revolute joints + 3 prismatic joints . . . 21
20 Alignment mechanisms 3 cylindrical joints . . . 21
21 Alignment mechanisms 1 spherical joint + 3 prismatic joints . . . 22
22 Position fixture of a ball joint [140] . . . 22
23 One-touch sliding locks [32] . . . 22
24 One-touch indexing clamp [32] . . . 23
25 Linear-motion stopper [32] . . . 23
26 Pneumatic shaft-locking clamps [32] . . . 23
27 Manual quick shaft-locking clamp [32] . . . 23
28 Manual quick locking for cylindrical joints [32] . . . 24
29 Lasers intersection [113] . . . 24
30 Balancing mechanism using counterweights [145] . . . 25
31 Balancing mechanism using springs [145] . . . 26
32 Balancing mechanism using auxiliary actuators [63] . . . 27
33 Parallelograms-type kinematics [108] . . . 28
34 Synchronous belt transmission kinematics [108] . . . 28
35 isocenter kinematics [108] . . . 29
36 Circular tracking arcs kinematics [108] . . . 29
37 Spherical linkages' kinematics [108] . . . 29
38 mechanical design for RCM mechanism of concept 1 . . . 31
39 mechanical design for RCM mechanism of concept 2 . . . 31
40 mechanical design of the L shape for RCM mechanism of concept 3 . . . 32
41 mechanical design for RCM mechanism of concept 3 . . . 33
42 mechanical design of the RCM mechanism of concept 4 . . . 34
43 mechanical design of the RCM mechanism of concept 4b . . . 34
44 mechanical design of the RCM mechanism of concept 5 . . . 35
45 mechanical design of the RCM mechanism of concept 5, highlighting the possible mechanical interface with the trocar . . . 35
46 Absolute reference frame . . . 41
47 Local reference frame for the RCM mechanism . . . 42
48 Nomenclature of the joints of the RCM mechanism . . . 42
49 Nomenclature of the joints of the alignment mechanism . . . 43
50 Design for the alignment that uses the DOFs of the RCM mechanism for alignment . . . 43
51 Step 1 for the alignment process . . . 44

52 Step 2 in the alignment process . . . 44
53 Step 3 in the alignment process . . . 44
54 Geometrical structure of the RCM design, with input (red) and geometrical constant values (blue) . . . 45
55 Geometrical structure of the design, reference frames for each joint . . . 46
56 Definition of the workspace constraint for extended configuration . . . 49
57 Calculation for the dimensions of the alignment mechanism . . . 51
58 Calculation for the dimensions of the alignment mechanism . . . 51
59 Calculation for the dimensions of the alignment mechanism . . . 52
60 Schematic of the overall system for the calculations for ensuring no collision with the patient . . . 52
61 Visualization of Forward kinematics: d=0 cm . . . 53
62 Visualization of Forward kinematics: d=13 cm . . . 54
63 Position of trocars for gallbladder removal [86] and values of the dimensions after averaging the values of this dimensions in section 20 . . . 55
64 Position of trocars for appendectomy: configuration 1 [86] and values of the dimensions after averaging the values of this dimensions in section 20 . . . 56
65 Position of trocars for appendectomy: configuration 2 [86] and values of the dimensions after averaging the values of this dimensions in section 20 . . . 56
66 Position of trocars for hernia [86] and values of the dimensions after averaging the values of this dimensions in section 20 . . . 57
67 Range of motion of the RCM mechanism on the the plane defined by rotating the (y, z) plane of an angle equal to the one found on the (x, y) for Gall bladder removal . . . 58
68 Range of motion of the RCM mechanism on the the plane defined by rotating the (y, z) plane of an angle equal to the one found on the (x, y) for Appendectomy configuration 1 59
69 Range of motion of the RCM mechanism on the the plane defined by rotating the (y, z) plane of an angle equal to the one found on the (x, y) for Appendectomy configuration 2 59
70 Range of motion of the RCM mechanism on the the plane defined by rotating the (y, z) plane of an angle equal to the one found on the (x, y) for inguinal hernia surgery . . . 59
71 Classification of motors [7] . . . 63
72 specification of gears [47] . . . 64
73 comparison in performance, speed and gear ratio [47] . . . 65
74 Cable capstan reducer with the automatic tensioning system [112] . . . 65
75 Block-and-tackle of MA23 [129] . . . 65
76 Comparison of position/orientation sensing modalities [139] . . . 66
77 Position sensors [14] . . . 67
78 Arc and force configuration . . . 68
79 Graphical representation of Young modulus and strength of materials [122] . . . 69
80 Cross section areas for the beams of the robotic arm . . . 74
81 Results of the simulation for the rectangular cross section area assembly . . . 75
82 Results of the simulation for the ellipse cross section area assembly . . . 76
83 Results of the simulation for the U shape cross section area assembly . . . 77
84 Schematic of the forces applied for the inertia calculation . . . 79
85 Results of the simulation for the U shape steel cross section area assembly . . . 81
86 Results of the simulation for the U shape aluminium cross section area assembly . . . 82
87 Outline drawing of the gearmotor LRPX32, front view[11] . . . 83
88 Components designed from the specification of the Pololu Universal Aluminum Mounting Hub for 6mm Shaft, M3 Holes . . . 84
89 Connection between the Universal Aluminum Mounting Hub and the beam . . . 84
90 Overview of the Pololu Universal Aluminum Mounting Hub for 6mm Shaft, M3 Holes . 84
91 Flange that connects to the motor in revolute joint 1 and 2 . . . 85
92 Overview of the design of the flange . . . 85
93 Final assembly of revolute joint 1 . . . 86
94 Screw's holes for coupling the beam one to the flange and the motor in revolute joint 2 . 86
95 final assembly of revolute joint 2 . . . 86
96 Dimension of the hole patterns in the linear actuator [41] . . . 87

97 Profile of the beam 2 that connect the linear actuator . . . 87
98 Drawing of the beam two that connect the linear actuator . . . 87
99 Outline drawing of the flange for connecting the instrument's actuator . . . 88
100 Flange connecting the linear actuator with the instrument's actuator . . . 88
101 Connecting design of the arm 1 . . . 89
102 Drawing and dimensions of beam 1 (right) and beam 2 (left) . . . 90
103 Results of the simulation for the U shape steel cross section area assembly in extended configuration: final dimensions . . . 91
104 Results of the simulation for the U shape steel cross section area assembly in elbow configuration: final dimensions . . . 92
105 Schematic for torque calculations of motor in first revolute joint . . . 93
106 Schematic for torque calculations of motor in second revolute joint . . . 93
107 Results of the simulation for the U shape steel cross section area assembly in extended configuration: final motors . . . 95
108 Results of the simulation for the U shape steel cross section area assembly in elbow configuration: final motors . . . 96
109 3D view of the final design of the RCM mechanism . . . 97
110 Drawing of the final design of the RCM mechanism with bill of material . . . 97
111 Outline drawing of the gearmotor LRPX32, back view [11] . . . 98
112 3D representation of the connector between the alignment and the RCM mechanism . . . 98
113 Parameterized design of the alignment mechanism . . . 99
114 Overview of the 5 parts . . . 100
115 Clamps for the sliders alongside the surgical table [44] . . . 101
116 Design of the bar connecting the clamp to the linear system . . . 102
117 Dimensions of the smallest rail [52] . . . 102
118 Dimensions of the slider [52] . . . 102
119 Redesign of flange connecting the RCM mechanism to the alignment mechanism . . . 103
120 Design of beam b with slider width equal to 63 mm . . . 103
121 Dimensions of beam c . . . 104
122 Dimensions of beam d . . . 105
123 Dimension of handle for locking the beam b . . . 105
124 Drawing of the *Joint 2* of the alignment system . . . 106
125 3D visualization of the *Joint 2* of the alignment system . . . 106
126 Pin inserted in the revolute joint . . . 107
127 Base of the pin inserted in the revolute joint . . . 107
128 J_a3 . . . 108
129 Design of the extra piece that connects Part 1 with the bar a . . . 108
130 Connection between Part 1 and Part 2 . . . 108
131 Satisfied constraints . . . 109
132 3D view of the final design . . . 109
133 Drawing of the final design . . . 110
134 Simulation 1: all parts in aluminium 6061 . . . 111
135 Simulation 2: all parts in aluminium 6061 . . . 111
136 Simulation 3: all parts in aluminium 6061 . . . 112
137 Simulation 4: all parts in aluminium 6061 . . . 112
138 Simulation 5: all parts in aluminium 6061 . . . 113
139 Simulation 6: all parts in aluminium 6061 . . . 113
140 Simulation 7: beam c and d in Steel 1035 . . . 114
141 Simulation 8: beam c and d in Steel 1035 . . . 114
142 Points of insertion of the lasers . . . 115
143 Quick release mechanism [24] . . . 117
144 Flange attached at $J_{rcm}1$ . . . 118
145 Flange attached at J_a4 . . . 118
146 Final design of the connector between the two parts . . . 119
147 3D visualization of the spacer between the beam c and beam d . . . 119
148 Drawing of the spacer between the beam c and beam d . . . 119

149 3D view of the final design . . . 120
150 3D overview of the simplified alignment mechanism . . . 123
151 3D printed alignment mechanism: overview of all the components . . . 123
152 3D printed alignment mechanism: set up for the experiment . . . 124
153 Scale for the SUS score [46] . . . 126
154 Plot of the misalignment after all the procedures and the acceptance boundaries . . . 127
155 Comparison between the first and the third trial for all participants . . . 130
156 Surgical bed [45] . . . 146
157 Position of primary trocars for gallbladder removal [4] . . . 150
158 Position of trocars for gallbladder removal [4] . . . 150
159 Position of trocars for gallbladder removal [16] . . . 151
160 Position of trocars for appendectomy [124] . . . 151
161 Position of trocars for appendectomy [25] . . . 152
162 Position of trocars for appendectomy [137] . . . 152
163 Position of trocars for appendectomy [26] . . . 153
164 Position of trocars for appendectomy [27] . . . 153
165 Position of trocars for appendectomy [51] . . . 154
166 Position of trocars for inguinal hernia surgery [78] . . . 154
167 Position of trocars for inguinal hernia surgery [28] . . . 155
168 Position of trocars for inguinal hernia surgery [21] . . . 155
169 GeoGebra used for calculating the motion for step 2 and 3 in the alignment procedure for Gall Bladder removal . . . 159
170 GeoGebra used for calculating the motion for step 2 and 3 in the alignment procedure for Appendectomy configuration 1 . . . 160
171 GeoGebra used for calculating the motion for step 2 and 3 in the alignment procedure for Appendectomy configuration 2 . . . 160
172 GeoGebra used for calculating the motion for step 2 and 3 in the alignment procedure for Inguinal hernia surgery . . . 161
173 Dimension of the hole pattern in the linear actuator [41] . . . 178

List of Tables

1 Advantages and disadvantages of MIS [84] . . . 2
2 Comparison MIRS and MIS [76, 53, 107] . . . 7
3 Workspace of the procedures . . . 17
4 Morphological table . . . 30
5 Concepts solutions . . . 36
6 Concepts solutions . . . 39
7 Denavit–Hartenberg parameters . . . 46
8 Optimized parameters . . . 50
9 Final optimized parameters . . . 50
10 Values of the parameters of the alignment mechanism . . . 51
11 Position of incision point and workspace inclination . . . 57
12 Range of inclination of the workspace axis on the plane of inclination on (x,y) plane . . . 60
13 Values of the parameters of the alignment mechanism . . . 60
14 Comparison of linear system [50] . . . 61
15 Quick selection guide [13] . . . 62
16 Comparison between manufacturing procedures . . . 71
17 Specification of Miniature Linear Module QM02-12477-120 . . . 72
18 Range of parameters of ElectroCraft RPX motors [9] . . . 73
19 Range of parameters of ElectroCraft LRPX planetary gearmotors [10] . . . 73
20 Volume of the design with the three cross section areas . . . 78
21 Optimized cross section parameters: t is the thickness, h is the height . . . 79
22 Parameters for the two cross section areas in two materials . . . 80
23 Standardize dimensions of cross section: t is the thickness, h is the height, w is the width 80
24 Final dimensions of the beams: w is width, h is height, t is thickness . . . 89
25 List of all the components with the manufacturing process to produce them . . . 121
26 Docking and covering time for the most used systems . . . 124
27 Docking time for the most used systems . . . 124
28 Questions and options for the System Usability Score Scale [46] . . . 125
29 Questions and options for the Net Promote Score Scale [35] . . . 126
30 Results on time and misalignment for all the participants . . . 128
31 Average score of the answers for SUS . . . 129
32 Scores of the answers for NPS . . . 129
33 Average time to set up the mechanism with respect to trial . . . 130
34 Average time to set up the mechanism with respect to step . . . 130
35 Quick overview of the linear motors [72] . . . 143
36 Continue of Table 36 [72] . . . 144

1 Introduction

In 1987, Mouret performed the first laparoscopic cholecystectomy, starting a revolution in the surgery field. From that moment, advances in surgery have focused on minimizing the invasiveness of the surgical procedures [83]. Only five years later, this procedure, called Minimally Invasive Surgery (MIS), was acknowledged as the "gold standard" procedure [83]. Over the last few decades, research in MIS has been continually increasing, as shown in Figure 1, showing a growing interest and a trend towards using this new technology in daily surgical operations.

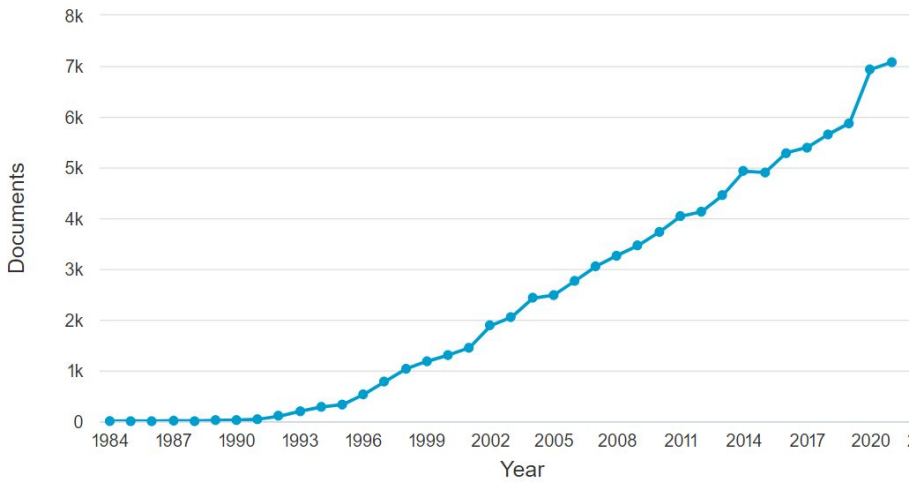

Figure 1: Graph depicting the number of documents indexed per year in a Scopus search containing the words "minimally invasive surgery"

MIS is a global concept that frames almost all the medical discipline (orthopedic surgery [81], neurosurgery [81], gynecology [99, 142, 81], urology [99], general and thoracic surgery [99, 81], vascular interventional surgery)[120] , gathering a set of modern practices which allow the surgeons to perform traditional procedures via small incisions in the patient's skin. In fact, in this procedure the surgeon works through a set of three to five incisions of 1.5 cm. Long-handled tissue manipulators are inserted in the body, and a video endoscope provides a view of the internal operating field [125]. Therefore, MIS requires the performance of small and precise movements for manipulating the tissue in a confined space [79].

The introduction of MIS in the Surgical field has been described as "the most dramatic change in surgery since the introduction of anaesthesia" (Khajuria, 2015). After early critics that warned about a longer operative times, unusual complications, and a potentially broader inferiority of oncological outcomes [101], nowadays this procedure is performed daily all over the world [151]. Moreover, its advantages with respect to the traditional open surgery technique are recognised in the scientific field [120, 99, 151, 81].

In spite of the early critics, some studies show that the MIS has established itself as mostly equivalent, or even better, for oncological outcome, [73, 97, 85]. Moreover, researches demonstrated a lower probability of surgical site infection [73, 97, 103, 142, 85], lower blood loss [73, 97, 98], and shorter hospital stay [97, 103, 142, 98, 90]. However, the particular configuration of MIS instrumentation imposes limitations in the manipulation and hand-eye coordination [69]. The use of rigid tool and the fixed access port constraints the lateral movements of the instruments, the surgeon's wrist motion, and creates a remote center of motion (RCM) [53]. The RCM of a mechanism is geometrically a point at which one or more rotational motion are centered [108]. This creates a lever arm effect that only amplifies the amplitude of the movements, decreasing the precision and accentuating any hand tremor. Furthermore, the indirect vision of the operating area with a 2D display creates a loss in hand-eye coordination [95, 151]. Additionally, it was shown that the instruments used are usually ergonomically inadequate and inefficient in force transmission, creating significant surgeon fatigue and discomfort

[65]. Finally, a lack of tactile and force feedback makes the surgery harder to perform [53, 95, 151]. In Table 1, the advantages and disadvantages of the MIS technology are listed.

Table 1: Advantages and disadvantages of MIS [84]

Advantages	**Disadvantages**
Reduction of tissue traumatization and smaller scar tissue	Difficulty with spatial perception
Reduction of blood loss	Lost hand-eye coordination
Reduction of infections	Constricted dexterity
Reduction of postoperative pain and discomfort	Loss of tactile feedback
Fewer complications in the surgical wounds	Longer operating time
Reduction of postoperative hospital stay	Long learning curve
Less risk of deep-vein thrombosis	
Better post-operative aesthetic	

1.1 Lead actors in MIS

In the performance of a MIS procedure, the lead actors that play a fundamental role are different. It is necessary to understand their roles and requirements during the procedure to better understand and have a deeper insight on the MIS itself. The main lead actors in MIS are:

- *Surgeon*: The surgeon is the one performing the surgery. It is necessary for the surgeon to have an ergonomic position while performing the surgery. Additionally, it is necessary for the surgeon to receive feedback form the surgery site: the feedback can be visual, haptic, or force.
- *Patient*: The patient is the one being subject to the surgery. It is necessary that the procedure does not create any injury or medical problems to the patient.
- *Assistants team and Anesthesia team*: the teams in support of the surgeon help in the success of the procedure. A fast accessibility of the patient helps the teams to assist the procedure and act in case of emergency.

1.2 Laparoscopic procedure

MIS can be subdivided in different subgroups, by the type of procedure performed. It is important to emphasize that different MIS procedures require different movements of the surgical tool. In this work the focus is on laparoscopic procedure. The decision to refer to this procedure is based on the fact that laparoscopy is the main application of surgical robots, as 70.1% of all surgical robots are used for laparoscopic surgery [110].
Laparoscopy is a an operation performed through small incision inside the abdominal cavity and pelvis, with the help of a camera attached at the tip of an instrument called laparoscope. The abdomen in the human anatomy is the body cavity lying between the chest or thorax above and the pelvis below and from the spine in the back to the wall of abdominal muscles in the front. The diaphragm is its upper boundary. There is no wall or clear-cut boundary between it and the pelvis. It contains organs of digestion and the spleen, which are surrounded by a serous membrane, the peritoneum. The dimensions in the coronal plane of the abdominal cavity for an average person is 31.5 cm x 29.5 cm [60]. The instruments are inserted in this cavity.
The procedure begins with the introduction of CO_2 in the abdominal cavity, with a pressure of 9-18 mmHg and a flow rate of 6-15 liters/min [107], for allowing a better view and more dexterity in the

abdomen and pelvis. Consequently, an incision is made, and a trocar is inserted in the abdominal cavity. Thus, a video camera is located at the tip of the laparoscope and introduced in the cavity. A visual feedback is given to the surgeon, that can perform the procedure inserting other instruments in the cavity. The set up of the laparoscopy is shown in Figure 2.

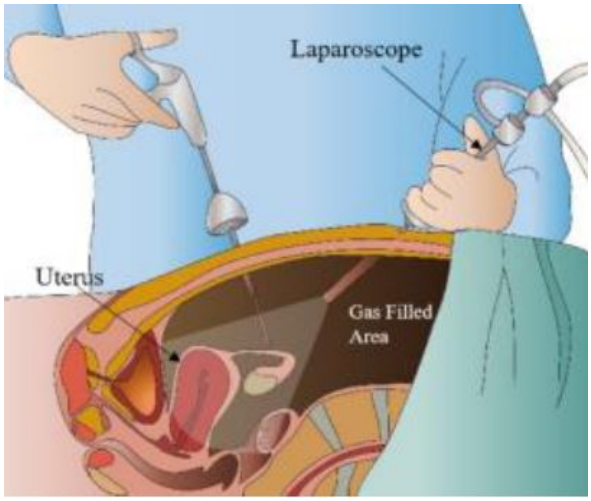

Figure 2: Laparoscopic surgery [107]

Laparoscopy is carried out under general anaesthetic and, along with the surgeon, assistants and anesthetists work close to the patient.

General laparoscopic surgery requires 4 Degrees Of Freedom (DOFs):

- translation along the line of insertion of the instruments into the patient's body;
- rolling motion;
- pitching motion;
- yawing motion.

The four DOFs are shown in Figure 3.

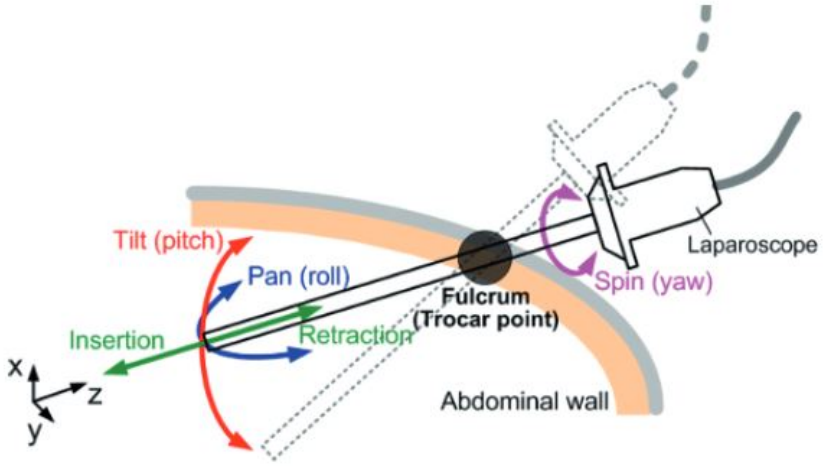

Figure 3: Total 4 DOFs in a laparoscopic robotic system

The roll-pitch-yaw motion is centered on the entry point.

Generally a laparoscopy has as a workspace a conic region shown in Figure 4.

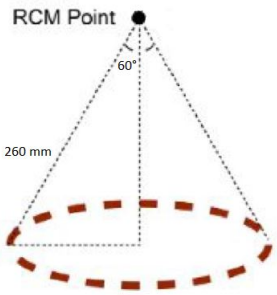

Figure 4: Workspace of a laparoscopic surgery inside the abdominal cavity

However, the angle of 60° presented in Figure 4 is a generic estimation of it. Each procedure has a specific workspace.
In this project three of the most performed MIS laparoscopic procedures are taken into consideration. These three procedures are performed in three of the four abdominal cavities, which makes the robot more versatile.

- **Cholecystectomy, Gallbladder removal**: The gallbladder is a pear-shaped sac in a depression on the liver's under surface. It stores bile between meals, reabsorbs water to concentrate bile, and contracts to release bile into the small intestine. Cholesterol in bile may precipitate under certain conditions and form crystals called gallstones. Gallstones in the bile duct may block bile flow into the small intestine and cause considerable pain. A surgical procedure called *cholecystectomy* can remove the gallbladder when gallstones are obstructive.
  In the cholecystectomy procedure, four small incisions are performed in the abdominal cavity

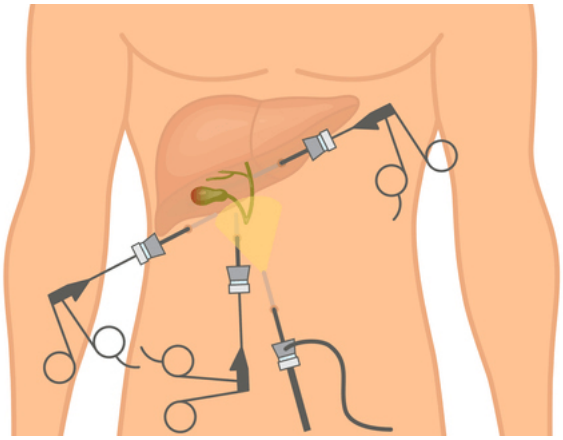

Figure 5: Gallbladder removal: laparoscopy set up [4]

  as shown in Figure 5. Three instruments and one laparoscope are inserted in the patient's body. The instruments have to move along the gallbladder, and cut the edges that connects it to the patient body. After, the Gallbladder is removed taking it out from the biggest incision port. The workspace of the tip of the instrument is a sphere of radius equal to the longest dimensions of the gallbladder. The normal adult gallbladder measures from 7-10 cm in length and 3-4 cm in transverse diameter [100].

- **Appendectomy**: appendix is a small, finger-shaped organ that branches off from the first part of the large intestine. When it becomes swollen or infected, the condition is called appendicitis. The appendix has, thus, to be removed.
  One laparoscope and two surgical tools, are inserted, as shown in Figure 6. The tools have a

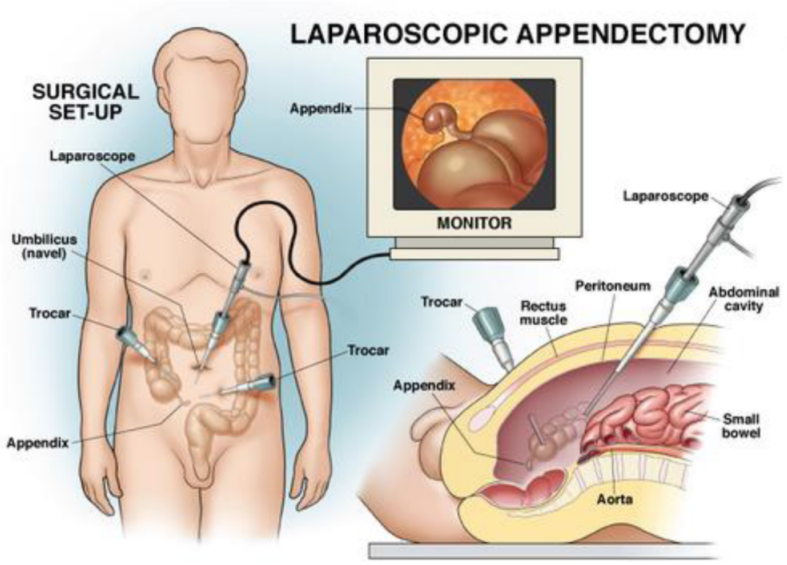

Figure 6: Appendectomy: laparoscopy set up [3]

spherical workspace of diameter equal to the length of the appendix. The values of the physical parameters of the appendix are presented in Figure 7.

	Mean	SD	Minimal	Maximal
Diameter (mm)	8.19	1.6	4.2	12.8
Length (mm)	81.11	28.44	7.2	158.8
Thickness (mm)	2.22	0.56	1.15	3.85

doi:10.1371/journal.pone.0096476.t001

Figure 7: diameter, length and thickness of appendix on CT [144]

- **Inguinal hernia surgery**: Inguinal hernia repair is a surgery procedure to repair a hernia in a groin. A hernia is tissue that bulges out of a weak spot in the abdominal wall. The intestine may bulge out through this weakened area. The hernia sac is removed from the defect in the abdominal wall, and a prosthetic mesh is then placed to cover the hernia defect. It requires the insertion of three trocar, two for the instruments and one for the laparoscope, as shown in Figure 8. The usual size of the mesh commonly placed for inguinal hernia repair ranges from 3

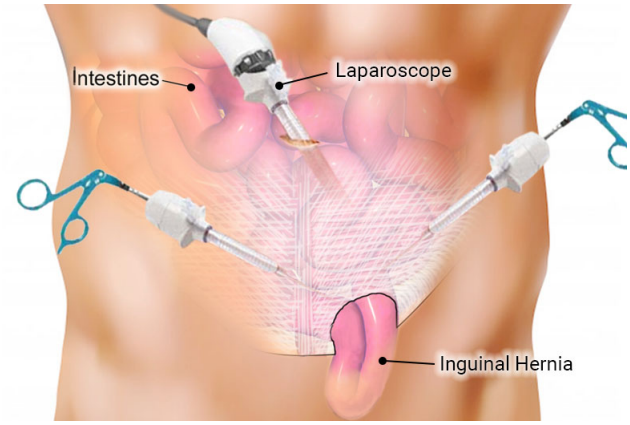

Figure 8: Inguinal hernia surgery: laparoscopy set up [19]

x 3 inches to 3 x 6 inches (7.5 x 7.5 cm to 7.5 x 15 cm) [61]. This means that the instrument has to move with a sphere of at least 15 cm diameter.

1.3 Trends in Minimally invasive surgery

After a general understanding on MIS, the main lead actors, and the specific procedure, a deeper look into the development and the emerging trends in this field is presented. Below, the two main trends in MIS are explained.

1.3.1 Minimally invasive robotic surgery (MIRS)

One of the main trend in this field is the use of robotic system for overcoming the disadvantages/limits of MIS. When it comes to the surgical field, the robot has to be intended as an instrument that expand the possibilities and the ability of the surgeon, as a 'surgeon's extension' rather than a 'surgeon's replacement' [69, 95, 53].The use of robots in surgery is first mentioned in 1985 [131], when the PUMA 560 was used for the first time to perform a neurosurgical biopsies [57]. But it is only after their use in MIS that it was able to fully appreciate and better understand their advantages. Over the last few decades, research in the use of robots for MIS has been continually increasing, as shown in Figure 9, underling a growing interest and a trend towards using them in MIS.

The use of robotic systems in MIS, Minimally invasive robotic surgery (MIRS), is aimed at solving

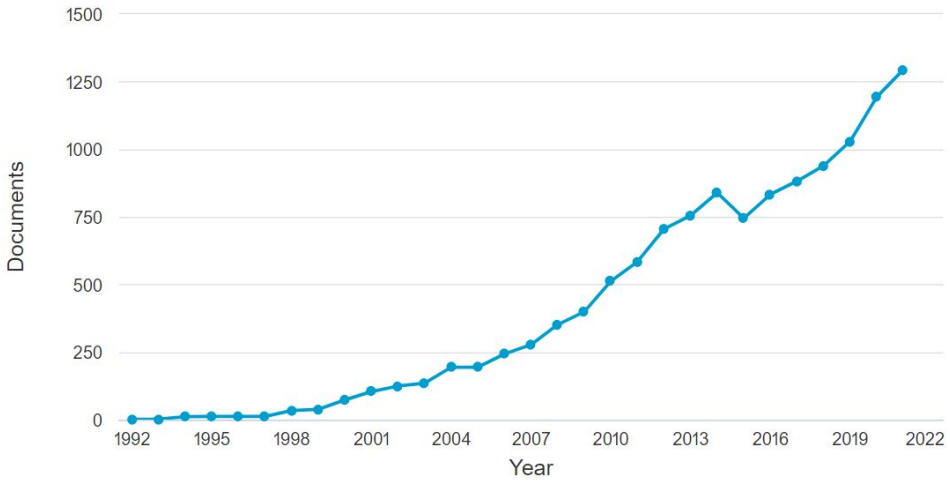

Figure 9: Graph depicting the number of documents indexed per year in a Scopus search containing the words "minimally invasive robotic surgery"

many of the disadvantages of this procedure [120]. The robots provide an improved control and dexterity [109], compensating for the loss of wrist articulation caused in the traditional MIS [53]. This has been proven by different studies [55, 96]. Moreover, imaging modalities have been integrated for improving the visual-motor coordination [53, 109]. Additionally, the surgeon controls the robot through a master console, that is designed to be more ergonomic [53, 109]. Finally, haptic feedback can be added, but its implementation still represents a challenge [53, 115]. The robots can be used also for reducing the human tremor [59, 109] and fatigue [59]. This makes the system more precise and accurate [95]. The accuracy and the precision have been proven by comparative outcome studies [55, 79, 102, 96]. Moreover, different studies has shown that the MIRS resulted to be safer than the MIS [74, 130, 126, 71, 147]. Another important feature of the MIRS is the possibility to scale down the motion of the surgeon till achieving micro motions [116]. Finally, it was proven that MIRS has some advantages in length of hospital stay [74, 85, 102, 71].

A comparison between the MIRS and MIS is shown in Table 2.

Despite many studies showing the feasibility of using the surgical robots, there are several disadvantages in these technologies that needs to be taken into consideration [109, 57]. The main disadvantage is the price of these robots, being around a million dollars [109]. In this case, the cost has been intended as purchase cost and maintenance cost. Additionally, MIRS requires a longer operative time [131].

Table 2: Comparison MIRS and MIS [76, 53, 107]

Evaluated aspect	**MIS**	**MIRS**
Surgical instruments	Camera, small instruments	Camera, surgical console, dexterous instruments
Surgeon position	Next to the patient	At console
Vision	2-dimensional	3-dimensional (3D endoscopic camera, high resolution)
Instrument manipulation	Limited	360°
Cost	Low	High
Visual-motor coordination	Poor	Good
Ergonomics	Poor	Very good
Dexterity	Poor	Good

This is due to the set-up time and the frequent replacement of the instruments [57]. Moreover, the risk of malfunction should not be underestimated [68]. Finally, the current robots used in MIS requires a big space and extensive training [68, 109]. They are very heavy, making it difficult to move around the room [76, 109]. The robot itself is bulky [76].
In the robotic MIS procedure it is necessary to ensure that the patient is never hurt by the robotic arm during its motion. For doing so, the incision point is considered as the fulcrum point, and the robotic arm should move such that this point acts as remote center of motion. Moreover, it is important that the insertion point remains free from components. For these reasons, RCM mechanism is a good concept to apply in the design of MIS robotic arm. RCM (Remote Center of Motion) mechanism is characterized by the presence of a remote fixed point (insertion point), with no physical revolute joint there, around the mechanism of it can rotate.

1.3.2 Reduction in size of the MIRS robotic systems

MIRS is an evolving field, and as the length of time this technology has been in use increases, a number of trends can be identified.
The most emerging trend in this field is the reduction in the size and cost of systems. This trend has been discussed and acknowledged by various researchers.
In 2019, Kumar and Ravi [107] conducted a comparative study of laparoscopic robotic systems. They compared the most commonly used master-slave systems: Zeus, Da Vinci, SPORT, and Versius. The result of their study is presented in Figure 10 and shows a reduction in size, set up time, and cost in time.

In addition, Khandalvala and colleagues published [105]"Emerging surgical robotic technology: a progress towards microbots" in 2019. In this paper, they present novel surgical robots that reduce cost and size and increase diversification in the field. The paper categorises the robotic systems presented as "moderate size," "small size," and "capsule robots." It is thus emphasised that robots are getting smaller and smaller.
Peter Berkelman and Ji Ma, in their paper [66], also claim that the robotic systems developed before 2009 occupy a large area in the operating room and are expensive and difficult to move and set up. Therefore, they present a more recent approach (from 2009), which was to develop smaller, simpler, and lighter surgical robotic systems. The same point is supported by Peters [132], who writes, "The available devices are becoming smaller and more procedure-specific as technology becomes cheaper, smaller, and faster". The trend is, also, recognised by Vitiello in the paper "Introduction to robot-assisted minimally invasive surgery (MIS)" [53].

	ZEUS	Da Vinci	Versius	SPORT
No. of Ports Required	Three	Four	Three	One
Setup Time	High	High (30 min)	Less (As reported)	Less
Dexterity	Good (4 DoF)	Excellent (7 DoF)	Good (Like arms)	Good (Flexible links)
Size	Less Bulky	Very Bulky (800 kg)	Compact (15 kg)	Compact
Cost	High	Very High (20 crores INR)	Low (Not in Market yet)	Low (Not in Market yet)
Haptics	No	No	No	No
Compensate for hand tremors	No	Yes	Yes	No

Figure 10: comparison between master-slave systems performed by Kumar and Revi in 2019 [107]

Additional, in the work *"Identification and deeper insight of the most emerging trend in minimally invasive surgery robotic systems"* [67], an attempt to perform a quantitative analysis and a statistical analysis is presented. The results found are shown in Figure 11 and Figure 12, and they show the presence of the trend towards smaller, lighter and less complex MIS robotic system.

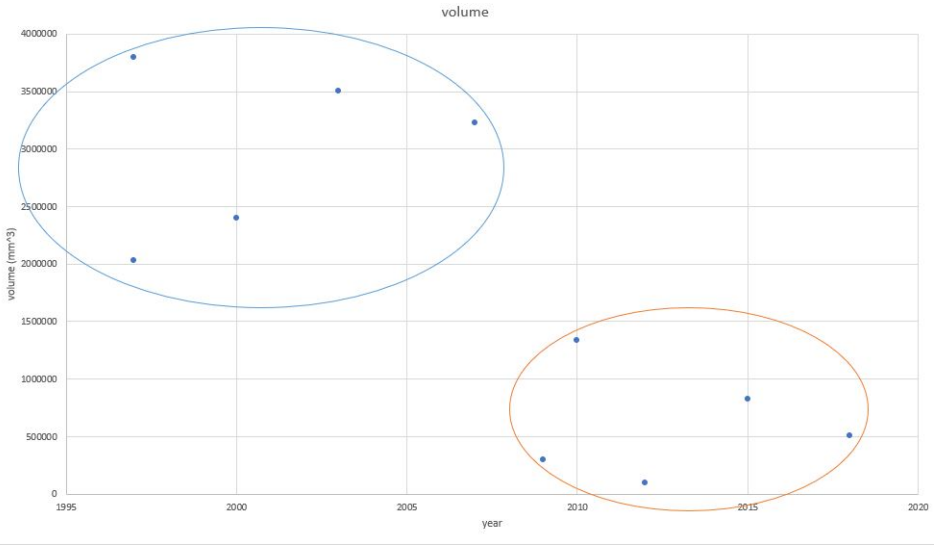

Figure 11: Graph of volume with respect of year of manufacturing of the MIS robotic systems

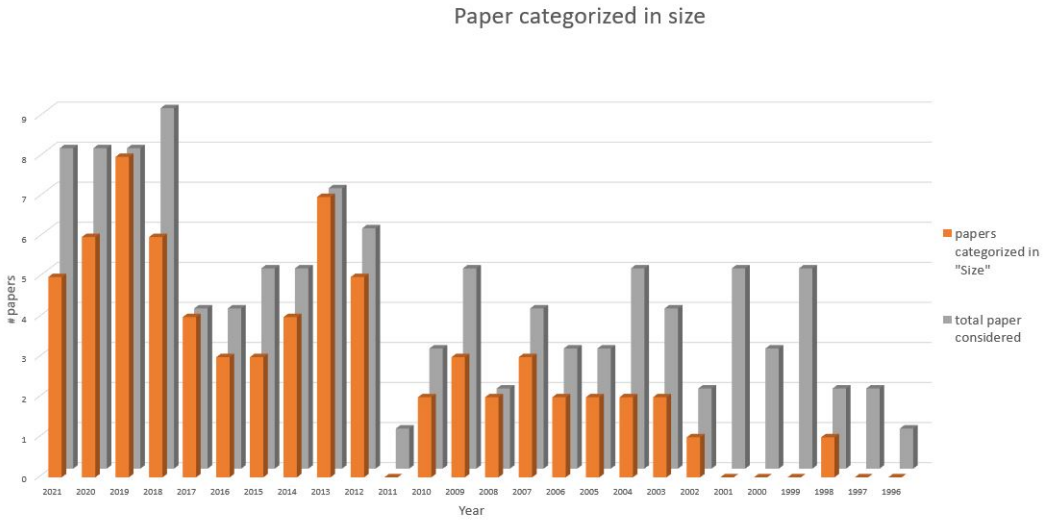

Figure 12: Graph of comparison between categorized papers in size and total papers with respect to the year of publication

2 Project definition

2.1 Problem Analysis

After an accurate study of the state-of-the-art of Robotic system in MIS, a general trend towards smaller, lighter, and less complex robotic arm has identified and presented in Figure 12. A quantitative and a statistical analysis, presented in Figure 11, showed that this trend is present and more noticeable after the expiration of the patents own by Intuitive Surgical on robotic minimally invasive surgery. After the expiration of the patents, in fact, novel smaller robots have been designed.
After recognising the trend, it seems necessary to have a deeper look and understanding on the reasons and the benefits of this trend. The following concepts are improved.

- *Avoidance of collisions* : safety is the first concern for surgical robots. The robotic arm must be designed to avoid collisions and excessive force on the target [53] for ensuring a safe and successful performance. Small robotic systems, due to their dimensions and light weight, are less likely to damage internal tissues due to unintended movements [66]. In fact, reducing the accelerating mass increases safety for both the surgeon and the patient [89]. In the event of an impact, a lower mass causes less harm to both the patient and the surgeon. The main goal in designing a medical-surgical system is to reduce hazards, and a lower mass reduces the severity of consequences in the event of a collision [89]. Moreover, reduced size reduces the likelihood of a collision itself [66, 107, 53].

- *Integrity of the robot* : large arcs of execution of the arms, as occurs in large systems, can lead to collisions and resulting damage to the robot, leading to possible failure of the last [107]. In reviewing various preclinical and clinical studies, it was found that a percentage of abortions of procedures by the robotic system were due to collisions of the arms. This prolongs operating time, but also carries the risk of injuring the patient. In addition, damage to the robot can lead to an increase in maintenance costs.

- *Setup time* : a smaller robot, usually clamped directly to the operating table, is easy to move, adjust, and intuitive to operate and commission [66]. Although there are no direct studies and comparisons between the set up time of smaller and larger robotic systems, it is generally accepted that smaller robotic systems can be set up more quickly and that larger systems take quite a long time to dock and undock [135, 105, 89, 70].

- *Operating Room* : the small size allows the robot to be easily integrated into the operating room [66, 104]. In addition, small surgical robotic systems can be easily transported from one operating room to another, allowing them to be used for multiple purposes [70]. Moreover, large robots require a larger operating room, while most operating rooms are small [70].

- *Patient accessibility* : A small robot allows staff to reach the patient while the robot is still mounted [66, 91, 135]. A system with a smaller footprint in the operating room facilitates the viability of personnel who can access the patient more quickly in an emergency [66, 53]. All of these benefits reduce the risk of the system and reduce the hazards and/or severity of the consequences.

- *Expansion of MIS treatments* : smaller robots expand the capabilities of single-port laparoendoscopic surgery or natural orifice translumenal endoscopic surgery [105], making the robot more than just an enhancement of traditional MIS, but rather an expansion of the field itself, enabling procedures that are otherwise infeasible [105].

- *User's perception* : user's perception is the way the surgeon, surgical team, and patient feel during the use of the surgical robot. Studies have shown that the surgeon feels more comfortable with robots that are less complicated and easy to dock, undock, maneuver, and position [49]. This is true for smaller robots [70]. Indeed, large robots are more difficult to transport and position [104, 64].
  Besides, some other studies have been conducted on robots in terms of their human interaction and the feelings of the user himself. However, not many studies have been conducted on surgical systems. Most of the studies deal with robots in general and concluded that the user feels less

mistreated with smaller robots [117]. Hiroi [93] studied perceived safety and trust as a function of the physical characteristics of the robot (especially size). In his work, he concluded that "size does matter" and influences user-perceived safety: smaller robots are perceived by the user as safer and more human. Although the research was not conducted directly with surgical robots, this is still an important point to include in this literature review and should be analysed in more detail in future studies.

- *Workflow interruptions* : a large group of researchers are focusing on assessing workflow interruptions during surgery, a factor that can affect the efficiency and safety of the procedure. In the study by Ahmad et al. [54], it is highlighted that the set up of the operating theatre plays a crucial role in reducing interruptions. It is noted that interruptions are avoided where communication and access to the patient is faster [54]. This is generally easier with smaller robotic systems [54]. On the same topic, Allers et al. [58] concluded that a safe procedure requires a good set up of the operating theatre, a set up that reduces unnecessary components. Therefore, smaller and compact robots can improve the performance of the surgery.

- *Anesthesia and sterilization* : anesthesia and sterilization are also fundamental steps in surgery. Smaller robots are easier to sterilise [104]. In addition, large robotic systems make anaesthesia more difficult, as it is difficult to reach the patient throughout the procedure [94].

All these benefits underline the importance of the trend. It is interesting to note that, even if the trend towards smaller and lighter robotic systems has been recognised, there are still no cheap, small, light robotic arms confirmed in the market.

2.2 Goal of this thesis

After identifying the most emerging trend and the benefits that it brings, a novel area of development in the field could be identified, and a design for a minimally invasive surgical robotic arm that fills this new area of development is presented in this work. The robotic arm aims to meet the trend, and the design is carried out so that all the requirements necessary for MIS are satisfied, such that the weight, size, and complexity of the system are optimized.

Thus, the goal can be summarized:
To design mechanically and electronically, a simple, lightweight, small robotic arm for laparoscopic cholecystectomy, appendectomy, and inguinal hernia surgery that can maneuver a laparoscopic instrument.

2.3 Environment definition

Before proceeding with the design, the definition of the environment in which the robotic arm has to function is necessary. For this project, it is decided to consider as application's environment a standard operating room, that presents a standard patient's bed and a standard level of technology. Moreover, it is desired to avoid the presence of specialized staff or specialized external components.
For these reasons, the design is supposed to maintain a low level of complexity and technology, for allowing not trained staff to use it.

2.4 System definition

The robotic arm has to be incorporated in bigger systems, composed by the other parts that make the overall MIS robotic system. It is necessary to ensure the function of the system itself, and thus have a look into the collaboration and interaction of all the parts. Therefore, a deeper look into the other components is done, and specific requirements are extrapolated.
The two sub-systems that collaborate with the robotic arm are:

- *Tool holder* : The tool holder is a tool driver that needs to be attached to the robotic arm. It has the feature to perform the axial rotation of the instruments. It is designed such that it is attached to the robotic arm through a flange, shown in Figure 13. Additionally, it presents an interface for the attachment of sterile drape that are used for covering robotic arms in the surgical environment. It has a mass of 0.9 kg.

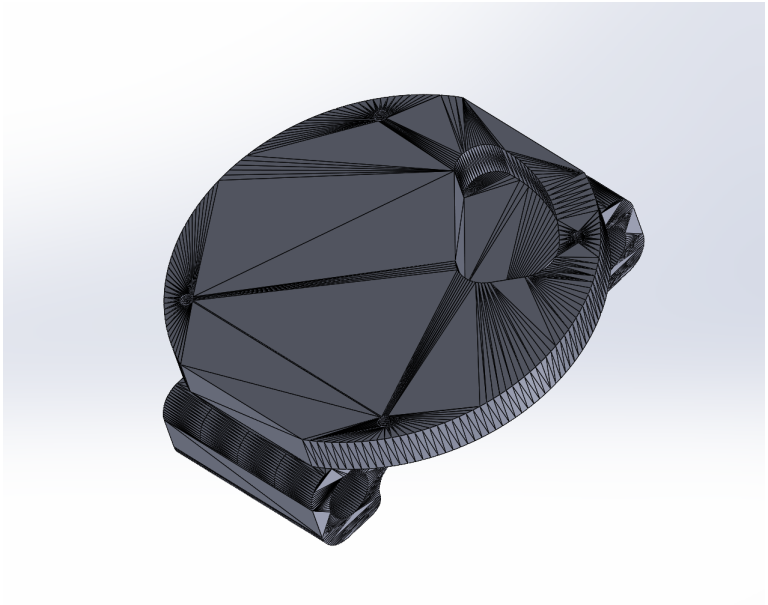

Figure 13: Flange for connecting the instrument's actuator

- *Trocar* : For inserting the end effector, the instruments, and the endoscope in the body of the patient, the *Trocar* is used. It defines the dimensions of the incision. Different sized trocars are used, commonly 5-8 mm for instruments and 12 mm for endoscope in multiport robots [133]. In multiport robots, the trocar is the fulcrum of the instruments and the endoscope [133]. The main components of a trocar are:
  - *The cannula*: The cannula is a tube-shaped metal or plastic shaft placed in the patient to allow access into the abdominal cavity during a laparoscopic procedure.
  - *The seal*: A seal is located at the top of the cannula, which allows instruments to pass through the cannula while preventing carbon dioxide (CO2) from escaping from the abdominal cavity. A gas-tight valve is located at the top of the cannula to allow instruments to be inserted and removed during a procedure without permitting the insufflated carbon dioxide escape. Various types of valves are available (spring loaded, magnetic trap door, trumpet, silicone, and so on), offering different characteristics in terms of leakage, mode of operation, and location on the cannula.
  - *The obturator*: This is the tool, either sharp or blunt, that enables the cannula to make the initial penetration into the abdomen.

  Considering the trocar presented in Figure 14, the procedure can be summarized as in Figure 15. The obturator is connected to the cannula by a fitting gripper, and is removed after the incision. The robotic arm has to consider the presence of such component close to the incision point.

2.5 Early decisions

The main decision taken for this project, before proceeding with the design, is the motion of the robotic arm. The system has to be moved in a first phase such that the rotational center of motion coincides with the incision point and the workspace of the procedure is aligned to the one of the system. Once this condition is satisfied, the instrument is attached to the robotic arm and manually inserted in the body and is ready to perform the surgery moving inside the patient's body.
In this project is decided to define a **global passive placement movement** and a **local active surgery movement**. In the first, an auxiliary mechanism is used for globally positioning the robotic arm. It is decided to be a passive motion, manually performed by the assistants, for satisfying the environment definitions presented in subsection 2.3. In the second, the RCM mechanism performs the surgery motion in an active way.

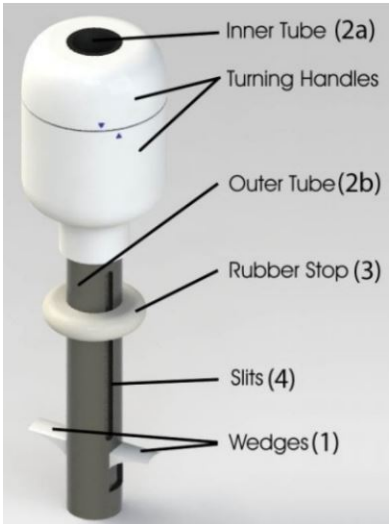

Figure 14: Trocar with its components [143]

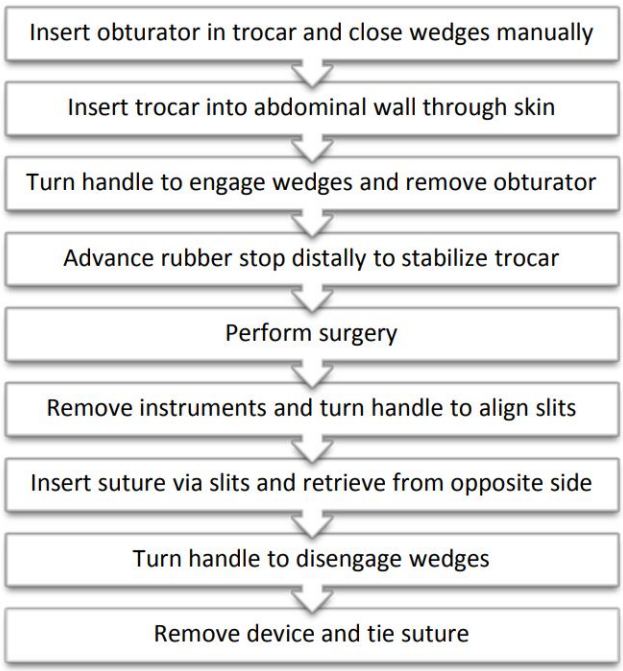

Figure 15: Work flow of surgery, concentrating on the trocar [143]

This decision of separating the motions, and designing specific mechanism for each of them, improves the intuitiveness of the system. Additionally, it permits to reduce the necessary workspace of the RCM mechanism. In fact, it is possible to define two workspaces. The first, regarding the alignment mechanism that has to cover all the abdominal area, and the second regarding the RCM mechanism that performs the active surgery movements. If the alignment is reached in a pre-phase, then the end-effector of the RCM mechanism should be able to move only on the working area near the organ/incision point, that is much smaller than the overall workspace if it is fixed. This permits to have smaller and more precise motions.

2.6 Approach and outline

A number of nine distinctive design phases are presented in this report. The first phase, section 3, is the identification of design goals and requirements. The section 4 and section 9 are dedicated to

the identification of the fundamental principles of the robotic arm and conceptual design of solutions and strategies to satisfy the aforementioned principles. This resulted in a morphological table. The morphological table is used for concept generation in section 5, where five concepts are generated and developed in details. In section 6, the five concepts are evaluated, and the final concept is selected. The design is optimized and finalized in section 7, section 10, section 11, and section 12. A validation of the design is presented in section 8. Finally, an experiment for evaluating the ease of set up of the mechanism is performed and the results are discussed in section 13. The paper is wrap up with a discussion, section 14, and a conclusion, section 15.

3 Specifications

This section describes the design goals and the requirements that the robotic arm must satisfy and optimize for filling the novel area of development.
The *design goals* are defined as variables to be optimized and minimized, and derives from the study of the trend and the insight of the benefits it brings. They are the variables by which the final design is selected.
The *design requirements* are derived from a literature review and a study of MIS robotic systems. The design must meet all of the requirements listed below. They relate to laparoscopic surgical systems.

3.1 Design goals

The *design goals* are the parameters that the design of the robotic arm wants to optimize. All the aforementioned benefits, subsection 2.1, can result in the identification of seven main *design goals* that the robotic arm has to optimize for filling the novel area of development of MIS robotic systems:

- **Minimize size and weight**: because of the trend towards smaller and lighter robotic systems in MIS shown in subsection 1.3, and the benefits of this trend presented in subsection 2.1, the goal of the paper is to design a small, light size robotic arm for MIS. Thus, it is necessary to identify the size and weight as variables to minimize.
- **Minimize hard-to-sterilize areas**: the specific parts must be designed to avoid hard-to-sterilize areas in contact with the patient or to allow easy attachment of sterile material.
- **Maximize ease of set up and control of the robotic arm**: this can be achieved by designing intuitive and simple interfaces for setting up the robotic arm before starting the surgery. Additionally, a simple control system that allows intuitive use of the robotic arm and reduces the risk of errors and improves the performance of the system itself. A lower number of output and an higher number of input improve the ease of control.
- **Minimize cost**: The design should allow ease of maintenance. Parts that are hard to maintain should be avoided. Additionally, it has to be made with standard parts that can be easily retrieved (standard shapes, materials, dimensions). When the part cannot be standardized, a part that can be manufactured by cheap and standard procedure is preferred.

3.2 Design Requirements

In this work, the design will focus on the mechanics and electronics of the slave robot arm. Thus, the requirements that the design has to satisfy can be divided into:

- *Mechanical requirements*: take care of the mechanical integrity, the kinematics and the dynamics that the robot arm must have, along with the physical dimensions that optimize the mechanical performance;
- *Mechatronical requirements*: take care of the actuation of the arm, the control and the selection of the actuators;
- *Production and material requirements*: take care of the medical requirements for material selection;
- *Interface requirements*: take care of the overall system picture and thus the integration of the arm into the MIS robotic system.

3.2.1 Mechanical requirements

- **Position in place**: The robot arm should be able to passively stay in place without retreating. This can be expressed mathematically as constant potential energy in any configuration.

- **Alignment of center of rotation(RC) with incision point**: Additionally, the RC of the mechanism has to align with the incision point. It is accepted that the RC is aligned in a sphere of radius 7.5 mm center in the incision point. This is because the incision has a length of 1.5 cm. The mechanism has to rotate around the incision port for to not hurt the patient.

- **Back-drivability**: The arm should be mechanically backdrivable. Backdrivability is the ability of the robot to be moved by external forces [69], and it is an index of safety in case it is necessary to move the robot away manually.

  The robot arm must only move under certain forces and must avoid being moved back by external unwanted interference. The minimum mean force that an human can apply in pushing/pulling is 62.24 N [82]. It is possible to define that the arm should be backdrivable with an applied force of 60N.

- **Mechanical Integrity**: The robotic arm must avoid collisions. For safety reasons, the robot-patient collision is unacceptable. Instead, the robot-robot collision should be avoided, and be of concern during the design of the robot and of the relative position. This means that the dimensions and position of the components of the robotic arm must be optimized so that this does not happen.

- **Motion**: A robotic arm for laparoscopy must have four DOFs, three rotational around the incision point, and one translational along the incision point. However, in this project, the robotic arm must have only three DOFs, one translational and two rotational. In fact, the rolling of the instruments is performed by an actuator for the instruments, which is placed at the beginning of the instruments. Besides, the robotic arm should be kept at a distance from the incision point. The motion is, thus, called Remote Center of Motion (RCM).The three DOFs that the robot arm must provide are thus shown in Figure 16.

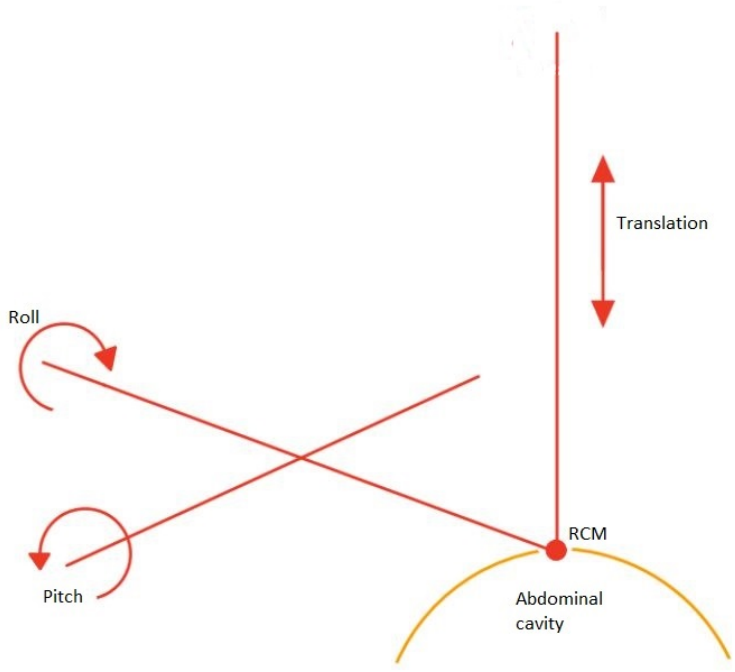

Figure 16: total DOFs of the robot arm

One of the DOFs that needs to be further discussed is the translational one. This DOFs is responsible of two main features:

  – *Insertion and extraction of instrument* : this feature permits to insert and extract the instrument in and out of the patient body. This motion has a large range of motion and

required to be precise and safe. It is decided to perform it **manually**.

- *Translation motion in the patient body* : this feature permits to move the instrument inside the patient's body. This motion has a small range of motion (13 cm) and requires high precision and repeatability.

The two features have different requirements in term of range of motion, required velocity, precision, and force.

Additionally, it is worth to notice that decoupling the DOFs enhance the dexterity, due to the fact that each dedicated DOF is going to be driven by a separate driver unit, that can allow maximum force and velocity. Thus, it is preferable to have dedicated DOFs.

- **Workspace**: The robot's workspace has to allow the robot arm to reach all the points necessary for the operation without being positioned more than once.
  As defined in subsection 2.5, the motion is going to be divided in two: *global passive placement motion* and *local active surgery motion*. For the first motion, the workspace is defined as a rectangular parallelepiped, which area is coincident with the abdominal volume (31.5 cm x 29.5 cm x 20 cm).
  The second local active surgery motion has a workspace that depends on the kind of procedure that is carried out. The workspace overall presents two equal and symmetric cones that meet at the RCM points of the mechanism.
  As expressed in subsection 1.2, in this project the design is made for performing *cholecystectomy*, *appendectomy*, and *inguinal hernia surgery*.

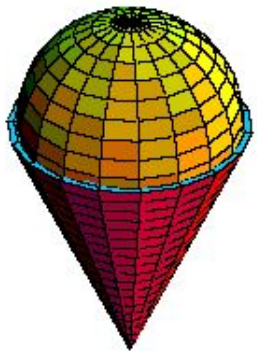

Figure 17: Workspace of the tip and of the instrument(yellow) and the instrument (red)

This conic structure represents the workspace of the instrument. However, the robotic arm's end effector has a workspace equal to the tip of the instrument. Thus, the workspace is expressed as a sphere, which diameter depends on the procedure. For the selected procedures, the workspace is expressed in Table 3. Then, from the spherical workspace, a conical structure is constructed, symmetric to the incision point, Figure 17.

Table 3: Workspace of the procedures

Procedure	**workspace**
Cholecystectomy	sphere of 10 cm
Appendectomy	sphere of 15.88 cm
Inguinal hernia surgery	sphere of 15 cm

To conclude the workspace of the robotic arm is:

- *Alignment design*: it needs to have a **rectangular parallelepiped workspace with dimensions 31.5cm x 29.5cm x 20cm**;
- *RCM mechanism*: it needs to have a **spherical workspace of radius 15.88cm**.

- **Payload**: The mechanical structure should be able to attach the instrument's driver and the instrument without deformation or change behaviour/control. The mass of the instrument's driver is 0.9 kg, thus for safety reasons, the payload of the robotic arm can be considered 1.0 kg.

3.2.2 Mechatronical requirements

- **Actuation**: The arm should be mechatronically controlled. This includes the presence of drive units and a system of energy transfer that enable the robotic arm to perform its tasks.
- **Position feedback**: In order to actuate the end effector in the correct manner, position feedback must be included in the loop to increase accuracy and reduce the risk of error. The quantity that has to be given as feedback is the exact position in space of the end-effector.
- **Precision**: The desired precision is 0.01 mm for translation and 0.8° for rotation [127].
- **Force and velocity**: Other important characteristics for surgery are the applied force and the speed of the instrument. These two characteristics are necessary to determine the success of the procedure and to maintain the required level of safety. The BioRobotics Lab at the University of Washington (with BlueDRAGON) has conducted some experiments. The most accurate and available data relative to force and velocity are: Fx,Fy 5N, Fz 20N, wx 0.486 rad/s (4.641 RPM), wy 0.432rad/s (4.125 RPM), wz 1.053 rad/s (10.05 RPM) [118, 136]. In addition, the velocity along the axis of the instrument is at most 0.2 m/s [88].

3.2.3 Material requirements

- **Material**: The parts near the access point should be bio-compatible (ISO10993), easily sterilizable or easily covered with sterile material.

3.2.4 Interface requirements

- **Instrument connection**: The connection with the instrument should be intuitive, allow the change of instruments without moving the robot and hold the instrument firmly.
- **Connection to the ground**: The connection to the ground can be made in different ways, but must be firm and intuitive.

4 Conceptual Design

In this chapter, the fundamental principles of the robotic arm are expressed and explored. Based on these, a number of features that the robotic arm must have is selected. The main features are, again, subdivided in area of design as in subsection 3.2. Next, an overview of possible conceptual solutions for each feature are presented.

4.1 Material design

4.1.1 Sterilize robotic arm

For having a safe environment, the external part of the robotic arm must be sterile. Two are the main approaches. Maintaining a sterile barrier between the robotic surgical device and outside contaminates is critical in the operating room.

- **Sterile material**: The robotic arm must be enclosed in a sterilizable case, with material selected between the ones that satisfy the requirement ISO10993.
- **Cover with sterile sleeve/drape**: Another well known and used strategy is covering the robotic arm by a sterile sleeve while the tool is separately sterilized by an autoclave procedure. Thin, plastic drapes are commonly used as a sterile barrier before, during, and after a surgical procedure.

Preliminary decision

The explored solutions that have been presented above, brought in light some aspects that already allow to make some preliminary decisions. For the complexity of the concept of sterilization of all mechanics and electronics of the robot itself and the simplicity and availability of the drapes, for this design the use of **drape** has been selected.

4.2 Interface design

4.2.1 Instrument and ground connections

The first level of interaction that needs to be taken into consideration is the connection of the robotic arm with the ground and with the instruments' holder.

- **Impactive Gripper**: These grips exhibit physical grasping directly impacting the object. **Friction grippers** press two or more parts together so as to hold them firmly. The two objects are constricted together due to the force that is applied at the interface. It is necessary that this force is higher than the ones applied at the end effector for guaranteeing the connection through all the procedure. Additionally, there are **shape grippers**, where the grip is created by a perfect fitting of the shapes of the two parts. The inside part is slightly larger than the outside one, and the fitting creates some force that Hold the instrument. However, this fitting increases the time for changing instruments. Additionally, it is less controllable with respect to the clamp one.
- **Ingressive Gripper**: These are sharp-point surfaces like pins, needles or hackles which exhibit physical penetration inside the surface of the object. These grippers slow down the change of instruments, and need a redesign of the instruments' holder.
- **Astrictive Gripper**: These grippers apply attractive forces using a vacuum, magneto- or electroadhesion. In this group there are **magnetic forces grippers**, that create a connection by the magnetic forces. It can be quite strong and can reduce the time for changing tools. However, this enforces to insert magnetic parts and magnetic forces in the system. In the **electrostatic forces grippers** the connection is created by the electrostatic forces between the two parts. Also in this case, the grip is strong, but, this enforces to insert a extra electric interconnections and electrostatic forces in the system. Finally, the **suction grippers** uses the difference between atmospheric pressure and a vacuum to lift, hold and move objects. Typically, the vacuum is generated by a miniature electromechanical pump or a compressed air-driven pump. The vacuum flow must be uninterrupted to ensure that the instrument is always attached to the robotic arm.

- **Contigutive Gripper**: These grippers require direct contact to exhibit adhesion, such as glue, surface tension or freezing/heating. The lasts are also called **thermal grippers**.

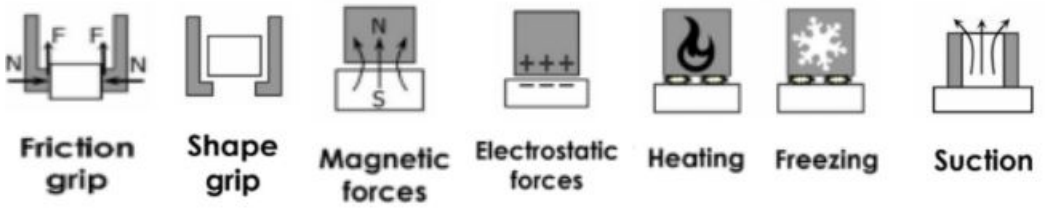

Figure 18: Grippers

Preliminary decision

The explored solutions that have been presented above, brought in light some aspects that already allow to make some preliminary decisions. Ingressive grippers required a redesign of the instruments' holder, which is something out of scope for this project. Astrictive and contigutive grippers require additional parts and electrical/mechanical components. Additionally, it is preferable not to have extra forces as magnetic or electrostatic, since they can interfere with the close parts of the robotic arm, and creates a malfunctioning. The suction grippers require additional parts for creating the vacuum. Finally, the thermal grippers require special structures and design for allowing freezing and heating. These phenomenons can also ruin the electromechanics that surround the gripper. Finally, all of the aforementioned strategies requires a constant and expensive maintenance.

Thus, the final selection is between **friction grip** and **shape grip**.

4.3 Mechanical design

4.3.1 Align the RC with the incision point

It is necessary, before the surgery, that the mechanism's RC is aligned to the incision point. As already expressed in the subsection 2.3, the robotic arm has to be integrated in every hospital with standard level of technology. Thus, the alignment of the robotic center of rotation and the incision point is reached by a passive motion of the system, without requiring any extra technology. For doing so, an *auxiliary-locating mechanism* is designed and attached to the robotic arm. The auxiliary mechanism should allow the location of the robotic arm in the space. It needs to have 6 DOFs, 3 Translations and 3 Rotations (3T3R). The mechanism should be locked after the alignment.

The **design of this pre-stage** needs to be easy, small, and intuitive, for meeting the goals defined in subsection 3.1. The auxiliary design should allow the motion of the robotic arm on the abdominal cavity, since the instruments in the laparoscopy is inserted in this cavity. This means that the end effector of the robotic arm should be able to be positioned everywhere on the area of the abdominal cavity (31.5 cm x 29.5 cm [60]) and be able to rotate in any directions.
Mechanically, the motion of mechanism can be achieved by the use of joints. The joints are:

- **Revolute/Hinge joint**: it allows 1 rotation around a fixed point (1R);
- **Prismatic/Slider joint**: it allows 1 translation along a prefixed axis (1T);
- **Cylindrical joint**: it allows 1 translation along a prefixed axis and 1 rotation along the same axis (1T1R);
- **Spherical/Ball joint**: it allows 3 rotations (3R).

The design of the preliminary stage is made by the combination of these joints.

- **3 revolute joints + 3 prismatic joints (1R+1R+1R+1T+1T+1T)**: in this concept six joints that allow the motion in space of the robotic arm are placed in series. The joints can be arranged in any order, however, for reducing the interference between the assistants and the auxiliary mechanism, the order of the prismatic joints want to be as follow: first translation along y, then translation along z, and finally translation along x. Additionally, it is preferred to

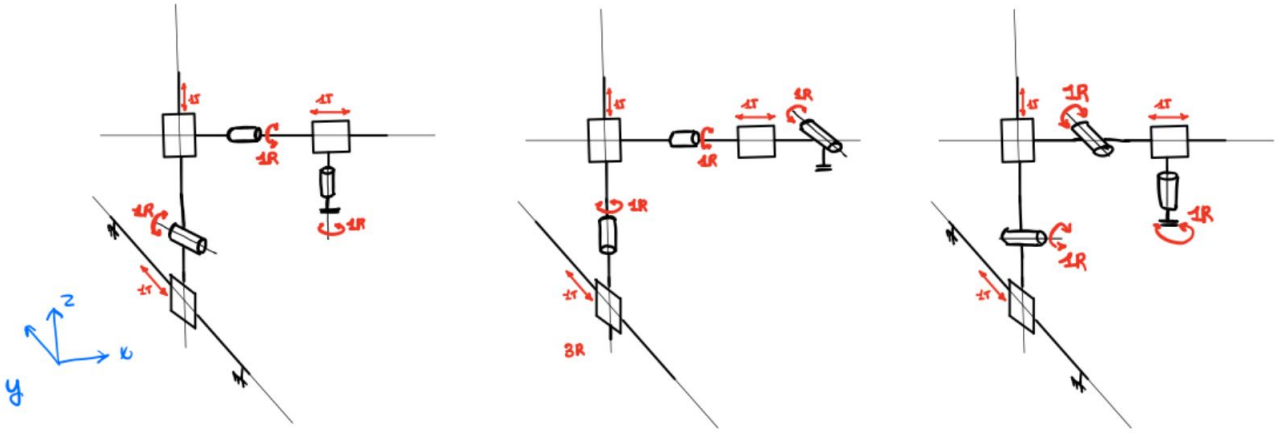

Figure 19: Some alignment mechanisms 3 revolute joints + 3 prismatic joints

have the revolute joints in between of the prismatic ones. Some possible designs are reported in Figure 19.

- **3 cylindrical joints (1R1T+1R1T+1R1T)**: in this concept solution, three cylindrical joints in series creates the required DOFs. Also in this case, the order of the cylindrical joints is for reducing the possible interference between the assistants and the auxiliary mechanism. The concept is shown in Figure 20.

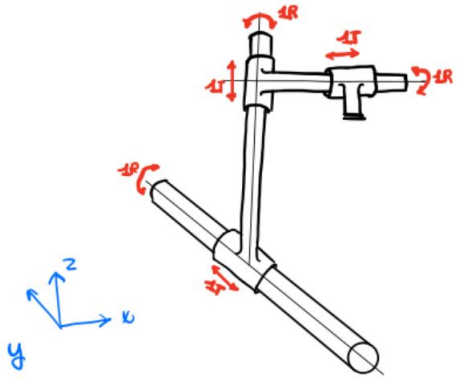

Figure 20: Alignment mechanisms 3 cylindrical joints

- **1 Spherical joint + 3 Prismatic joints (3R+1T+1T+1T)**: in this concept solution the three rotations are allowed by the spherical joint. All the joints are arranged in series. The spherical joint has to be positioned on the base, for facilitating the functioning of the locating mechanism, since the presence of linkages after the ball joints will increase the precision and the easiness of the motions. Along with this, it is also true that rotating extra parts can create additional hazards. Additionally, the order of the prismatic joints follows the previous one, for the same reasons expressed in the previous two points. Thus, the possible designs are presented in Figure 21.

Finally, as soon as the robotic arm is positioned, it is necessary to **lock the auxiliary mechanism**. This can be done by mechanical locks that the surgeon has to insert before starting the operation and as soon as the alignment is reached. A deeper look in the locking mechanism is taken.

- **Locking ball joint: Positioning fixture**: there exist already lockable ball joints. Once the arm is located, the surgeon/assistant can directly lock the joint from itself.

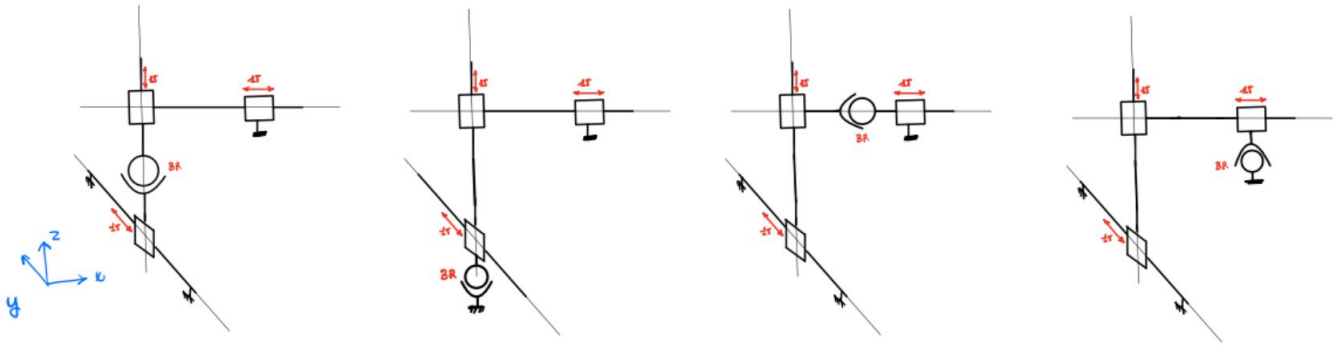

Figure 21: Alignment mechanisms 1 spherical joint + 3 prismatic joints

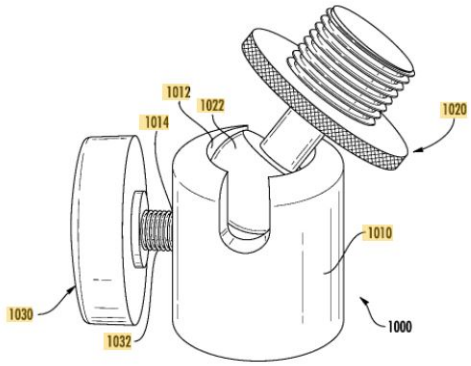

Figure 22: Position fixture of a ball joint [140]

- **Locking sliders: One-touch sliding locks**: One-touch Sliding Lock is a fixing component that enables easy and secure locking in sliding adjustment [32].

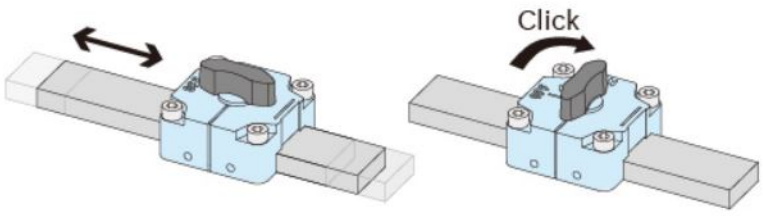

Figure 23: One-touch sliding locks [32]

- **Locking sliders: One-touch indexing clamps**: One-Touch Indexing Clamps are quick fasteners with precise locating for position adjustment by sliding or rotation. Tapered surface contact provides +/- 0.05 repeatability. ON/OFF marking and click eliminate human error. Quick and easy clamping by turning the handle slashes workpiece set up time and spiral cam mechanism provides high clamping force [32].
- **Locking sliders: Linear-motion stoppers**: Turning the handle to the clamping position allows clamping the linear rail [32].

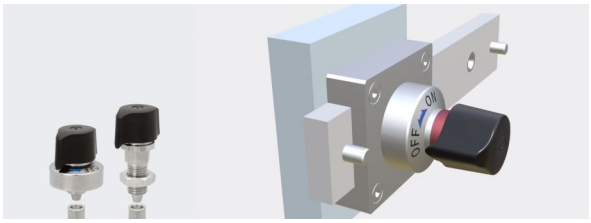

Figure 24: One-touch indexing clamp [32]

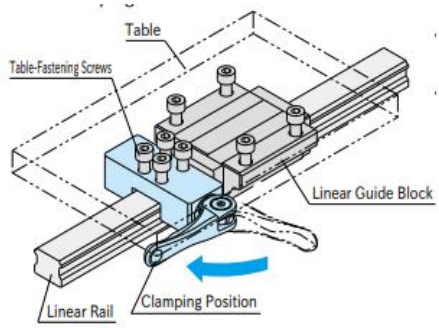

Figure 25: Linear-motion stopper [32]

- **Locking sliders: Pneumatic shaft-locking clamps**: Pneumatic Shaft-Locking Clamps are automated quick locks for machine changeover. Perfect for clamping sliding shafts and spindles after positioning and adjusting the equipment [32].

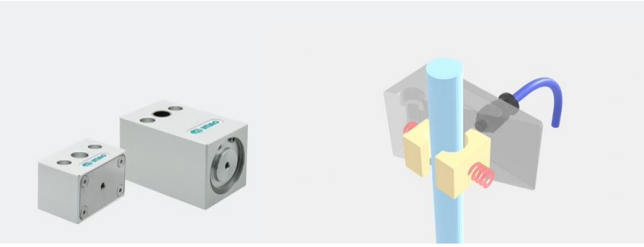

Figure 26: Pneumatic shaft-locking clamps [32]

- **Locking sliders: Quick shaft-locking clamps**: As the handle is turned down, it pushes the locking block toward the shaft for clamping. When the handle is released, the flat spring allows the locking block to be returned to the original position [32].

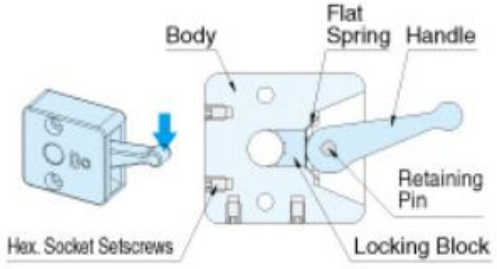

Figure 27: Manual quick shaft-locking clamp [32]

- **Locking cylindrical joints: pressure locking**: The cylindrical joint can be locked with a pressure locking system. A screw is turned to create pressure on the shaft, since it does not allow any other motion due to the pressure created [32], shown in Figure 28.

Figure 28: Manual quick locking for cylindrical joints [32]

Preliminary decisions

For the selection of the locking mechanism for the linear sliders, it is possible to make some preliminary decision that permits to narrow down the solutions. First, the pneumatic shaft locking clamps needs extra components that are expensive and heavy. For this reason, this concept is withdrawn. Additionally, the linear motion stopper requires an additional part, that increases the weight and the dimensions of the stage. The remaining options for locking the linear motions are **one-touch sliding locks**, **one-touch indexing clamps**, and **manual quick shaft-locking clamps**.

Finally, since the alignment is manual, a **technology that points the Remote center of motion** of the mechanism is necessary. An overview of the possible theoretical technologies is reported below. For what expressed in subsection 2.3, the use of external camera systems has not been taken into consideration.

- **Lasers**: inserting in the system two lasers that meet each others in the RC of the mechanism. The intersection gives a visual feedback to the assistant that is aligning the mechanism, Figure 29.

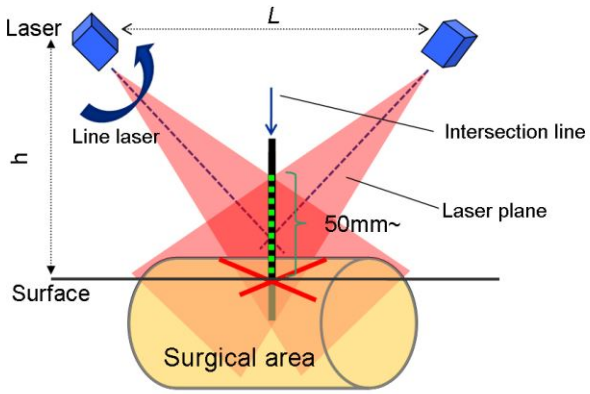

Figure 29: Lasers intersection [113]

- **Rigid body extensions**: this strategy uses bodies that meet in the rotational center. These bodies have to be mounted during the alignment, and removed after it.

- **Estimation with force sensing**: since the body wall has a non-negligible thickness, there will be always some forces and torques generated as the instrument is pivoting about the incision point. The larger the dis-alignment between the RC and the incision point, the larger the generated force will be. By measuring the forces generated it is possible to estimate the offset and the position of the fulcrum point. However, this conceptual solution needs the insertion of force sensors on the robot. Additionally, force sensors are noisy and prone to drift, they require calibration, pose difficulties when it comes to sterilization and are expensive.

- **Algorithm and computer models**: this concept solution is based on the use of computer models and algorithms for calculating and displaying the remote center of motion of the mechanism. However, this concept solution increases the risk of collision, since there is no real time feedback but only a feed-forward model.

4.3.2 Maintenance of position in place passively

In case of total system failure, the mechanism should be able to maintain its position, for safety reasons such as not hurting the patient and not colliding with itself. Additionally, if a gravity stability is reached, the actuation load is used only for the control of the motion and not for counteract the gravity, reducing the amount of torque necessary, thus the size and weight of the actuators. Finally, for the same reason as before, the motors needs a lower low-speed reduction ratio.

This feature can be reached by different approaches. Mathematically, the mechanism should be in stable equilibrium (state of least energy) at all possible configurations. For doing this it is necessary to achieve static balancing: continuous equilibrium; constant potential energy; neutral stability. This is reached by passive gravity compensation.

- **Counterweight**: it balances the mechanism by putting weights on the opposite side of the center of rotation. They can be mounted on the *links of initial system* or on *auxiliary linkages* connected to the initial system [62]. The first one can use as mass the motors themselves. It is more appropriate for serial and planar parallel mechanism. The second uses an auxiliary linkage, a mechanical system that is mounted between the balancing element and the robotic arm. These structures improve the compensation and design conditions via optimum location of the balancing elements [62]. However, they increase the footprint and the overall size of the robotic arm.
  With this approach, it is easy to mechanically assemble the linear actuator, but it increases the overall mass, the overall size, and the inertia. Another advantage is the independency of the direction of gravity vector. An example of balancing with counterweights is shown in Figure 30.

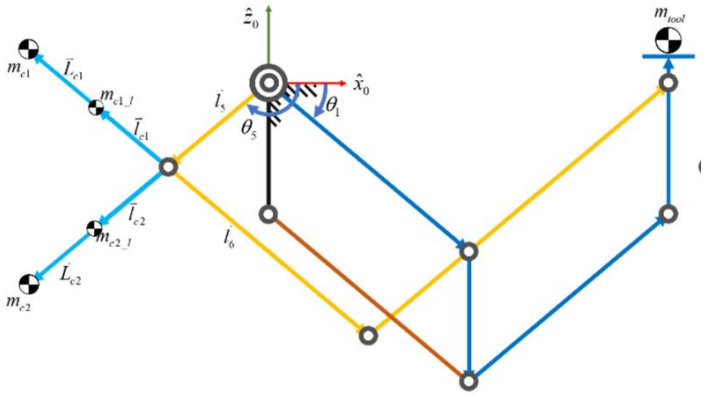

Figure 30: Balancing mechanism using counterweights [145]

- **Springs**: it balances the mechanism by the restoring force of springs. The spring can be divided in *zero-free length* and *non-zero free length*. The first one is a term for defining special designed

spring that would exert zero force when at zero length. Physically, it is impossible for a spring to reach zero length, thus the zero-length spring is achieved by manufacturing a coil spring with built-in tension [62]. The zero-length spring is usually used when the gravity compensation is done directly on the robot's links.
Also in this case, we can define different strategies to insert the balancing element in the existing structure. The first is *springs joined directly to the robot's links*, and in this case a zero-length spring is used. Other strategies are *using the cable and pulley arrangement*, *balancing with auxiliary mechanical systems*, *balancing by using auxiliary linkage*, and *balancing by using a cam mechanism* [62].
With this approach, the users feel less inertia, but the behaviour of the stiffness of the springs is non-linear, and it is difficult to assemble the linear actuator. An example of balancing with springs is shown in Figure 31.

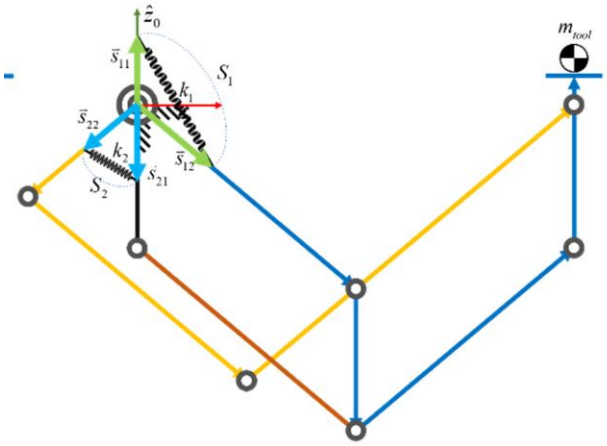

Figure 31: Balancing mechanism using springs [145]

- **Spring and counterweight equilibrator**: in this strategy both springs and counterweight are used for reaching the gravity balancing[145]. In this case the user feels low inertia and it is mechanically easy to assemble. Additionally it allows a wide range of adding mass. However, it has an high cost [145]. Usually this configuration is used when the load at the end effector changes, using the springs as initial balancing and the counterweights to handle the variable payload, or vice versa [145].

- **Auxiliary actuators**: *pneumatic or hydraulic cylinder* can be used for gravity compensation, by connecting them to the robot's links [62]. Continuous balancing is achieved by the pumping of the fluid from the first reservoirs-counterweight to the second. Example are shown in Figure 32. Additionally, *electromagnetic effects* can be used for balancing.

- **Inertia control**: another strategy for reaching gravity balance is achieving the optimal control of input torque. The control law combines terms that cancel the gravity effects on the robot link dynamics with a PD-type error feedback on the motor variables. However, this strategy will not help in case of full failure of the electronic/sensory system [62].

Another possible solution is the following:

- **Non-backdrivable transmission**: a non-backdrivable transmission systems allow a joint to hold a position independently of the torque applied to the joint output, without providing any motor torque [75]. A transmission can be non-backdrivable till a maximum force, and be back-drivable for forces higher than the maximum one. A study of the forces that the system needs to sustain in case of failure needs to be calculated, but it is roughly calculated that they are lower than the force that an human person can apply (*le* 60 N). As expressed in subsection 3.2, the system needs to be manually backdrivable from assistants. It is necessary, then, to select a

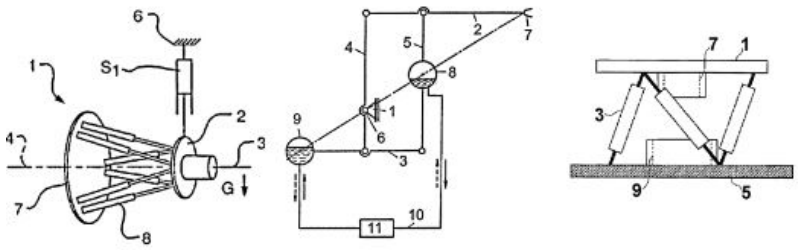

Figure 32: Balancing mechanism using auxiliary actuators [63]

motor and a transmission that can be backdrivable above and when an average human force is applied, but not otherwise.

Preliminary decision

The explored solutions that have been presented above, brought to light some aspects that already allow to make some preliminary decisions. The auxiliary actuators need extra parts and systems to work. Additionally, the insertion of liquids or compress air in the system increase the hazards of it. For these reasons, they are discarded from the possible solutions. Moreover, a inertia control may fail during the blackout of the system.
Thus, the final decision is between the **counterweights**, **springs**, **combination of both**, or **non-backdrivable transmissions**.

4.3.3 Motion

The mechanism that creates the desired motion is an RCM mechanism. Usually, a RCM can be realized in three ways:

- **Mechanical RCM**: the mechanical approach is safer because it is less sensitive to errors. This design has to provide 2 rotational (R) DOFs and one translational (T) DOF. This can be reach by combining different mechanisms, mounting them in series or in parallel. There are different combinations possible: 1R+1R+1T; 1R+1R1T; 2R+1T; 2R1T. Decoupling the DOFs makes the robot safer (each DOF can be stopped and controlled alone) and less expensive in energy (1 actuator for 1 DOF).
- **Virtual RCM**: this approach is less safe. However, the mechanical approach requires a perfect alignment between the remote center and the incision port prior to any surgical maneuver. In this case the RCM is achieved with dynamic posture decomposition, forward kinematics optimization, adaptive force control, or Cartesian control algorithm.
- **Hybrid**: in this approach, the RCM is achieved both mechanically and virtually. An example is the robotic system Zeus.

For what expressed in subsection 2.3, the robotic arm needs to be easy to use and maintain a low level of technology and complexity. For these reasons, in this work, the RCM is achieved with the **mechanical approach**, being it safer and less sensitive to errors.
Additionally, the mechanism can be a **rigid-body mechanism** or a **compliant mechanism**. It is generally accepted that compliant designs, even though requires less parts, create generally bigger mechanisms with respect to their linkage mechanism counterparts. Additionally, the compliant design is more complex for achieving the desired motion with the desired precision. Finally, they are not stiff or rigid enough for this application, reducing the absolute precision of the motion. Additionally, they suffer of plastic deformation. For these reasons, in this project the design will be created by a **rigid-body mechanism.**

Based on the mechanism types, the mechanical RCM mechanisms used in MIS robots can be classified in six types:

- **Revolute+Prismatic joints (1R+1T)**
  This method that sees the concatenation of revolute and prismatic joints is simple, does not need additional link, and has a smaller footprint.

- **Parallelograms-type (1R or 1R1T)**
  This mechanism is composed by two parallelogram structures, the RCM can be located where two adjacent sides of either parallelogram are intersected [108]. This mechanism has one rotational DOFs. When the mechanism is pivoted with a revolute joint whose axis passes through the RCM, an additional rotational DOF will be added [108]. These two situations can be seen in Figure 33. This configuration is clinically proven, but the footprint is big. The main concern with this configuration is the stiffness, necessary for meeting the required precision.

Figure 33: Parallelograms-type kinematics [108]

- **Synchronous belt transmission(1R or 1R1T)**
  In this mechanism, the parallelograms are simulated with synchronous belt transmission [108]. The mechanism can be seen in Figure 34, and has one DOF.

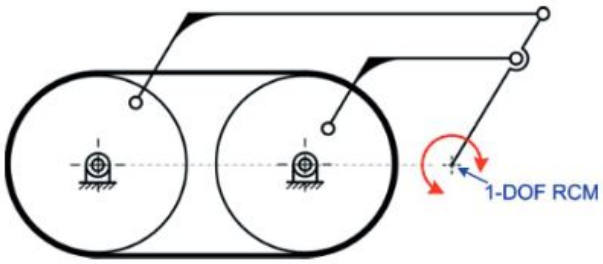

Figure 34: Synchronous belt transmission kinematics [108]

- **Isocenter (3R+1T)**
  This mechanism is composed of a circular ring that constrains an object which moves inside the ring [108]. It can be seen as a 4-DOF pin-in-ring joint, as shown in Figure 35.

- **Circular tracking arcs (1R or 2R)**
  This mechanism is composed of a circular arc that behaves as a track for the passive member, that slides on it [108]. This creates a 1-DOF. Additionally, if the track is pivoted with a revolute joint whose axis passes through the RCM, an additional rotational DOF will be added [108]. These two situations can be seen in Figure 36. This design is compact and down-scalable. However, it requires high manufacturing and assembly precision. The main problem is that the range of motion is directly proportional to the radius of the mechanism, thus for satisfying the required workspace it is necessary to have a circular arc mechanism with a big footprint.

- **Spherical linkages (2R or 3R)**
  This spatial mechanism enforces all the moving bodies to rotate around a unique point, permanently fixed in space [108]. It is composed by 2 or 3 revolute joints that do not coincide.

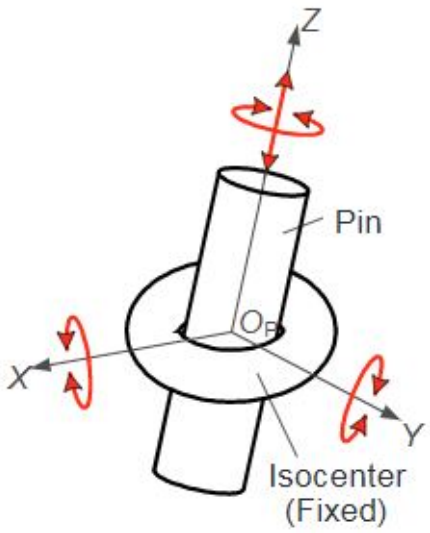

Figure 35: isocenter kinematics [108]

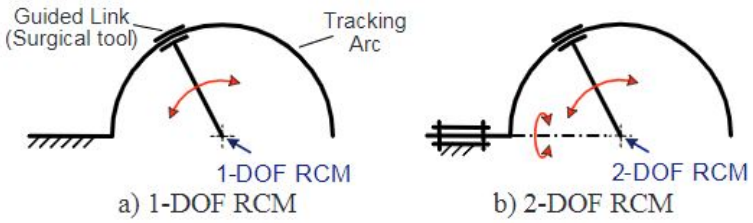

Figure 36: Circular tracking arcs kinematics [108]

The mechanism is shown in Figure 37. The main problem is that the DOFs are coupled, and, additionally, the mechanism is not planar, thus it has a big footprint.

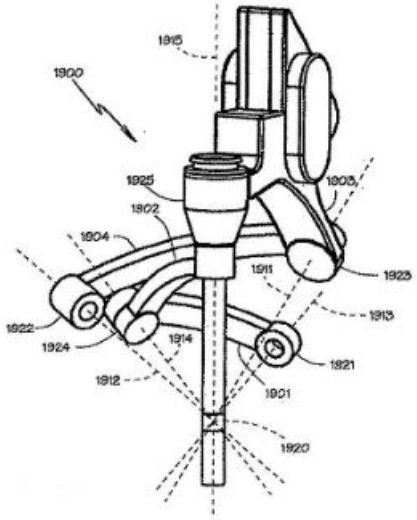

Figure 37: Spherical linkages' kinematics [108]

5 Concept generation

Even if the challenges and their concept solutions were worked separately, it is necessary to study the interdependency of them and to come up with cumulative concept solutions that consider the collaboration of all the different parts. For doing so, a morphological chart, Table 4, was made.

Table 4: Morphological table

Function					
Interface	friction grip	shape grip			
Position in place passively	Counterweight	Springs	Spring and counterweight equilibrator	Non-backdrivable transmission	
Align pre-stage	3 revolute joints + 3 prismatic joints (1R+1R+1R +1T+1T+1T)	3 cylindrical joints (1R1T+1R1T +1R1T)	1 Spherical joint + 3 Prismatic joints (3R+1T+ 1T+1T)		
Block sliders of the alignment mechanism	One-touch sliding locks	One-touch indexing clamps	Manual quick shaft-locking clamps		
Feedback of RC point	Lasers	Force sensing	Rigid body extensions	Algorithm and computer models	
Motion	Revolute+ Prismatic joints (1R+1T)	Parallelograms - type (1R or 1R1T)	Isocenter (3R+1T)	Circular tracking arcs (1R or 2R)	Spherical linkages (2R or 3R)

5.1 Four concept designs

Using the morphological chart, Table 4, through the combination of different solutions, a variety of concept designs were made. In this paper, five of them have been reported. Additionally, the mechanical design for creating a RCM mechanism has been farther developed in each concept. The first three concepts present independent DOFs. The first one aims to minimize the dimensions of the RCM mechanism. The second one aims to minimize the steps in the alignment, simplifying the alignment mechanism. The third one aims to minimize the number of linkages.

5.1.1 Concept design 1: The seven-bar mechanism

In this concept, the mechanical design was realized by a seven-link linkage, which provides as input a rotation in I and as output a rotation in A with a center of rotation far from the bar mechanism. The mechanism is then connected to a revolute joint that allows the second rotational degree of freedom. Finally, a prismatic joint is inserted at the end to allow the translation of the instrument. The choice of this mechanical design is due to the fact that the RCM is quite far from the mechanism. Moreover, the arc generated for a small mechanism is still large enough to meet the requirements. For this reason, it is possible to reduce the size of the linkage to create a small robotic system that provides better position feedback. It is important to emphasize that the radius R and the angle θ depend on the length of the bars and on the distance between the two fixed points F and I. In addition, the mechanism is a linkage with seven rods, so there are several parts that can break or create slash. Another positive aspect of this concept is the symmetry of the design.
The robotic arm is held in position by a counterweight because of the symmetry of the design.
The alignment pre-stage consists of three cylindrical joints and is manually aligned using two lasers whose intersection points identify the RCM of the mechanism. The cylindrical joints are locked with a manual quick-release fastener.

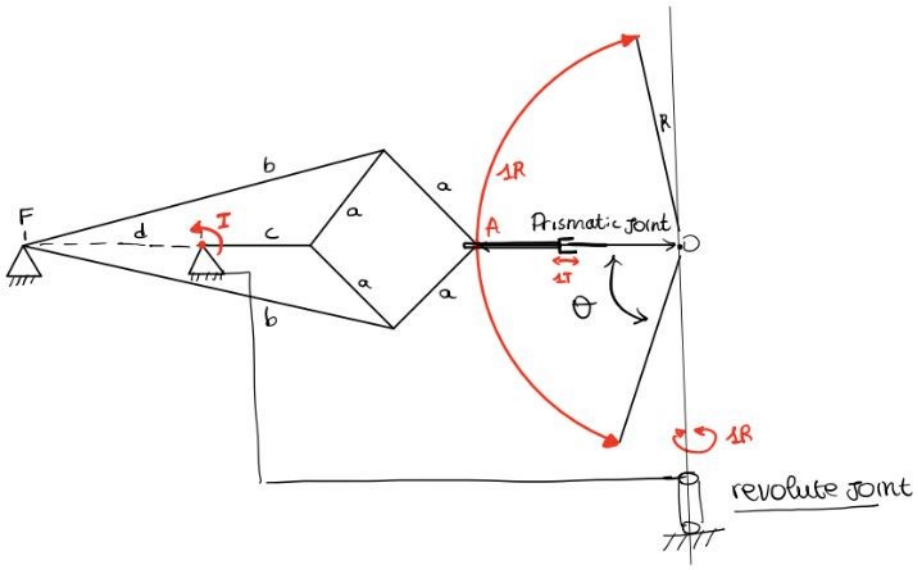

Figure 38: mechanical design for RCM mechanism of concept 1

Finally, the grip is created by a friction grip, for the fact that the design requires a long beam from the point that rotated to the RCM. This factor can creates high forces and moments, that needs to be overcame. A shape grip may not overcome them.

5.1.2 Concept design 2: The cubic design

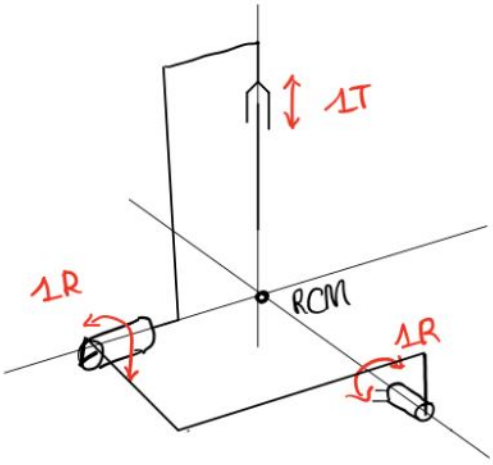

Figure 39: mechanical design for RCM mechanism of concept 2

In this conceptual design, the mechanical RCM is achieved by using two revolute joints and one prismatic joint, as shown in Figure 39. The joints are all connected in series, creating a center of rotation free of any physical connection. Finally, The design has independent DOFs, but the main drawback is the positions of the two revolute joints. Since the RCM is on the same plane as them, part of the mechanism (two rotational joint) would have to be on the patient. However, this can be helpful in aligning the mechanism. In fact, the height and inclinations (rotations) of the mechanism are already determined by the positioning of the two revolute joint on the plane of the RCM (abdominal

plane). Thus, only the two translations need to be aligned and the alignment mechanism can consist of only two prismatic joints that can be locked by one-touch sliding locks. The alignment is manual, and two lasers positioned on the revolute joints cross at the RCM point. Another drawback is the large frame connecting the two revolute joints, which is necessary for the independent DOFs.
Gravity compensation is achieved by using non-backdrivable gears.
The overall system is connected to the ground with friction grips.

5.1.3 Concept design 3: The "L" mechanism

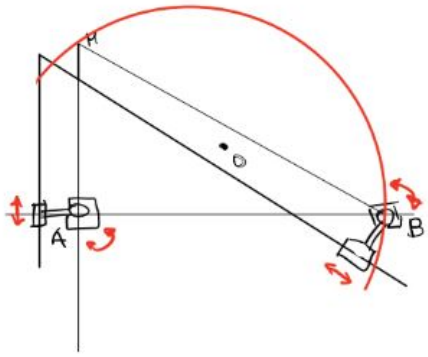

Figure 40: mechanical design of the L shape for RCM mechanism of concept 3

In the third conceptual design, an attempt was made to achieve the previous concept by using an auxiliary mechanism that generates one of the rotations. This mechanism consists of an L-shaped rigid body connected to two cranks, Figure 40. One of the cranks (A or B) is activated and the L-shaped rigid body moves and generates a rotational motion at the point M. The circle is the circumcircle of the triangle with vertices A, M and B. An extension is added to this L-shaped body and a prismatic joint is connected to allow the instrument to move, as shown in Figure 41. In addition, the mechanism is connected to a revolute joint that allows the final rotational movement. The three different configurations shown in Figure 41 differ in the position of the revolute joint. The lower and upper configurations have independent DOFs, but must "hug" the patient's body to avoid a physical collision between the body and the mechanism. To achieve this, the designs must be large enough. Therefore, the dimensions of the designs are limited and must be larger than the width of the abdominal cavity (30 cm). The top right design, on the other hand, is not subject to the same constraints as the other two. However, the DOFs are dependent. The overall dimensions of the L-shape determine the arc of rotation from M to B and thus the workspace of the design.
The entire robot is connected to the floor by a friction grip. This allows for greater forces in all directions.
The overall gravity balance is achieved by using non-backdrivable transmissions to allow a limited number of joints and maintain a simple design.
The alignment pre-stage consists of a spherical joint and 3 prismatic joints, in the order of prismatic joint 1, prismatic joint 2, spherical joint, prismatic joint 3, since the mechanical design already has a large number of extended bodies and it is preferable to have fewer rotating bodies. The alignment is done manually, and the incision point is indicated by lasers. The prismatic joints are locked by means of one-touch sliding locks.

5.2 Mechanical design: dependent and independent DOFs

As already expressed, it is preferred to have dedicated DOFs.
Concepts 1, 2, and 3 clearly attempted to have independent DOFs. From these designs, it is clear that for independent DOFs, it is always necessary to design a long frame that connects the original mechanism with a 'turn-it-around' joint. This creates a large frame that must move around the patient. The system cannot be reduced in size because of this frame.
For this reason, two other concepts were developed allowing the dependency of DOFs, and taking into account that the design must be compact and small, and should reduce the presence of the swap region

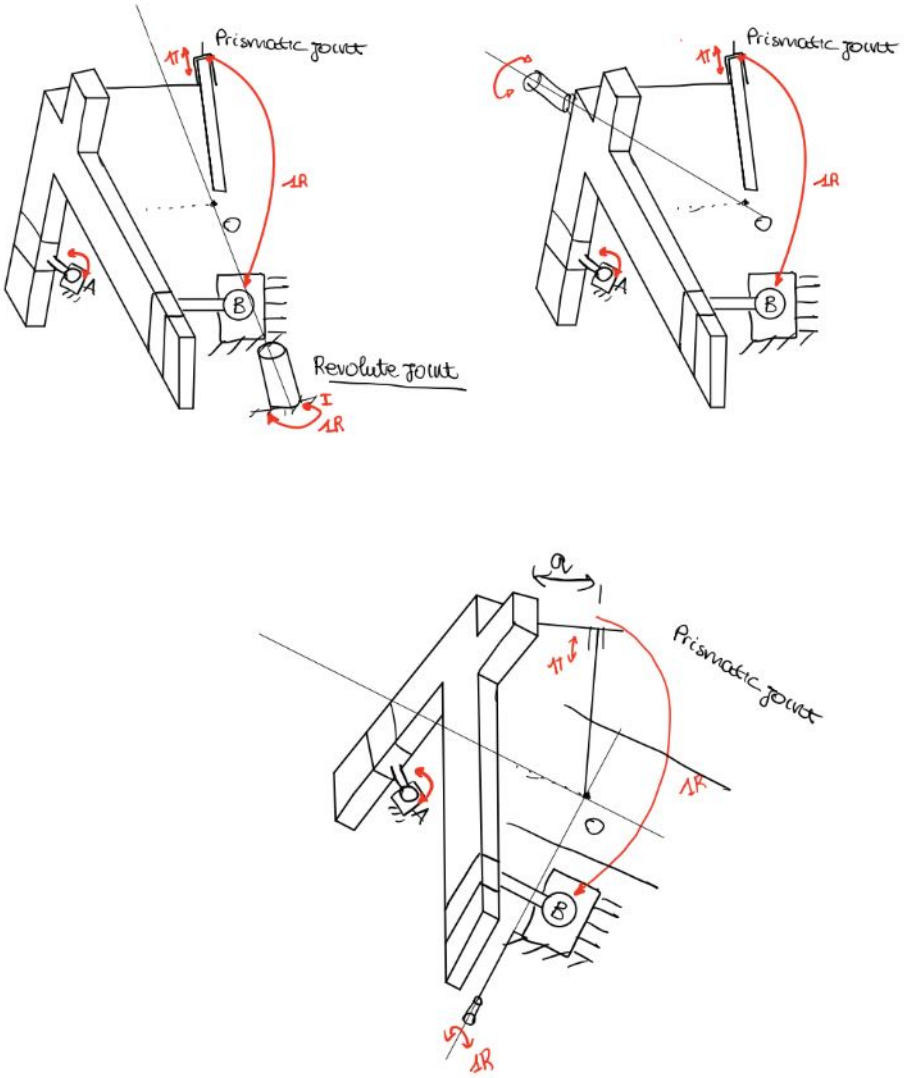

Figure 41: mechanical design for RCM mechanism of concept 3

when in motion. The concept 4 follows a classic approach, and aim to minimize the size of the RCM maintaining the functionally. The concept 5, instead, presents the center of rotation in the mechanism itself. Additionally, thanks to the position of it, presents a revolutionary concept in the alignment mechanism, attaching the latter to the trocar rather than to the ground.

5.2.1 Concept solution 4: The double arced mechanism

This concept is inspired by the spherical linkage theoretical solution. It is created by three joints in series. In Figure 42, the two revolute joints that allow rotation have axes that intersect at the RCM point. An additional linkage is added for attaching the prismatic joint that allows instrument translation. A similar approach is used in Figure 43, where the joints are replaced by arcs. In both cases, the angles between the two rotation axes are between 0° and 90°.
The main disadvantage is the dependence of the two rotations, so that the movement of a single DOF may require the use of two motors. However, this arrangement allows for a small mechanism that still provides the required workspace. In addition, the design is simple and can be used intuitively.
The system is coupled with an alignment mechanism consisting of three cylindrical joints in series. They allow manual alignment between the incision point and the RC of the mechanism, which is

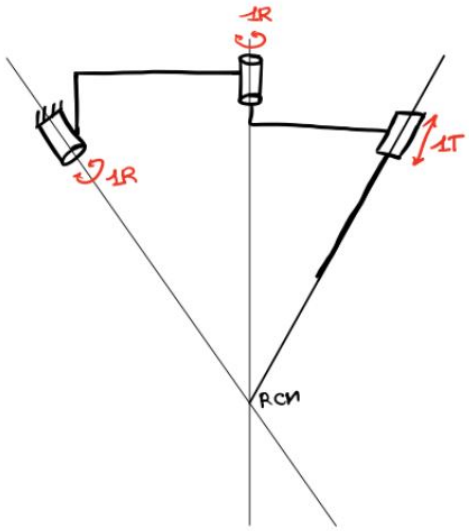

Figure 42: mechanical design of the RCM mechanism of concept 4

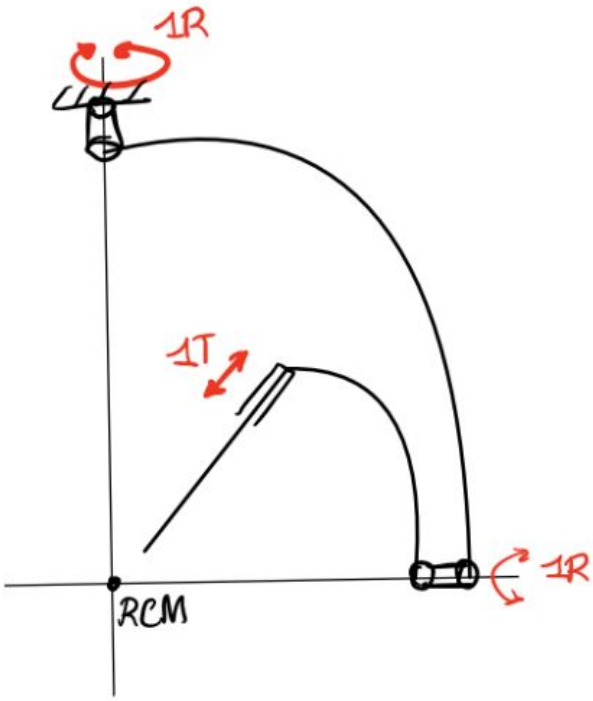

Figure 43: mechanical design of the RCM mechanism of concept 4b

indicated to the surgeon by means of two laser beams.
The design is passively held in position with gears that cannot be bacdrivable to reduce the overall weight of the mechanism and simplify the structure. The overall system is connected to the ground with friction grippers.

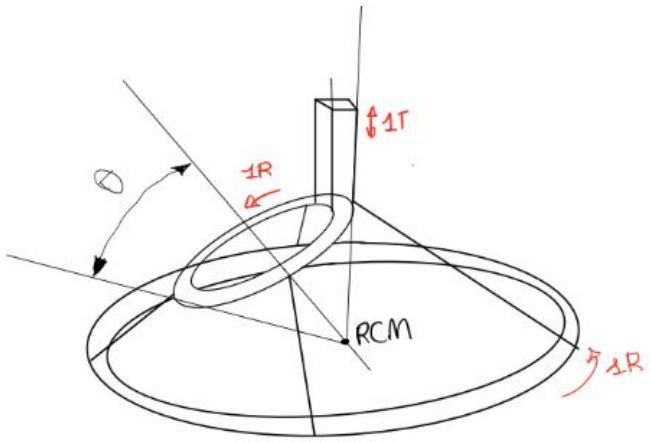

Figure 44: mechanical design of the RCM mechanism of concept 5

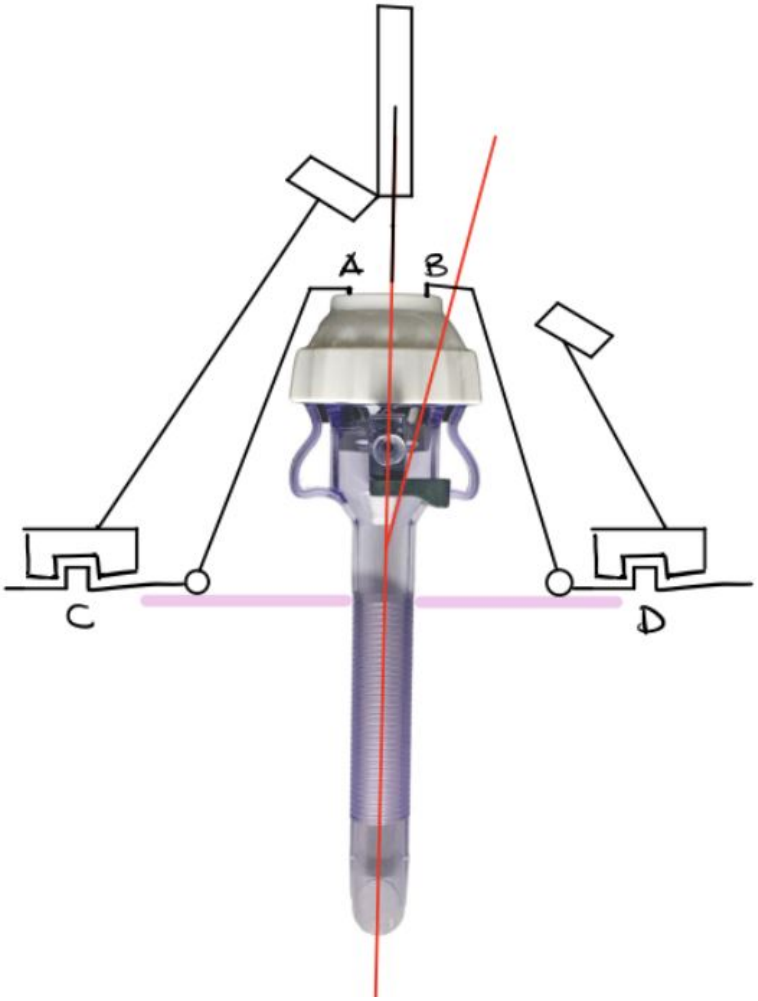

Figure 45: mechanical design of the RCM mechanism of concept 5, highlighting the possible mechanical interface with the trocar

5.2.2 Concept solution 5: The double rings

The design presented in Figure 44 is an RCM mechanism consisting of two stages: a lower stage that generates rotation around the vertical z-axis, and an upper stage that allows rotation around a second axis at an angle θ with respect to the previous axis. The two stages are connected with rigid bodies or a shell. In this way, there are no joints, which improves rigidity and possibly precision. A slider is connected to the second stage so that the instrument can move along the insertion line.
The RCM of the mechanism is manually aligned via a preliminary stage consisting of only three prismatic joints for translations in space. The rotations for the alignment are not necessary because the orientation is already defined by a patient's attached frame. The prismatic joints are locked with one-touch sliding locks. Additionally, the RC of the mechanism is marked by the intersection of two lasers. The whole system is connected to the floor by friction grippers.
Another option is an interface that connects the mechanism directly to the trocar so that the RC coincides with the incision point. As described earlier in subsection 2.4, a trocar is created by an obturator, which is then removed. The obturator clicks with the trocar through a form closure (point A and B in Figure 45). It is contemplated to design a click frame that attaches directly to the head of the trocar and allows the mechanism to be mounted on top (point C and D in Figure 45). It is important to understand and compensate for trocar head movement, as the trocar head will not perfectly align with the incision point. Passive joints can be used to compensate for it. The concept idea is shown in Figure 45.
For this concept, a deeper look at actuation solutions was taken. The motors have to drive the two rings and generate rotations. The solutions are discussed in section 18, and the final decision is between using a *ring-type piezoelectric motor* or a *frame-less torque motor*.
Gravity compensation is achieved by adding counterweights.
The major drawback of the design is that the DOFs of the rotations are dependent. This creates a swap region that needs further analysis. Also, it is not intuitive to cover the entire design with a plastic film, so a sterilizable sleeve is proposed to cover the mechanism. However, this design can also work with small dimensions and reduce the required parts by integrating the alignment pre-stage into the RCM mechanism.

An overview of the five concepts is summarized in the Table 5.

Table 5: Concepts solutions

Function	**Concept 1**	**Concept 2**	**Concept 3**	**Concept 4**	**Concept 5**
Motion	Peaucellier mechanism	independent prismatic and revolute joints in series	L shape design	Spherical linkage	Double rings mechanism
Interface	Friction grip	Friction grip	Friction grip	Friction grip	Friction grip
Equilibrium in place passively	Counterweight	Non-backdrivable transmission	Non-backdrivable transmissions	Non-backdrivable transmission	Counterweight
Align pre-stage	3 cylindrical joints (1R1T+1R1T +1R1T)	2 prismatic joint (1T+1T)	1 Spherical joint + 3 Prismatic joints (3R+1T+ 1T+1T)	3 cylindrical joints (1R1T+1R1T +1R1T)	3 cylindrical joints (1R1T+1R1T +1R1T) *or* Intrinsic radial design
Block sliders of the alignment mechanism	Manually quick locking	One-touch sliding locks	One-touch sliding locks	Manually quick locking	Manually quick locking *or* Fit gripper
Feedback of RC point	Lasers	Lasers	Lasers	Lasers	Laser *or* Rigid bodies

6 Concept selection

Strength and weaknesses of the generated concepts are evaluated in this chapter, to select the most promising one.
Evaluation criteria are extracted from the design goals, and are ordered based on importance, decided after desk research and critical thinking. The five concept solutions are, thus, evaluated with the Harris profile, Table 6. After evaluating them, a reasoning and discussion concluded that the concept solution 4 is most suitable design for the project.

6.1 Evaluation criteria

For evaluating and comparing the different designs, a list of evaluation criteria was created, keeping on the top the most important criterion, till the least important added in the bottom.
Considering the fact that it is assumed that all the design can satisfy the requirements through a detailed dimensional design, the evaluation criteria are composed by the design goals. However, the design goals are further divided, and evaluation criteria are:

- *EC1: Minimize size*: this design goal is the main outcome of the literature review, [67], and the main goal of the project itself. Minimizing the size has the benefits presented in subsection 2.1. For this reason, it is considered the most important criterion.
- *EC2: Optimize weight*: as for the EC1, the same applies for EC2. However, this can be considered as second most important criterion, due to the criticality of reducing size before optimizing weight [67]. Additionally, this design goal is mainly relative to the designs that apply weight on the patient body. For this reason, this requirement is more important for the conceptual design 5.
- *EC3: Minimize hard-to-sterilize areas*: one important aspect of a surgical robotic system is the easiness of sterilization. In subsubsection 4.1.1, a decision in using sterile covering drape is made, however for concept 5 this is not possible, due to the design of the mechanism. For this reason, concept 5 has a rigid cover that can be design with sterilizable material.
- *EC7: Maximize standard manufacturable parts*: as expressed in EC5, reducing the overall cost of the surgery procedure is one of the most emerging trend that this project wants to fit in. Maximizing the standard manufacturable parts will reduce the manufacturing cost and, thus, the purchase cost.
- *EC5: Minimize maintenance time and cost*: a third important point that was carried out in the work [67] was the desire of reduction of cost of the surgery itself. For accomplish this, a reduction of the maintenance time and cost will reduce the overall cost of the surgery. These costs, in time and money, are the routine ones, and, hence, are more impactful in long term than the purchase cost.
- *EC4: Maximize easiness of set up of the robotic arm*: it is necessary for the robotic arm to be manually set up. One of the main design goal is to allow this set up to be intuitive. This reduce the errors in the alignment procedure and the length of the learning curve.
- *EC6: Maximize easiness of control of the robotic arm*: having a easiness of control is one of the design goal. This also reduces the overall cost and the intuitiveness of the robot. However, the effect on these two points is marginal, thus this design goal is at the bottom of the list for importance.

6.2 Harris profile

After ordering the evaluation criteria in base of the importance, Harris profile is the method used for evaluating the designs. The evaluation is done by comparing the designs one to the other. Thus, a list from one to five of the most and less suitable designs is make.

6.2.1 EC1: Minimize size

As discussed in subsection 5.2, it is noticed that the designs with independent DOFs required the presence of a 'turn-it-all-around' joint, that enforced the presence of a big external frame for connecting the mechanism with this joint. For this reason, concept 4 and 5 are the smallest one. *Concept 5* can have very small dimensions, depending on the force necessary for moving the instrument, that can be partially external to the mechanism. *Concept 4* can, also, have small dimensions, however the arcs/links need to cover the overall workspace and allow the motions of the instruments that is internal to the mechanism. Additionally, concept 5 may be designed such that it does not need an alignment pre-stage, while concept 4 needs one. For these reasons, concept 5 is evaluated as the one concept that minimize size the most, followed by concept 4. As already said, *concept 1*, *concept 2*, and *concept 3* present a big frame. Between the three, *concept 2* is the one that can reduce the size the most, followed by *concept 1*, since it can reach quite small dimensions in the bars lengths. Finally, the *concept 3* is the one that less reduces the size.

6.2.2 EC2: Optimize weight

Concept 4 can have very light weight, because the two bars can be light enough and still sustain the instruments. *Concept 5* can, also, have light weight, but the double rings need to sustain the instruments and to allow the motions all around the arc. However, concept 5 can be designed such that it does not need an alignment pre-stage but present the alignment mechanism in the RCM mechanism itself, while concept 4 needs one, and this increases the weight of the overall system. For this reasons, concept 5 is evaluated as the one that minimize size the most, followed by concept 4. *Concept 1*, *concept 2*, and *concept 3* present a big frame. Between the three, *concept 1* is the one that can reduce the weight the most, followed by *concept 2*. Finally, the *concept 3* is the one that less reduces the weight.

6.2.3 EC3: Minimize hard-to-sterilize areas

Concept 4 is the one that minimize the most hard-to-sterilize areas. It is one of the smallest concept and it can be wrapped up in plastic bag. Following, *concept 1* can be easily wrap up in plastic drape, and the mechanism in motion can be positioned far from the drape. For these reasons, this is the second concept that minimizes hard to sterilize areas. Following, *concept 3* can be wrapped up in plastic. It presents a larger moving body that can interfere with the plastic drape with respect to concept 1. For this reason it is considered the third concept to minimize hard to sterilize area. *Concept 2* can be wrapped up in plastic, but there is an interface with the patient itself. For this reason, concept 2 is the hardest in sterilize interface between the design wrapped in plastic.
On the other hand, *Concept 5* cannot be wrapped in a plastic drape due to the design itself, especially if presenting a patient's interface. In fact, it is though to design a shell that can be dismounted and sterilized every use. This make the sterilization of concept 5 the hardest.

6.2.4 EC7: Maximize standard manufacturable parts

All the designs are thought such that they can be manufactured with standard parts. However, *concept 3* requires a specific design and dimensions of the L shaped body. For this reason, it is considered the concept that has less standard manufacturable parts. Additionally, *concept 2* and and *concept 1* need an external big frame. Even if the frame is not supposed to be too large to be manufactured, the dimensions may limit some manufacturing strategies. Between the two, concept 1 needs a larger frame, and requires more parts to be manufactured. For this reason, concept 2 is considered to standardize more parts than concept 1. Both *concept 4* and *concept 5* can be easily standardized. Concept 4 may require a specific angles between the two linkages, or a specific curvature of the curved rigid body. For this reason, concept 5 is considered the one that can be most standardized, followed by concept 4.

6.2.5 EC5: Minimize maintenance time and cost

Concept 4 is the one that most minimize cost and time of maintenance. The RCM mechanism presents only two bars and three joints for the motion, and there are not hard areas to reach. Additionally, the pieces can be standardized, and the maintenance can be fast and cheap. The alignment mechanism

is composed only by 3 cylindrical joints, that can be easily tested and, in case of necessity, changed. Following, *concept 2* and *concept 5* are directly in contact with the patient. For this reason, they have to be checked for integrity more often. Between the two, the concept 5 requires accurate maintenance of the alignment mechanism, that is much more complex than the alignment pre-stage. Thus, concept 2 is the second in minimizing maintenance time and cost, and concept 5 is the third. *Concept 3* presents two cranks for the motion of a single DOFs. The two cranks need to be maintained and in case lubricated more often. For this reason, the concept 3 is the second last in decreasing maintenance time and cost. Being *concept 1* formed by a 7 bars linkage, the possibility of dysfunction and the necessity of maintenance is increased. In fact, the joints are considered as weak points, and need to be checked more often. For this reason, it is the concept that requires more maintenance time and cost, being the maintenance required more often.

6.2.6 EC4: Maximize easiness of set up of the robotic arm

The easiness of set up of the robotic arm depends on the pre-alignment stage and the presence of technologies that feedback the RC point of the mechanism. The designs are all made for being easily to control and understand. However, the set up depends also on the mechanism itself. Setting up bigger mechanism is harder than the smaller ones. For this reason, *concept 4* and *concept 5* are the easiest to set up. Between the two, the intuitiveness of the design has been asked to experts during the experience reported in section 17. After the informative talks, concept 5 results to be less intuitive than concept 4. Following, *concept 3*, *concept 2*, and *concept 1* are the less easy to set up. Between them, concept 2 is the easiest to set up, since it needs to be just set up in a plane. Following, concept 1 present 3 cylindrical joints, and the dimensions of the seven-bars-linkage mechanism can be reduce, while concept 3 has a ball joints that control the all rotations, and it is bigger than the concept 1. For this reason, it is easier to set up concept 1 than concept 3.

6.2.7 EC6: Maximize easiness of control of the robotic arm

Independent DOFs allows an easier control than dependent ones. For this reason, *concept 1*, *concept 2*, and *concept 3* are easier to control than the last two concepts. *Concept 2* is the easiest to control, since each motion is independent and is directly transmitted to the end effector through a direct linkage. *Concept 1* is the second easiest to control, however, respect to concept 2, the velocity depends on the local position of the end effector in the first rotation (created to the Peaucellier mechanism). Finally, *concept 3* is the hardest to control in the group of mechanisms with independent DOFs. This is for the same reason pointed in concept 1, plus the presence of two cranks in A and B that needs to be controlled. *concept 5* is easier to control than *concept 4* because of the absence of linkages. In fact, in concept 5 the motion is translated directly to the instruments.

The discussed points are graphically represented in the Harris profile, Table 6. This profiles are used for deciding the final design.

Table 6: Concepts solutions

	Concept 1	**Concept 2**	**Concept 3**	**Concept 4**	**Concept 5**
EC1	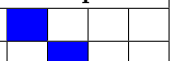	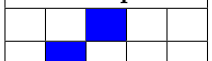	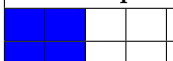	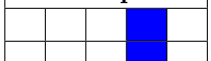	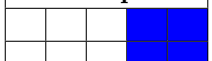
EC2				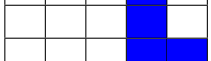	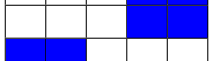
EC3	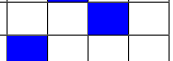	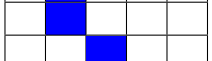			
EC7					
EC5					
EC4	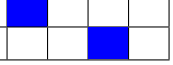	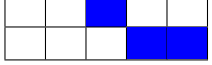			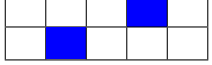
EC6					

6.3 Final selection

The Harris profile shown in Table 6 is a graphical tool to help select the final design. However, a deeper understanding of the results is required. Concepts 1 and 3 perform the worst on the most important design objectives, and they also perform mediocre on the least important objectives. These

two concepts are discarded outright. Concept 2 performs mediocre on all design goals, while Concepts 4 and 5 perform much better on most of them than Concept 2. Thus, the main discussion revolves around the choice between Concepts 4 and 5. Although both perform poorly on the last design goal, a point already discussed in subsection 5.2, the other differences will be discussed. Concept 5 performs better than Concept 4 on the two most important design goals. In fact, this concept may result in a smaller, lighter, and more standardized design. The difference in intuitiveness of setup that makes Concept 4 better than Concept 5 is due to the radial trocar platform. The main problem with Concept 5 is the dependence of the DOFs. The design seems to indicate that the swap area formed by the dependence of the DOFs will be quite large. However, this aspect cannot be analyzed now.
Overall, Design 5 may revolutionize the very concept of the robotic arm: a small, easy-to-fix robotic arm that is easier to operate and setup. Once the operation is completed, the robot can be easily disassembled and transported. In addition, the main advantage of Design Concept 4 is that it attaches to the patient itself. This eliminates misalignment and the patient's breathing movements are already filtered out. With an inverted conical structure, the problem of staying in place and being mechanically stable is easily solved. However, there are still many issues that need to be discussed and solved in Concept 5 to make it functionally valuable. Therefore, further analysis and discussion need to be done.

6.3.1 Alignment design on the trocar

The alignment design presented in Figure 45 is analyzed. Structurally possible, it is important to consider that the trocar represents the access door to the patient's interior and is in direct contact with the wound itself. In addition, the trocar is inserted into the patient's body at different angles. This means that the movable arms used to attach the flat platform to the trocar must take into account the angulation of the trocar, be fixed and secured for that angulation before attachment. Moreover, the global alignment is not complete with the attachment of the platform, but must include a final step in which the top ring is manually rotated until the instrument is aligned with the trocar. Additionally, this alignment mechanism is in direct contact with the patient, so an alternative to the plastic drape is needed to meet minimum sterilization requirements. Finally, it must be lighter in weight, as it acts directly on the patient.
However, the most important point of discussion with this alignment system is the medical analysis. Forced movement or constraint on the trocar can cause mild trauma to the wound. All experts who participated during the experience reported in section 17 felt that this design was more difficult to set up and less safe than that used in Concept 4. Through medical reasoning and discussions with experts, the main concern was the high risk that this alignment system posed. The main reasons are summarized:

- the incision point has to be reached during all the procedure;
- the trocar motion depends on the length of instrument out of the abdominal cavity, till reaching a motion of rotation of radius 6cm. This means that the passive joints have to compensate for a large motion, reducing stability and accuracy;
- the alignment design is felt less intuitive from the experts, since it is completely different from the already existing adds on's set up;
- this alignment is felt from the experts to be less safe, since the incision point is less easily reachable in case of emergency.

These reasons brought to discard this concept solution for the global alignment and proceeding with the 3 cylindrical joints (1R1T+1R1T+1R1T) design.

6.4 Final selection

Due to the change of *Concept 5*, where the mechanism for the alignment of the trocar is replaced by the design with 3 cylindrical joints, a new considerations in relation to the Harris profile must be done. The presence of the alignment mechanism with 3 cylindrical joints increases the weight and size of *Concept 5*, reaching values close to those of *Concept 4*. However, *Concept 4* is easier to sterilize and reduces the risks that *Concept 5* poses from patient contact. For these reasons, **concept 4** is selected as the final design.

7 Dimensional design

The final mechanical design is divided in the design of the RCM mechanism and the design of the passive global alignment mechanism.

7.1 Definition of reference frames and nomenclature

Before designing the system, a general definition of the reference frames is made for readability. Two reference frames are defined:

- **A global reference frame**: This reference frame defines the position is space with respect to a reference frame fixed with the surgical room. It is defined as shown in Figure 46, with the *z-axis* perpendicular to the surgical table, the *x-axis* along the longer side of the surgical table, and the *y-axis* along the shortest side of the surgical table.

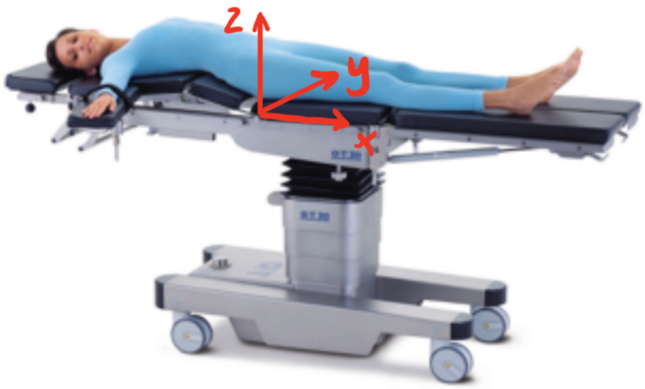

Figure 46: Absolute reference frame

- **A local reference frame for the RCM mechanism**: This reference frame defines the position in place with respect to the first revolute joint of the RCM mechanism. Defined as presented in Figure 47, the z_l*-axis* is along the axis of rotation of the first revolute joint, the x_l*-axis* is perpendicular to the z_l-axis and on the plane with the two revolute joints of the RCM mechanism lay in the planar configuration. The y_l*-axis* is perpendicular to the z_l-axis and the x_l-axis.

Finally, a nomenclature for the Joints is decided:

- $J_{rcm}i$: Refers to the ith joint of the RCM mechanism. The joints are numbered from left to right, as shown in Figure 48.
- $J_a i$: Refers to the ith joint of the alignment mechanism. The joints are numbered from bottom to top, as shown in Figure 49.

7.2 Design of the global alignment mechanism

In the subsubsection 5.2.1 the chosen global alignment was made with the three cylindrical joints in series. However, another option is to manually align the mechanism globally using the active DOFs of the RCM mechanism passively. This allows the DOFs of the alignment mechanism to be reduced. Due to the required reversibility of the mechanism under human forces, the DOFs of the RCM mechanism can be moved passively. The main advantage is that the global alignment mechanism can be reduced in size and still cover the entire required workspace.
The alignment procedure consists of two phases:

- *Phase 1*: Aligning the RC of the mechanism with the incision point in space;

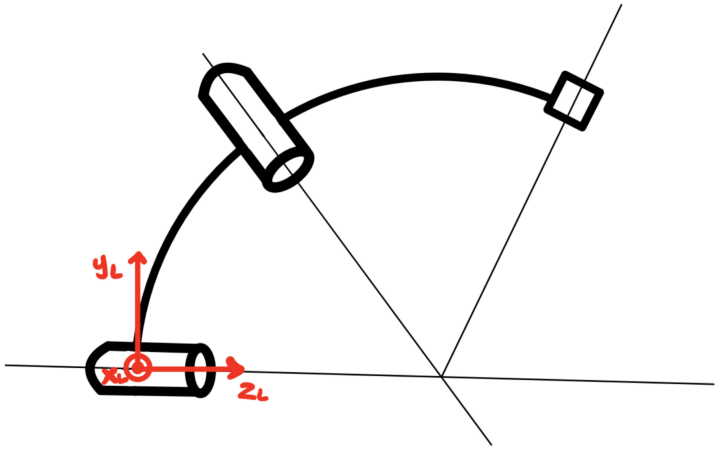

Figure 47: Local reference frame for the RCM mechanism

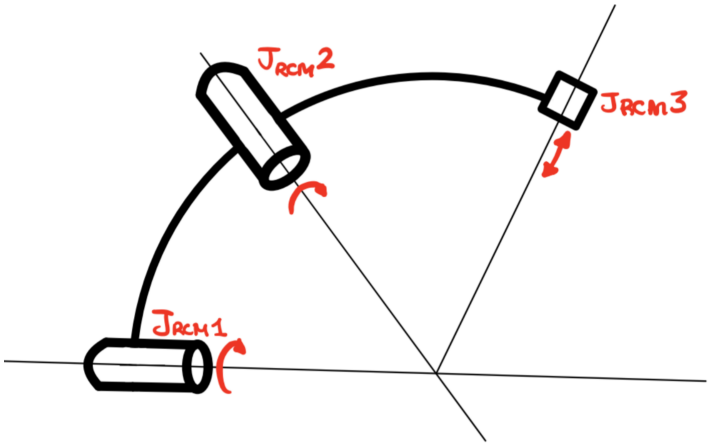

Figure 48: Nomenclature of the joints of the RCM mechanism

- *Phase 2*: Align the axis of the RCM's workspace with that of the operation.

Because the bed has rails on both of the long side, only half of the abdominal cavity has to be reached, while the other half can be reached by mounting the robotic arm on the other side. It is decided to continue with this design.

The mechanism is composed by a revolute joint (J_a3) , that rotates around the x-axis, that attaches a prismatic joint (J_a4) that translates along the z_l-axis. The alignment mechanism is mounted on the lateral sliders of the bed through a prismatic joint (J_a1) that allows the motion along the x-axis. Finally, a third prismatic joint, (J_a2), allows the motion vertically, along the z-axis. The design is shown in Figure 50.

For the dimensional design of the mechanism the maximum dimensions height of the abdominal cavity when the patient is laying on the sagittal plane is extracted by the website DINED, considering dutch population between 20 and 60 year. The average is 301 mm, while the standard deviation is 30 mm [123]. Thus, in this study the range considered is between [27.1 cm, 33.1 cm]. The alignment procedure is described by the following steps:

- **Step 0: motion along z axis:** The overall system is translated along the z axis, J_a2, such that the axis of rotation $J_{rcm}1$ is at a fixed height with respect to the horizontal plane on the

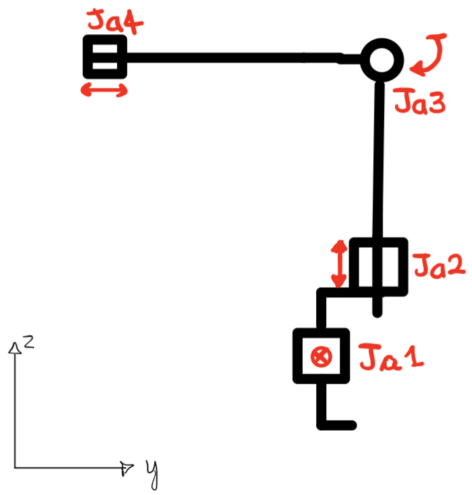

Figure 49: Nomenclature of the joints of the alignment mechanism

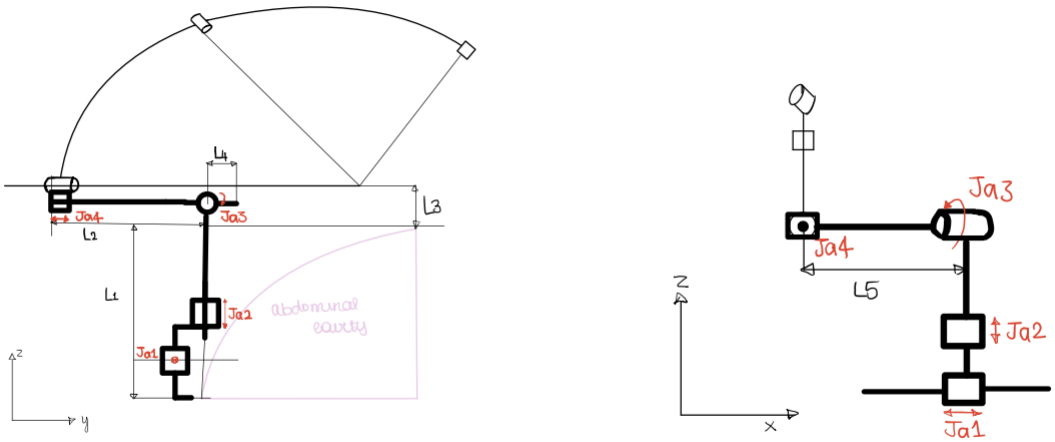

Figure 50: Design for the alignment that uses the DOFs of the RCM mechanism for alignment

abdominal cavity highest point. The fixed height is defined by L3 and shown by a laser beam.

- **Step 1: sliding on the patient bed**: The mechanism is moved along the x-axis by sliding J_a1, till $J_{rcm}1$ and $J_{rcm}2$ are on the on a plane perpendicular to the sliding direction passing trough the incision point. J_a1 is, thus, manually blocked. This process is shown in Figure 51.
- **Step 2: rotating the RCM mechanism**: The RCM mechanism is rotated around the x axis by J_a3. The mechanism is rotated till the axis of rotation of $J_{rcm}1$ passes through the incision point. Then J_a3 is manually blocked. This process is shown in Figure 52.
- **Step 3: sliding of the RCM mechanism**: J_a4 permits to move the all RCM mechanism along a line always parallel to the axis of rotation of $J_{rcm}1$. The mechanism has to be slid till the axis of rotation of $J_{rcm}2$ passes though the incision point. Then J_a4 is manually blocked. This process is shown in Figure 53.

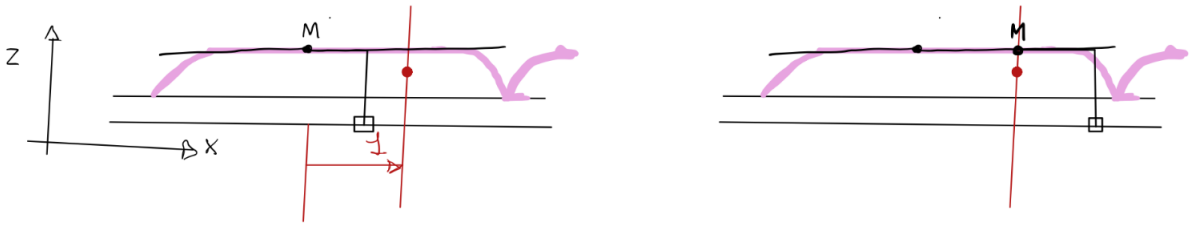

Figure 51: Step 1 for the alignment process

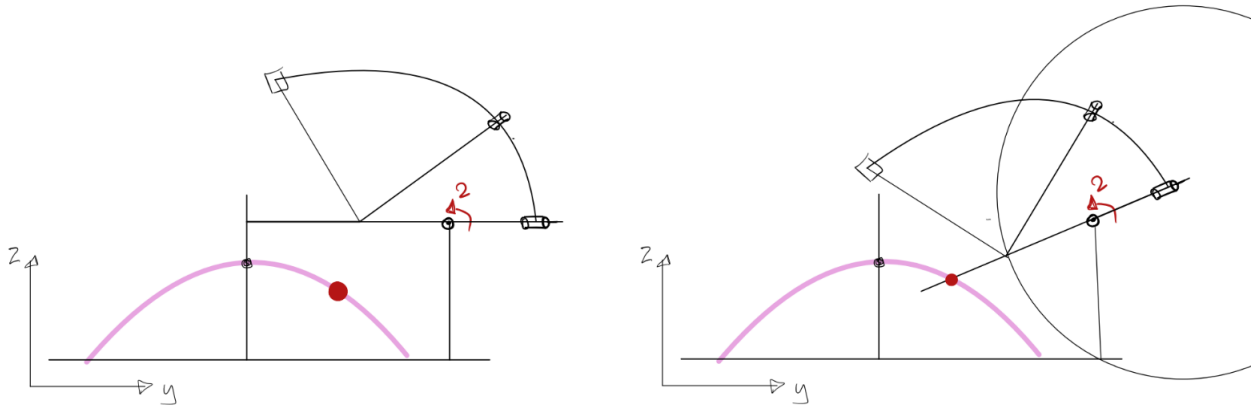

Figure 52: Step 2 in the alignment process

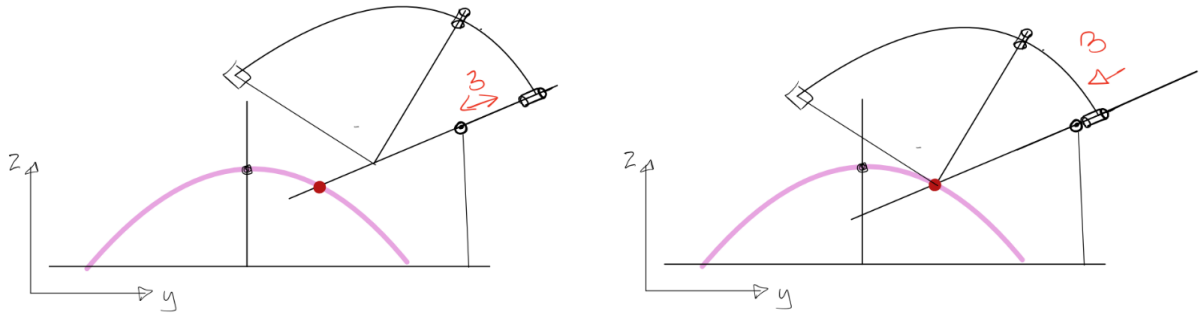

Figure 53: Step 3 in the alignment process

- **Step 4: manual rotation of θ1 and θ2**: At this step the RC of the mechanism is aligned with the incision point. However, the workspace inclination of the RCM mechanism still is not coincident with the one inside the body. For doing so, $J_{rcm}1$ and $J_{rcm}2$ need to be manually moved, till the two axes coincide. It is enough to stop to input the forces for the system to be stable, this because the joints are non-backdrivable under the forces of the robot itself. The alignment is completed, and the instrument can be inserted. For giving a feedback of what is the inclination of the workspace, a laser is inserted in the RCM mechanism, such that the line coincide with the axis of the workspace of the RCM mechanism.

7.3 Design of the RCM mechanism

In this subsection, the design refers to the local reference frame.

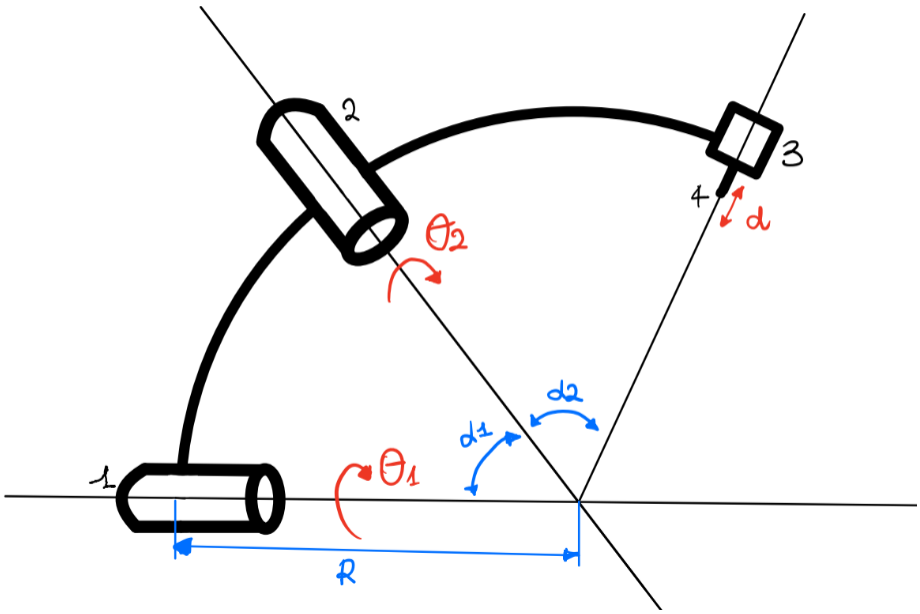

Figure 54: Geometrical structure of the RCM design, with input (red) and geometrical constant values (blue)

The RCM mechanism of the concept 4 is studied. The final structure of it is reported in Figure 54. The mechanism is composed by two revolute joints ($J_{rcm}1$ and $J_{rcm}2$) and one prismatic joint ($J_{rcm}3$). The inputs are:

- $\theta 1$: rotation along the axis of $J_{rcm}1$;
- $\theta 2$: rotation along the axis of $J_{rcm}2$;
- d: translation along the line connecting the end point of the mechanism and the incision point.

The geometrical parameters that define the mechanism are:

- $\alpha 1$: the angle between the two axes of rotations;
- $\alpha 2$: the angle between the axis of rotation of $J_{rcm}2$ and the translation line of $J_{rcm}3$;
- R: the radius of the two arcs. In this case it is considered equal for both the arcs.

In all the following calculation two abbreviations are used: c*angle* is the cos(*angle*) and s*angle* is the sin(*angle*).

7.3.1 Forward kinematics

In the forward kinematics, a study of the motion of the end effector is done, considering the structure, the geometrical constraints, and the inputs motion. The inputs are $\theta 1$, $\theta 2$, and d. The geometrical structure is reported in Figure 54.

The Denavit–Hartenberg parameters are calculated,Table 7, considering the local reference frames reported in Figure 55. In the table, θ is the angle from x_{ln-1} to x_{ln} along z_{ln-1}; α is the angle from z_{ln-1} to z_{ln} along x_{ln}; d is the distance between Ol_{n-1} and Ol_n along z_{ln-1}.

The DH parameters are used for calculating the forward kinematics of the mechanism.
The final result is:

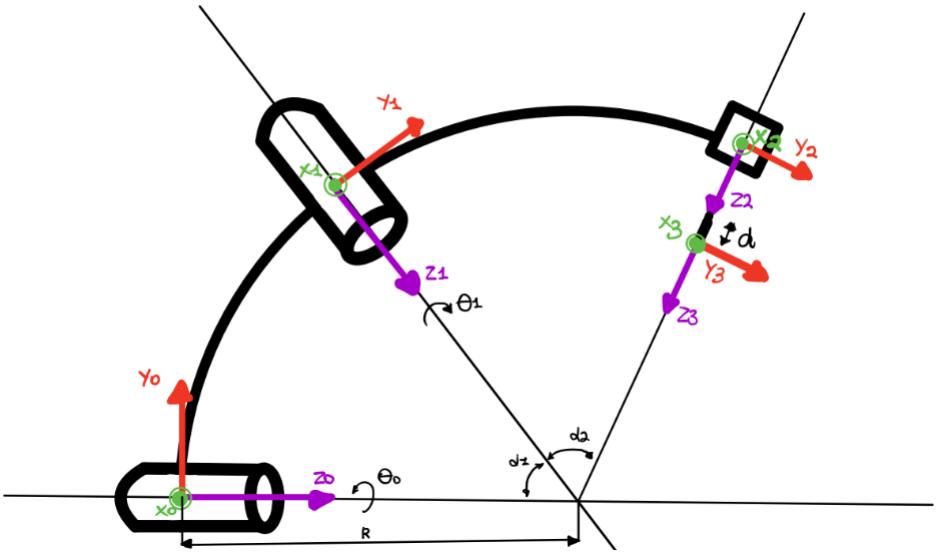

Figure 55: Geometrical structure of the design, reference frames for each joint

Table 7: Denavit–Hartenberg parameters

	θ	α	**d**
Frame 1-2	$\theta 1$	$\alpha 1$	R-R*cos($\alpha 1$)
Frame 2-3	$\theta 2$	$\alpha 2$	R-R*cos($\alpha 2$)
Frame 3-4	0	0	d

$$\begin{bmatrix} px_1 \\ py_1 \\ pz_1 \end{bmatrix} = \begin{bmatrix} -(R-d)(c\alpha 2 s\alpha 1 s\theta 1 + s\alpha 2 c\theta 1 s\theta 2 + c\alpha 1 s\alpha 2 c\theta 2 s\theta 1) \\ (R-d)(c\alpha 2 s\alpha 1 c\theta 1 - s\alpha 2 s\theta 1 s\theta 2 + c\alpha 1 s\alpha 2 c\theta 1 c\theta 2) \\ R + (d-R)(c\alpha 1 c\alpha 2\text{-}s\alpha 1 s\alpha 2 c\theta 2) \end{bmatrix} \tag{1}$$

The Matlab code that calculated the forwards kinematics is reported in subsection 19.1.

7.3.2 Jacobian matrix

The Jacobian matrix maps the relationship between the velocities of the end effector and the velocities input in the joints. In this case, it is found through partial differentiating the equation of px_l, py_l, pz_l. The last three rows, instead, are found with the relation:

$$^3w_3 = \begin{bmatrix} ^3R_0 \begin{bmatrix} 0 \\ 0 \\ 1 \end{bmatrix} & ^3R_2 \begin{bmatrix} 0 \\ 0 \\ 1 \end{bmatrix} & \begin{bmatrix} d\theta 1 \\ d\theta 2 \\ dd \end{bmatrix} \end{bmatrix} \tag{2}$$

The overall Jacobian matrix is then :

$$J = \begin{vmatrix} (d-R)(c\alpha 2 s\alpha 1 c\theta 1 - s\alpha 2 s\theta 1 s\theta 2 + c\alpha 1 s\alpha 2 c\theta 1 c\theta 2) & (d-R)(s\alpha 2 c\theta 1 c\theta 2 - c\alpha 1 s\alpha 2 s\theta 1 s\theta 2) & c\alpha 2 s\alpha 1 s\theta 1 + s\alpha 2 c\theta 1 s\theta 2 + c\alpha 1 s\alpha 2 c\theta 2 s\theta 1 \\ (d-R)(c\alpha 2 s\alpha 1 s\theta 1 - s\alpha 2 c\theta 1 s\theta 2 + c\alpha 1 s\alpha 2 s\theta 1 c\theta 2) & (d-R)(s\alpha 2 s\theta 1 c\theta 2 - c\alpha 1 s\alpha 2 c\theta 1 s\theta 2) & s\alpha 2 s\theta 1 s\theta 2 - c\alpha 2 s\alpha 1 c\theta 1 - c\alpha 1 s\alpha 2 c\theta 1 c\theta 2 \\ 0 & (R-d)(s\alpha 1 s\alpha 2 s\theta 2) & c\alpha 1 c\alpha 2\text{-}s\alpha 1 s\alpha 2 c\theta 2 \\ s\alpha 1 s\theta 2 & 0 & 0 \\ c\alpha 1 s\alpha 2 + c\alpha 2 s\alpha 1 c\theta 2 & s\alpha 2 & 0 \\ c\alpha 1 c\alpha 2\text{-}\ s\alpha 1 s\alpha 2 c\theta 2 & c\alpha 2 & 1 \end{vmatrix}$$

Due to the decoupled rotation DOFs and translation DOF, the rotation capability of the robotic arm can be optimized independently.

Thus, the J matrix is:

$$\begin{bmatrix} s\alpha 1 \mathrm{s}\theta 2 & 0 \\ c\alpha 2 \mathrm{s}\alpha 1\text{-}\mathrm{c}\alpha 1 \mathrm{s}\alpha 2 \mathrm{c}\theta 2 & \end{bmatrix} \tag{3}$$

The Matlab code that calculated the Jacobian matrix is reported in subsection 19.2.

7.3.3 Inverse kinematics

The inverse kinematics is used for expressing the inputs as a function of the position in space of the end effector. It is used for the control of the robotic arm.
The functions that expressed the inputs are derived by the Equation 1 or geometrically calculated.
Geometrically, d can be expressed as:

$$d = \sqrt{px_1{}^2 + py_1{}^2 + pz_1{}^2} \tag{4}$$

This value is replaced in the Equation 1. From the third equation in Equation 1, it is possible to find the value of $\cos(\theta 2)$ as a function of geometrical constants and position of end effector:

$$cos(\theta 2) = -\frac{R - pz_1 + (d - R)c\alpha 1 c\alpha 2}{(R - d)s\alpha 1 s\alpha 2} \tag{5}$$

and thus:

$$\theta 2a, \theta 2b = atan2(\sqrt{1 - cos^2(\theta 2)}, cos(\theta 2)) \tag{6}$$

This value is inserted in the remaining two equations in Equation 1, and the $\cos(\theta 1)$ and $\sin(\theta 1)$ are derived.

$$cos(\theta 1) = \frac{py_1(c\alpha 2 s\alpha 1 + c\alpha 1 s\alpha 2 c\theta 2) - px_1 s\alpha 2 s\theta 2}{(R - d)((c\alpha 2 s\alpha 1 - c\alpha 1 s\alpha 2 c\theta 2)^2 + s\alpha 2^2 s\theta 2^2)} \tag{7}$$

and:

$$sin(\theta 1) = \frac{px_1(c\alpha 2 s\alpha 1 + c\alpha 1 s\alpha 2 c\theta 2) + py_1 s\alpha 2 s\theta 2}{(d - R)(((c\alpha 2 s\alpha 1 - c\alpha 1 s\alpha 2 c\theta 2)^2 + s\alpha 2^2 s\theta 2^2)} \tag{8}$$

Thus:

$$\theta 1a, \theta 1b = atan2(sin(\theta 1), cos(\theta 1)) \tag{9}$$

The Matlab code that calculated the inverse kinematics is reported in subsection 19.3.

7.4 Optimization of the RCM design dimensions

A multidimensional, non linear optimization problem can be formulated as follow:

$$\begin{gathered} \min \mathrm{F_k(I)}\ \mathrm{k{=}1,...,t} \\ \text{subject to: } \mathrm{g_i(I)} < 0\ \mathrm{i{=}1,...,n} \\ \mathrm{h_j(I){=}0}\ \mathrm{j{=}1,...,m} \end{gathered}$$

where F(I) is the cost function, I is the vector of parameters to optimize, and $\mathrm{g_i}$ and $\mathrm{h_j}$ are inequality and equality constraints.
In this design the parameters to optimize are:

$$\mathrm{I{=}[\alpha 1,\ \alpha 2,\ R]}$$

The cost functions F(I) are:

- **Compactness**: the design goal of minimize size and make the design compact can be mathematically expressed by the function:

$$c1 = \frac{\alpha 1^3 + \alpha 2^3}{(\frac{\pi}{2})^3} \tag{10}$$

This function has to be minimize. The cube is added because the inertia of an arc is directly proportional to the cube of the angle.
Additionally, the radius R has to be minimized, for reducing the size of the robotic arm and ensuring the compactness:

$$c2 = \frac{R}{R_{\max}} \tag{11}$$

- **Kinematic performance index**: to maximize the kinematic performance, different parameters can be evaluated. The two most used performance metric in the literature are mechanism manipulability and mechanism isotropy. The isotropy is the ratio between the minimum and the maximum eigenvalue of the Jacobian matrix. When isotropy is zero, the mechanism is in a singular configuration. An isotropy of 1 means that the mechanism can move equally well in all direction. This means that the ISO value expressed in Equation 12 wants to be maximize.

$$ISO = \frac{\lambda min}{\lambda max} \tag{12}$$

The manipulability is, instead, directly proportional to the Jacobian determinant. Larger Jacobian determinant means that, for a given displacement of the end effector, less actuation is needed in the joint, that allows to have smaller and lighter actuators. A frequently used measure is the Yoshikawa's manipulability [150], which is selected also for this work, and is expressed as:

$$m = \sqrt{det(JJ^{\mathrm{T}})} \tag{13}$$

The larger this measure, the closer the manipulator is to the isotropic configuration. Additionally, it is necessary to ensure it on all the workspace, thus it requires to be averaged. For this reason, it is necessary to consider the cost function:

$$c3 = \frac{1}{avg(m)} \tag{14}$$

For the given J matrix:

$$c3 = \frac{2}{1+s}$$

$\alpha 1 s \alpha 2$ (15)

The inequality and equality constraints g_i and h_j are:

- **Workspace**: the mechanism has to be able to satisfy the required workspace. The workspace is presented in subsection 3.2. However, it is necessary to refer to the workspace as function of the angles. It is, thus, easier to define the workspace as an angle that the instrument can travel. Since the actual workspace of the end effector of the robotic arm is a sphere of radius 7.94 cm with a center at a distance R for the incision point, the angle of the workspace of the instrument is *atan(7.94/R)*. In the following calculations, $i1$ is the angle of inclination of the workspace with respect to the z_l axis of the first revolute joint.
The Figure 56 shows the **planar configuration** of the mechanism, where $\alpha 1$ and $\alpha 2$ lay on the same plane without overlapping. This configuration is taken for visualization of the constraints. The workspace constraint can be expressed as in Equation 16.

$$\epsilon \geq atan(\frac{R}{7.94}) \tag{16}$$

with:

$$\epsilon = \frac{-\pi}{2} + i1 + \alpha 1 + \alpha 2 \tag{17}$$

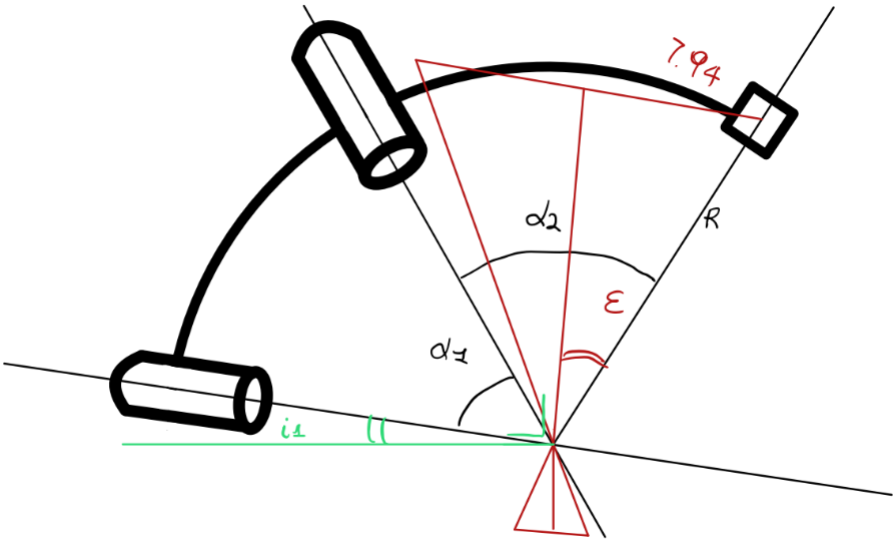

Figure 56: Definition of the workspace constraint for extended configuration

- α **angles**: for a better stability and stiffness it is required to ensure:

$$\alpha 1 \geq \alpha 2 \tag{18}$$

- **Angles and radius**: the angles $\alpha 1$ and $\alpha 2$ have to be in the range (15°,75°), while the radius has to be between 16.5 cm and 30 cm.
  $i1$ is the angle between the axis of rotation of $J_{rcm}1$ and the perpendicular to the y axis. It is noticed that having a greater $i1$ allows to reduce the dimensions of the RCM mechanism. However, at the same time, it increases the dimensions of the alignment mechanism and reduces the precision of the alignment, increasing the effect of the minimum noticeable distance on the accuracy of the pre-alignment. It was decided, thus, to find a compromise, imposing as minimum value of $i1$ 15°.

  Additionally, for all the configuration this is valid:

$$15 \leq \alpha 1, \alpha 2 \leq 75 \tag{19}$$

$$16.5cm \leq R \leq 30cm \tag{20}$$

7.5 Final geometrical design of the RCM mechanism

To achieve the final design, the parameters $\alpha 1$, $\alpha 2$, and R are optimized subjected to the cost functions and the constraints. Because more than one cost function was identified, it is necessary to select a methodology that permits to optimize them together. The used strategy is to perform an optimization with aggregation of objective functions, where the objectives are multiplied by weights that are directly proportional to their importance in the specification.

$$F(I) = w1c1 + w2c2 + w3c3 \tag{21}$$

where *w1, w2, w3* are the weight for the respective cost functions.
The weights are decided as follow:

$$w1 = 0.5 \tag{22}$$

$$w2 = 0.3 \tag{23}$$

$$w3 = 0.2 \tag{24}$$

The overall problem can be summarized in:

$$minF(I) = w1\frac{\alpha1^3 + \alpha2^3}{(\frac{\pi}{2})^3} + w2\frac{R}{R_{\max}} + w3\frac{2}{1 + s\alpha1s\alpha2} \tag{25}$$

subject to:

$$atan(\frac{7.94}{R}) + \frac{\pi}{2} - i1 - \alpha1 - \alpha2 \leq 0 \tag{26}$$

$$\alpha1 \geq \alpha2 \tag{27}$$

$$15 \leq \alpha1, \alpha2 \leq 75 \tag{28}$$

$$16.5cm \leq R \leq 30cm \tag{29}$$

The genetic algorithm method (GA) has been adopter for finding the optimal solution. The three parameters than has been optimized are R, $\alpha1$, $\alpha2$, and the results of the optimizations are reported in Table 8.

The optimized parameters that geometrically define the RCM mechanism are reported in Table 8.

Table 8: Optimized parameters

	α**1**	α**2**	**R**
iteration 1	53.6105°	47.1166°	16.5 cm
iteration 2	53.0416°	47.6644°	16.5003 cm
iteration 3	51.8584°	48.8716°	16.5 cm
iteration 4	50.6231°	50.0565°	16.5 cm
iteration 5	51.1428°	49.5265°	16.5001 cm
iteration 6	50.6901°	49.9883°	16.5 cm
iteration 7	52.5133°	48.1938°	16.5 cm

Due to the fact that the mechanism is designed such that the arm 1 characterized by $\alpha1$ is subjective only to one DOFs, while the arm 2, characterized by $\alpha2$, is subjective to two DOFs, between the optimized couple it is decided the one that minimize $\alpha2$ the most. This improves the stiffness of the overall system. The final decided values are reported in Table 9.

Table 9: Final optimized parameters

α**1**	53.6°
α**2**	47.1°
R	16.5 cm

7.6 Final geometrical design of the alignment mechanism

After dimensioning the RCM mechanism, it is possible to dimension the alignment system.

The value reported refers to parameters presented in Figure 50. Since the minimum value of $i1$ is decided 15°, then the value of L3 should be 4.42cm (16.5cm * tan(15°)). L1 is set as the highest of the abdominal cavity 33.1cm.

The length that the RCM mechanism has to slide on L2 depends on the position of the incision point. The maximum area of the abdominal cavity where the incision point can be is considered to be a circle of radius 16.5 cm [123]. To understand what the dimensions of L2 and L4 are, the maximum distance that the RCM mechanism has to travel is calculated and shown in Figure 57 and Figure 58. L2 is equal to 6.36cm and L4 equal to 0.8cm. The values are reported in Table 10.

After designing the alignment system, it is necessary to ensure that during the motion and the alignment no collision with the patient happens. The robot is mounted folded in the first place, and then moved. For this reason it is enough to ensure that the Equation 30 is satisfied. The equation is

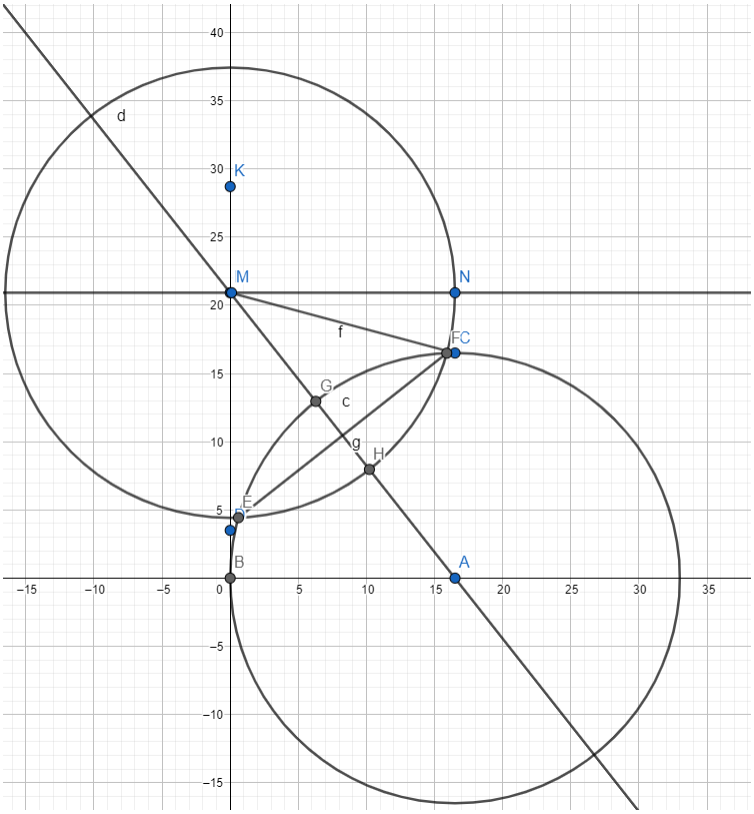

Figure 57: Calculation for the dimensions of the alignment mechanism

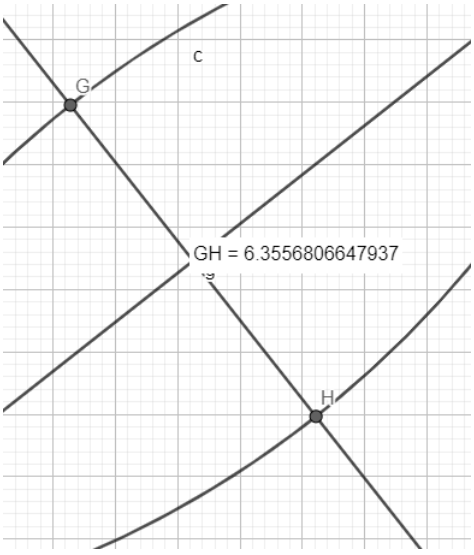

Figure 58: Calculation for the dimensions of the alignment mechanism

Table 10: Values of the parameters of the alignment mechanism

L1	33.1 cm
L2	6.4 cm
L3	4.42 cm
L4	0.8 cm

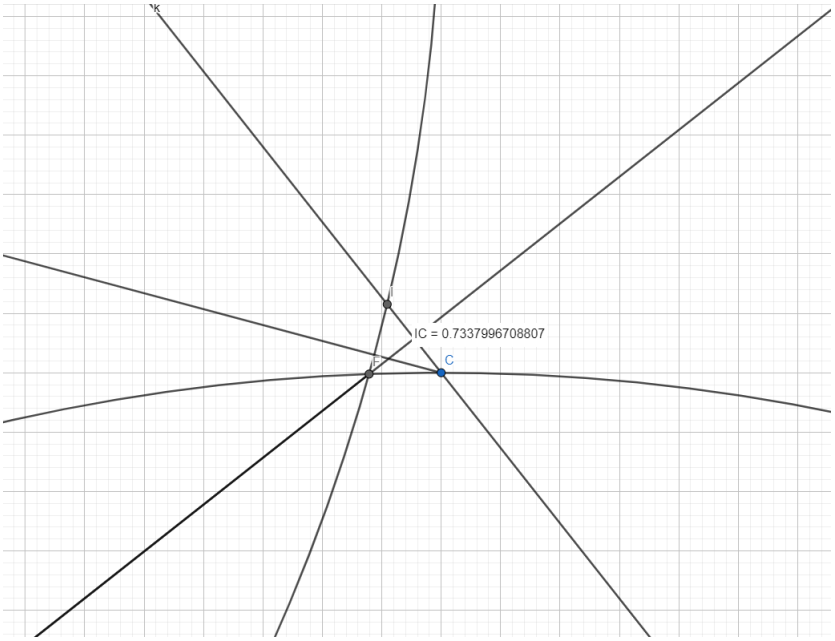

Figure 59: Calculation for the dimensions of the alignment mechanism

derived from the schematic in Figure 60.

$$16.5 - 16.5c\alpha 1 \leq L1 + 4.42 \tag{30}$$

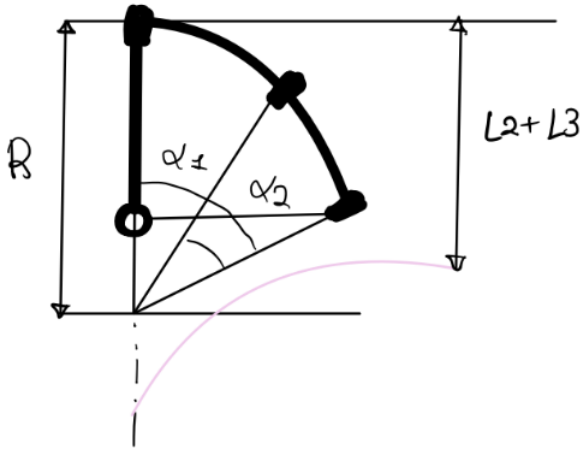

Figure 60: Schematic of the overall system for the calculations for ensuring no collision with the patient

For the decided values, the Equation 30 is satisfied.
Finally, it is necessary to ensure that all the rotations are possible, and that the area is free of obstruction in the (x, z) plane. In some configurations, it may be convenient to have $\theta 1$ larger than 90°. However, it is necessary to ensure that there is never contact between the parts. Thus, $\theta 1$ can reach a maximum of 110° for the parameters optimized. Finally, the distance along the x axis between the RCM mechanism and the the slider, L5 in Figure 50, is set to be 19.6 cm (16.5 cm + 16.5 cm x cos($\alpha 1$ + $\alpha 2$ - 90°)), for avoiding any interference between the bars.

8 Analysis of the mechanical design

In this section, the mechanical design is analysed. Firstly, the RCM mechanism is analyzed to verify that it can reach all the points on the workspace during the active phase. This validation is done by visualizing the forward kinematics of the robotic arm, in subsection 8.1. Subsequently, the three procedures are further analyzed and defined, subsection 8.3. Then, in subsection 8.4, it is shown that the passive alignment can reach all the incision points required for the three procedures and can align the workspace of the RCM mechanism with the one in the patient's body.

8.1 Visualize the forward kinematics

The forward kinematics, worked in subsubsection 7.3.1, links the joint angles with the motion at the end effector. With the result in subsubsection 7.3.1, it was possible to plot the relation between them. The graphs Figure 61 and Figure 62 show the value of x_l, y_l, z_l that the end effector can reach, as a function of $\theta 1$ and $\theta 2$. The colors are indication of the value. In the simulation, the angle $\theta 1$ is considered to be zero when the arm is on a planar configuration; $\theta 2$ is zero when the robotic arm is fully extended. Additionally, the ranges of motion of $\theta 1$ and $\theta 2$ are respectively chosen to be [$-\pi/2$; $\pi/2$] and [$-5/6\pi$; $5/6\pi$], to avoid collision with the patient and between the parts of the robotic arm. The only studied variables are $\theta 1$ and $\theta 2$, while d is set as a constant. d is an active parameter responsible of the linear translation of the instruments. However, it is only responsible of the linear motion along the axis of the workspace. In this study, the focus is on the plane perpendicular to this axis, to prove that the robotic arm can reach a circle of diameter 15.88 cm, subsection 3.2. For this reason, the variable d can be neglected.
The graphs reported in Figure 61 and Figure 62 are the visualization of the forward kinematics for d=0 cm and d=13 cm, and are performed with the code reported in section 21.

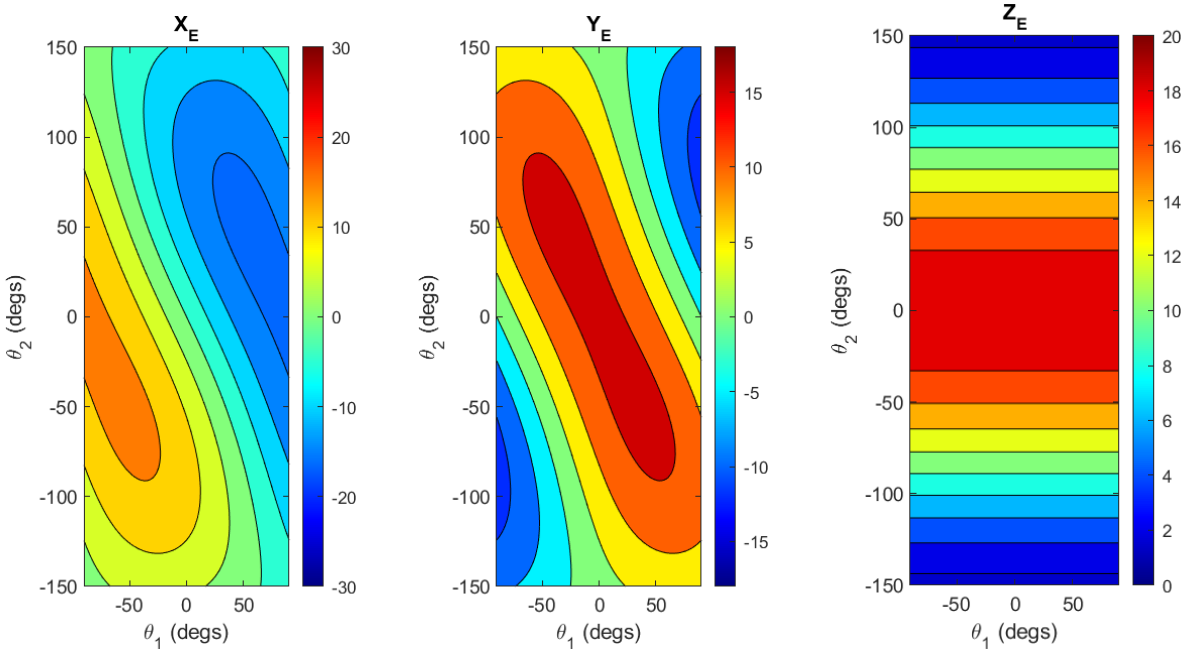

Figure 61: Visualization of Forward kinematics: d=0 cm

The graphs, Figure 61 and Figure 62, show that the end effector of the RCM mechanism has a range of motion of x=[-16.5 cm, 16.5 cm], y=[-11.5 cm, 16.5 cm], and z=[0.13 cm, 19.55 cm]. Thus, it covers all the points of the workspace. Additionally, it can be seen that the robot can reach the same point in space in different configurations of $\theta 1$ and $\theta 2$. This define a non-monotonic behaviour: the same output can be reached with different inputs.

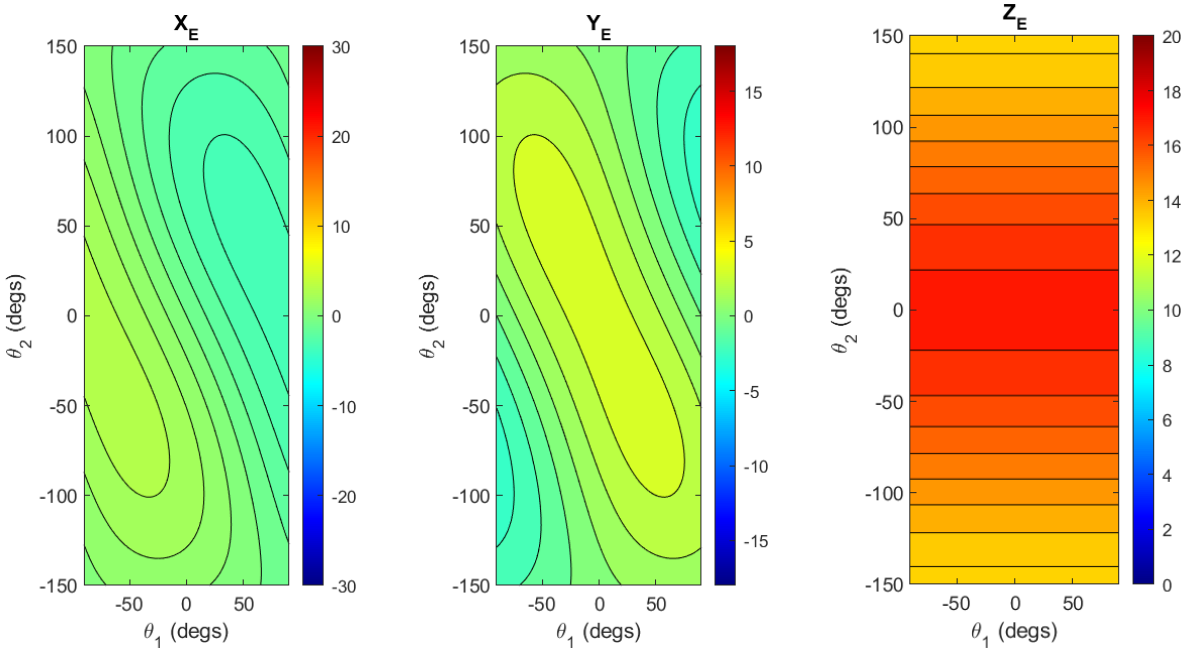

Figure 62: Visualization of Forward kinematics: d=13 cm

8.2 Verification of workspace positioning

In this section, it is verified that all the configurations of the trocar position and workspace's axis inclination can be reached with the designed alignment and RCM mechanisms.
The alignment is defined by two stages:

- *Alignment of the RC of the RCM mechanism with the incision point*: This condition is characterized by three equations that needs to be satisfied: x_{rc}=x_{ip}, y_{rc}=y_{ip}, z_{rc}=z_{ip}, where *rc* is for remote center and *ip* is for incision point. The incision point can be located anywhere on half of the abdominal cavity. This stage is satisfied by the *step 1*, *step 2*, and *step 3* of the alignment procedure, subsection 7.2, and depends on the motion of J_a1, J_a2, J_a3, and J_a4.

- *Alignment of the workspace of the RCM mechanism with the one of the surgery*: This condition is characterized by two equations, that refers to the angles of the axis of the workspace on the (x, y) plane and on the (y, z) plane. $anglexy_{rcm}$=$anglexy_{body}$, $angleyz_{rcm}$=$angleyz_{body}$. However, it is possible to redefine these equations considering the angle of the axis of the workspace on the (x, y) plane and the one on the plane defined by rotating the (y, z) plane of an angle equal to the one found on the (x, y) plane. This approach is preferred, since with analyzing the procedures it is possible to define the angle relative to the (x, y) plane, and the second angle results more intuitive and meaningful. This stage is satisfied by the *step 4* in subsection 7.2, and depends on the motion of $J_{rcm}1$ and $J_{rcm}2$, thus varying $\theta 1$ and $\theta 2$.

Since this robotic arm has been design for the three procedures *Cholecystectomy*, *Appendectomy*, and *Inguinal hernia surgery*, a deeper study on these three procedures is performed, for understanding which are the required incision points and inclinations of the workspace to be reached, section 20. The study is performed over different images, which results in a final selection of trocar positions and inclinations. In the calculation it is assumed that the body's abdominal shape can be simplified with a cylinder of radius 16.5 cm, since the mechanism needs to perform for the largest abdominal cavity.
In this section, four different configurations for the three procedures are taken into account, two of them for the appendectomy. For reference, the images in the work [86] are reported. In the schematics, the placement of the trocars and the line of action of those in the plane (x, y) is presented. The distance between the trocar incision and the origin of the RCM mechanism is measured for calculating the angle decided in the *Step 2* of the alignment procedure. All the dimensions are scaled such that the width of the human body is set to be 33 cm, while all the angles are absolute values and are referred to the vertical axis.

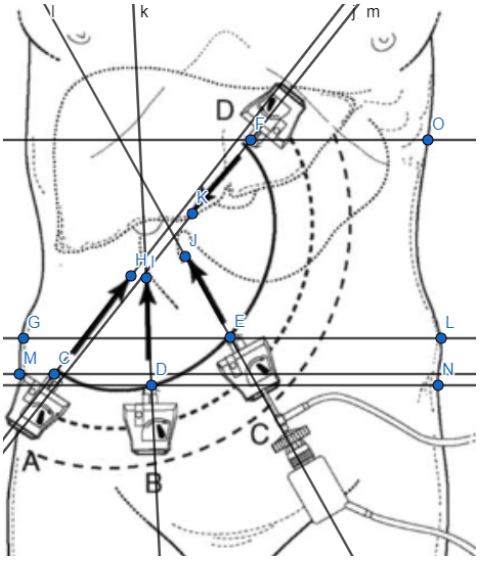

Dimension	Value
FO	14 cm
CM	2.75 cm
EL	16.5 cm
DN	22.5 cm
angle FK	38°
angle EJ	29°
angle DI	2°
angle CH	38°

Figure 63: Position of trocars for gallbladder removal [86] and values of the dimensions after averaging the values of this dimensions in section 20

8.3 Procedures analysis

In the following analyses, a study of images regarding the position of the trocars for the procedures is reported, section 20. Here, the images of [86] are used as reference. The angles of the insertion of the trocars can be estimated by the position of the trocar and the position of the organ. In the work [86] the angle of inclination of the workspace's axis in the (x, y) plane is reported with an arrow. In Figure 63, Figure 64, Figure 65, and Figure 66, the length values refer to the distance between the incision point and the edge of the body, while the angles refer to the inclination of the axis of the workspace on the (x, y) plane.

8.3.1 Gallbladder removal

In the gallbladder removal, four trocars are inserted in the body as shown in Figure 63. For better understanding and referring to the incision points, in this procedure the incision point C is referred as *Incision point 1*, the incision point D is referred as *Incision point 2*, the incision point F is referred as *Incision point 3*, and the incision point E is referred as *Incision point 4*.

8.3.2 Appendectomy

In the appendectomy, three trocars are inserted in the body as shown in Figure 64 or as shown in Figure 65. For better understanding and referring to the incision points, in this procedure, configuration 1, the incision point C is referred as *Incision point 1*, the incision point D is referred as *Incision point 2*, the incision point E is referred as *Incision point 3*. In the configuration 2, instead, the incision point H is referred as *Incision point 1*, the incision point F is referred as *Incision point 2*, the incision point D is referred as *Incision point 3*.

8.3.3 Inguinal hernia surgery

In the inguinal hernia surgery, three trocar are inserted in the body as shown in Figure 66. In this procedure the incision point D is referred as *Incision point 1*, the incision point E is referred as *Incision point 2*, the incision point C is referred as *Incision point 3*.

The values found need to be modified such that it is possible to refer at them as rotation in *Step 2* and translation in *Step 3* in the alignment procedure. The rotation in *Step 2* is calculated using the relative position of the incision point along the y axis with respect to the edge of the body. Later,

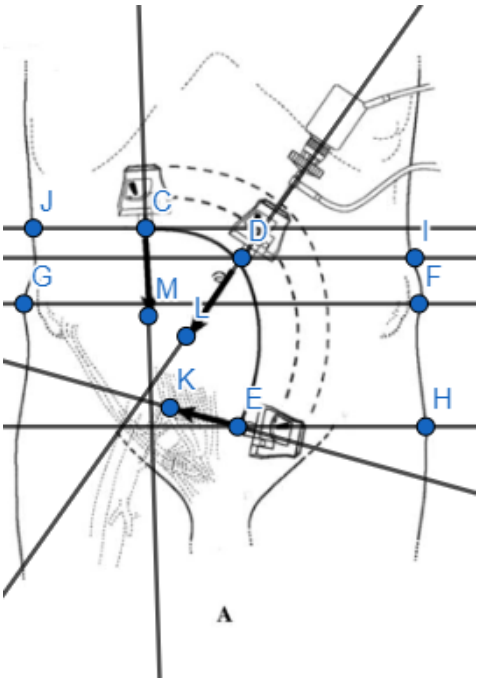

Dimension	Value
CJ	9.4 cm
DI	14.45 cm
EH	15.7 cm
angle CM	1.5°
angle DL	35°
angle EK	74°

Figure 64: Position of trocars for appendectomy: configuration 1 [86] and values of the dimensions after averaging the values of this dimensions in section 20

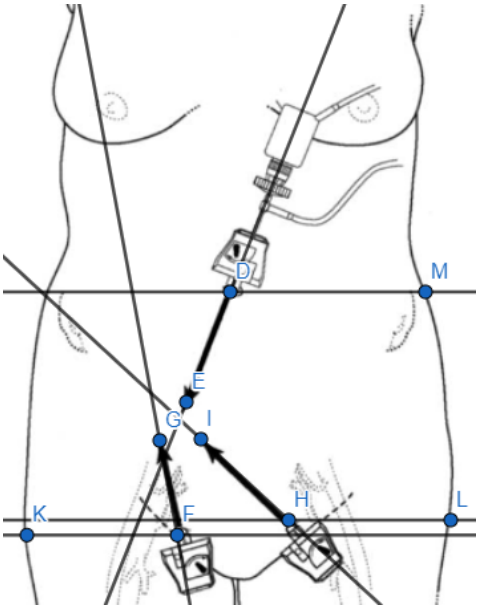

Dimension	Value
DM	16.5 cm
HL	13.45 cm
FK	12.45 cm
angle DE	22°
angle HI	47°
angle FG	10.5°

Figure 65: Position of trocars for appendectomy: configuration 2 [86] and values of the dimensions after averaging the values of this dimensions in section 20

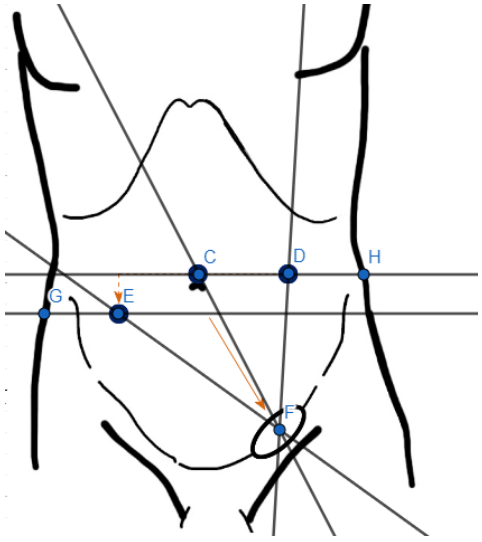

Dimension	Value
DH	6.5 cm
CH	16.5 cm
EG	7 cm
angle EF	56°
angle CF	28.5°
angle DF	3°

Figure 66: Position of trocars for hernia [86] and values of the dimensions after averaging the values of this dimensions in section 20

the translation necessary in *Step 3* is calculated using GeoGebra, as shown in Figure 169, Figure 170, Figure 171, and Figure 172. The values reported in Table 11 are found.

Table 11: Position of incision point and workspace inclination

Procedure	Rotation Step 2	Translation Step 3
Gall bladder removal		
Incision point 1	76.88°	-4.38436 cm
Incision point 2	28.455°	-4.727806 cm
Incision point 3	18.228°	-1.76033 cm
Incision point 4	15°	0.58179 cm
Appendectomy 1		
Incision point 1	32.7585°	-5.34606 cm
Incision point 2	17.455°	-1.3420 cm
Incision point 3	15.7894°	-0.19 cm
Appendectomy 2		
Incision point 1	21.5825°	-3.11131 cm
Incision point 2	19.3401°	-2.2774 cm
Incision point 3	15°	0.58179 cm
Inguinal hernia surgery		
Incision point 1	49.8958°	-6.34755 cm
Incision point 2	47.8691°	-6.31853 cm
Incision point 3	15°	0.58179 cm

8.4 Proof alignment of workspace

8.4.1 Stage 1: Alignment of the RC of the RCM mechanism with the incision point

This stage depends on the range of motions of the first 4 steps of the alignment procedure.
In *Step 0* J_a1 is moved along the x axis, till the RCM mechanism is aligned with the incision point on the (y, z) plane. This is always reachable, since the rails on which J_a1 slides run along the x axis from the shoulder to the toe of the patient.
In *Step 1*, the height of the alignment mechanism is adjusted by sliding J_a2. J_a2 can move 6 cm along the z axis, ensuring this condition for the lowest and the highest abdominal cavity in the dutch population [123].

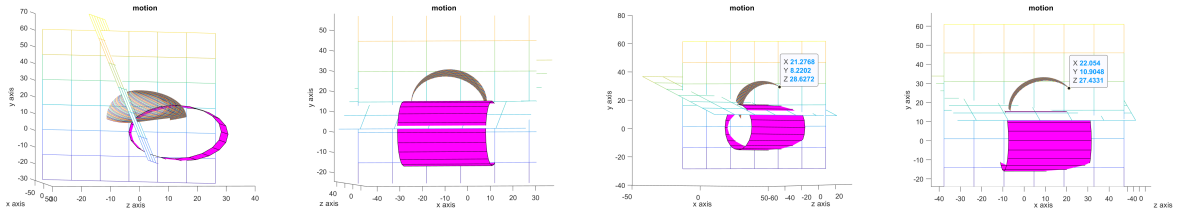

(a) Incision point 1 (b) Incision point 2 (c) Incision point 3 (d) Incision point 4

Figure 67: Range of motion of the RCM mechanism on the the plane defined by rotating the (y, z) plane of an angle equal to the one found on the (x, y) for Gall bladder removal

In *Step 2*, the rotational axis of $J_{rcm}1$ is rotated till it passes though the incision point. In these three procedures the angles of rotations of J_a3 should range between 76.88° and 15°. Since J_a3 is designed such that it can rotate in a range (0°, 90°) without colliding with the patient, this condition of alignment is satisfied for every incision point.
In *Step 3*, J_a4 is slid till the axis of rotation of $J_{rcm}2$ passes trough the incision point. The distance J_a4 has to travel for achieving this condition is calculated using GeoGebra, section 22, and has a minimum value of -6.31853 cm and maximum value of 0.58179 cm. The design in Figure 50 allows a translation along the axis between [-6.35 cm, 0.8 cm]. For this reason, in all the trocars the axis of rotation of the second revolute joint in the RCM mechanism can be aligned.

All the conditions in the four steps are satisfied. The RC of the RCM mechanism can be aligned with the incision point.

8.4.2 Stage 2: Alignment of the workspace of the robotic arm with the one of the surgery

This condition depends on the range of motion reached in *step 4* of the alignment procedure.
In *Step 4*, $J_{rcm}1$ and $J_{rcm}2$ are manually moved to align the axis of the workspace of the RCM mechanism with the one of the surgery. The inclination of the trocar is considered to coincide with the inclination of the workspace in the patient's body.
The satisfaction of this condition is defined by the range of angles of the axis of the RCM workspace on the (x, y) plane, and the one on the plane defined by rotating the (y, z) plane of an angle equal to the one found on the (x, y) plane. From images, section 20, it was possible to extract the inclination of the trocar in the (x, y) plane for each procedure. Thus, the condition is meet by satisfying the range of angles on the plane defined by rotating the (y, z) plane of an angle equal to the one found on the (x, y) plane. Due to the fact that in the images it is possible to understand the direction of the instrument on the (x, y) plane, it is necessary to ensure that for all the procedure the found range of motion is equal or grater than [0°, 90°].

This condition was tested with Matlab, code in section 23, and the results are graphically shown in Figure 67, Figure 68, Figure 69, and Figure 70. In Figure 67, Figure 68, Figure 69, and Figure 70, the pink cylinder represents the body of the patient, the plane parallel to the image represents the plane defined by rotating the (y, z) plane of an angle equal to the one found on the (x, y) plane, the other plane represents the inclination during the *step 2* of the alignment procedure, and the dark lines represent the possible position of the end effector.
In the *Incision point 2* for appendectomy configuration 2 the trocar inclination is towards the inside of the RCM mechanism. However, the angle of the line of the trocar in the (x,y) plane with respect to the horizontal is close to π, allowing to still have a wide range of inclination.

8.4.3 Results

The results of the simulations are reported in Table 12, where the possible ranges of inclination of the workspaces in the plane defined by rotating the (y, z) plane of an angle equal to the one found on the (x, y) plane are reported. Additionally, the position of the robot on the patient's bed is considered when calculating the angles. Finally, the range considered goes from 0° to 180°, which is the space

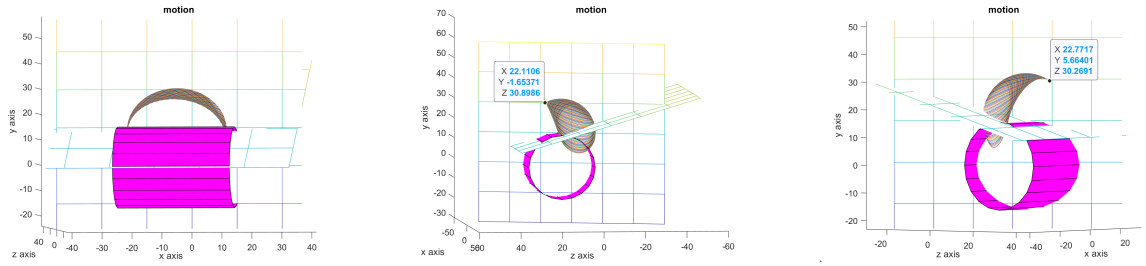

(a) Incision point 1 (b) Incision point 2 (c) Incision point 3

Figure 68: Range of motion of the RCM mechanism on the the plane defined by rotating the (y, z) plane of an angle equal to the one found on the (x, y) for Appendectomy configuration 1

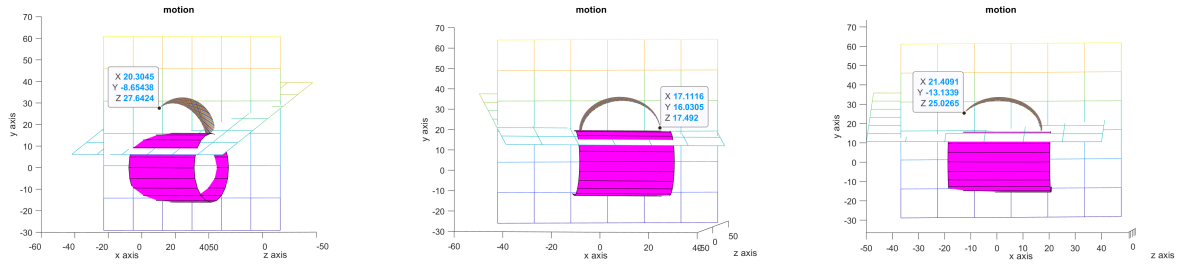

(a) Incision point 1 (b) Incision point 2 (c) Incision point 3

Figure 69: Range of motion of the RCM mechanism on the the plane defined by rotating the (y, z) plane of an angle equal to the one found on the (x, y) for Appendectomy configuration 2

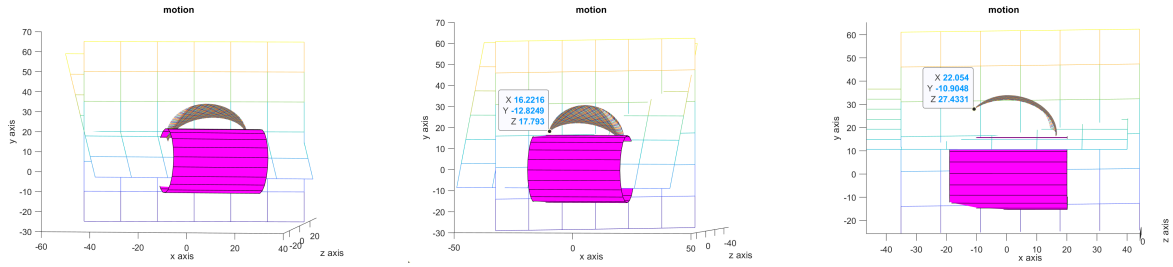

(a) Incision point 1 (b) Incision point 2 (c) Incision point 3

Figure 70: Range of motion of the RCM mechanism on the the plane defined by rotating the (y, z) plane of an angle equal to the one found on the (x, y) for inguinal hernia surgery

above the patient body. Since in all the incision points the range of motion is greater than [0°,90°], the robotic arm can align all the workspace's axes.

Table 12: Range of inclination of the workspace axis on the plane of inclination on (x,y) plane

Procedure	**Minimum inclination angle**	**Maximum inclination angle**
Gall bladder removal		
Incision point 1	0°	155.3°
Incision point 2	0°	155.3°
Incision point 3	0°	107.64°
Incision point 4	0°	121.66°
Appendectomy 1		
Incision point 1	0°	155.3°
Incision point 2	0°	95.64°
Incision point 3	0°	103.13°
Appendectomy 2		
Incision point 1	0°	107°
Incision point 2	0°	153.93°
Incision point 3	0°	124°
Inguinal hernia surgery		
Incision point 1	0°	155.3°
Incision point 2	0°	113.94°
Incision point 3	0°	115°

After this analysis, it was shown that none of the incision points require to rotate $\theta 1$ for an angle greater than 90° or lesser than -90°. For this reason, it is possible to reduce L5 of the alignment mechanism and set it equal to zero. The new dimensions of the alignment mechanism are shown in Table 13.

Table 13: Values of the parameters of the alignment mechanism

L1	33.1 cm
L2	6.4 cm
L3	4.42 cm
L4	0.8 cm
L5	0 cm

9 Background on mechatronical components and material

Once the mechanical design is completed and validated, researches about the actuators, backdrivability, position feedback, and material selection are performed.

9.1 Actuators and transmission system

9.1.1 Linear system for linear translation

For the translation along the z axis a linear system is selected. However, the linear motion systems can be of different kind. A comparison of the most used and available is done:

- *Timing belts*: They have high velocity and they are not expensive. However, they have limited accuracy and acceleration. The slipping and stretching of the belts leads to high maintenance cost, low efficiency, and heat generation from the mechanical contact. They also lead to backlash and wear of the parts. Additionally, another downside is the mechanical complexity of the system [50].
- *Rack and pinion drivers*: They can move large masses at high velocity. The use of metal gears requires lubrication, and therefore regular maintenance. They have limited accuracy, due to possible backlash between the gears, and limited acceleration [50].
- *Ball screws*: They have high efficiency and decent accuracy. However, they have acceleration and velocity limits [50].
- *Linear motors*: they have high force density, high acceleration and, therefore, extremely dynamic movements. They eliminate the need of mechanical transmission. They run over magnetic plates without any friction. Thus, they have high lifetime. The design is compact and can be modular. Additionally, they are direct drive without transmission, thus they have no backlash, no translation and are easy integrated [50]. However, they are heavy, and their initial cost is high.

An overview of other aspects about these systems is presented in Table 14.

Table 14: Comparison of linear system [50]

	Timing belt	**Rack and pinion**	**Ball screw**	**Linear motor**
Accuracy	50 μm	40 μm	5 μm	0.1 μm
Max. acceleration	50 m/s^2	40 m/s^2	10 m/s^2	100 m/s^2
Max. velocity	+	+	-	+
Reliability	-	-	-	+ +
Maintenance	-	-	-	+ +
Modularity	-	+	-	+ +
Ease of installation	-	+	+	+
Noise	-	- -	-	+ +
Cleanliness	- -	-	-	+
Initial cost	+	+	-	-

From Table 14 and from the discussion presented above, the use of **linear motor** is selected. For this reason, an overview of the **different linear motors** is done:

- *Voice Coil*: The voice coil motor is the simplest type of linear motor. A permanent magnet is placed inside a coil of wire. As current is sent through the coil the permanent magnet moves away from the coil. These motors can generate a lot of force but are limited in travel of 2.5 cm or so [13].
- *Force Tube*: This type of linear motor places a stack of disk-shaped permanent magnets inside a hollow non-magnetic tube. This tube is placed inside an assembly of coils. By selectively applying current to the coils, the tube moves through the coils or the coils move down the length of the tube. This type of linear motor can generate a lot of force and does not have the travel limits of voice coil motors [13].

- *Stepper*: This linear motor works just like a rotary step motor and has all of the same advantages and disadvantages. They are most often operated open loop and move in discrete steps. Linear stepper motors are simple to commutate but have poor speed force characteristics, are inefficient, and have low stiffness because they are operated open loop [13]. Their main advantage is that the rack base of the motor is passive. The rack is basically a slab of iron with slots milled into it. Since the magnets and motor coils are located in the forcer, the rack base does not attract and capture ferrous materials [13].

- *Hybrid*: The hybrid linear motor's construction is almost identical to the linear stepper motor. The motor's magnets and coils are just configured differently. The main difference is in its performance. It is operated closed loop so it has higher stiffness and is more efficient [13].

- *Brush DC*: In the brush DC linear motor, the rack base contains all of the motor winding while the forcer has the permanent magnets and the brushes. The motor is self commutating so in some applications no controller is needed. The rack base is complex and the motor has all of the disadvantages of all brush type motors – brush wear and arcing[84].

- *Induction*: The induction linear motor is the only linear motor that does not use permanent magnets. The rack base consists of rods that are encapsulated such that all of the ends of the rods on each side are shorted together[13]. The windings in the forcer induce currents in these rods to create a magnetic field. It is best suited for applications that have low duty cycle and long travels [13].

- *Synchronous*: This is the most common type of linear motor. It is also known as a DC brushless linear motor or AC linear motor. They come in two styles - iron core and ironless core [84]. The forcer of the iron core motor consists of a section of laminated iron with embedded motor windings. The rack base has permanent magnets affixed along its entire length. The ironless core linear motor uses a U-shaped rack base that has permanent magnets affixed to both inside legs of the U-shaped channel [13]. The forcer windings are embedded in a nonmagnetic core material that slides inside of the U-shaped channel. There is no iron used in the forcer. The iron core type linear motors dissipate heat better that the ironless core motors. To overcome the heat build-up in ironless core motors, they are available with cooling tubes built into the core through which air or a fluid is pumped to remove the heat [13].

A quick overview for the best selection per application is given in Table 15.

Table 15: Quick selection guide [13]

Application	**Linear motor type**
Short stroke, light load, high frequency	Voice coil
Short stroke, moderate load	Force tube
Low mass, open loop	Stepper
Long travel, low duty cycle	Induction
Low cost, low duty cycle	Brush DC
Smooth Motion	Ironess Core PM Synchronous
General automation	Iron core PM Synchronous *or* Hybrid

9.1.2 Actuators for rotational DOFs

The actuators for rotation can be classified in base of their working principle. An overview of the motors' classification is reported in Figure 71. For the requirements of the robotic arm, compact size, precision, accuracy, and efficiency of the motors are critical. For these reasons, among the motors listed in Figure 71, *Brushed DC*, *Brushless DC*, and *Stepper motors* are further investigated.

- **Brushed DC motors**: the main advantage of the brushed DC motors is the speed control over a wide range both above and below the rated speed. They have high starting torque, thus they can be used for driving heavy loads in starting conditions. They are quick in starting, stopping,

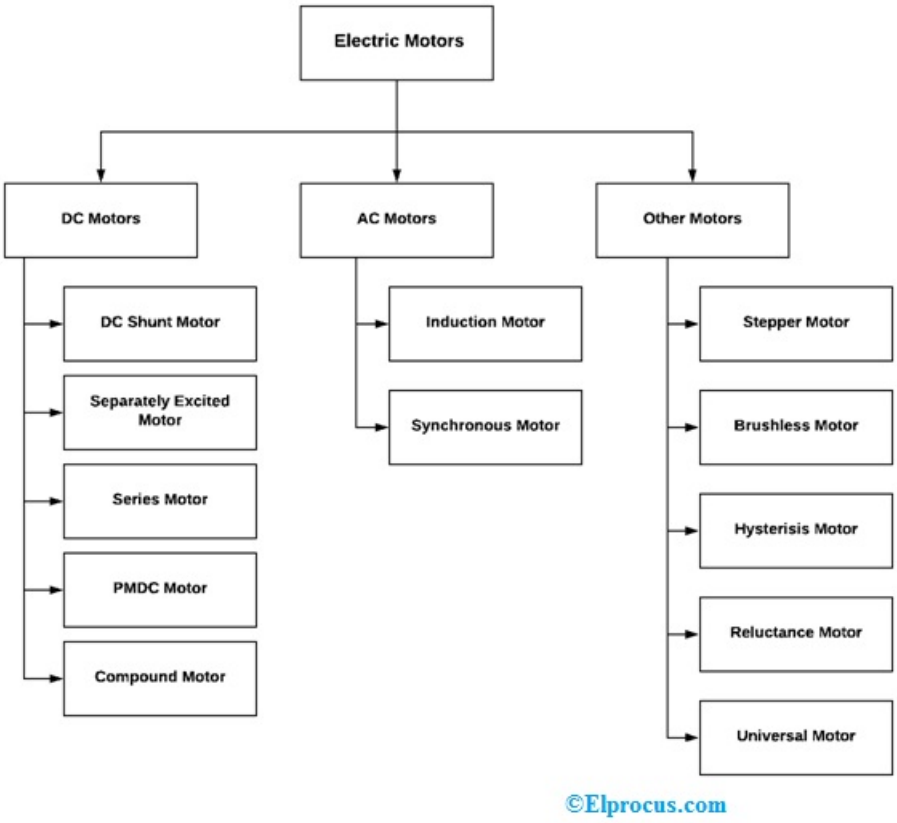

Figure 71: Classification of motors [7]

reversing and accelerating [92]. However, they are costly, and requires additional maintenance cost due to the presence of the brush. Additionally, they create damages due to sparking occur at brush [92].

- **Brushless DC motors**: The absence of brush reduce cost maintenance, replacement, and damage. They perform better than the brushed DC motors, having a better efficiency and life span [87]. Additionally, brushless DC motors have no excitation loss compared to AC motors. They are available in small and compact size. This makes these motors lighter than the brushed DC motors and the AC motors. They provide high torque to weight ratio making it suitable for many robotics and medical applications involving robotic arms [87]. Moreover, brushless DC motor has low no-load current making it suitable to run it at low or no load. Brushless DC motors can provide maximum torque continuously during rotation, while brushed DC motor can provide maximum torque at an only specific point of the rotation. With respect to AC motors, they have no core losses, thus they have a better efficiency [87]. Brushless DC motors can have a feedback control to monitor and control the speed and torque, resulting in accurate torque and speed control providing higher efficiency, low power consumption. However, their cost is high, and at low speed they may create small vibrations [87].

- **Stepper motors**: the advantage of these motors is good precision at open loop. The precision of every step is controlled within the range from 3% to 5% [92]. Plus, the error in the last step won't be accumulated in to the next step. The steppers in general have a better holding torque for the power rating. The configuration of stepper motors can be comparatively simple [92]. The manufacturing cost is low. As stepper motors are brushless ones, the lifetime of stepper motor is determined by the bearings' lifespan only. The drawback of a stepper is that the torque of a stepper stays at its peak even in no load condition [92]. Apart from this, the steppers, due

to open loop control, are quite noisy as well. Additionally, Stepper motor has no advantages in aspects of size and weight. Energy utilization ratio is comparatively low [92].

For the shown advantages and disadvantage, brushed DC motors are discarded. The main decision is between **DC brushless** and **Stepper motors**.

9.2 Backdrivability

The best way to achieve backdrivability is through a direct connection between the motors and the robotic arm, without transmission systems. However, available motors do not reach the necessary level of torque, so a transmission is necessary for increasing the torque. However, the transmission needs to be backdrivable under forces higher than 60 N. This is not always true for conventional transmissions [129]. The following are backdrivable transmissions:

- **Gearbox**: one of the most common transmission between the motors and the mechanism is the gearbox. The backdrivability of it depends on the kind of gears and the gear ratio.
  Gears can be categorized in base of their designs and their working principle. The main gears are: *spur*, *helical*, *worm*, *bevel*, *spiroid*, *harmonic drive*. The characteristics, advantages, disadvantages, and backdrivability are presented in Figure 72.

Type	Notes
Spur	Majority of gears are spur. Relatively easy to design and make. Parallel shafts. High efficiency (99% per train). No side thrust. Can back drive. Single Ratio up to 1:10. Can be made very accurate with low vibration /noise. Normally steel pinions require lubrication. Plastic gears can be used requiring no lubrication
Internal Spur	Similar performance to normal spur. Results in compact drive geometry. Used in manufacture of epicyclic / planetary gears.
Helical	Single Helical have similar properties to spur. However drive results in axial thrust. Gears are smoother/quieter for the same size/spec. The gears can run at high speeds up to large diameters. Higher torque/life capabilities for same size as spur.
Double-Helical	Similar benefits to single helical but with no generated side thrust. Higher performance compared to single helical
Crossed-Helical	Shaft at 90^{o}. Difficult to make accurately. Smooth drive.
Worm	Offset shafts at 90^{o}. Very high ratios possible in single stage. Sliding action. One gear is normally copper allow (bronze). Low efficiency at higher ratios and low speeds. Lubrication essential for mechanical and thermal reasons. Cannot backdrive at high ratios.
Bevel Gear	Mainly used for drive transmission through 90^{o}. Only low ratios used (4:1 and less). Lubrication required. Some vibration on spur type: Helical type smoother.
Spiroid	Perform a similar function to worm boxes but the gears have characteristics which combine those of the bevel and worm gears. High powers and speed ratios are possible and mechanical efficiencies higher than worm boxes for equivalent ratios.
Harmonic Drive	Performance advantages include high-torque capacity, concentric geometry, lightweight and compact design, zero backlash, high efficiency, high ratios (up to 320:1), and back drivability. Harmonic drive systems suffer however, from high flexibility, resonance vibration. Used in robotics

Figure 72: specification of gears [47]

From this brief comparison, it can be seen that only some gears are backdrivable, and can be used in this design: **spur gears**, **helical gears**, **bevel gears**, **harmonic drivers**.
A second factor that influences the backdrivability is the gear ratio. Generally, **reducing gear ratio** increases the backdrivability. Finally, the backdrivability of a gearbox is highly correlated with the friction and the efficiency. Hence, a look to the efficiency of different types of gears to get a initial impression of the backdrivability of them is made in Figure 73.

- **Capstan drive**: Capstan drives are rotary transmission elements widely used in robot mechanisms because of their low inertia, low backlash, high stiffness and simple implementation [129]. Figure 74 shows a typical capstan drive used in haptic devices. Their working principle is based on a capstan located on the motor shaft wrapped with a cable having its both ends linked to a large diameter wheel. An automatic tensioning system, composed of a spring and a fixed post on the wheel, can also be implemented in order to avoid manual adjustment of the pre-load after a certain period of time due to creep in the cable [112]. The cable in a capstan drive is typically wrapped around the input and output drums in a figure-eight pattern to transmit the power. The transmission error of a capstan drive mechanism results from the drum eccentricities and can be modelled.

Type	Normal Ratio Range	Pitch Line Velocity (m/s)	Efficiency Range
Spur	1:1 to 6:1	25	98-99%
Helical	1:1 to 10:1	50	98-99%
Double Helical	1:1 to 15:1	150	98-99%
Bevel	1:1 to 4:1	20	98-99%
Worm	5:1 to 75:1	30	20-98%
Crossed Helical	1:1 to 6:1	30	70-98%

Figure 73: comparison in performance, speed and gear ratio [47]

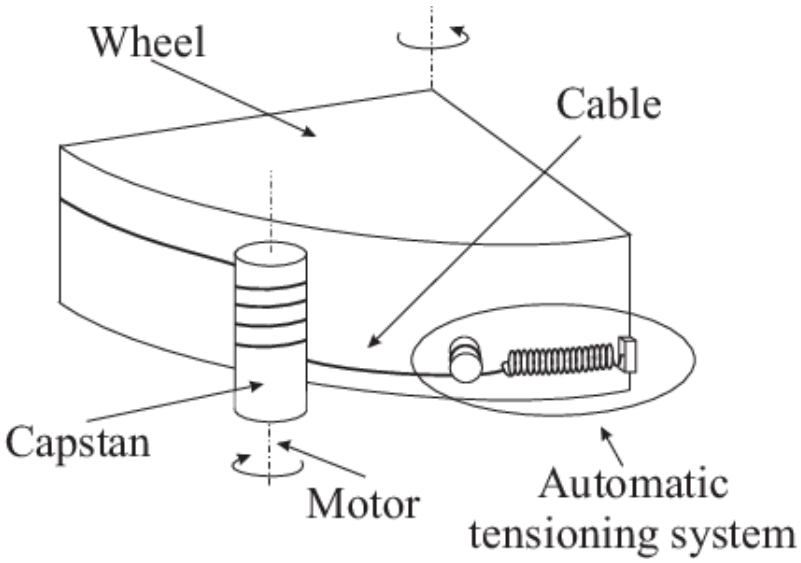

Figure 74: Cable capstan reducer with the automatic tensioning system [112]

- **Block-and-tackle**: this transmission is made of cables, it is very efficient in terms of transmitted force, but it is bulky, fragile, and hard to maintain [129]. The block-and-tackle implemented in the MA23 robot is shown in Figure 75

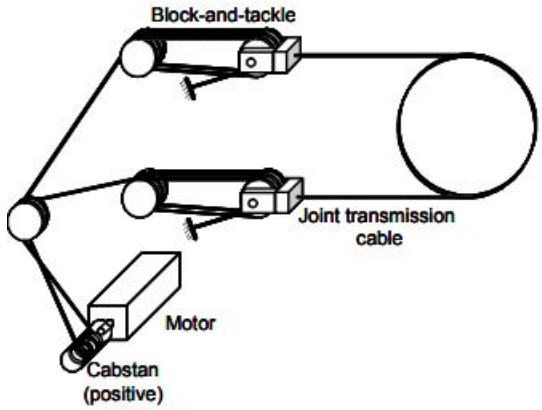

Figure 75: Block-and-tackle of MA23 [129]

Another way to achieve and optimize backdrivability is trough:

- **Strategy of Torque control**: the paper *"Back-drivability improvement of geared system based on disturbance observer and load-side disturbance observer"* [148] proposes a method of improving the back-drivability of torque control according to the dynamic characteristics of forward-drivability based on the concept of proposed equivalent expression. The control strategy is composed of disturbance observer (DOB), a load-side DOB (LDOB) and the designed controller for torque control. The DOB realizes robust motion control by compensating for friction and modelling error of the system, and the LDOB estimates the external torque input from the load-side.

Preliminary decision

The explored solutions that have been presented above, brought in light some aspects that already allow to make some preliminary decisions. Because of the complexity of the torque control strategy, and the fact that in absence of power this would not work, this strategy is already excluded from the morphological table. Thus, the remaining options are **Gearbox**, **Capstan drive**, and **Block-and-tackle**.

9.3 Position Feedback

The ultimate goal of this design is to feedback the absolute position of the end effector. The main characteristics are the used sensors, the position of those, and the quantities they give as feedback. It is decided to use **wireless sensors**, for reducing the amount of components and complexity of the system.
In this overview, all the systems that track the position through the use of external components (cameras, markers, etc) are removed, as well as systems that will need the presence of specialized staff, for the considerations expressed in subsection 2.3.

- **Position sensors**: Position/orientations sensors are divided in four sub-classes that refer to the modalities of sensing: *mechanical*, *optical*, *magnetic*, *acoustic*. A good comparison of the different sensors categorized in base of the modalities of sensing is done in the work [139], and reported in Figure 76.

	Mechanical	Optical	Magnetic	Acoustic
Accuracy	0.1 - 2.5 mm	0.1 - 0.5 mm	~5 mm	~1 mm
Resolution		best ~0.01 mm		~ 0.1 mm
Bandwidth	>3000Hz	100-2500 Hz	20-100Hz	500-1000Hz
Interference Sources	physical occlusion	heat, occlusion	ferrous objects, magnetic fields	temp., humidity, occlusion
Examples	Faro Arm, NeuroNavigator	Optotrak 3020, Flashpoint	Polhemus, Flock of Birds	Sonic Wand
Contact / Non-contact	Direct Contact	Contact w/ targets	Contact w/ targets	Contact w/ targets
Passive / Active	Passive	Active	Active	Active

Figure 76: Comparison of position/orientation sensing modalities [139]

Additionally, the most used and important sensors of these categories are reported in Figure 77. The *potentiometric* is a mechanical sensors, and calculates the position in base of the measured resistance. *LVDT* and *RVDT* are acronyms for Linear and Rotatory Variable Differential Transformer. They are inductive sensors, and calculate the position in base of the change in the characteristics of a magnetic field that is induced in the coils of the sensors [14]. The *optical sensors* work with two principles: in the first, the light is emitted by an emitter and sent over to a receiver; in the second, the emitted signal is reflected back from the object that needs to be recognized in space [14]. In base of the characteristics of the light received, the position of the receiver/object can be calculated. The *magnetic Hall effect sensor* uses the hall effect: development of a transverse electric field in a solid material when it carries an electric current

and is placed in a magnetic field that is perpendicular to the current [14]. Finally, the *magnetostrictive sensors* use ferromagnetic materials and the phenomena that creates a change in size or shape when these materials are in presence of an applied magnetic field. The advantages and disadvantages of these sensors are reported in Figure 77.

TYPE OF SENSOR	NON-CONTACT	ADVANTAGES	DISADVANTAGES	NOTES
Potentiometric		• High accuracy • Inexpensive	• High wear and tear • Sensitive to dust • Sensitive to extreme temperatures	• Linear or angular sensor
LVDT or **RVDT**		• High accuracy • Heavy duty • Low sensitivity to harsh environments	• Quite expensive • Bulky and heavy	• RVDT: rotation limited to 40° more or less
Optical		• High accuracy • High resolution	• Fragile • Sensitive to dust • Sensitive to extreme temperatures	• More expensive than a magnetic sensor
Magnetic Hall effect	X	• Heavy duty • Low sensitivity to liquid	• Sensitive to impact • Disrupted by magnetic materials and electrical wires • Hysteresis	
Magnetostrictive	X	• Heavy duty • Accurate for long lengths	• Sensitive to temperature changes • Lack of accuracy for short lengths • Quite expensive	

Figure 77: Position sensors [14]

The use of these sensors in the end effector and/or joints can give a position feedback of the end effector.

- **IMU**: One possible solution for position tracking is the implementation of IMU in the system. The IMU can be implemented at the end effector directly, and gives as output the position and the orientation of it. Another option is to implement the IMU in the joints, and calculate the position of the end effector by maths.
  However, as stated in paper *Improving low-cost inertial-measurement-unit (IMU)-based motion tracking accuracy for a biomorphic hyper-redundant snake robot* [149], IMU-based position tracking calculates the position by double integration of measured acceleration from the IMU itself. However, with double integration, calculation errors increase[149]. To eliminate the effects of accelerometer errors, most of the papers use sensor fusion algorithms, among which the Kalman filter is the most used. In [77, 152, 138], standard Kalman filter, unscented Kalman filter (UKF), and extended Kalman filter (EKF) are employed in high data rate signal processing. EKF has lower accuracy; however, UKF requires more computational time.

- **Encoders**: Apart from the previous technologies, magnetic encoders can be used to measure the angular velocity and position of a motor, as shown in the work [146]. Motors were mounted in a robot that integrate encoders and magnetic compasses to calculate the absolute position [111]. However, using the encoder for position feedback of end effector leads to errors in case of backlash, that results in increase of hazards for the patient. In fact, a wrong position feedback of the end effect may result in a wrong motion and collision with the patient's body/tissue.

- **Hybrid**: Finally, some academic studies make use of a fusion of the aforementioned technologies

for position tracking. In the paper *Inertial-robotic motion tracking in end-effector-based rehabilitation robots*, [128], a hybrid system design that uses wearable inertial sensors and real-time sensor fusion methods was presented. The proposed approach accurately tracks the motion of the end-effectors. Another paper using a similar method is *End-Effector Pose Estimation in Complex Environments Using Complementary Enhancement and Adaptive Fusion of Multisensor*, [119], where a pose estimation method is proposed with the fusion of vision sensors, inertial sensors, and encoders. Firstly, according to the complementary characteristics of each measurement unit in the sensors, the original data is corrected and enhanced. Furthermore, an improved Kalman filter (KF) algorithm is adopted for data fusion by establishing the nonlinear motion prediction of the end-effector and the synchronization update model of the multirate sensors [119]. Finally, the radial basis function (RBF) neural network is used to adaptively adjust the fusion parameters. The disadvantage of this approach is the cost and the redundancy of the position tracking.

9.4 Material and Manufacturing processes

The selection of material and shape of the shaft is one of the main parts of the design and is going to help in the selection of motors and transmissions.
The first variable to be selected is the minimum stiffness that the structure has to have for achieving a precision of 0.8° in the rotation motion. Since the overall rotational motion is a circle of diameter of 15.88 cm, the accuracy of motion has to be lesser or equal than 0.355 mm. Thus, the maximum deflection for satisfying this requirements is 0.355 mm at the end effector.
The total force applied on the structure is unknown, but it is known that the mass of the attached instrument's driver and instrument is 1 kg. Thus, the force applied at the end effector is 9.81 N. Considering the Figure 78, W can be set equal to zero, while P can be set equal to 9.81 N. This configuration gives the highest amount of deflection, that can be expressed as in Equation 31 and Equation 32. In the formulas, I is the second moment of area of the cross section and E is the young modulus of the material.

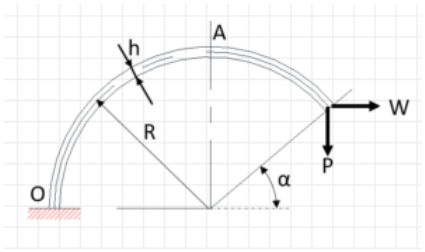

Figure 78: Arc and force configuration

$$deflection_{\mathrm{y}} = \frac{PR^3}{IE}[(\pi - \alpha)(0.5 + c^2\alpha) + 0.75s2\alpha] \tag{31}$$

$$deflection_{\mathrm{x}} = \frac{PR^3}{IE}[(\pi - \alpha)(0.5 + s^2\alpha) - 0.75s2\alpha - 2s\alpha] \tag{32}$$

In the designed robotic arm, the α in the Figure 78 is equal to π-α1-α2, thus α=79.3°. This give an estimation of minimum product EI. For the y deflection, $(\mathrm{EI})_{\mathrm{min}}$ is around 10^{10} Nmm^2. For the x deflection, $(\mathrm{EI})_{\mathrm{min}}$ is around 2.9x10^{10} Nmm^2.

Since the first design goal is to minimize size, the maximum allowed dimension of the cross section Area is set to be 5 cm. This means that the minimum allowed E is of the order 10^5 N/mm^2.
From Figure 79 it can be seen that metals and ceramics are in the range of Young modulus required. However, ceramic material have high brittleness which leads to unexpected fractures [40]. Additionally, manufacturing metals is cheaper and more convenient than manufacturing ceramics [40]. For these reasons, **metal** is selected as material class for the robotic arm. The selection of the final metal is reasons afterwards.

Additionally, an overview of the **manufacturing processes** that allow to manufacture a arced beam is done. The main methods are listed below.

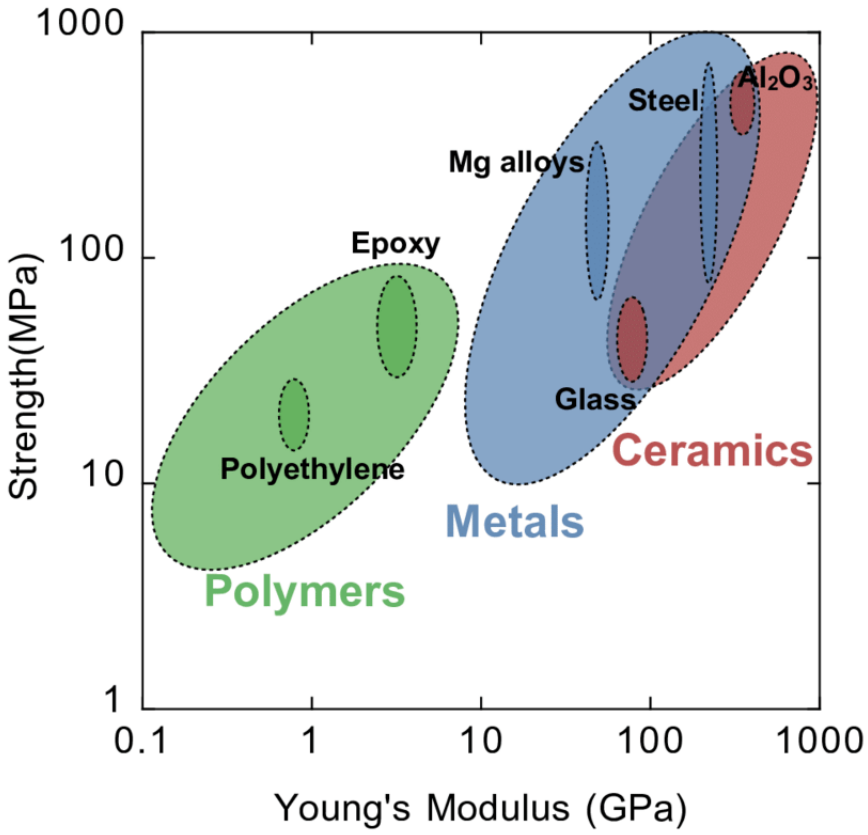

Figure 79: Graphical representation of Young modulus and strength of materials [122]

- **Casting**: Metal casting is a production method in which molten metal is poured into a cavity and left to cool and solidify to obtain the part [106]. The main advantage of this procedure is the high variety of shape it can produce. In fact, a cavity that shape the arc can be easily made. Additionally, the shape and size of the castings are very close to the workpiece. Therefore the metal casting process reduces the amount of further machining work and saves the metal materials. However, the pieces have poor accuracy, repeatability, and dimensional consistency [106]. Additionally, this change of states of the material can modify the chemical structure of the material, and thus the mechanical properties of it. It can create small defects that can be fatal in a high precision and safety environment as the medical one [106]. Finally, this procedure is quite expensive, since it requires to liquefy the material and to create and fabricate specific molds.

- **Forming**: Metal forming is a production method in which stresses like tension, compression, shear, etc. are applied to the part to deformed the raw material [106]. The main procedure that can produce the arc shape beams is the *Metal Bending*. Bending is the process of forming where an angle is used in order to press by a compressive force a metal piece. The main advantages of this procedure is the easiness of the tools, which are low cost and versatile. Additionally, it can accommodate all shapes from thin sheet metal to even complex cross section areas [106]. The products made through Forming Processes are stronger and more durable than those made through casting. It is cheap, quick, easy, reducing the amount of waste, which is negligible or zero [106]. Moreover, it has an higher potential strength than forging or casting: when using other methods like casting or forging, all stress concentrates at the surface making them more likely to crack or shatter if exposed to fatigue loads [106]. The disadvantage of the process is susceptibility to error ratios where defects are hard to detect after processing [106].

- **CNC machining**: Another possible manufacturing process for creating the desired arced beam is CNC machining. CNC machining is the process of using a computer-driven machine tool to produce a part out of solid material in a different shape [106]. It has high accuracy and requires less time to complete a task. Additionally, it works with a wide range of materials [106]. However, CNC machines are more expensive and require a greater initial investment than machines that can be operated manually, however it is less expensive than a comparable 3D printed part. The main disadvantage is the material wastage. For producing the arced beams, it is necessary to have a block of material with thickness equal to the thickness of the part, and height and length equal to R*cos(α) and R*sin(α). The most of the material is going to be wasted. Additionally, it is impossible to have hollow cross sections.

- **Origami**: Creating origami style parts allows to have arc shaped beams. This can be done by sheet metal water jet cutting that creates a teeth origami, which can be shapes as arced by folding and welding the teeth together. This can be applied to any shape material, also tubes, or hollow cross section area parts. This procedure is cheap and allows to have light structures. The advantages of water jet cutting are flexibility, precision, repeatability, speed, cost-effectiveness, great quality, contactless cutting, versatility and automation possibilities [106]. However, water jet cutting has a limitation in the maximum thickness of the manufactured metal.
  The second procedure is welding, which creates superior strength piece, and allows to join the cut parts together. Usually, the welded connections are very strong more than the parent's materials [106]. Additionally, it is a quite inexpensive procedure. However, the welding sub-procedure creates materials distortion. Since there are uneven heating and cooling of different components, there is a possibility of generating residue, which is normally stressful. This residual stress reduces the load-carrying capacity of the welded parts.

- **Additive manufacturing**: This process allows to have any desired shape for the part. However, the procedure is very expensive, requiring post-processing for restring the mechanical properties of the material [106]. Another disadvantage of this procedure are the internal defects, which are not visible but probable for parts manufactured with additive manufacturing. In the medical field, safety and control over the structure are vital features. For these reasons, this manufacturing process is not optimal.

A comparison of the advantages and disadvantages of these procedures is done in Table 16, with a higher attention on material, cost, and cross section area they can produce.

The most used and most available metals for this processes are *stainless steel 1035* and *aluminium 6061*. Thus, in this project, this two are the materials that are going to be compared for the final design.

Table 16: Comparison between manufacturing procedures

	Casting	**Forming**	**CNC**	**Origami**	**Additive manufacturing**
Materials	Iron, steel, aluminium, magnesium and copper-based alloys [106]	Steel, aluminum, brass, and copper [106]	Any metals	All types of metals. More reflective metals like aluminium are more difficult to cut.[106]	Steel, Titanium, Aluminium, Cobalt Chrome Alloy [106]
Cross section area	Any [106]	Rectangular, circular, hollow and full	Only full rectangular	Rectangular, circular, hollow and full, limited in size: thickness affect the feasibility [106]	Any
Cost	Very expensive for smaller to medium quantities [106]	Cheap	Expensive (large amount of waste)	Cheap	Very expensive
Mechanical properties	Local tensile properties vary widely with solidification conditions [106] UNEVEN	Better mechanical properties than by casting or machining products[106] Yield strength and tensile strength higher	Excellent mechanical properties [106]	Good mechanical properties	Porosity and worst fatigue resistance. Yield strength, corrosion resistance, ductility sensible to change of density, unpredictable. [106]

10 Mechatronical and Material design

10.1 Sizing of actuators, transmission systems and material selection

After the overview performed in section 9, a recap of the requirements for selecting actuators, transmissions, and materials is done. The requirements are the following:

- *Precision*: The precision has to be 0.8° for the rotation and 0.01 mm for the translations [127].
- *Velocities*: The required velocities are: wx 0.486 rad/s (4.641 RPM), wy 0.432rad/s (4.125 RPM) [118, 136], vz 0.2 m/s [88].
- *Backdrivability*: The system has to be backdrivable for forces $\geq$ 60N.
- *Non-Backdrivability*: The system has to be non-backdrivable for forces $\leq$ 60N.
- *Maximum force*: For ensuring position in place in case of failure of the motors the overall force applied in static to the motors has to be $\leq$ 60 N.
- *Range of motion*: the linear system needs to ensure a range of motion of [0mm, 130mm], while the rotating motors must have a range of motion of [-90°, 90°] for $\theta 1$ and [-150°, 150°] for $\theta 1$.

10.1.1 Motor selection for the translational DOF

In this section, a linear motor that satisfy the requirements in subsection 10.1 and that meets the design goal in subsection 3.1 is selected.
Several linear motors were reviewed to see if they met the requirements, [33], [29], [30], and [41]. It is desirable to minimize the weight and size of the motors for this application.
The selected module is part of the *Miniature Linear Modules QM02 with tubular Linear Servo Drives* catalog, which lists small, lightweight and efficient linear modules. It is decided to choose the whole linear system equipped with two ball bearing [41]. The motor installed in the linear module is a tubular ironless linear motor [41]. It has single-cable technology with an optimized, compact and direct connection [41]. The selected module is the **Miniature Linear Modules QM02-12477-120**. The specifications are given in Table 17.

Table 17: Specification of Miniature Linear Module QM02-12477-120

Specifications	
Maximum mechanical stroke	140.6 mm
Maximum force	10.5 N
Continuous force	3.6 N
Maximum velocity	3 m/s
Mass	206 g
Dimensions	30x57x206 mm^3
Position accuracy	50 μm

10.1.2 Motor selection for rotational DOFs

As already discussed in subsubsection 9.1.2, the main decision to be taken on the type of motors is between *Stepper motors* and *DC Brushless motors*. Different motors were compared, [15], [43], [8].
For the requirements presented in subsection 3.2, the resolution of the motion must be 0.8°. It was found that most stepper motors operating in open loop have a resolution of 1.8°, and the minimum was 0.9° [15], [43], [8] . In addition, DC brushless motors can reach a weight of 50 g, while the minimum weight of steppers is about 200 g. For these reasons, the **DC brushless motors** are selected for this application. This reduces the size, noise and increases the efficiency of the system. The precision of these motors is determined by the drives. In [8], most drives compatible with the DC motors have a position resolution of 32 bits, which provides the required resolution of 8.38190317 x 10^{-8}. In [15], the resolution of the drives is 24 bits, 2.14576721 x 10^{-5}, which still meets the requirements. Due to the large size and high mass of the drivers, they are positioned at the base of the robotic arm and the

wires are routed along the arm to the motors, which are inserted into the joints. For this reason, one of the main requirements for the motors is to be small.
The universal servo drives in [12] are compatible with most of their DC brushless motors. These motors are specifically designed for medical purposes to reduce size, improve resolution, and have the required specifications and materials.
The **ElectroCraft RPX** DC brushless motors are very compact, highly controllable motors with class-leading torque per frame size and power [9]. They are extremely energy efficient and ideal for embedded applications [9]. The range of parameters for these motors is shown in Table 18.

Table 18: Range of parameters of ElectroCraft RPX motors [9]

	Motor RPX22	**Motor RPX32**	**Motor RPX40**	**Motor RPX52**
Weight	72 g	260 g	370 g	657g
Length	49 mm	74 mm	60 mm	68 mm
Diameter of motor	22 mm	32 mm	40 mm	52 mm
Diameter of shaft	4 mm	5 mm	6 mm	7 mm
Continuous Stall Torque	42 mNm	150 mNm	325 mNm	750 mNm
Continuous rated Torque	42 mNm	150 mNm	270 mNm	600 mNm
Peak Torque	91 mNm	438 mNm	991 mNm	3150 mNm
Continuous rated velocity	9000 RPM	7500 RPM	2950 RPM	2500 RPM

10.1.3 Transmission selection

In section 6, it was decided to maintain the position in place passively by a non-backdrivable transmission. This can be achieved with the help of a **Gearbox**. However, one of the requirement is that the gearbox is backdrivable for forces higher than 60 N. For this reason, it is necessary to select a gearbox backdrivable for all forces higher or equal to 60 N, and non-backdrivable for smaller forces.
The gearbox must be compatible with the motor and have small dimensions. In this application, it is necessary to choose a gearbox that increases torque and reduces speed. The desired output speed is 4.641 RPM, so the gearbox selected must have a ratio greater than 4.641 RPM /speed of the motor. For the motor presented in Table 18, existing gearmotors (assembly with gearbox and motor) are found. Depending on the number of gear stages in the gearbox, the output torque and speed vary. It is decided to choose a **gearmotor** for this application. The gearmotors are listed in Table 19.

Table 19: Range of parameters of ElectroCraft LRPX planetary gearmotors [10]

	GearMotor LRPX22	**GearMotor LRPX32**	**GearMotor LRPX40**
Weight	136.4-171.5 g	283-364 g	527-727 g
Length	77.2-93.6 mm	84.6-104.1 mm	82.3-123.6 mm
Diameter of motor	22 mm	32 mm	40 mm
Diameter of shaft	6 mm	6 mm	10 mm
Continuous running Torque	0.098-1.6 Nm	0.162-6.6 Nm	0.378-15 Nm
Peak Torque	0.28-3 Nm	0.81-8 Nm	2.27-22.5 Nm
Continuous running velocity	2408-17 RPM	2322-7 RPM	1265-5 RPM

10.1.4 Cross section area of the beams: Comparison of three different designs

The gearmotors, presented in Table 19, attach the beam through four screws placed at the four angles of the circumscribed square in the circular cross section of the motors. The connection is more stable and easier if the surface of the beam that attaches the motor is a flat surface. From Table 19, the possible edge dimensions of the mounting plane for the gearmotors can be seen to range from a square with a side length of 22 mm to 40 mm. This suggests that a cross-section with a horizontal face no

wider than 40 mm should be selected. In addition, it is favourable to have a hollow cross-sectional area, as it affects the weight and allows the passage of the wires in the cavity.
It is decided to model the robotic arm with the cross-sections shown in Figure 80, since they are the most commonly manufactured and have a horizontal, flat surface that allows stable mounting of the gearmotors on it. The width of the beams is assumed to be 40 mm, which corresponds to the maximum radius of the motors.

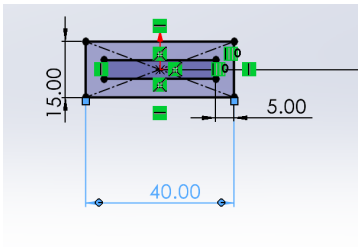

(a) Rectangular cross section area

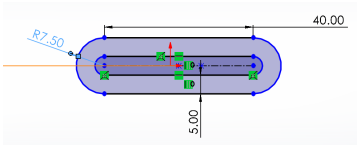

(b) Ellipse cross section area

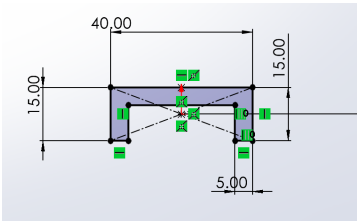

(c) U shaped cross section area

Figure 80: Cross section areas for the beams of the robotic arm

To determine which cross-section is best for this design, a comparison is made between the three designs presented in Figure 80. In this case, the comparison is only qualitative, since the thickness and height of the cross-sectional area are chosen arbitrarily. However, they are kept constant across the three cross-sectional areas. Thus, it is possible to qualitatively check the differences between them. The material chosen for this qualitative comparison is AISI 1035 steel.
In the simulation, the beam 1 of the robotic arm is fixed, while a force of 11.83 N (instrument, actuator of the instrument's and the linear system) is applied to the end of the beam 2. The results are displayed in Figure 81, Figure 82, Figure 83 and Table 20.

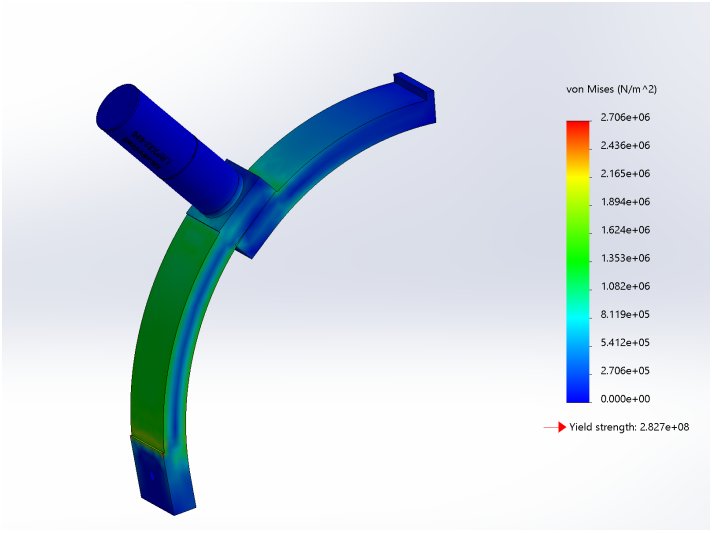

(a) Rectangular cross section area stress

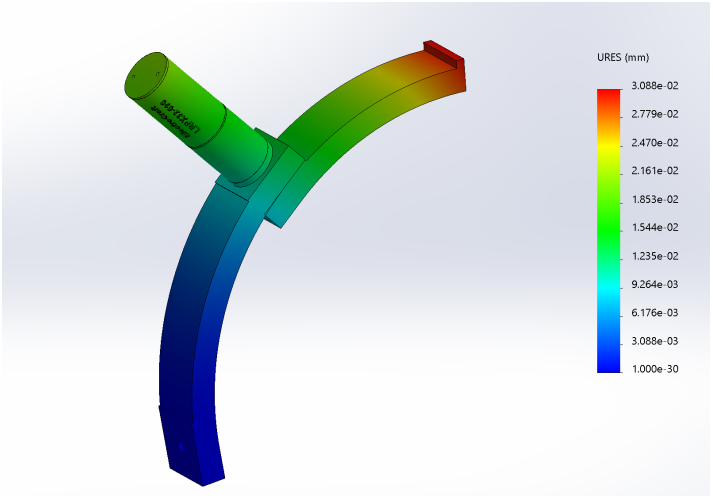

(b) Rectangular cross section area displacement

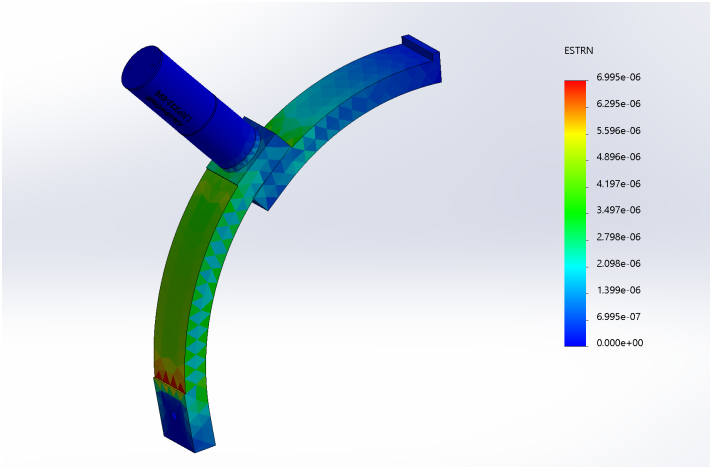

(c) Rectangular cross section area strain

Figure 81: Results of the simulation for the rectangular cross section area assembly

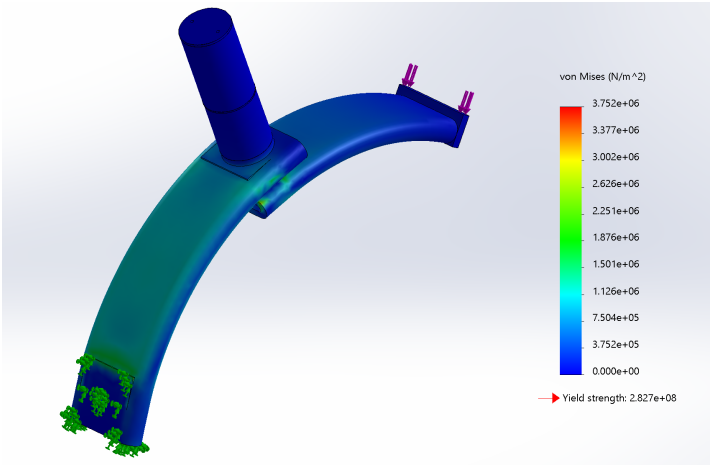

(a) Ellipse cross section area stress

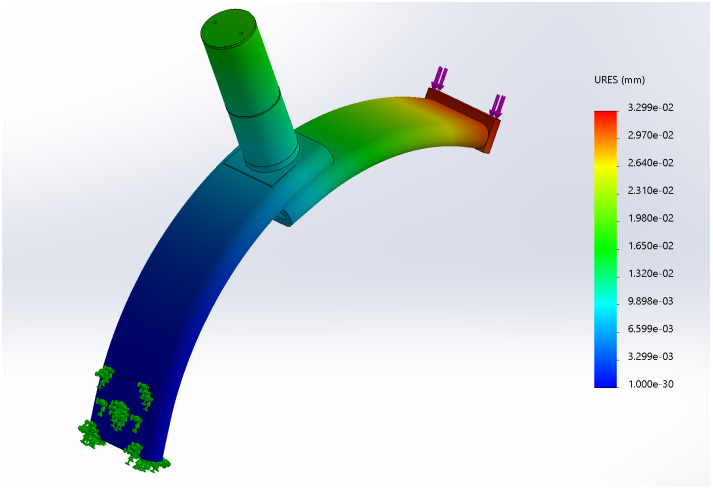

(b) Ellipse cross section area displacement

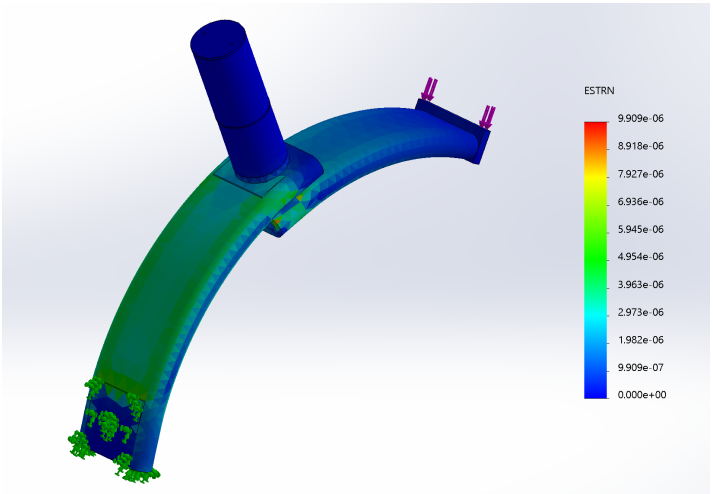

(c) Ellipse cross section area strain

Figure 82: Results of the simulation for the ellipse cross section area assembly

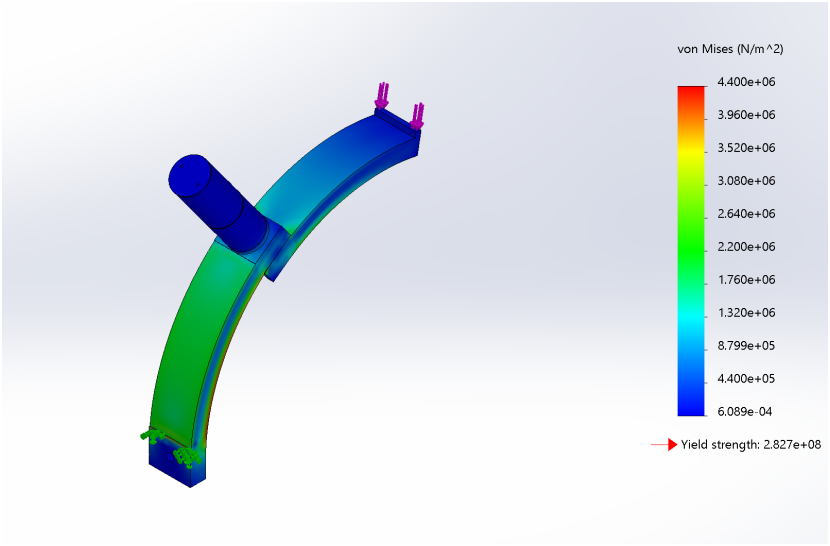

(a) U shape cross section area stress

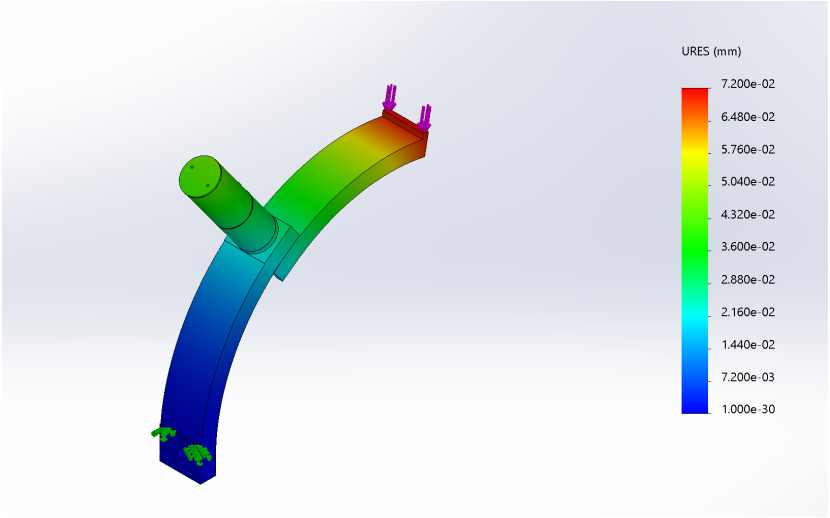

(b) U shape cross section area displacement

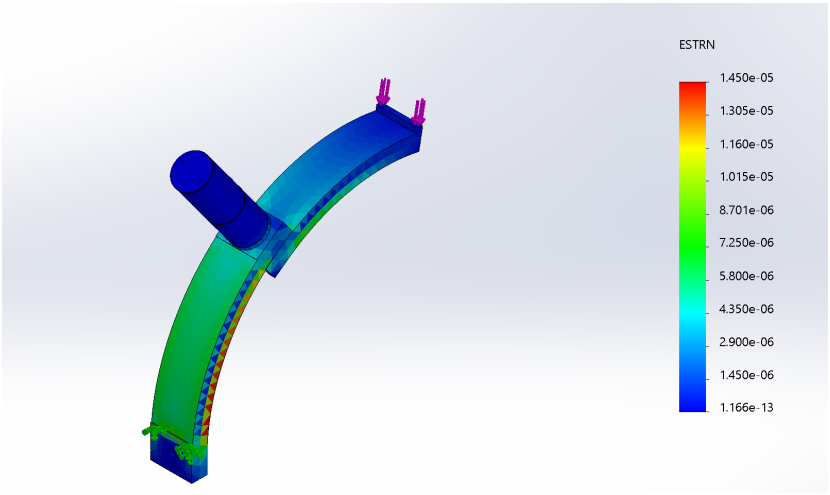

(c) U shape cross section area strain

Figure 83: Results of the simulation for the U shape cross section area assembly

Table 20: Volume of the design with the three cross section areas

Cross section	**Volume (mm^3)**
Rectangular	239480.75
Ellipse	286359.51
U shape	188790.50

From the simulations, the **Rectangular cross section** design has lower residual stress and strain, and lower estimated displacement compared to the other two designs. However, the **U-shaped** design is easier to fabricate and has a smaller volume. Therefore, further analysis and comparison between the *Rectangular* and *U shape* cross sections is performed in subsubsection 10.1.5.

10.1.5 Final selection of cross section and selection of material

The Rectangular cross section and the U shape one are optimized for both Aluminium 6061 and Stainless Steel 1035.

$$I_{\text{rect}} = \frac{base_{\text{out}} * height^3{}_{\text{out}}}{12} - \frac{base_{\text{in}} * height^3{}_{\text{in}}}{12} \tag{33}$$

$$I_{\text{ushape}} = \frac{(height - 2thickness) * thickness^3}{3} + 2\frac{base * thickness^3{}_{\text{in}}}{3} \tag{34}$$

From Equation 31 and Equation 32, the dimensions of the cross-sectional area can be optimized. Since the beam must support the motors, the footprint must be at least equal to the diameter of the gearmotors (22 mm to 40 mm). In addition, the thickness of the cross section is set between the standard values, because it is better to make the beams from standard components to reduce the overall cost of the system. The standard thicknesses are between 1 and 10 mm with a gradation of 0.5 mm [5], [17].
To perform the calculations and optimize the cross section area, a preselection of the rotation motor in $J_{rcm}2$ is made. A gearmotor with a diameter of 32 mm and three gear stages is selected, Table 19 motor LRPX 32-090. This motor provides a continuous torque of 5.6 Nm and has a mass of 336 g. This results in a width of the cross section area of 32 mm. Moreover, in the calculations, the two beams are considered as a single elongated beam, while all supports (connectors, flanges, bolts, screws) are neglected. For this reason, a safety factor is applied to the selected optimized values. The optimization of thickness and height is performed using a genetic algorithm in Matlab. The inertia is defined as Equation 10.1.5 and Equation 10.1.5, and the inequality constraint to be satisfied is Equation 37 $\leq$ 0.355 mm. The forces acting on the robotic arm are shown in Figure 84, where vector w is the weight of the gearmotor in the second revolute joint, vector u is the weight of the linear motor, and vector u is the weight of the instrument and the instrument actuator. DI is the distance between the application point of the motor and its center of mass. This value is determined using the CAD model of the gearmotor [11]. The value for the LRPX 32-090 motor with 3 gear stages is 49.2 mm.

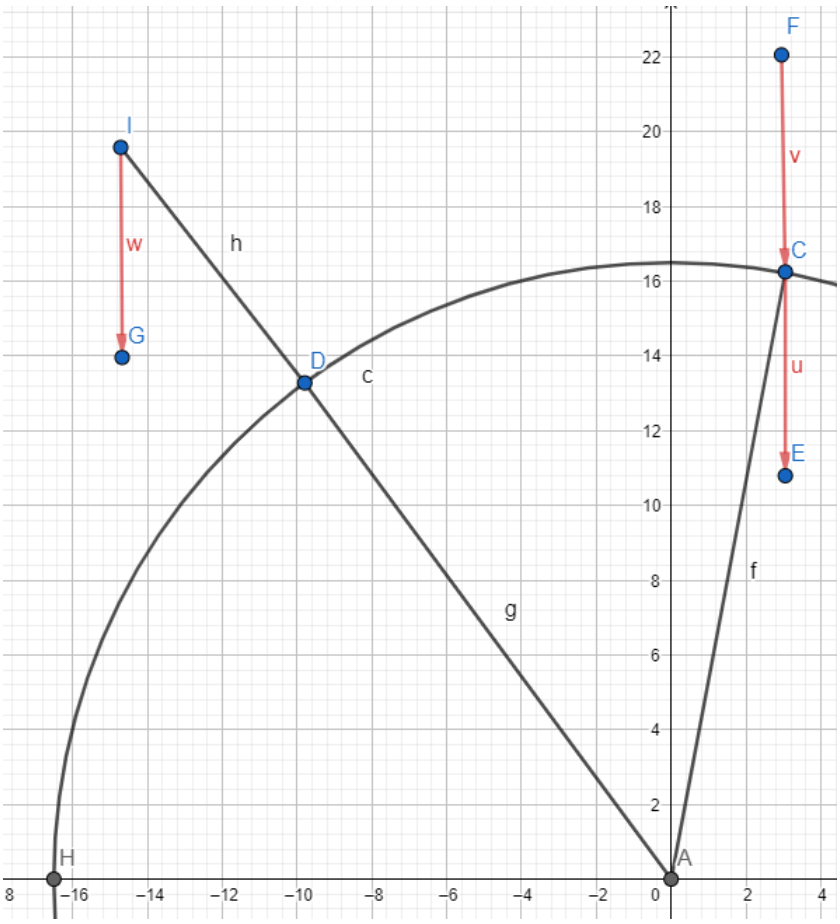

Figure 84: Schematic of the forces applied for the inertia calculation

It is, then, possible to define the overall deflection as in Equation 37.

$$deflection_{\mathrm{y1}} = \frac{(v+u)R^3}{EI}[(\alpha 2+\alpha 1)(0.5+c^2(\pi-\alpha 2-\alpha 1))+0.75s2(\pi-\alpha 2-\alpha 1)] \tag{35}$$

$$deflection_{\mathrm{y2}} = -\frac{(wh)R^2}{IE}[(\alpha 1)(0.5+c^2(\pi-\alpha 1))+0.75s2(\pi-\alpha 1)] \tag{36}$$

$$deflection_{\mathrm{y}} = deflection_{\mathrm{y1}} + deflection_{\mathrm{y2}} \tag{37}$$

The Matlab code for the optimization is reported in section 24. The optimization is performed for both the hollow Rectangular cross section and the U shaped cross section, and for Aluminium 6061 and Stainless Steel 1035. The results are reported in Table 21.

Table 21: Optimized cross section parameters: t is the thickness, h is the height

Aluminium 6061			**Steel 1035**		
Rectangular			*Rectangular*		
	t	3.7371 mm		t	2.7069 mm
	h	11.8815 mm		h	8.4634 mm
U shape			*U shape*		
	t	5 mm		t	3.7991 mm
	h	10.0247 mm		h	7.5971 mm

Additional important parameters are displayed in Table 22.

Table 22: Parameters for the two cross section areas in two materials

	Rectangular	**U shape**
Aluminium 6061		
Area	272.1145 mm ^{2}	210.2475 mm ^{2}
Mass/Length	0.7347g/mm	0.5677 g/mm
Height	11.8842 mm	10.0247 mm
Steel 1035		
Area	189.7533 mm ^{2}	150.4284 mm ^{2}
Mass/Length	1.4896 g/mm	1.1809 g/mm
Height	8.4634 mm	7.5971 mm

From the Table 22 it is evident that the U-shaped shape cross section area reduces both mass and dimensions. For this reason, the **U-shape cross section area** is chosen for the beams.
For both materials, a study of the stress and strain on the structure is performed. Once the cross-section is selected, the standard dimensions are studied in more detail. The values established are based on the fact that the width must be at least 32 mm, and the values found in Table 21 are taken as indicators and a safety factor is applied. The standardized dimensions of the cross-section area are given in Table 23, [1], [34], [2], [36], [38], [20], [18].

Table 23: Standardize dimensions of cross section: t is the thickness, h is the height, w is the width

	U shape
Aluminium 6061	
t	5 mm
h	15 mm
w	35 mm
Steel 1035	
t	4 mm
h	10 mm
w	35 mm

These profiles are tested on SolidWorks. The results of the simplified simulations with the dimensions found in Table 23 are reported in Figure 85 and Figure 86.

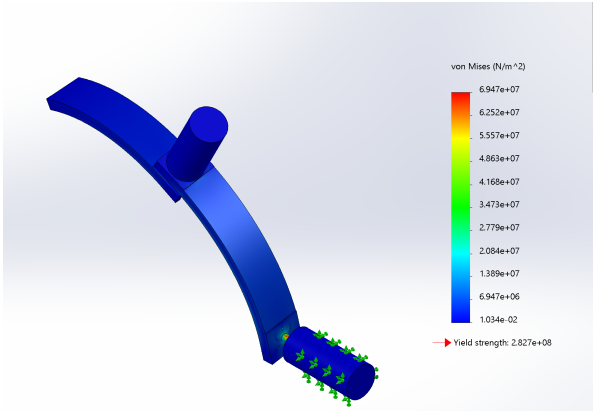

(a) U shape steel cross section area stress

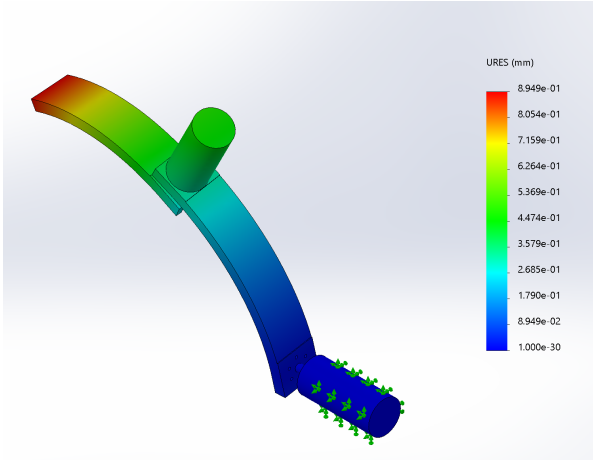

(b) U shape steel cross section area displacement

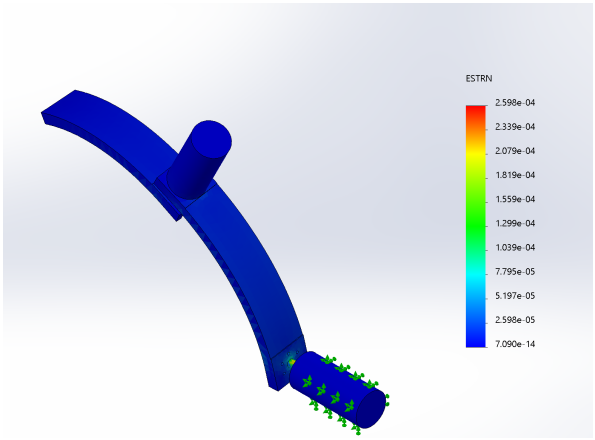

(c) U shape steel cross section area strain

Figure 85: Results of the simulation for the U shape steel cross section area assembly

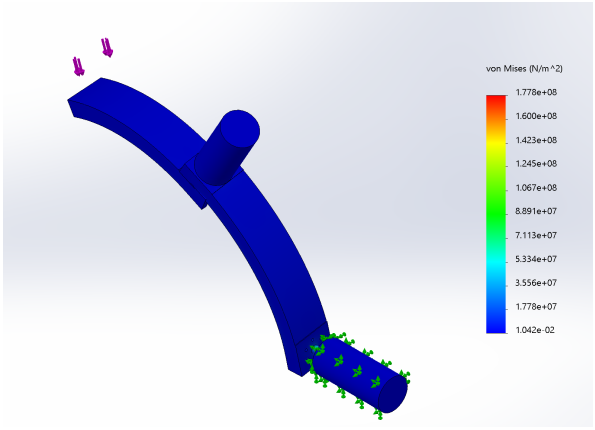

(a) U shape aluminium cross section area stress

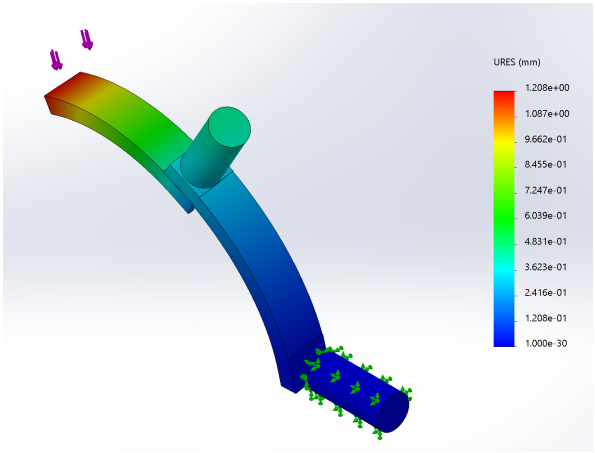

(b) U shape aluminium cross section area displacement

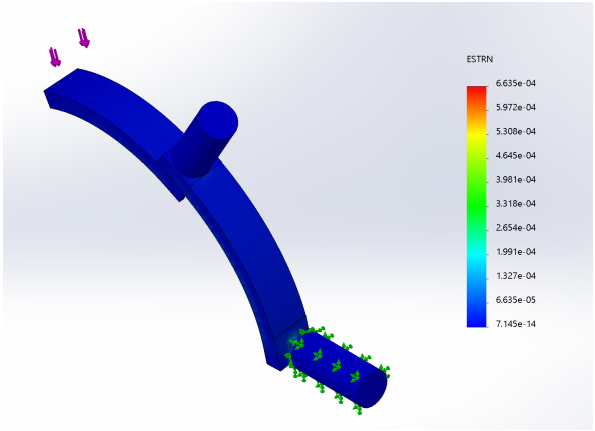

(c) U shape aluminium cross section area strain

Figure 86: Results of the simulation for the U shape aluminium cross section area assembly

It is clear from Figure 85 and Figure 86 that the dimensions of the cross section area must be further optimized. This is done by iterating the dimensions in SolidWorks. Before that, however, the connections between the gearmotors and the beams are designed. Their design affects the stress, strain and maximum displacement of the structure.

10.1.6 Design of connectors

The RCM mechanism requires four connectors:

- a connection in $J_{rcm}1$, between the first arced beam and the first gearmotor;
- a connection between the second motor and the two beams. It is decided to insert the gearmotor in $J_{rcm}2$ on top of the first beam, so that the dimensions of the bended beam remains small. This means that the gearmotor in $J_{rcm}2$ is fixed on top of the first beam but has to rotate the second one.
- a connection between the end of the second beam and the linear system.
- a connection between the linear system and the instrument.

The constraints on the *first and the second connections* are the following:

- The shape of the attaching area is a circle of diameter equal to 32 mm.
- The screws present are M3x0.5 6H are are positioned as shown in Figure 87.

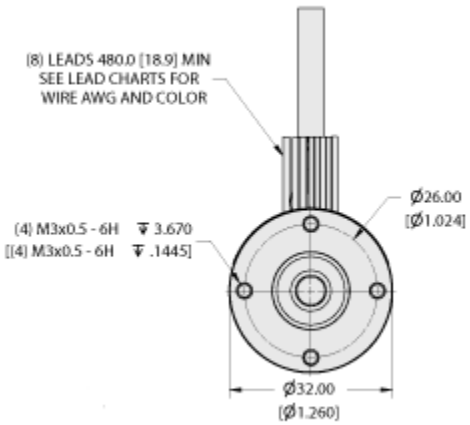

Figure 87: Outline drawing of the gearmotor LRPX32, front view[11]

The **first connection** can be made with a universal mounting hub for a 6 mm shaft, as shown in Figure 88, and then connect the universal mounting hub to the rotating armature, thought six M3 screws, Figure 89. These components are selected from existing catalogs to reduce manufacturing costs. For the universal mounting hub, [39] [31] [23], the **Pololu Universal Aluminum Mounting Hub for 6mm Shaft, M3 Holes** [39] is selected. The design of the hub is shown in Figure 90. In addition, a *flange* is added, Figure 91, to increase the strength of the system and distribute the load. The dimensions of the flange match those of the motors and are optimized to match the pattern of the bolts on the motors, Figure 91. The overall design of $J_{rcm}1$ is shown in Figure 93.

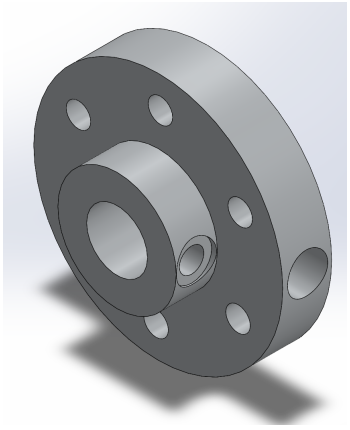

Figure 88: Components designed from the specification of the Pololu Universal Aluminum Mounting Hub for 6mm Shaft, M3 Holes

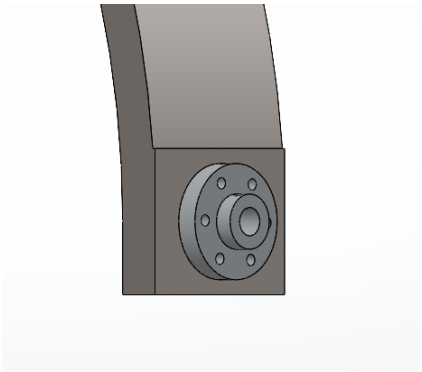

Figure 89: Connection between the Universal Aluminum Mounting Hub and the beam

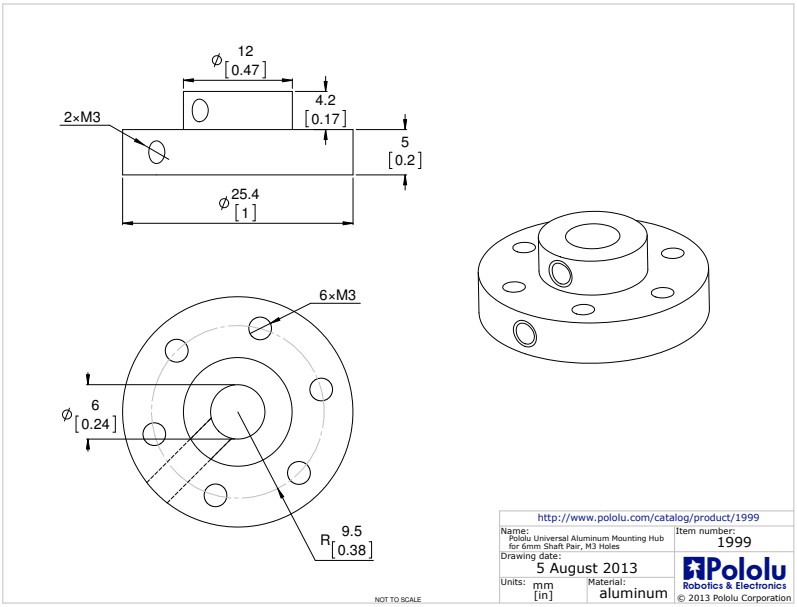

Figure 90: Overview of the Pololu Universal Aluminum Mounting Hub for 6mm Shaft, M3 Holes

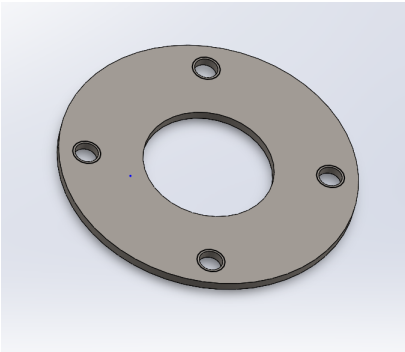

Figure 91: Flange that connects to the motor in revolute joint 1 and 2

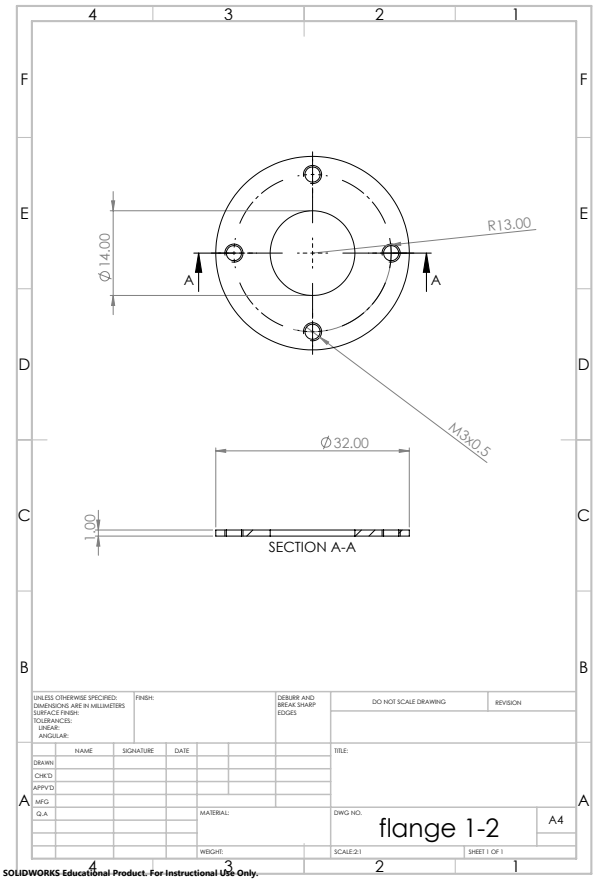

Figure 92: Overview of the design of the flange

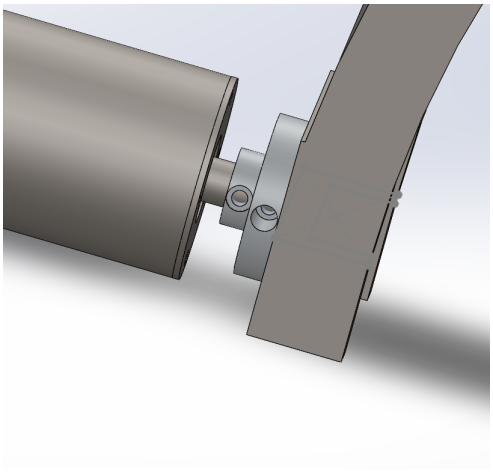

Figure 93: Final assembly of revolute joint 1

The **second connector** is used to fix the motor to the beam 1 and allows the rotation of the beam 2. In this case, the connection between the second motor and the first beam is made by means of a *flange*. The upper part of the flange enables direct fastening of the motor to the first beam, which is provided with appropriate screw holes, Figure 94. The shaft then features a universal mounting hub, Figure 88, to attach the rotating shaft to the beam 2. The overall connection is shown in Figure 95.

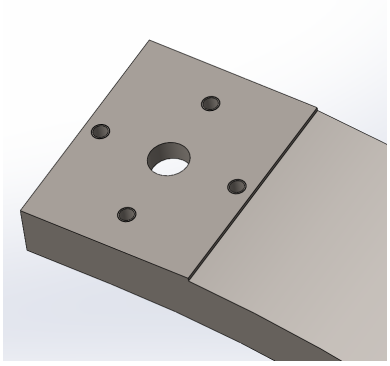

Figure 94: Screw's holes for coupling the beam one to the flange and the motor in revolute joint 2

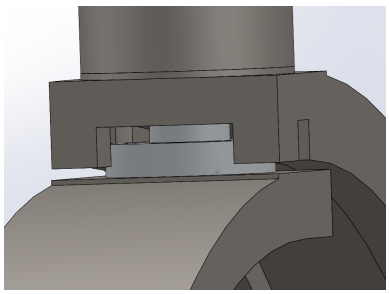

Figure 95: final assembly of revolute joint 2

For the third and the fourth connectors, the CAD model of the linear actuator was not found, thus the pattern of the holes in the flanges are approximated using the Figure 96, details in section 26.

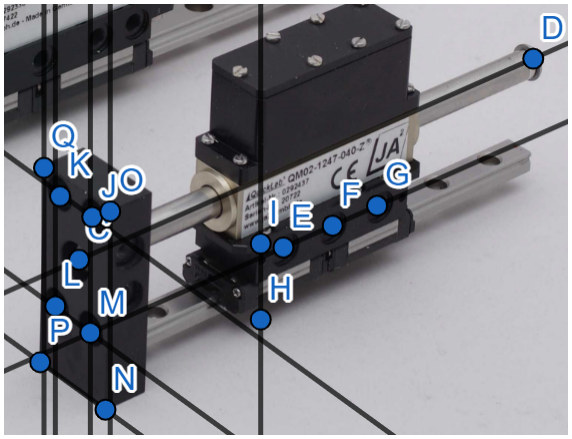

Figure 96: Dimension of the hole patterns in the linear actuator [41]

The constraints about the *third connection* are, thus, the following:

- The shape of the attaching area is composed by two parallel rectangles with dimensions 20 mm x 22 mm, and at a distance equal to 30 mm.
- The screws present are M3 and are positioned as shown in Figure 96, represented by the point E, F, G.

The design of the beam two is modified such that it presents the required mating surfaces, as shown in Figure 97 and in Figure 98.

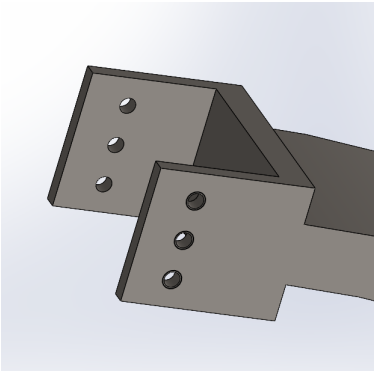

Figure 97: Profile of the beam 2 that connect the linear actuator

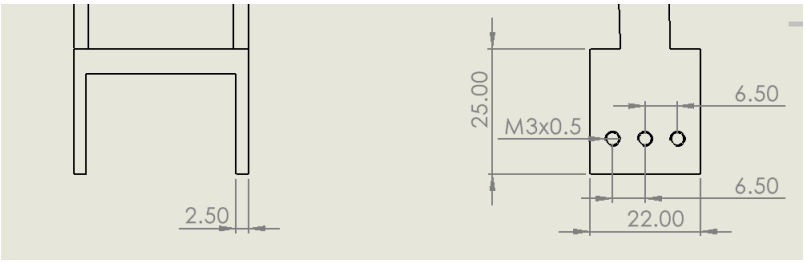

Figure 98: Drawing of the beam two that connect the linear actuator

The constraints about the *fourth connection* are the following:

- The connector has to attach to the linear module through M3 screws, with a pattern identified by K, J, L, M in Figure 96.

- The connector needs to attach the instrument's actuator flange, as in Figure 99

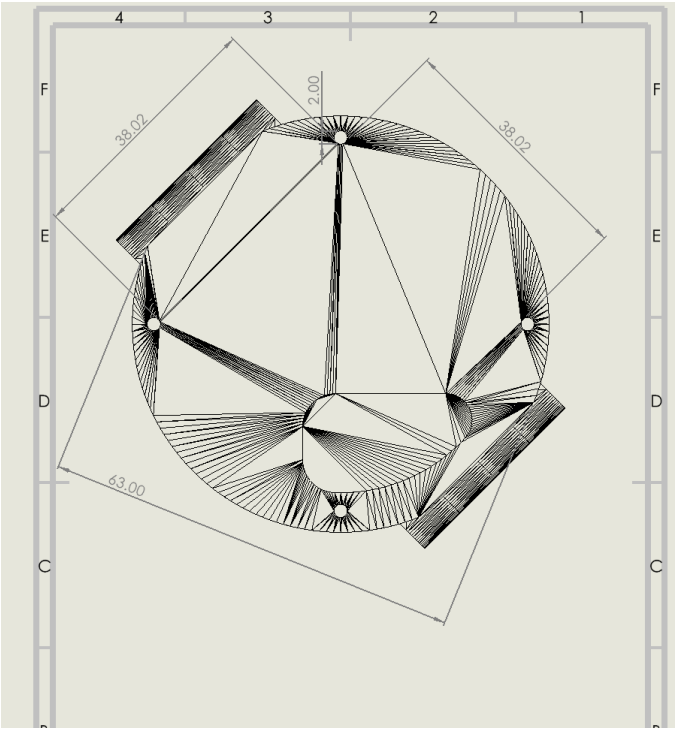

Figure 99: Outline drawing of the flange for connecting the instrument's actuator

- The screws present on the flange for connecting the instrument's actuator are M2.

The **fourth connection** is done by using a plate which attach both the interfaces, as shown in Figure 100.

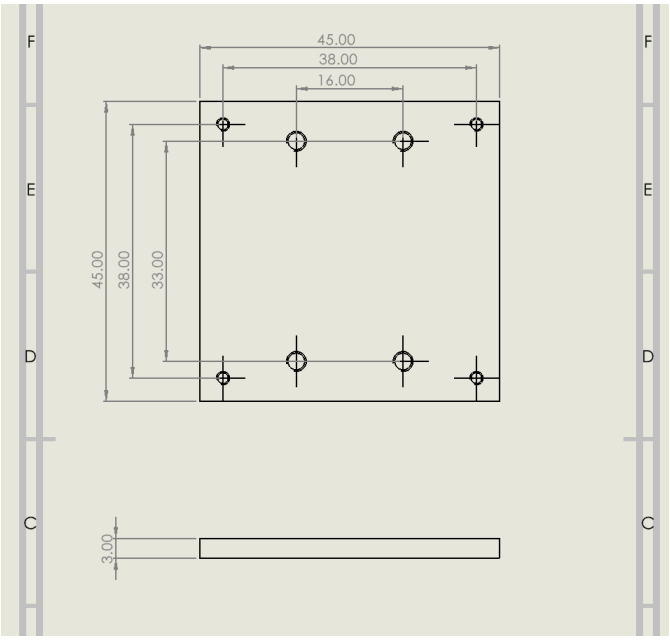

Figure 100: Flange connecting the linear actuator with the instrument's actuator

10.1.7 Finalizing the dimensions of the arced beams

After designing the connectors, an iterative approach was used in SolidWorks to finalise the dimensions of the cross sections. In this case, the two beams are treated separately, and the motors are represented by a hollow steel cylinder whose mass and centre of mass correspond to the selected motors. Finally, the linear module and the weights of the actuator and the instrument are simulated by a vertical force acting on the beam 2. Also, all the connectors are inserted in the assembly. The dimensions of the thickness and height of the two beams are iterated, starting from the optimal solution found in Matlab and increasing/decreasing it by 0.5 mm. The iterations performed for the aluminium profiles showed a large difference between the values calculated in Matlab and the actual value required. The total values had to be more than double to obtain a stable design that would meet the required maximum displacement. For this reason, it was decided to proceed with the 1035 steel beam. An overview of the stress, strain and displacement of the assemblies made of steel and aluminium is given in Figure 86 and Figure 85 as a reference of the initial values. The iterations show as solution the one present in Table 24.

Table 24: Final dimensions of the beams: w is width, h is height, t is thickness

Arm 1	
t	7 mm
h	13 mm
w	35 mm
Arm 2	
t	3 mm
h	10 mm
w	35 mm

Finally, the distance between the two arms is calculated using SolidWorks and corresponds to the 14 mm along the y_l axis. This distance is chosen so that the motor shaft is fixed on top of the flange and can reach the inner surface of beam 2. The Pololu Universal Aluminum Mounting Hub for 6mm Shaft, M3 Holes is inserted into the gap to connect the rotating shaft of the motor to the beam 2. As a result, there is a collision between the side wall of the U-profile of the beam 1 and the universal motor hub. For this reason, a cylinder with a diameter of 25.5 mm is cut from beam 1 in accordance with the hub. Also, two of the four holes that allow the connection between the gearmotor and the beam 1 are made on the side wall of the U-profile. To facilitate the assembly of the robotic arm, a square parallelepiped with an edge of 7 mm and a height of 6 mm is cut out of beam 1, corresponding to the steps. The details of the connecting zone in beam 1 are shown in Figure 101.

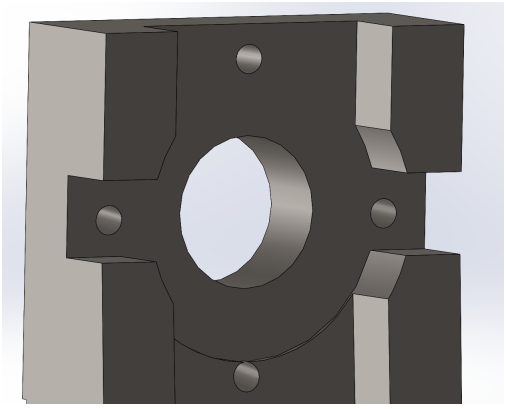

Figure 101: Connecting design of the arm 1

The design of the beams is summarized in Figure 102.

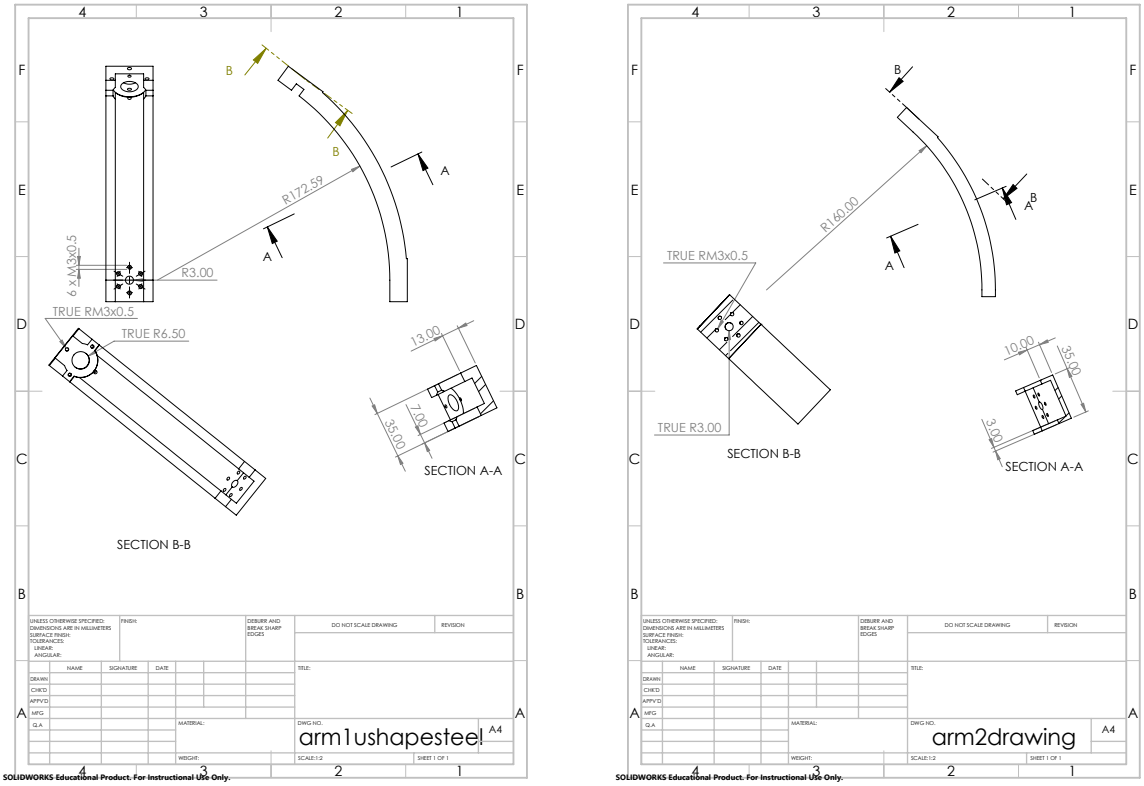

Figure 102: Drawing and dimensions of beam 1 (right) and beam 2 (left)

The structure is tested in static. The first test is done considering the linear actuator, the instrument, and instrument's actuator as forces acting on the edge of the beam 2 directly. This is considered the worst case scenario when the configuration of the arm is planar extended. The results are shown in Figure 103.

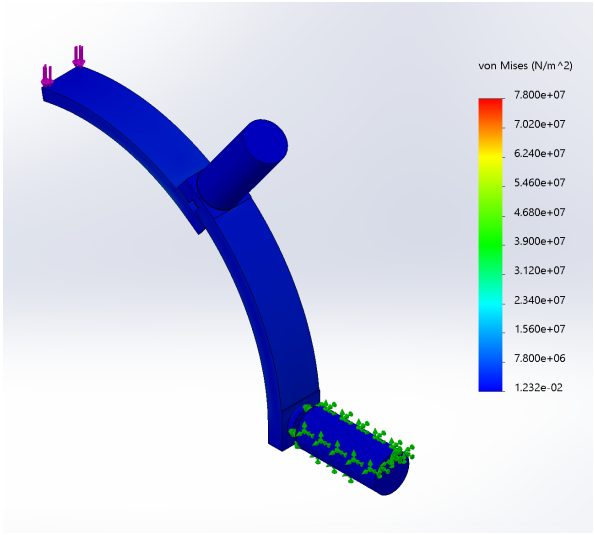

(a) U shape steel cross section area stress: final design

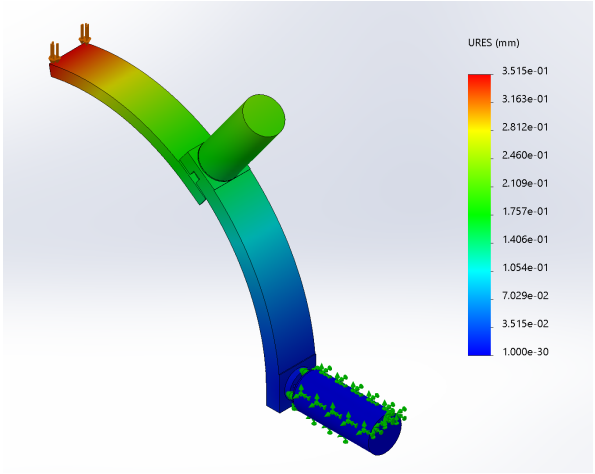

(b) U shape steel cross section area displacement: final design

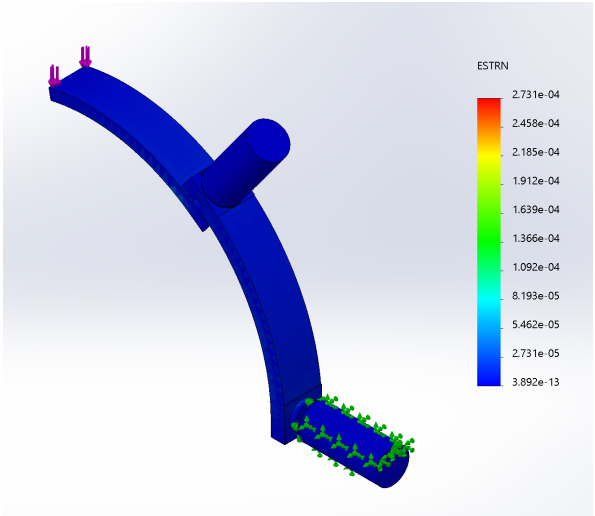

(c) U shape steel cross section area strain: final design

Figure 103: Results of the simulation for the U shape steel cross section area assembly in extended configuration: final dimensions

However, in the the elbow configuration, the main effect of the instrument and instrument's actuator is the development of a moment. Therefore, a new model where a hollow cuboid with the dimensions and weight of the linear module is attached was developed to simulate this condition. The weight of the actuator acting on a rod has its greatest effect at a distance equal to the maximum of d (13 cm) from the center of the beam 2. This is simulated by applying a force at the end of the parallelepiped equal to the weight of the instrument and the instrument actuator. The results are displayed in Figure 104.

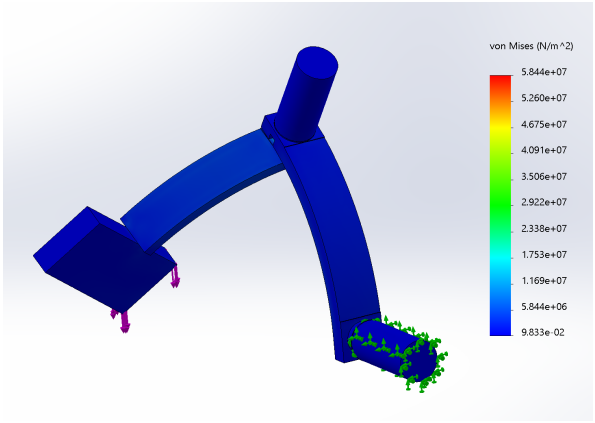

(a) U shape steel cross section area stress: final design

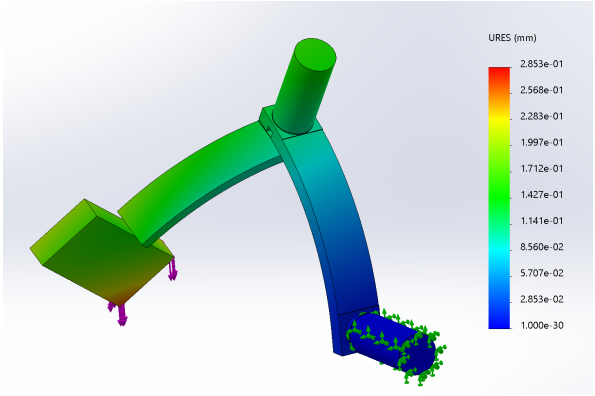

(b) U shape steel cross section area displacement: final design

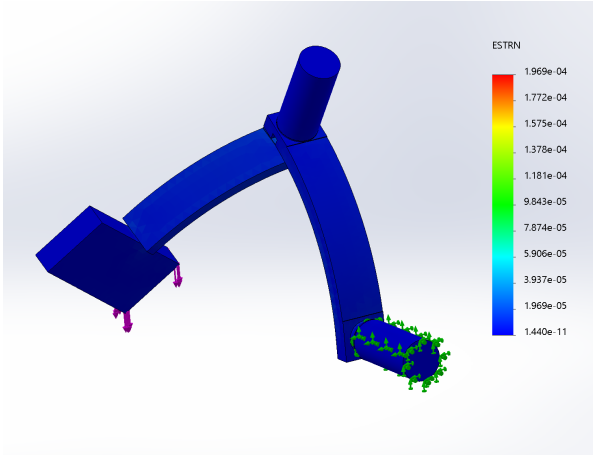

(c) U shape steel cross section area strain: final design

Figure 104: Results of the simulation for the U shape steel cross section area assembly in elbow configuration: final dimensions

Since the structure does not experience any high stress or strain, the dimensions are finalized.

Thus, torque calculation can be performed, and the gearmotors can be finalized.

10.2 Torque calculation for selecting the right rotational motor

Once all the components have been designed, it is necessary to check that the selected gearmotors can apply the torque necessary for holding the arm in place and moving it. The torque can be expressed as:

$$Torque\ (\tau) = Inertia\ (I)\ x\ Angular\ acceleration\ (\alpha) \tag{38}$$

$$Torque\ (\tau) = Force\ (F)\ x\ Length\ (L) \tag{39}$$

The angular acceleration of the robotic arm in this application is small compared to the acceleration due to gravity. Therefore, it is possible to size the rotation motor so that the first equation is valid. In order to estimate the required torque at each joint, the worst case scenario must be chosen. The scheme of forces and dimensions is shown in Figure 105 and Figure 106. The values related to the center of mass of the two beams and the two rotating motors were extracted from SolidWorks. The linear module, instrument, and instrument's actuator are assumed to exert a force on the edge of beam 2. The final required torques for $J_{rcm}1$ and $J_{rcm}2$ are calculated, section 25,and are equal to:

- $\tau 1 = 2.837158\ Nm$
- $\tau 2 = 0.65836\ Nm$

The torques found are smaller than the ones delivered by the gearmotors and the velocities are higher than required. Thus, it is possible to downsize them.

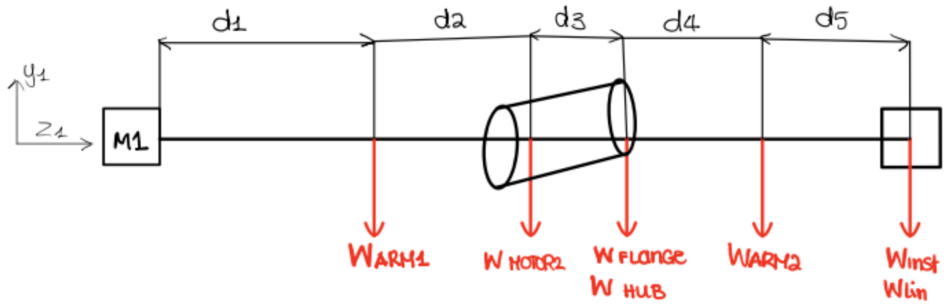

Figure 105: Schematic for torque calculations of motor in first revolute joint

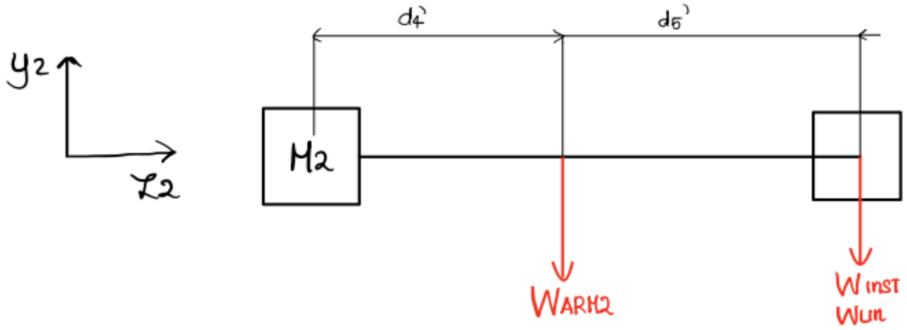

Figure 106: Schematic for torque calculations of motor in second revolute joint

10.2.1 Resized rotational motors

After calculating the required torque, it is possible to downsize the motors, reducing the mass and dimensions of the overall system.
The motor in $J_{rcm}2$ must provide a torque of $\tau 2 = 0.65836$ Nm. This requirement is fulfilled for the **Gearmotor LRPX32-90V12–019**. This motor has 2 gear stages and has a mass of 310 g. This is used in the equation to calculate the torque of $J_{rcm}1$. This results in a torque $\tau 1 = 2.82541$ *Nm*. This torque can be supplied by the **Gearmotor LRPX32-90V12-076**. These motors meet the required speed.

The structure is modified on SolidWorks, and tested again. The results are shown in Figure 107 and Figure 108. These tests show that the stress, displacement, and strain satisfy the requirements.

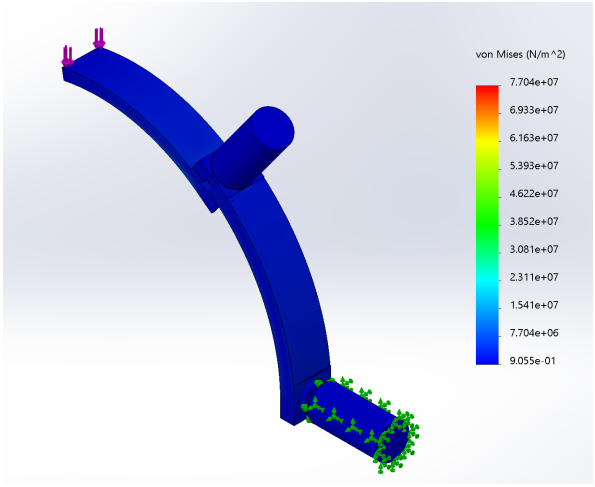

(a) U shape steel cross section area stress: final design

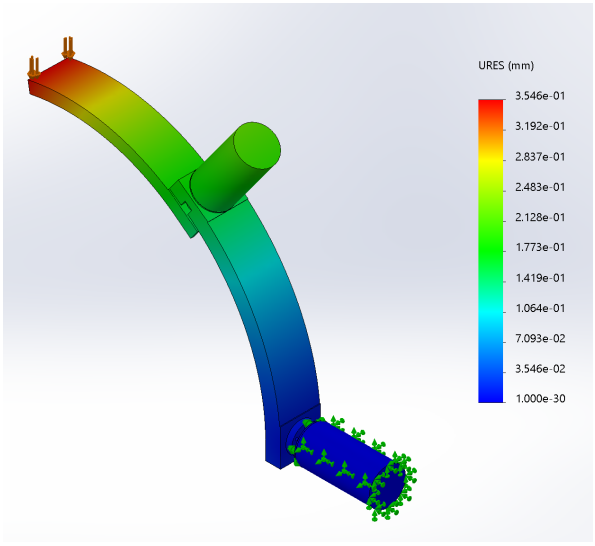

(b) U shape steel cross section area displacement: final design

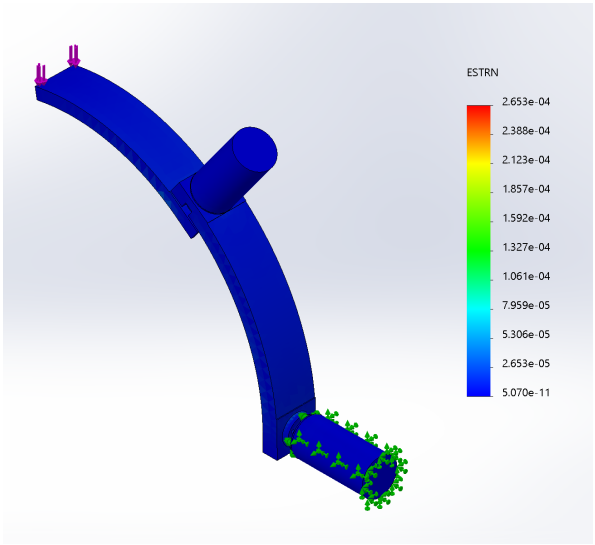

(c) U shape steel cross section area strain: final design

Figure 107: Results of the simulation for the U shape steel cross section area assembly in extended configuration: final motors

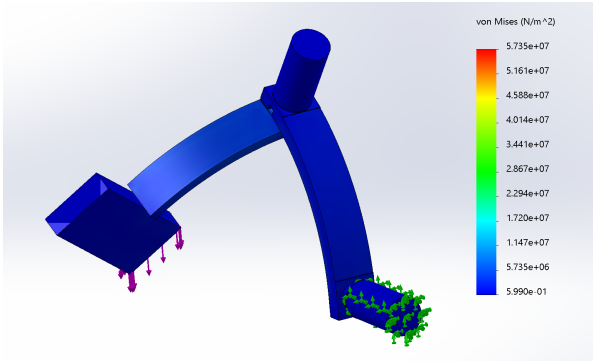

(a) U shape steel cross section area stress: final design

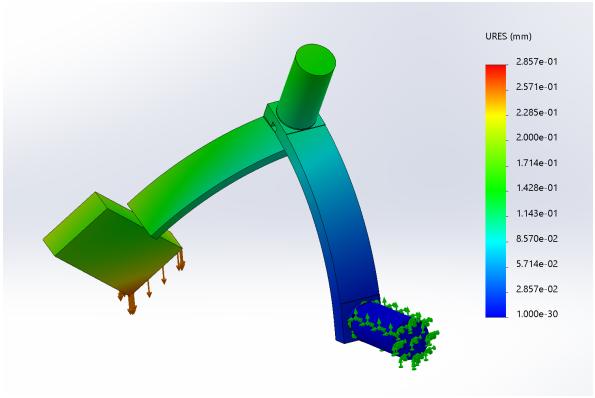

(b) U shape steel cross section area displacement: final design

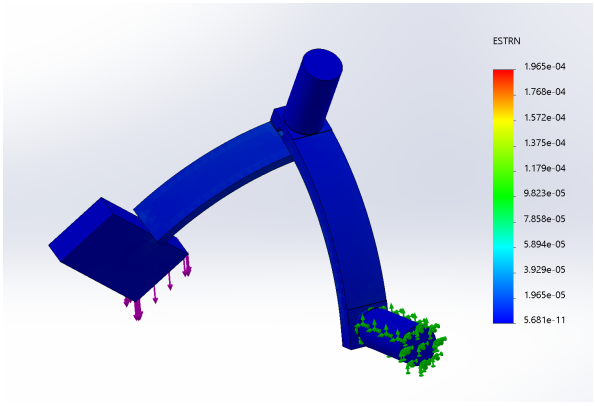

(c) U shape steel cross section area strain: final design

Figure 108: Results of the simulation for the U shape steel cross section area assembly in elbow configuration: final motors

10.3 Final design of the RCM mechanism

The final design of the RCM mechanism is summarized in Figure 109 and in Figure 110.

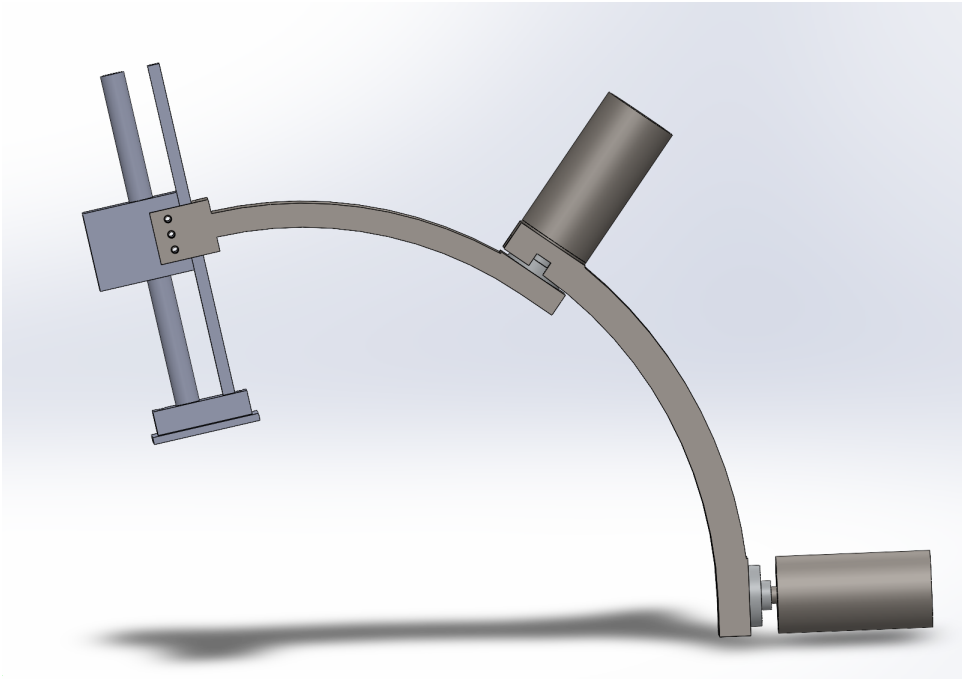

Figure 109: 3D view of the final design of the RCM mechanism

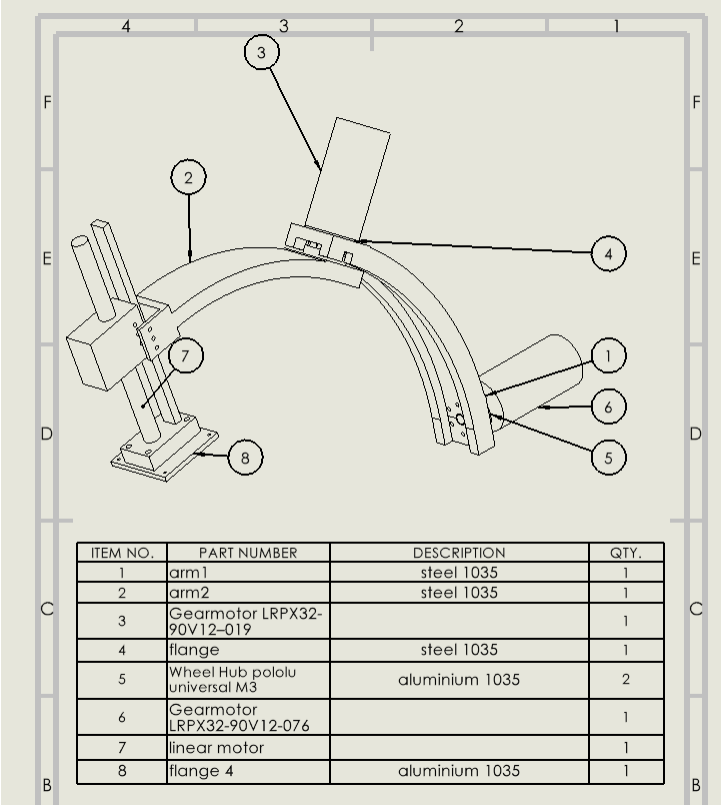

ITEM NO.	PART NUMBER	DESCRIPTION	QTY.
1	arm1	steel 1035	1
2	arm2	steel 1035	1
3	Gearmotor LRPX32-90V12–019		1
4	flange	steel 1035	1
5	Wheel Hub pololu universal M3	aluminium 1035	2
6	Gearmotor LRPX32-90V12-076		1
7	linear motor		1
8	flange 4	aluminium 1035	1

Figure 110: Drawing of the final design of the RCM mechanism with bill of material

11 Design of the global alignment mechanism

In this section, the global alignment mechanism is designed. The main goal of the design is to maintain low weight and size. Additionally, it is preferable to have out of shelf or easily manufacturable pieces.

11.1 Connection between the global alignment and the RCM mechanism

This subsection discusses the connection between the RCM mechanism and the alignment mechanism. The global alignment system and the RCM mechanism connect $J_{rcm}1$ to J_a4. J_a4 is assumed to have a flat surface on which screw holes can be placed. The connection has a flat mating surface that screws into the slider, and two vertical surfaces that screw into the front and back of the motors. This replaces the *flange* present in $J_{rcm}1$. The design is shown in Figure 112. The connection to the gearmotor refers to the pattern in Figure 87 and Figure 111. The alignment mechanism and flange must be sized so that the point on the axis of rotation of $J_{rcm}1$, which is 16.5 cm from the centre of rotation of the RCM mechanism, can move 0.8 cm forward and 6.4 cm backward on the slider. The sizing of this connector is presented in the following sections.

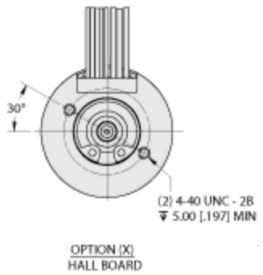

Figure 111: Outline drawing of the gearmotor LRPX32, back view [11]

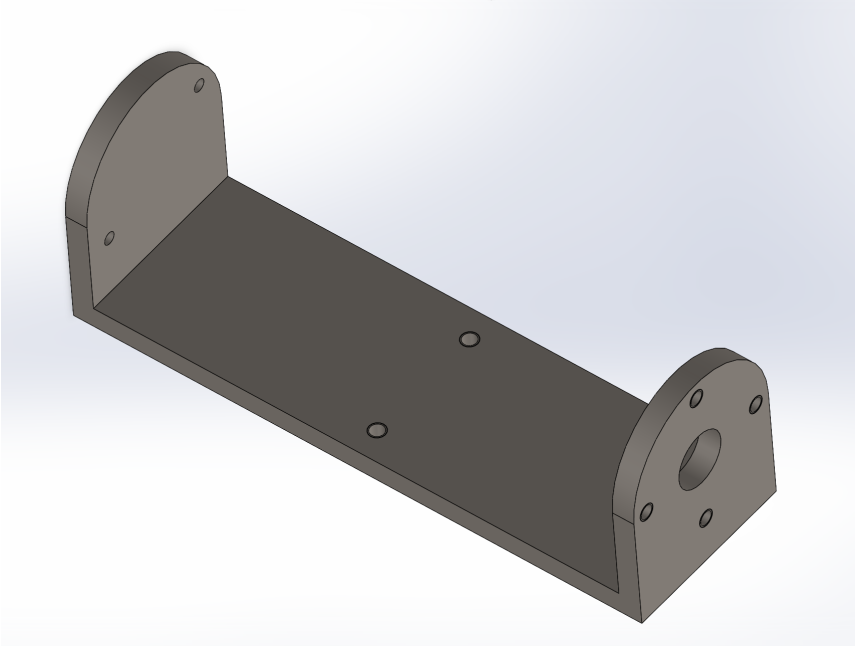

Figure 112: 3D representation of the connector between the alignment and the RCM mechanism

11.2 Mechanical design of the alignment mechanism

In this subsection, the design of the alignment mechanism is discussed, referring to the different parts of the design as presented in the Figure 113.

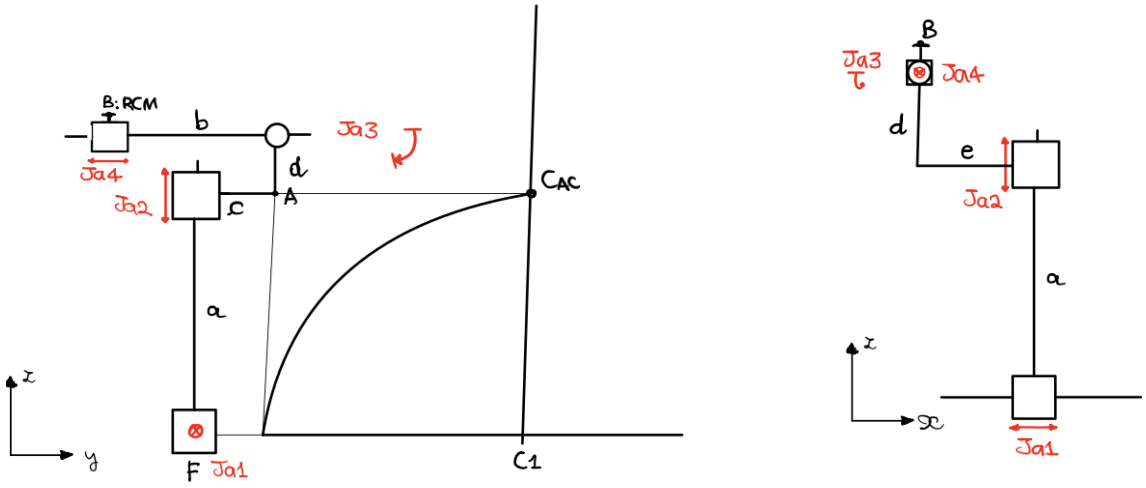

Figure 113: Parameterized design of the alignment mechanism

The design consists of the analysis of the following joints:

- J_a1: This joint allows movement along the x-axis. It slides directly on the rail on the side of the surgical bed. It must be lockable.
- J_a2: This joint allows for translation along the beam a. It was decided to have a range of motion of 6 cm, but it is possible to make the beam a fully compatible with the slider. This increases the possible range of motion along the z axis of the alignment mechanism.
- J_a4: This joint allows displacement along the beam b. The RCM mechanism must be mounted on it, using the flange presented in Figure 112.

In addition, there are some constraints on the dimensions of the mechanism.

- *Distance Ay-*C_{ACy}: Distance between J_a3 and the midpoint of the abdominal cavity along the y-axis. This distance must be 16.5 cm.
- *Distance Bz-*C_{ACz}: Distance between the point where the RCM mechanism is attached and the highest point of the abdominal cavity along the z-axis. This distance must be 4.42 cm.
- *Distance Fy-*C_{ACy}: Distance between J_a1 and the middle point of the abdominal cavity along the y-axis. This distance depends on the width of the surgical bed, which is 50.8 cm on average [45].

It is possible to divide the overall design in five parts, presented in Figure 114.

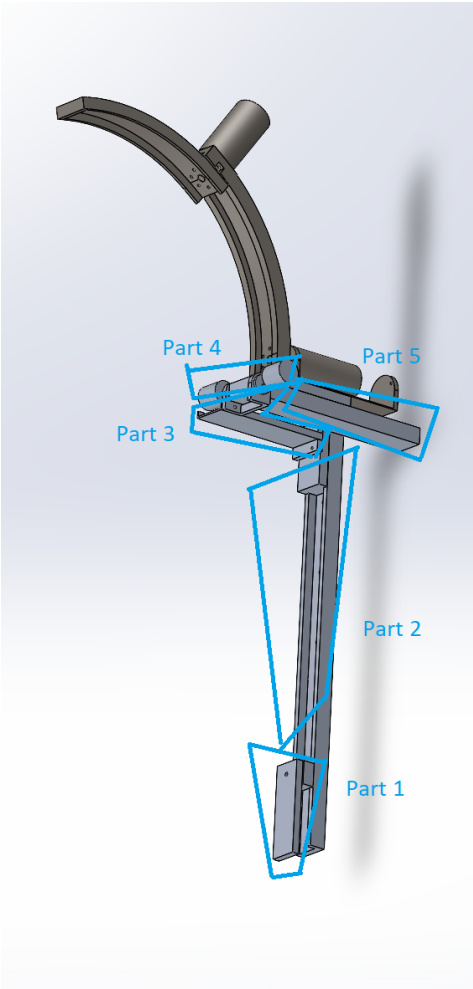

	Components
Part 1	J_a1
Part 2	beam *a*, J_a2
Part 3	beam *c*, beam *d*, beam *e*
Part 4	pin, base of the pin, J_a3
Part 5	beam *b*, J_a4

Figure 114: Overview of the 5 parts

In the following subsections, a deeper look in each of the parts is given, reporting the final design and the reasoning behind it.

11.2.1 Design of Part 1: Clamp and connecting beam

Part 1 allows the motion along the x-axis and is directly connected to the carriage along the operating table. It can be customized and fabricated, but there are already standard components that provide linear motion and blocking along the rail of the operating table. An overview of these components can be found in Figure 115. When designing the alignment mechanism, it is advantageous to mount a linear slider on top of J_a1, which allows J_a2 to move. These sliders usually have a rectangular shape. Therefore, J_a1 is chosen to have a rectangular mountage. The Bar Clamp - Standard is less expensive than the EZ Grip Bar Clamp and still meets the required functionalities. The standard dimensions of the cross section area of the bars that can be inserted into the clamp are 1" x 1/4" [37], [6] or 1" x 3/8" [48], [44]. The last selection is the **Standard clamp** compatible with a 1" x 1/4" rectangular section beam.

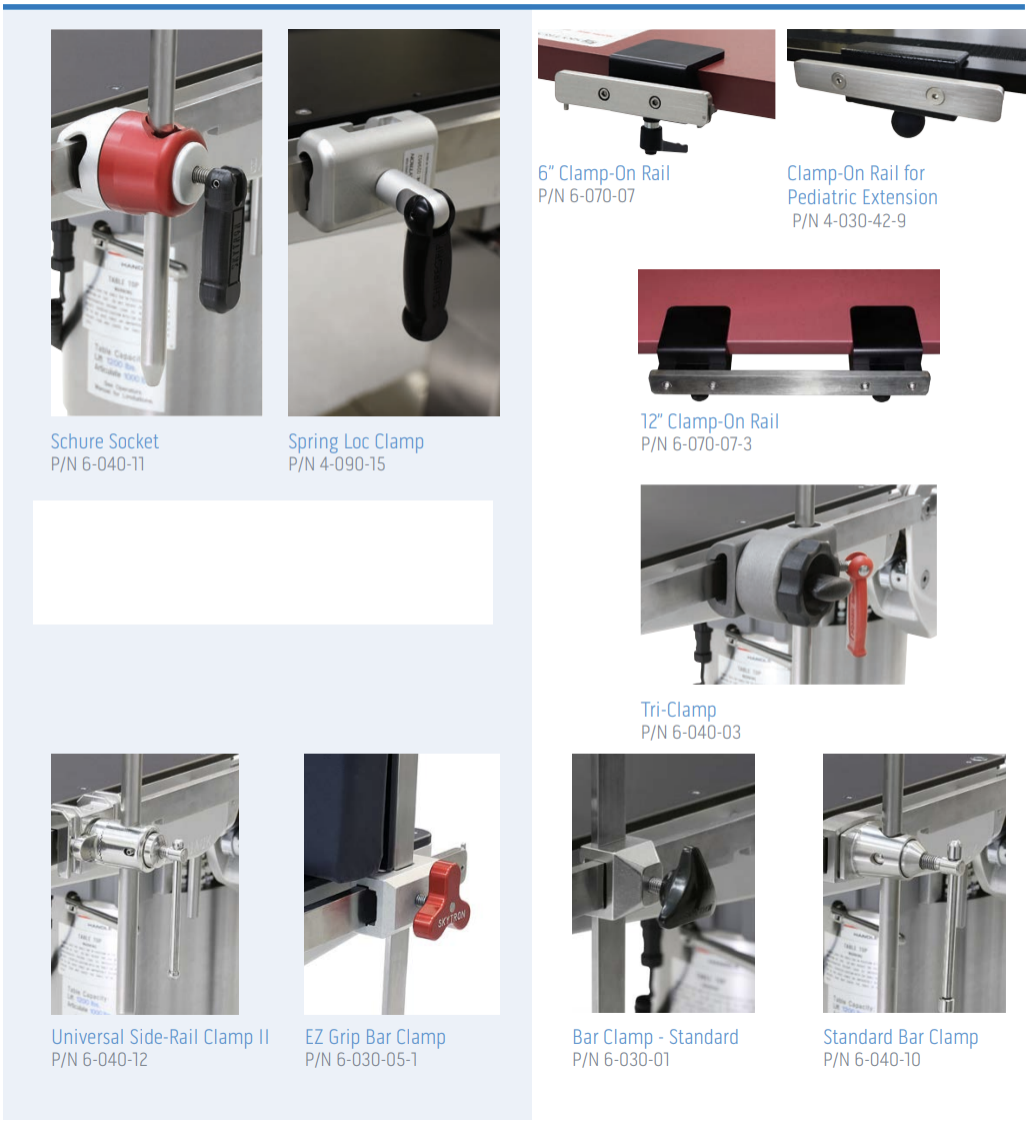

Figure 115: Clamps for the sliders alongside the surgical table [44]

11.2.2 Design of Part 2: Beam a and J_a2

Part 2 consists of a linear stage that allows the motion of J_a2. The linear stage is designed using standard components with a lockable joint that reduces weight and size. However, it was not possible to find a linear slider with a rectangular cross section area of 1" x 1/4". For this reason, the linear slider is connected to the clamp by a rod with a rectangular cross-section of 1" x 1/4" and a length of 80 mm. This rod has a screw hole that allows the connection to the linear module at a height of 70 mm. This calculation takes into account the height of the clamp (assuming it is 10 mm). The rod is shown in Figure 116.

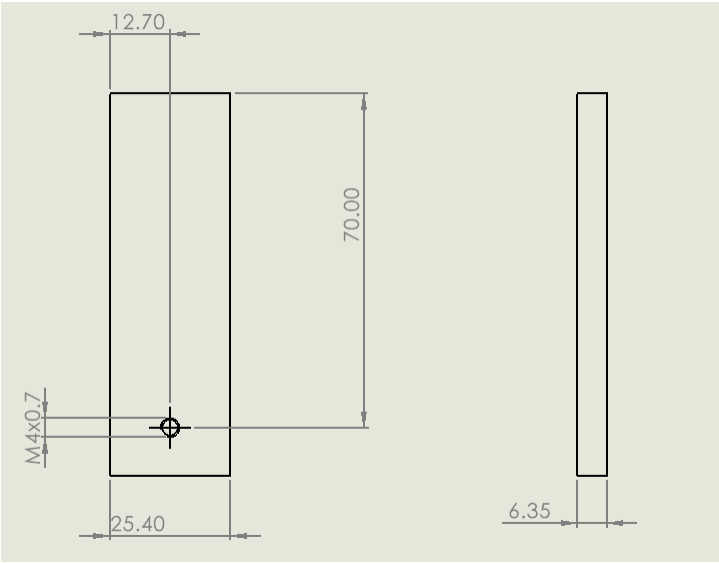

Figure 116: Design of the bar connecting the clamp to the linear system

Finally, a linear module is selected, [52], [42], [22]. It is decided to choose the smallest rail and slider, with dimensions given in Figure 117 and Figure 118. Also, the rail should have a maximum height of 33.1 cm from the terminal connection, so the total length of the rail must be 35.4 cm (33.1 cm + 2.3 cm). The end parts are closed with plastic masks to block sliding.

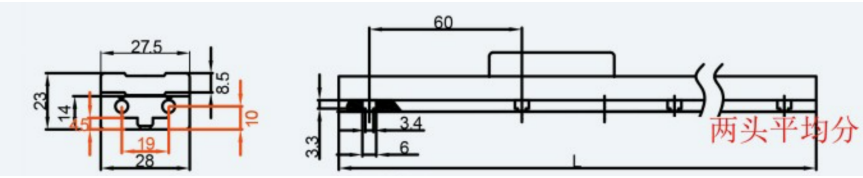

Figure 117: Dimensions of the smallest rail [52]

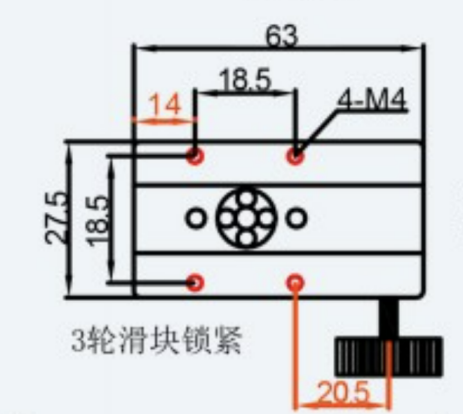

Figure 118: Dimensions of the slider [52]

11.2.3 Design of Part 5: Beam b and J_a4

Part 5 consists of a slider that allows the motion along the axis of $J_{rcm}1$. For the same reasons as *Part 1*, the same linear module is selected. Finally, a solid beam is attached to the end of the rail and a cylinder is cut into which the pin of the revolute joint can be inserted. The beam b is shown in

Figure 120, and the flange in Figure 91 is redesigned to minimize the length of the beam b, as shown in Figure 119. For a detailed calculation, see section 27.
In addition, it is necessary to insert a bolt hole in the beam b, which allows to connect and fix the beam to the pin of the revolute joint. Therefore, a tread is inserted 7 mm from the end of the beam b in Figure 120.

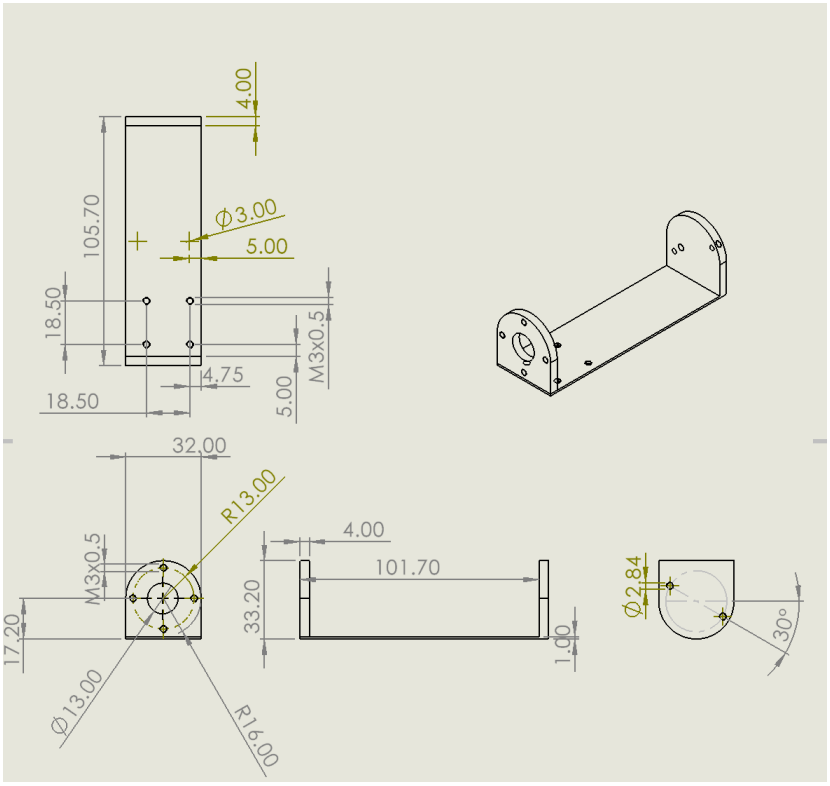

Figure 119: Redesign of flange connecting the RCM mechanism to the alignment mechanism

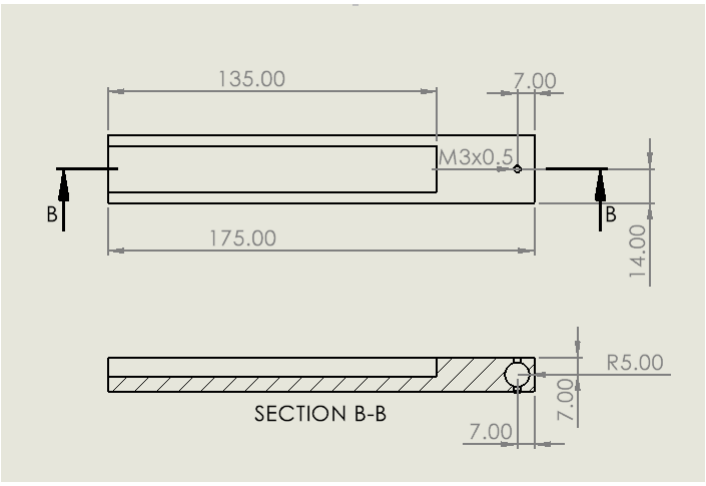

Figure 120: Design of beam b with slider width equal to 63 mm

11.2.4 Design of Part 3: Beam c, beam d, beam e

Part 3 consists of three beams. Beam d allows the center of rotation of the RCM mechanism to be positioned 4.42 cm above the highest point of the abdominal cavity along the z-axis. Beam c allows positioning J_a3 16.5 cm from the highest point of the abdominal cavity along the y-axis. Beam e

reduces the risk of collision with the components of the *Part 2* of the alignment mechanism.
The beams are dimensions such that the constraints in subsection 11.2 are satisfied. Additionally, bar e is composed by the thickness of the beam d and c.

To allow quasi-homogeneous stress and strain distribution, the cross section area of the beam d is dimensioned close to the dimensions of the slide rails. However, the internal dimensions of the U-shaped beam d are set to match the external dimensions of the slide rail plus 1 mm to allow for greater rotation in J_a3 without collision.
The cross section area of the beam c is instead optimized to satisfy the constraints in subsection 11.2 and avoid collision with other components of the mechanism. The length of the two beams is chosen to satisfy the constraints. In addition, a vertical surface is added to the end of beam c, which has a screw pattern corresponding to that of the slider, to allow the connection between beam c and beam a.

The final dimensions of the beams are reported in Figure 121 and in Figure 122.

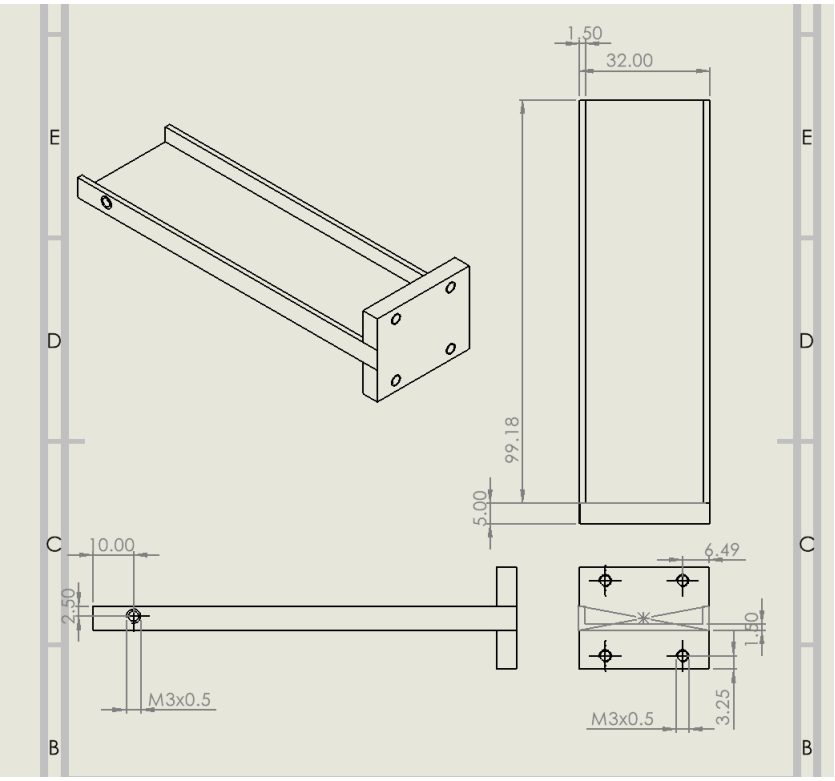

Figure 121: Dimensions of beam c

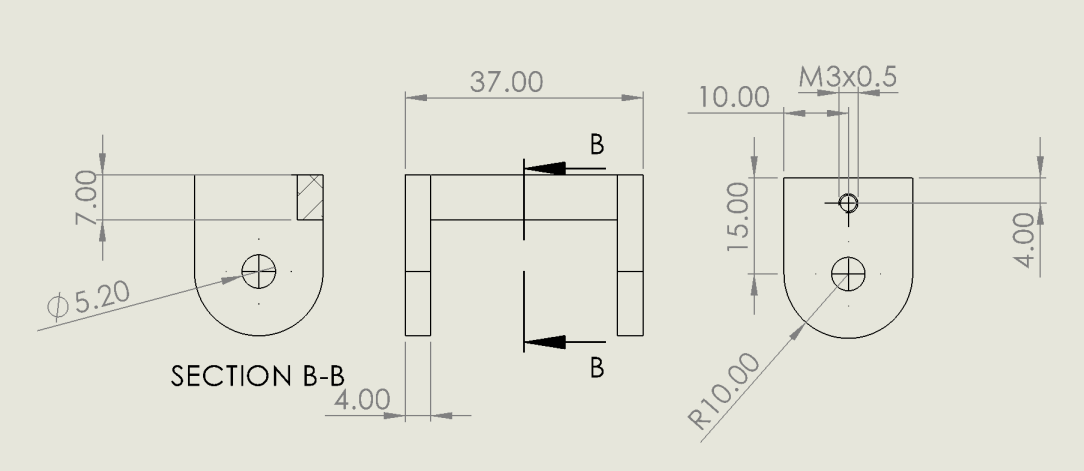

Figure 122: Dimensions of beam d

11.2.5 Design of Part 4: J_a3

Part 4 is composed of the J_a3. The revolute joint is lockable with two handles on the two sides of the beam d, which support the rotation and allow blocking by pressure screws. The handle is shown in Figure 123, and it is made of steel, with an end tip made of POM, to increase friction and hold the screws. Also, the head of the screws is a star knob to increase the strength of the handle. The pin is attached to the base with a screw. It is preferred to maximize the diameter of the pin so that it is less stressed. However, it is necessary to leave a free space to allow the pressure closure through the handles. It is therefore decided to set a diameter of 5 mm, Figure 124.
The revolute joint is supposed to be built on beam d. The pieces composing the revolute joint are welded to the beam d, and the final design of it is shown in Figure 125. The dimensions of 8 mm shown in Figure 125 is given by the fact that the beam b has to rotate 90°.

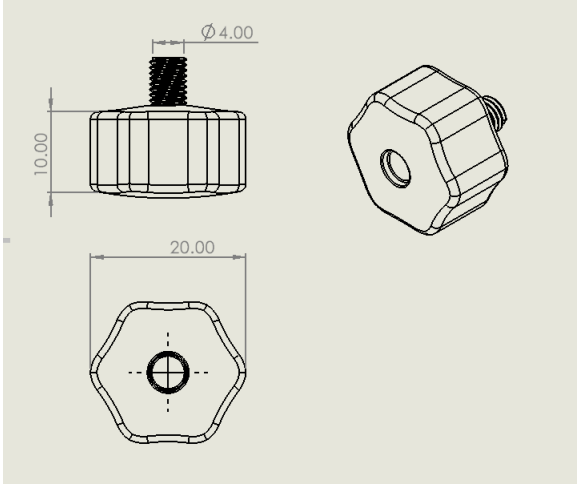

Figure 123: Dimension of handle for locking the beam b

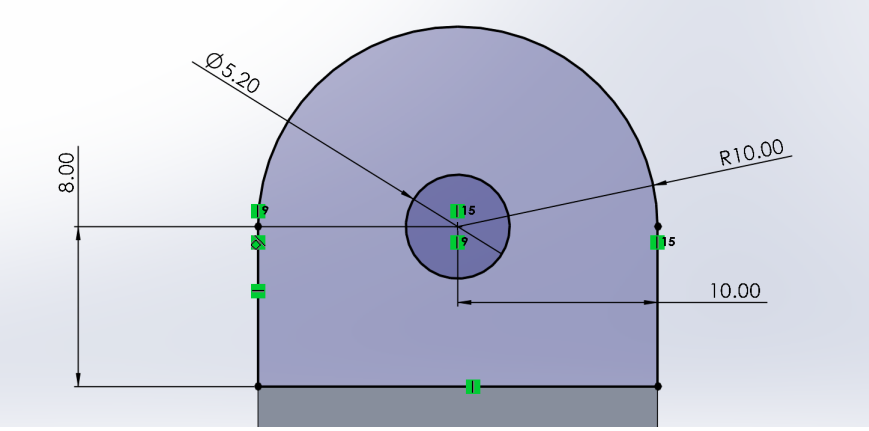

Figure 124: Drawing of the *Joint 2* of the alignment system

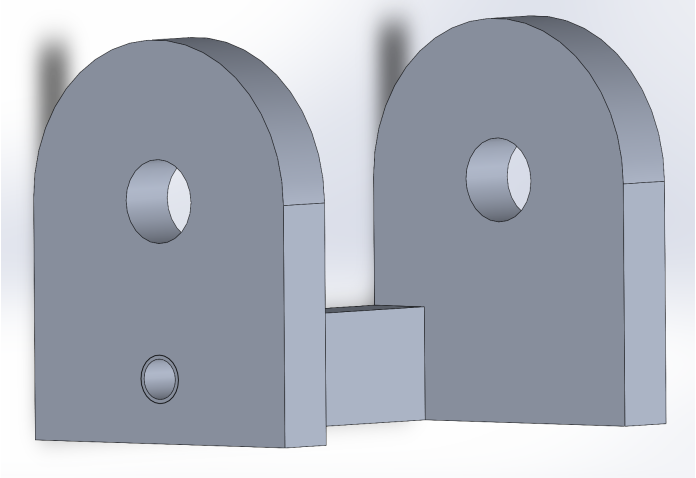

Figure 125: 3D visualization of the *Joint 2* of the alignment system

Additionally, two bases are screwed to the pin after it is inserted in the revolute joint, such that it does not slide out. These bases present a screw hole that allows to insert the handles, rotate the beam *b*, and block it. The pin is shown inFigure 126, and the base in Figure 127.

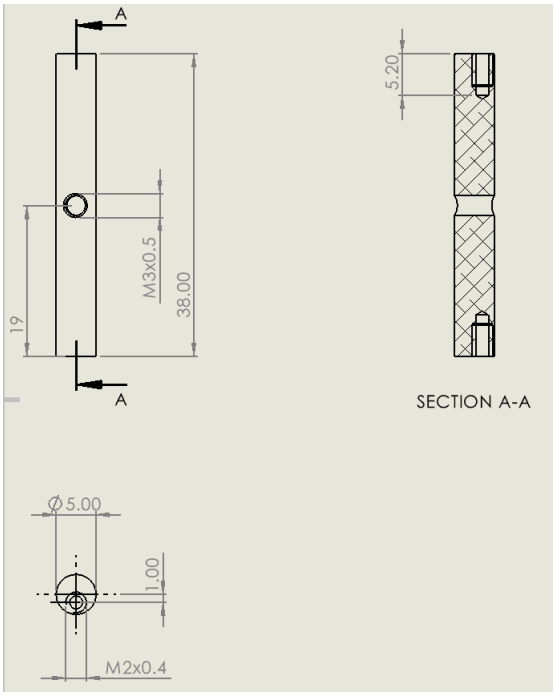

Figure 126: Pin inserted in the revolute joint

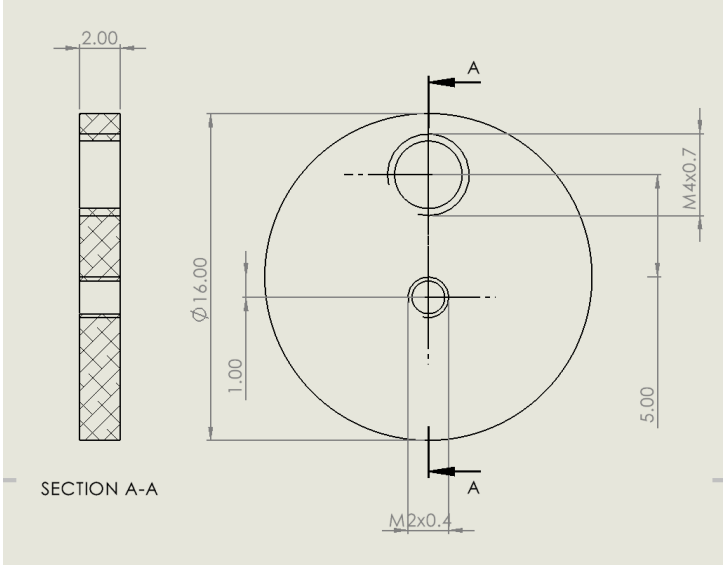

Figure 127: Base of the pin inserted in the revolute joint

The final assembly that composes the J_a3 is shown in Figure 128.

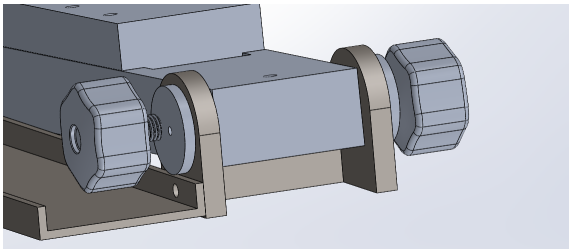

Figure 128: J_a3

11.3 Final design of the alignment mechanism

Before assembling all the parts, the constraints, presented in subsection 11.2, are satisfied, as shown in Figure 131. This requires to design an extra piece, between the bar in *Part 1* and the slider mechanism, beam a. This extra piece is necessary for avoiding collision between the RCM mechanism and the beam a when $\theta 1$ is set to be 90°. The extra piece is shown in Figure 129.

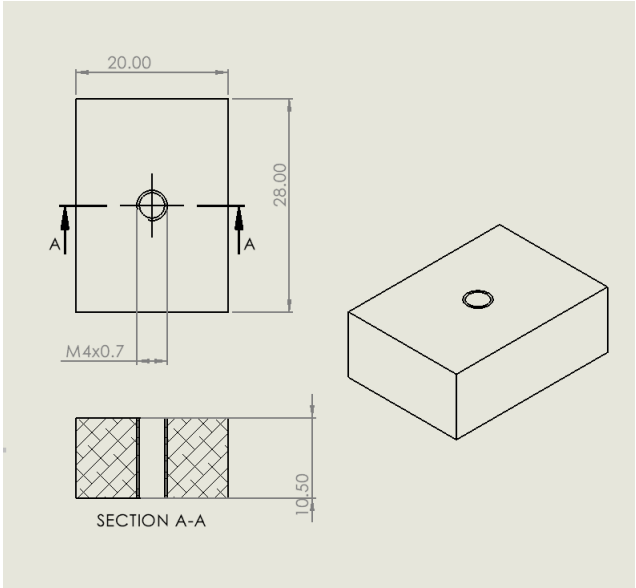

Figure 129: Design of the extra piece that connects Part 1 with the bar a

The connection of the Part 1, the extra piece, and bar a are shown in Figure 130.

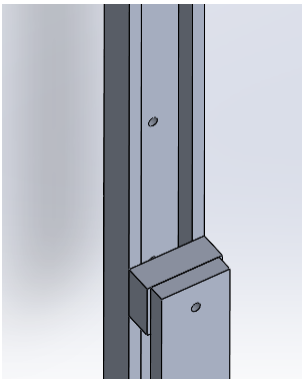

Figure 130: Connection between Part 1 and Part 2

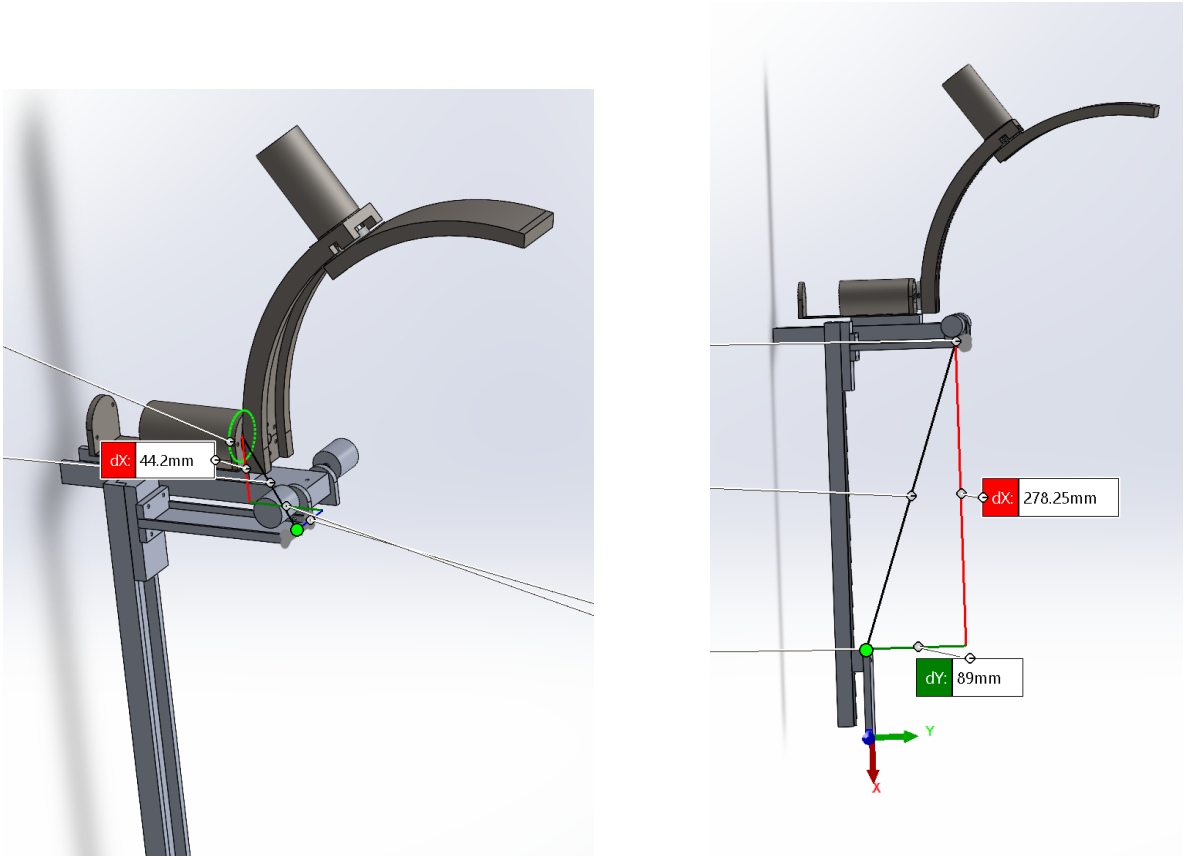

Figure 131: Satisfied constraints

The final design is presented in Figure 132 and in Figure 133.

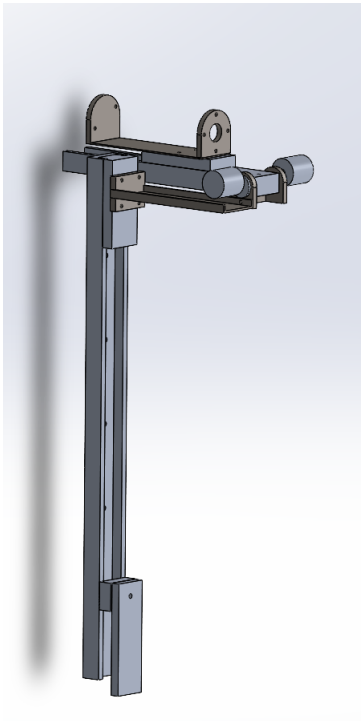

Figure 132: 3D view of the final design

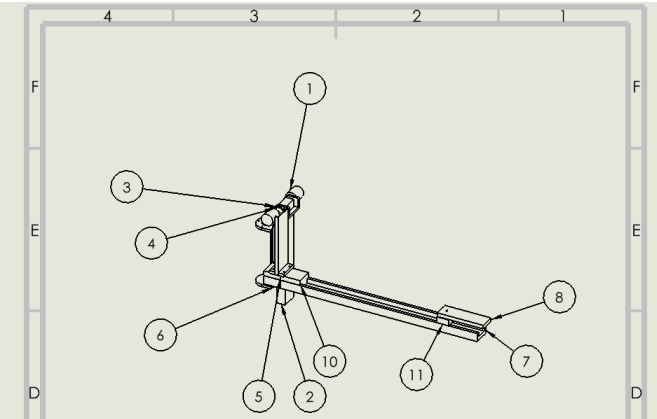

ITEM NO.	PART NUMBER	DESCRIPTION	QTY.
1	handles	steel 1035	2
2	beam b	aluminium 6061	1
3	beam d	steel 1035	1
4	base of pin	aluminium 6061	2
5	beam c	steel 1035	1
6	flange	steel 1035	1
7	beam a	aluminium 6061	1
8	connection to clamp	aluminium 6061	1
10	slider	aluminium 6061	2
11	connection to beam a	aluminium 6061	1

Figure 133: Drawing of the final design

11.4 Failure analysis of the structure

In section 10, it was shown that the RCM structure in planar configuration experiences higher stress, strain and displacement than in elbow configuration. For this reason, the alignment mechanism is tested with the RCM mechanism in planar configuration.
Six main configurations are considered: beam b at 0 or 90°, $\theta 1$ at 0 , 90° or -90°. The results are presented in Figure 134, Figure 135, Figure 136, Figure 137, Figure 138, and Figure 139.

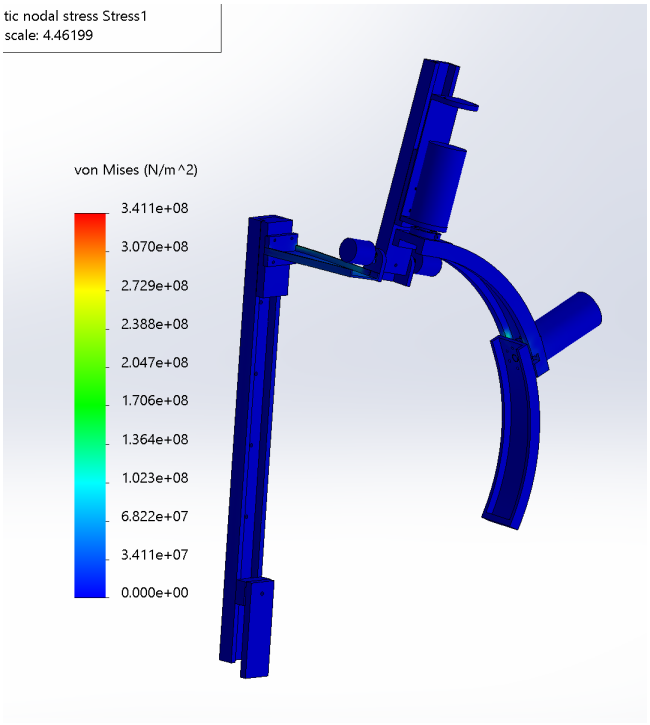

Figure 134: Simulation 1: all parts in aluminium 6061

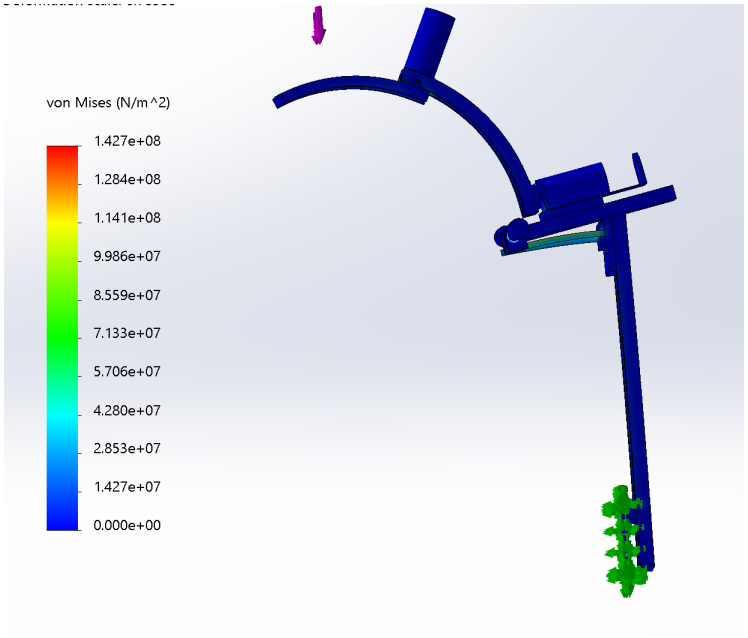

Figure 135: Simulation 2: all parts in aluminium 6061

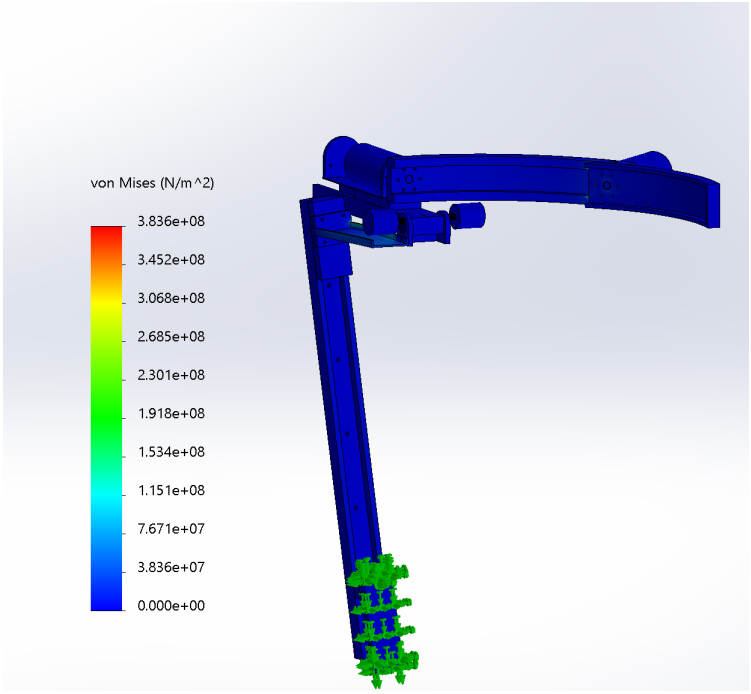

Figure 136: Simulation 3: all parts in aluminium 6061

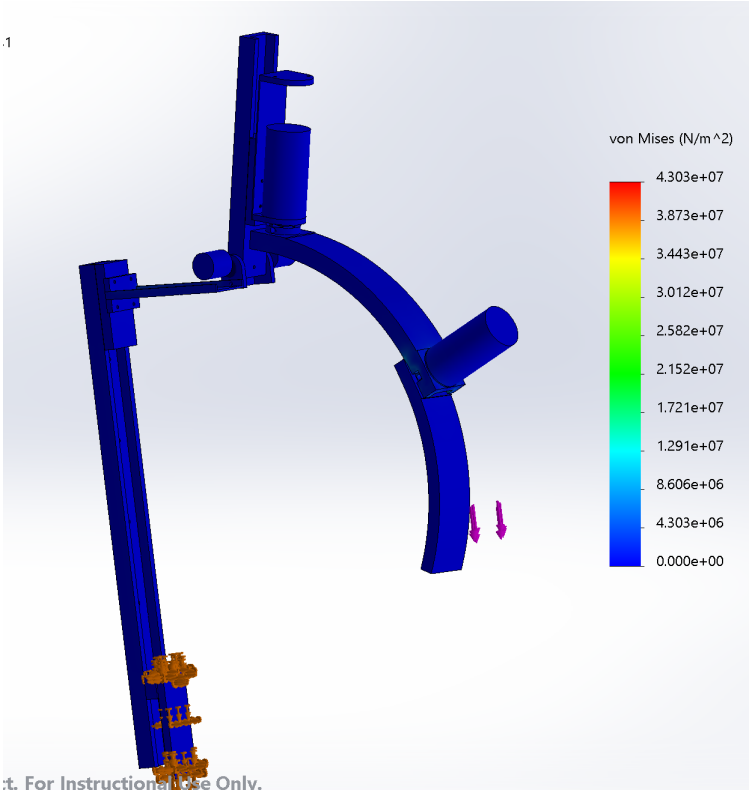

Figure 137: Simulation 4: all parts in aluminium 6061

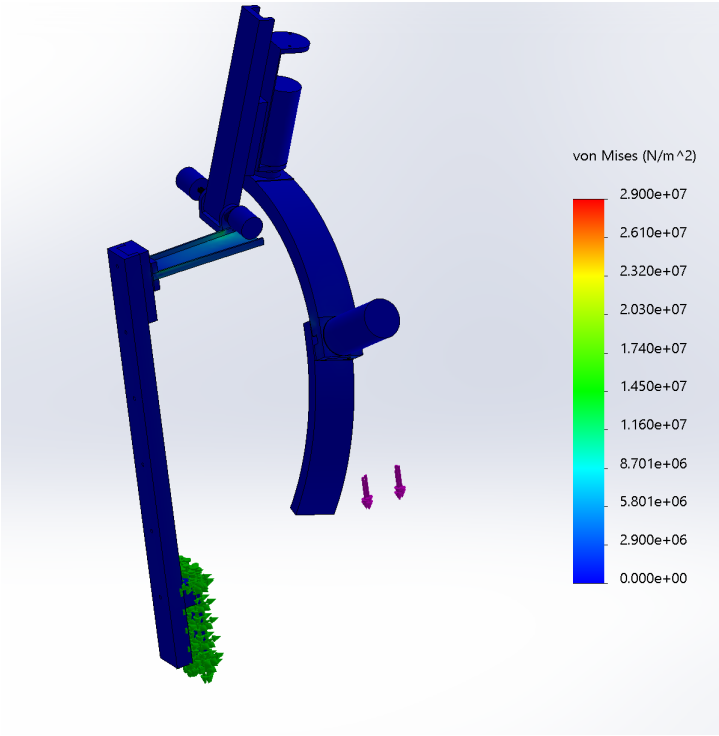

Figure 138: Simulation 5: all parts in aluminium 6061

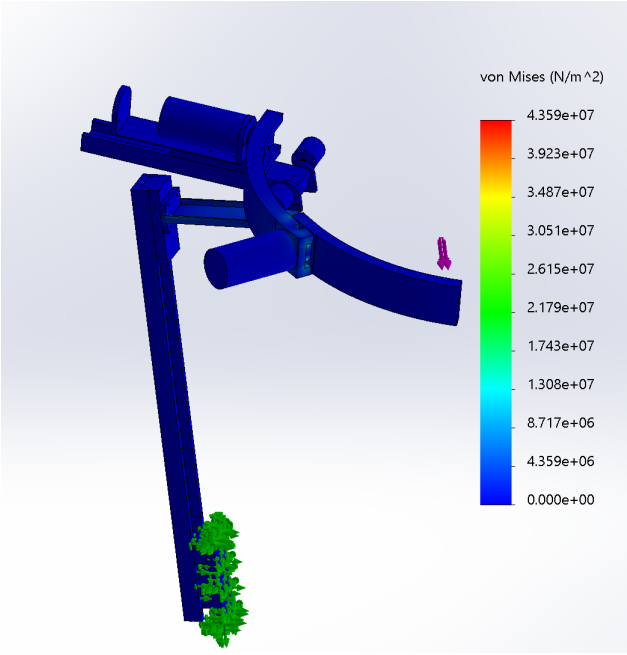

Figure 139: Simulation 6: all parts in aluminium 6061

For two of the simulations, the stress developed in the structure is too high, Figure 134 and Figure 136. Additionally, it can be seen that beam c is the component most subject to an high stress. For these reasons, it is decided to change the material of the beam c and beam d from Aluminium 6061 to Steel 1035. Thus, the structure is tested again in the two configurations shown in Figure 134 and Figure 136, giving a result that reduces the stress to a safe value, as shown in Figure 140 and in Figure 141.

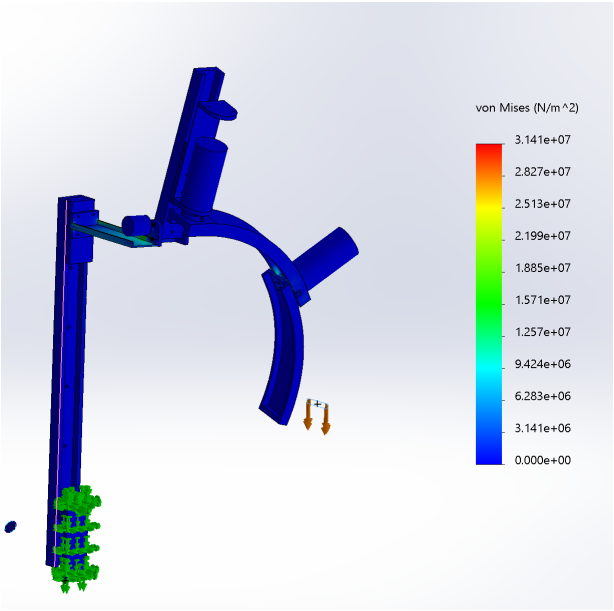

Figure 140: Simulation 7: beam c and d in Steel 1035

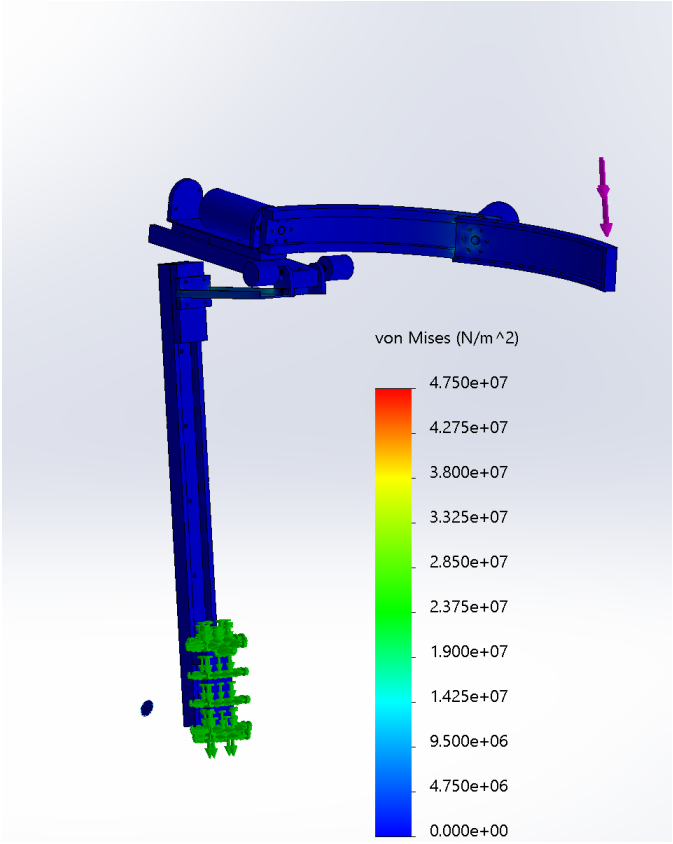

Figure 141: Simulation 8: beam c and d in Steel 1035

11.5 Position of lasers: indicators for the alignment

Five lasers needs to be inserted for allowing the overall alignment of the system. The points of insertion of the lasers are displayed in Figure 142.

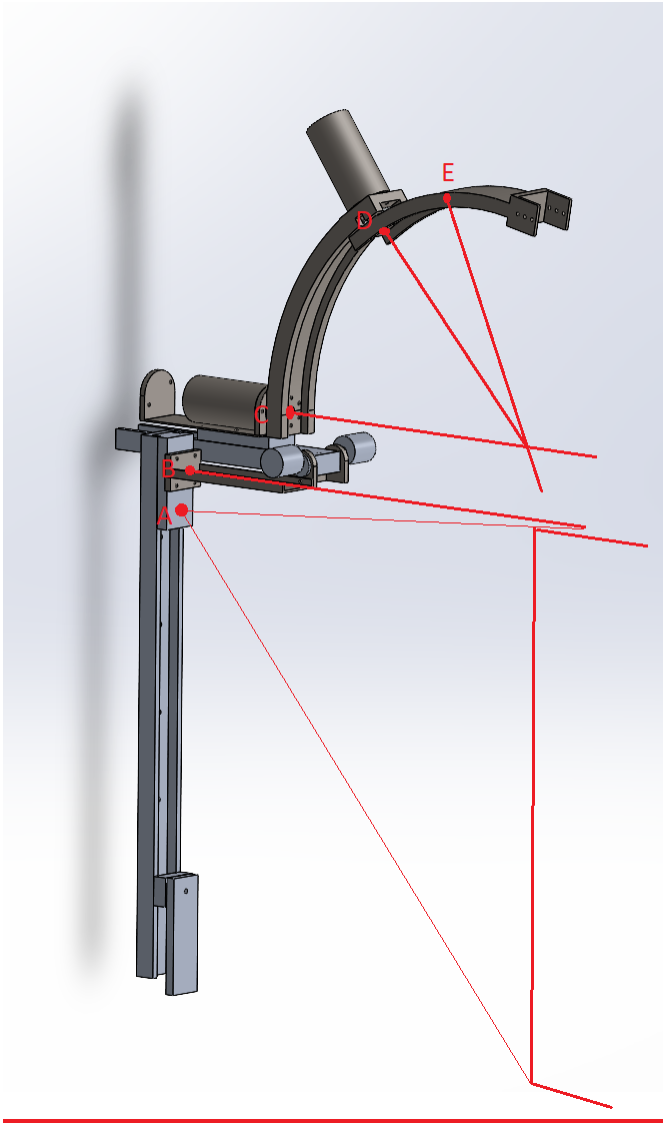

Figure 142: Points of insertion of the lasers

The functionality and the properties necessary for each laser are reported below:

- Laser that gives as feedback a plane for Step 0 positioned in point A in Figure 142;
- Laser that gives as feedback a point in Step1 positioned in point B in Figure 142;
- Two lasers that give as feedback a point for step 2 step 3 positioned in point c and point D in Figure 142 ;
- Laser that gives as feedback a line in beam 2 of RCM mechanism 25.7° away from the end effector, point E in Figure 142.

11.6 Design of position Feedback

Finally, a position feedback system is design. This system has to provide the position of the end effector for allowing the correction of possible position errors. Due to the fact that the deflection is calculated considering the $J_{rcm}1$ as absolute point, it is also necessary to feedback the position of $J_{rcm}1$ in space, and compensate for it during the final motions. For this reason, the outcomes of the position feedback system are:

- Position in space of $J_{rcm}1$;

- Position in space of the end effector.

In subsection 9.3, an overview of the possible sensors that can be used for the position feedback is presented and an early decision to incorporate *wireless sensors* is taken, for reducing the amount of wires and complexity of the system. In particular, for the position of $J_{rcm}1$, the inclination of the beam b is the value that is used for the feedback. A wireless gyroscope is implemented in the lateral side of the flange where the motor in $J_{rcm}1$ is attached. This will feedback any change of inclination of the beam b under the force applied by the RCM mechanism. For the end effector, instead, a relative position with respect to the $J_{rcm}1$ gives all the necessary information. Along with that, a feedback on the velocity and acceleration allows to have a more precise and safer surgical operation. For this reason, it is decided to implement in the flange connecting the robotic arm to the instruments' actuator the **IMU BNO055 wireless**. This IMU gives as a feedback the velocity, acceleration, and relative position after being calibrated.

12 Final design

12.1 Redesign of connection RCM mechanism to alignment mechanism

One of the features that makes the robotic arm practical is its portability. One method for calculating it is the NiOSH Lifting Equation, which calculates the recommended weight limit (RWL) that defines the maximum allowable weight (load) that can be lifted. To calculate the recommended weight limit the Equation 40 is used, where LC is the load constant and is 25 kg in Europe, HM is the horizontal location variable, VM is the vertical location variable, DM is the distance the object is moved vertically variable, AM is the asymmetry angle variable or twisting angle requirements variable, FM is the frequency and duration of the lift variable, and CM is the coupling variable. It is assumed that the robotic arm is on the floor and is raised to the operating table.

$$LC \cdot HM \cdot VM \cdot DM \cdot AM \cdot FM \cdot CM = RWL \tag{40}$$

HM, VM, DM, AM, CM, FM are calculated by using the European variable tables, considering H=25 cm, V=0 cm, D=80 cm, A=0 deg, C=1 good coupling, and F$<$ 0.2 lift/min and $<$ 1 hour duration of lifting. This gives: HM=1, VM=0.78, DM=0.87, AM=1, CM=1, FM= 1. Thus, the final **RWL=15.6078 kg**.
The overall weight of the system is:

- RCM mechanism weight = 1388.66 g
- alignment mechanism weight = 789.44 g

This means that both sub-mechanism are safe to be lift.
Finally, a look at the dimensions is done. The main purpose is to have small dimensions that easily fit into a standard box, so that the robot is transportable. The mechanisms have a maximum capacity of:

- RCM mechanism volume when extended: 318 mm x 241.4 mm x 35 mm
- Alignment mechanism volume: mm 385 mm x 178 mm x 101 mm

It is decided to redesign the connection between the RCM mechanism and the alignment mechanism to allow quick and easy assembly and disassembly, so that the two systems can be transported separately. For this reason, a brief look at the fast-click-on mechanism is provided.

12.1.1 Connection Mechanism Design

An overview of interconnect mechanisms is given in subsection 4.2. Due to the high forces acting on the systems, it is decided to proceed with a **friction grip**. One of the mechanisms that meets the requirements and the desired property is the quick release mechanism, Figure 143.

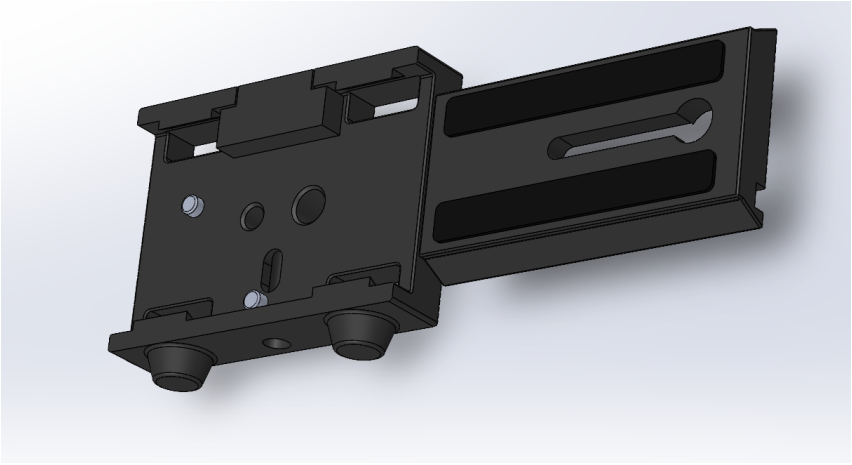

Figure 143: Quick release mechanism [24]

The mechanism is inserted in the design of the flange. The one presented in Figure 119 is changed. The new design incorporates two quick release mechanisms. The flange is composed by two parts, one attached to the motor of $J_{rcm}1$ and the other to J_a4. The two parts connect through the quick release mechanisms. The first part of the flange is shown in Figure 144, and the second in Figure 145. The overall mechanism is shown in Figure 146.

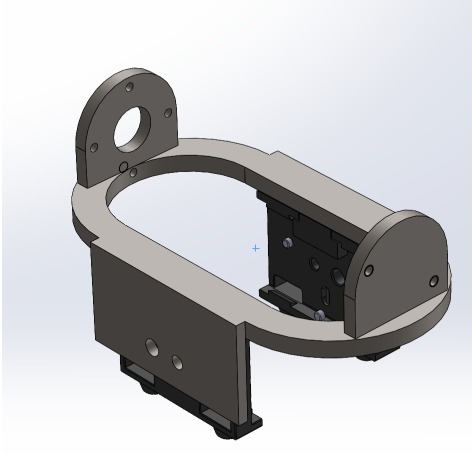

Figure 144: Flange attached at $J_{rcm}1$

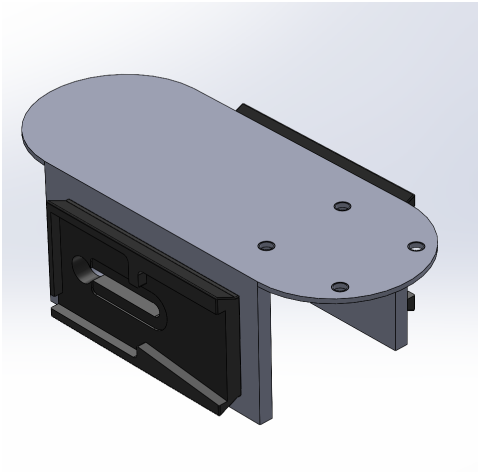

Figure 145: Flange attached at J_a4

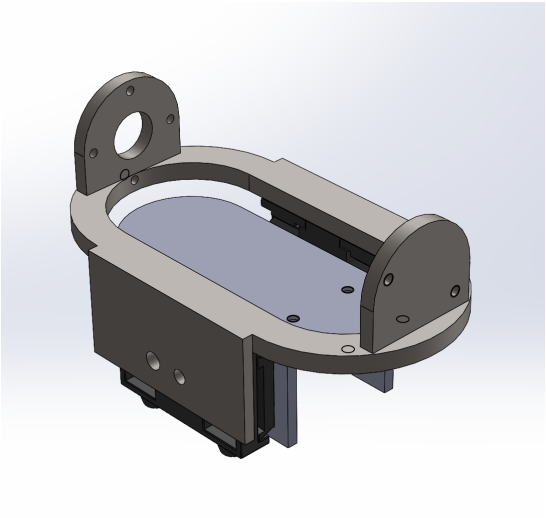

Figure 146: Final design of the connector between the two parts

Because of the new design, it is necessary to add a spacer between beam c and beam d, to avoid the collision between the new flange and the vertical beam a. The design of the spacer is simple and strong, and is shown in Figure 147 and Figure 148. The final design is shown in Figure 149.

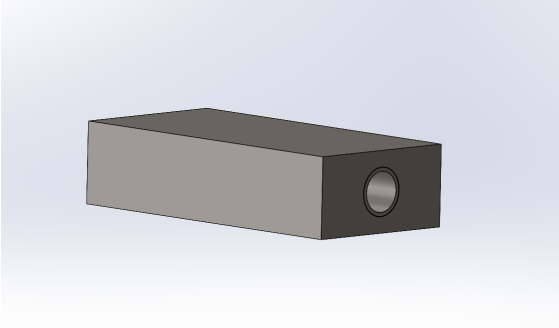

Figure 147: 3D visualization of the spacer between the beam c and beam d

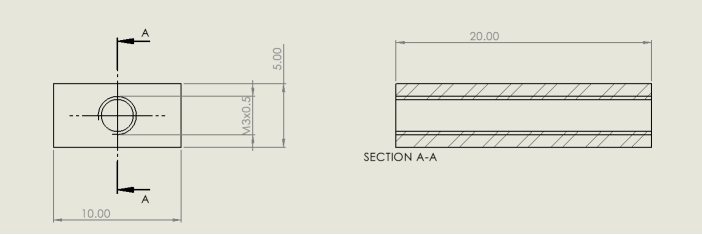

Figure 148: Drawing of the spacer between the beam c and beam d

12.2 Manufacturing processes

The final design of the overall system is shown in Figure 149.

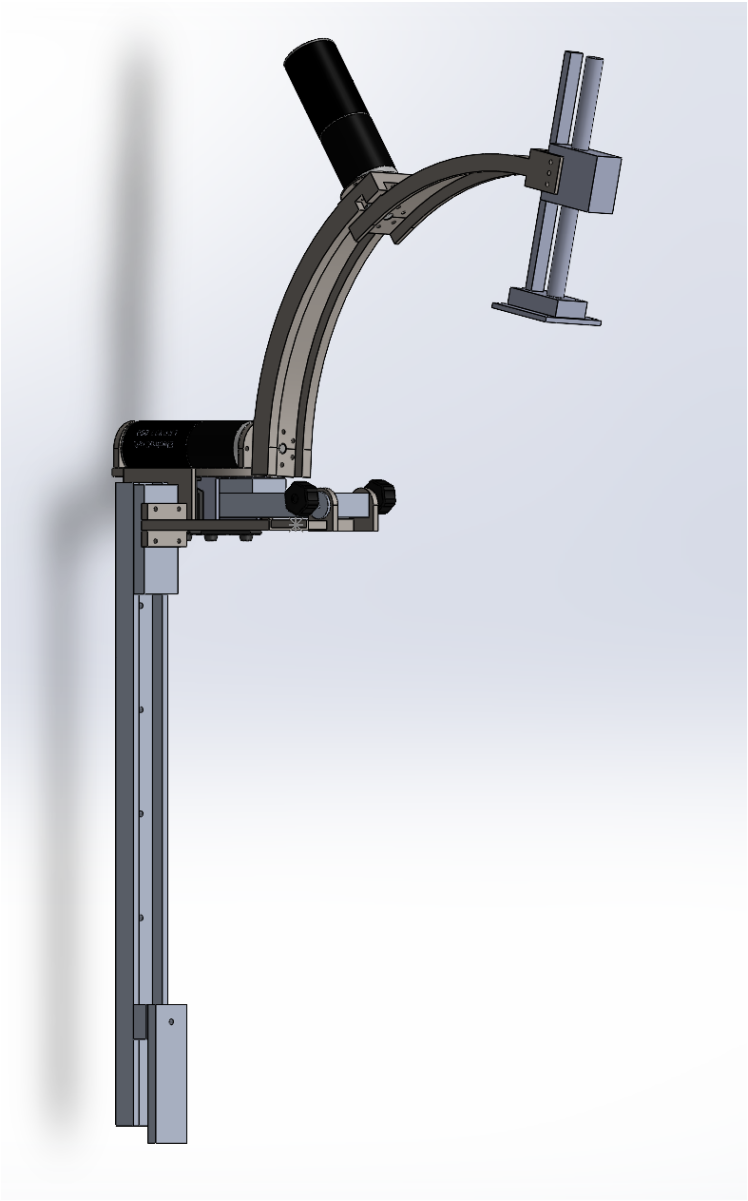

Figure 149: 3D view of the final design

In the Table 25, the customized parts of the final design are reported, along with the manufacturing process for producing them and the overall quantities of each of them.

Table 25: List of all the components with the manufacturing process to produce them

Part	**Quantity**	**Manufacturing process**
Beam 1 RCM mechanism	1	Metal forming, threading, drilling, and machining removal
Beam 2 RCM mechanism	1	Metal forming, threading, drilling, and welding for the lateral flanges
Flange $J_{rcm}2$	1	Threading and drilling
Flange $J_{rcm}3$	1	Threading and drilling
Motor hub RCM mechanism	2	Out of shelf Pololu Universal Aluminum Mounting Hub for 6mm Shaft, M3 Holes
Gearmotor $J_{rcm}1$	1	Out of shelf Gearmotor LRPX32-90V12-076
Gearmotor $J_{rcm}2$	1	Out of shelf Gearmotor LRPX32-90V12–019
Linear module $J_{rcm}3$	1	Out of shelf Miniature Linear Module QM02-12477-120
Beam a alignment mechanism	1	Out of shelf SGR10 15N Roller slider slide Aluminum profile
Beam b alignment mechanism	1	Out of shelf SGR10 15N Roller slider slide Aluminum profile, welding, drilling, and threading
Beam c alignment mechanism	1	Welding and threading
Beam d alignment mechanism	1	Welding, machining, threading
Connection to clamp alignment mechanism	1	Threading
Connection to beam a alignment mechanism	1	Threading
Pin alignment mechanism	1	Threading
Base of pin alignment mechanism	1	Drilling and threading
Handle alignment mechanism	2	Out of shelf
Connector alignment mechanism to RCM mechanism	1	Threading and drilling
Spacer beam c and beam d	1	Threading

12.2.1 Beam 1 and beam 2 of RCM mechanism

For the manufacture of the two curved beams, the manufacturing processes studied in Table 16 are compared and metal forming is chosen. This decision is due to the low cost and the simple process that can easily bend a U-shaped beam with the required dimensions. In addition, the beams are threaded and drilled to produce the hole patterns required for connecting the motors and connectors. Beam 1 is also machined to cut the material that collides with the universal hub and threads, as shown in Figure 101. Beam 2, on the other hand, is welded to the two flanges that connect to the linear module, as shown in Figure 97.

12.2.2 Beam *b* of alignment mechanism

Beam *b* of the alignment mechanism consists of two parts: the standard slider SGR10 15N Roller slider slide Aluminum profile and a customized part that allows the connection with the revolute joint. The two parts are welded together, and the custom part is made by a rectangular beam with the required dimensions, in which a hole is drilled and a thread is made, as shown in Figure 120.

12.2.3 Beam *c* of the alignment mechanism

Beam *c* of the alignment mechanism is customized and consists of two parts: the U-shaped beam and the flange that connects it to J_a2. The first part consists of a standard U-shaped beam with a thread at the position shown in Figure 121. The second part consists of a plate in which a thread is cut to produce the connecting pattern. The two parts are welded together.

12.2.4 Beam *d* of the alignment mechanism

Beam d of the alignment mechanism is custom-made and consists of three parts: the U-shaped beam and two flanges required to make J_a3. The first part consists of a standard U-shaped beam with a thread in the position shown in Figure 122. The second and third parts consist of a plate that is milled and machined to make the center hole and the shape of the profile. The three parts are welded together as shown in Figure 125.

13 Validation of the ease of set up: alignment of the incision point with the center of rotation

In this section the ease of set up of the system is validated, concentrating on the alignment of the incision point with the center of rotation of the RCM mechanism.
For doing so, an experiment is carried out. The alignment mechanism is redesigned and simplified as shown in Figure 150 and 3D printed, Figure 151. Additionally, the joints are created and fixed though wing screws and wing nuts. The set up of the experiment is shown in Figure 152

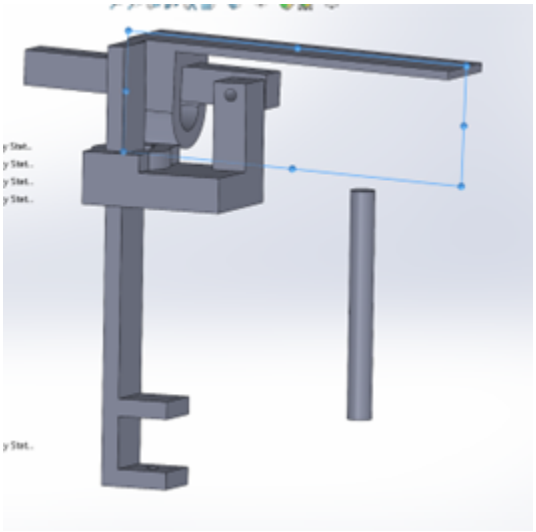

Figure 150: 3D overview of the simplified alignment mechanism

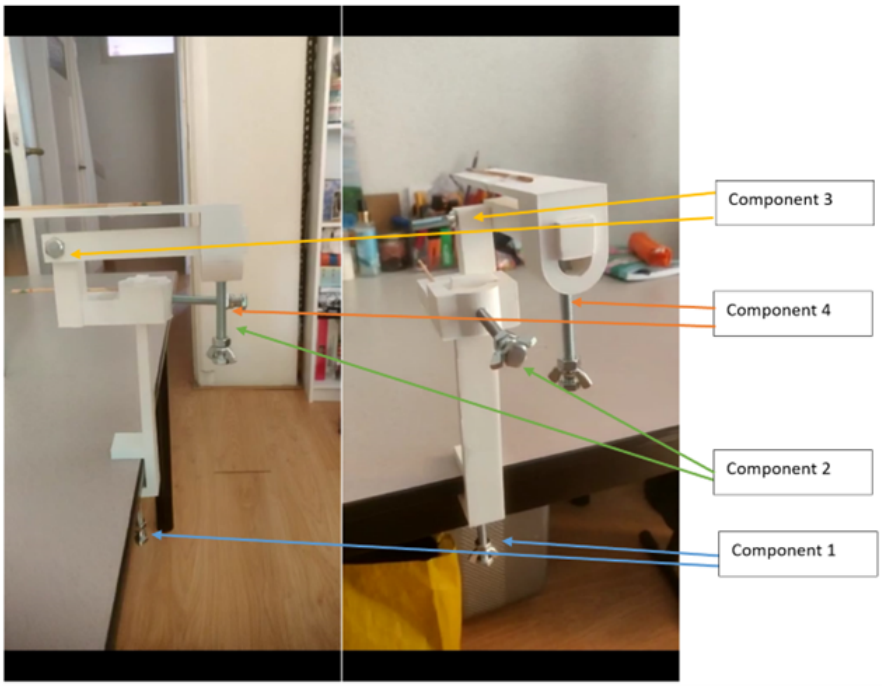

Figure 151: 3D printed alignment mechanism: overview of all the components

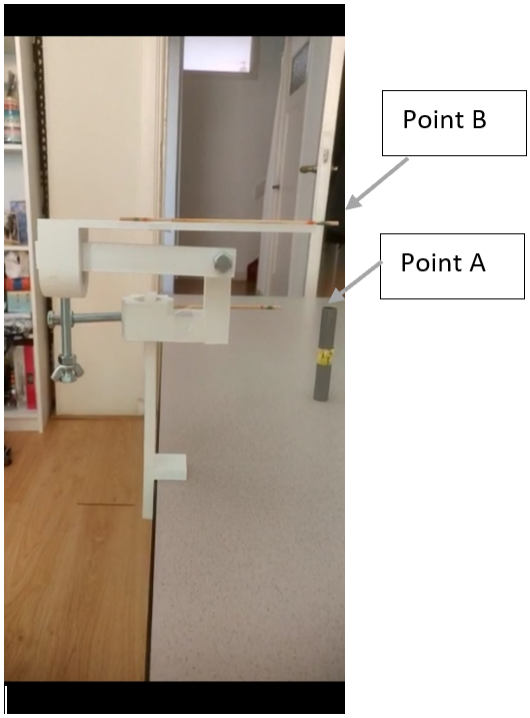

Figure 152: 3D printed alignment mechanism: set up for the experiment

A literature review was performed for estimating the set up time of the robots that were presented and studied in [67]. This resulted in the Table 26.

Table 26: Docking and covering time for the most used systems

Year	**Robotic system**	**Set up time**
1997	Zeus	18 mins [121]
1997	Da Vinci	7.8 mins docking time[141]
2003	Senhance	10 mins [80]
2007	Revo-i	10.6 mins [114]
2012	Medrobotic Flex System	15 mins [134]
2018	Versius	5 mins docking time [56]

In the set up time reported in Table 26, the overall time takes into consideration the alignment and the connection with the sterile material that covers the robot. In the experiment this second part does not happen, thus the average time to set up the sterile drape is taken out from the values find in the literature and it is equal to 5.6 minutes [141]. For this reason the Table 26 is modified, Table 27.

Table 27: Docking time for the most used systems

Year	**Robotic system**	**Set up time**
1997	Zeus	13.4 mins [121]
1997	Da Vinci	7.8 mins [141]
2003	Senhance	5.4 mins [80]
2007	Revo-i	5 mins [114]
2012	Medrobotic Flex System	9.4 mins [134]
2018	Versius	5 mins [56]

13.1 Hypotheses

The hypotheses of the experiment are:

- **H1**: the system requires a set up time shorter than then 5 minutes, which is the lowest set up time reported in Table 27.
- **H2**: the system is simple, easy to set up, and comfortable to use.
- **H3**: the user can quickly learn the procedure.

13.2 Independent tested variables

In the experiment, the participants are selected in the group of non-specialized staff. 5 to 10 participants are expected to take part at the experiment. It is asked to the participant to set up the robotic arm three consecutive times. The first and the third time they will align the same point, while the second they will align a different point in space.
The variables for testing the hypothesis are:

- *Time for the alignment*: for each alignment procedure, the time the participant takes to conclude it is registered. This is going to be used for discussing H1. The times of the first and the last repetitions are compared, for checking the H3.
- *System Usability Scale (SUS)*: this questionnaire, [46], is used for evaluating the H2. The questions asked are shown in Table 28.

Table 28: Questions and options for the System Usability Score Scale [46]

Question	**Possible answers(1=totally disagree, 5=totally agree)**
Q1: I think I would use the product frequently if I was a surgery assistant	[1,5]
Q2: I found it unnecessary complicated	[1,5]
Q3: I found the product easy to use	[1,5]
Q4: I think I need technical support to use the product	[1,5]
Q5: I found the different feature of the product well integrated with each other	[1,5]
Q6: I felt there were too many inconsistencies in the product	[1,5]
Q7: I can imagine that most people can quickly get on with this product	[1,5]
Q8: I fount it difficult to use	[1,5]
Q9: I felt confident while using the product	[1,5]
Q10: I had to learn a lot about the product before I could use it properly	[1,5]

The SUS score is calculated as following [46]:

  - To all odd number questions 1 point is subtracted to the score (X-1);
  - For all even number questions, to 5 is subtracted the score (5-X);
- The SUS score is calculated as *SUS=sum of all new scores* ·2.5.

The SUS score is interpreted as shown in Figure 153.

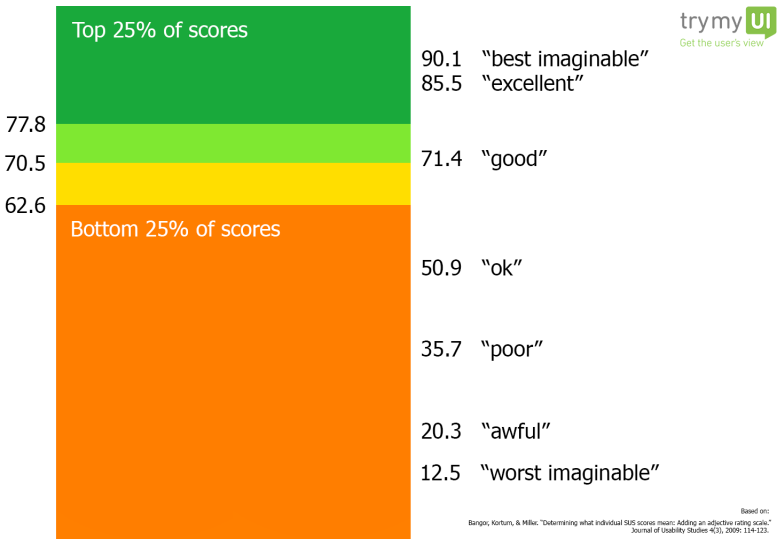

Figure 153: Scale for the SUS score [46]

- *Net Promoter Score (NPS)*: this questionnaire is used for evaluating the H2 [35]. The questions used are shown in Table 29.

Table 29: Questions and options for the Net Promote Score Scale [35]

Question	**Possible answers**
Q11: How do you rate the product?	[1,5]
Q12: How do you rate the comfort of the product?	[1,5]
Q13: How do you rate the ease of the product?	[1,5]
Q14: How do you rate the clarity of the steps?	[1,5]

Additionally the results of this questionnaire are read and interpreted considering:

  - Range score [1,3]: Detractors: not likely to recommend;
  - Score 4: Passive;
  - Score 5: Promoters: most likely to recommend.

The NPS is calculated as *NPS=%Promoters-%Detractors* [35]. The NPS value ranges from -100 to 100. A method for evaluating the value of NPS is the absolute method: an NPS score above 0 indicates that the participants are most likely to suggest the product, and felt comfortable using it [35].

13.3 Method

The method used for the experiment is summarized in the following steps:

- The alignment procedure is explained to the participant though a paper that explains the 4 steps with images, section 28.
- The alignment mechanism and a bar representing the incision point are fixed on the table. The center of rotation of the mechanism and the incision point are defined as point B and point A in Figure 152.

- It is asked to the participant to perform the alignment. The time required to reach the condition Point A = Point B is registered, with detailed time for each step, and the final misalignment.
- Another incision point with a different height and position is placed on the table, so that the experiment is conducted for larger and smaller rotational angle in J_a3. It is asked to the participant to perform the alignment again, with the new incision point.
- The third time, the participant is required to align the mechanism with the incision point that was aligned the first time.
- After the experiment, the participant compiled the questionnaires.

13.3.1 Results

The results of the experiment are reported in Table 30: the time in seconds represent the time needed to complete each step; the misalignment in millimeter is the distance between the Point B and Point A after the alignment, where radial is the distance on the plane parallel to the flat surface of the cylinder, and height is on the surface perpendicular to it. The misalignment is plot, and a acceptance area is decided to be in radial misalignment in range [0 mm,10 mm] and height misalignment in range [0 mm,10 mm]. This is checked in Figure 154, and all the procedure could be included in the study.

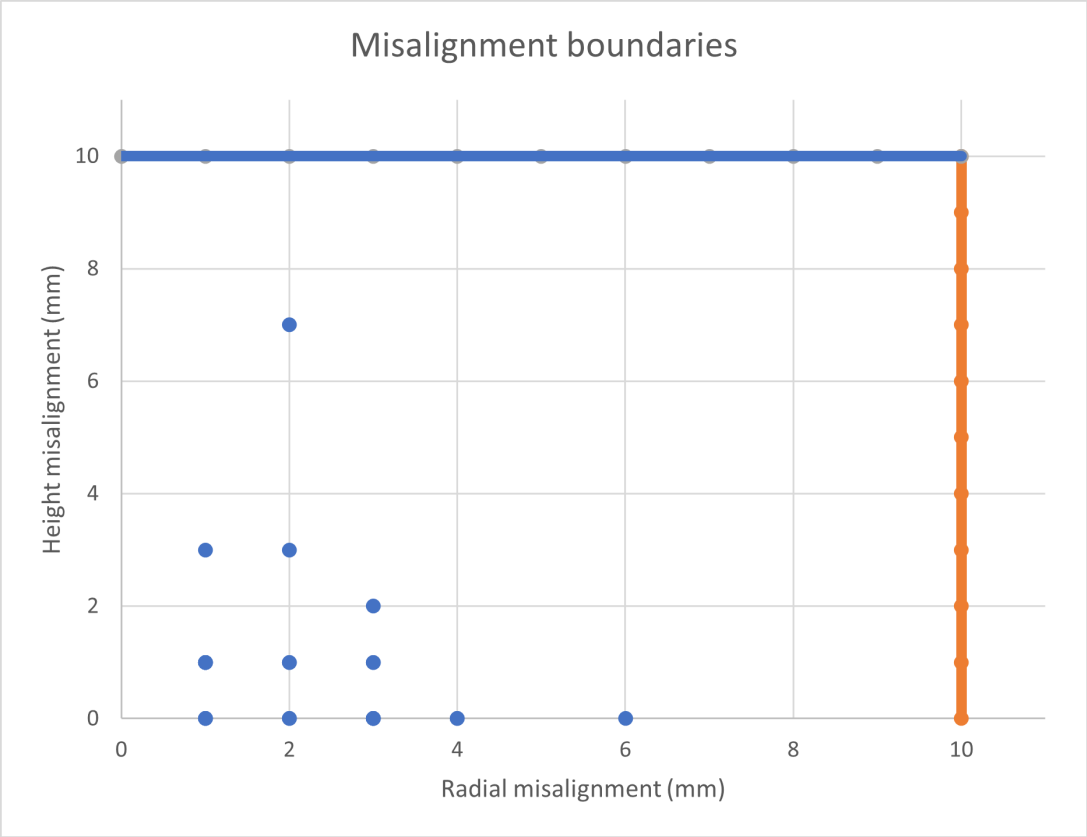

Figure 154: Plot of the misalignment after all the procedures and the acceptance boundaries

For all the questions in the SUS questionnaire the average points are calculated, Table 31.

Table 30: Results on time and misalignment for all the participants

Participant	Trial 1		Trial 2		Trial 3	
	Time(s)	Misalignment(mm)	Time(s)	Misalignment(mm)	Time(s)	Misalignment(mm)
1(long-short-long)						
Step 1	8.56		27.85		13.02	
Step 2	12.54		10.57		8.22	
Step 3	4.97		10.66		6.4	
Step 4	9.7		3.87		7.47	
Total	35.79	1(radial)3(height)	52.96	6(radial)0(height)	35.13	3(radial)2(height)
2(short-long-short)						
Step 1	12.66		8.57		7.87	
Step 2	16.58		9.62		12.41	
Step 3	11.93		10.3		7.44	
Step 4	8.99		8.39		7.63	
Total	50.18	3(radial)1(height)	36.88	2(radial)0(height)	35.36	1(radial)1(height)
3(long-short-long)						
Step 1	19.05		19.13		17.55	
Step 2	21.46		14.09		19.36	
Step 3	7.5		21.62*		8.63	
Step 4	0.8		12.07		6.69	
Total	48.83	4(radial)0(height)	66.92	1(radial)1(height)	52.25	3(radial)0(height)
4(short-long-short)						
Step 1	9.41		9.5		14.45	
Step 2	11.14		4.53		6.51	
Step 3	9.87		11.34		4.43	
Step 4	9.41		12.44		6.6	
Total	39.85	1(radial)0(height)	37.35	4(radial)0(height)	32.01	3(radial)1(height)
5(long-short-long)						
Step 1	6.83		11.84		14.6	
Step 2	18.4				6.04	
Step 3	14.16		17.65		3.02	
Step 4	42.4		15.51		8.75	
Total	81.81	2(radial)0(height)	45.22	1(radial)1(height)	32.43	3(radial)0(height)
6(short-long-short)						
Step 1	8.88		8.8		19.82	
Step 2	16.5		23.33		10.09	
Step 3	9:05		17.46		10.2	
Step 4	32.66		28.92		15.65	
Total	67.10	2(radial)1(height)	78.54	3(radial)0(height)	55.78	1(radial)0(height)
7(long-short-long)						
Step 1	5.72		12.78		5.74	
Step 2	39.15		14.2		11.91	
Step 3	9.99		12.72		24.98	
Step 4	25.38		12.26		24.4	
Total	80.27	2(radial)3(height)	51.98	2(radial)7(height)	67.04	1(radial)1(height)
8(short-long-short)						
Step 1	15.78		4.6		9.23	
Step 2	7.51		4.29		5.34	
Step 3	4.17		5.54		2.2	
Step 4	3.71		5.13		1.98	
Total	31.18	2(radial)1(height)	19.58	1(radial)0(height)	18.75	3(radial)0(height)

Table 31: Average score of the answers for SUS

Question	Average score
Q1	4.25
Q2	1.5
Q3	4.375
Q4	2.25
Q5	4.625
Q6	1.75
Q7	4.875
Q8	1.125
Q9	4.375
Q10	1.875

The values in Table 31 are use for calculating the SUS score: **SUS=(34.0005 x 2.5)=85.00125**. This means that the system is excellent for the participants that tried it.
Additionally, the NPS score is calculated using the results reported in Table 32. The value of NPS is **NPS=40.6%-3.12%=37.48 > 0**. This means that the participants are most likely to find the procedure comfortable and user-friendly.

Table 32: Scores of the answers for NPS

Question	Scores
Q11	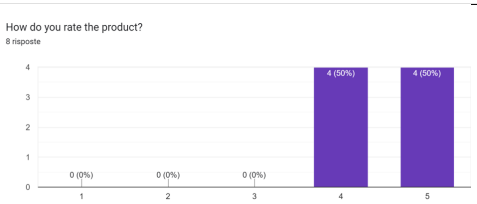
Q12	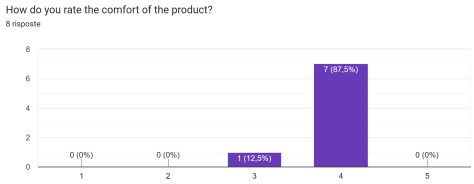
Q13	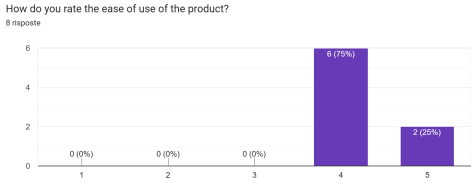
Q14	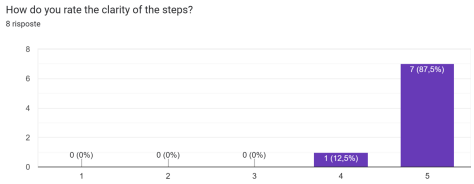

Finally, the results in Table 30 are further investigated, Table 33, Figure 155, and Table 34.

Table 33: Average time to set up the mechanism with respect to trial

Average time trial 1	54.37625s
Average time trial 2	48.67875s
Average time trial 3	41.09375s

Figure 155: Comparison between the first and the third trial for all participants

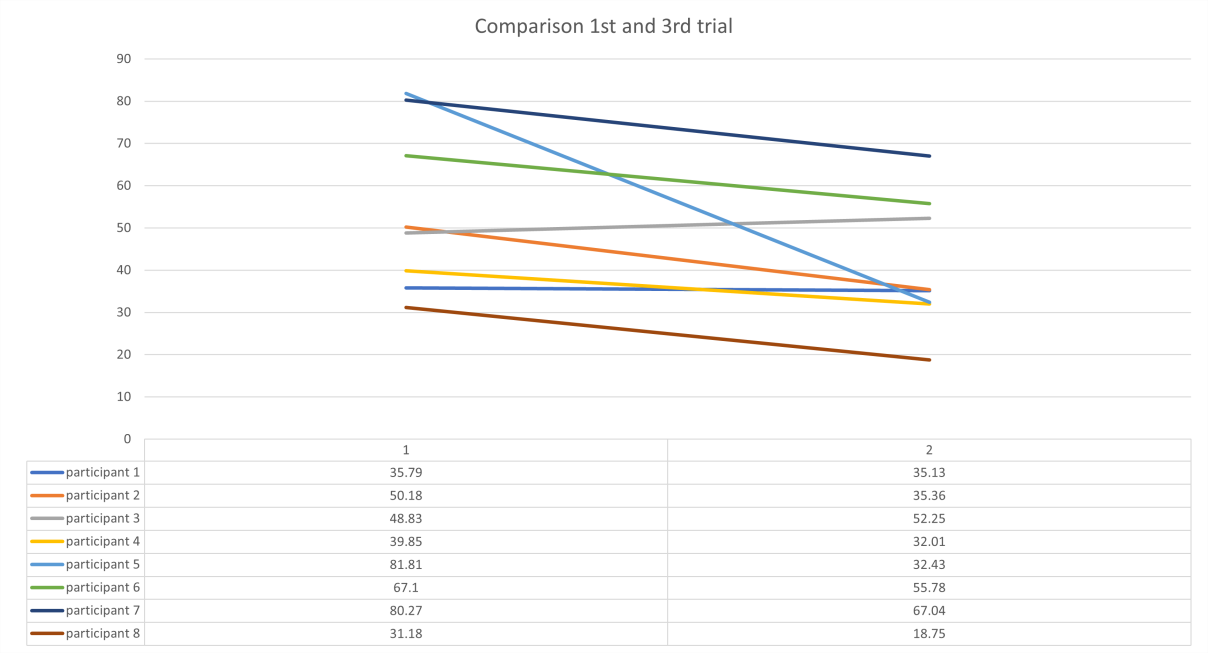

Table 34: Average time to set up the mechanism with respect to step

Step 1	12.1766s
Step 2	13.259s
Step 3	9.19s
Step 4	12.95041s

13.3.2 Discussion and conclusion on the experiment

Before discussing the limitations of the design and the findings obtained with the experiment, a look at the results is presented to infer the validity of the hypotheses.
From Table 33, it can be seen that the average time to set up the system is less than 5 minutes. This is also true for the maximum time each participant took to align the mechanism, Table 30. This proves the H1.
Furthermore, it can be concluded from Table 33 that the average time for aligning the mechanism decreases from the first to the third trial. A deeper insight into all participants can be obtained from Figure 155. The only participant for whom the time spent increased was participant 3, who performed step 1 twice in the last trial. In general, however, it can be seen that participants adapt and learn the procedure over time, so that H3 proves to be correct.
Finally, the evaluation of SUS shows that the system is in the range of excellent usability, which means that it is user-friendly and convenient. This proves the H2. This conclusion is supported by the value of the NPS score, which is $37.48 > 0$.
After proving the hypotheses, additional comments and observations are reported.
For a more in-depth look at the four steps, see Table 34. Although in some trials some steps took much longer than others, overall the steps have a similar average time. Therefore, the complexity of

them is considered similar. In general, it takes longer if the participant had problems with screwing and unscrewing, a problem that can be easily solved with more ergonomic and intuitive handles.
During the experiment, it was found that participants repeated step 1 after performing step 2 five times. All five times this occurred while aligning the lowest incision point. The cause is thought to be the type of visual feedback that was given in the experiment. Indeed, it was perceived as difficult to align the center of the cylinder with the stick when viewed from above in Step 1. However, this is considered a limitation of the prototype. In fact, the use of sticks for feedback and the guidance line for alignment is only an approximation and simplification of the lasers used in the final system, in subsection 11.5. Step 1 has as feedback a laser that creates a plane on the patient's abdominal cavity, which is much easier to read compared to that of the experiment. The use of this feedback should reduce the time difference found in the alignment of the two incision points and avoid the repetition of step 1.
Another limitation of the prototype is the type of handles that were used. The nuts and bolts worked, but attention had to be paid to how they were gripped. This problem primarily limited the performance of participant 7. However, it is expected that this problem will be overcome in the final mechanism by incorporating ergonomic and easy-to-use grips.
The final important finding about the mechanism is that the radial offset is on average larger than the height offset, Table 30. This can be explained by the fact that the height misalignment is corrected in the last step, when the rest of the procedure has already been executed. In radial position, on the other hand, the adjustment is made in the first three steps, based on the feedback from the sticks rather than the proximity of the points themselves. Due to the structure of the mechanism and the definition of the steps, an error in the alignment is predicted mainly in the radial plane. This observation must be taken into account in the final procedure so that compensation in the radial plane is possible.
To conclude, the experiment has shown that the alignment mechanism allows for an alignment of the incision point and the center of rotation that takes less than 5 minutes, even when performed by non-specialized personnel who quickly learn the procedure. In addition, it has been shown to be simple, convenient and straightforward to use.

14 Discussion

In this masters thesis, a robotic arm for laparoscopy has been developed with a focus on reducing size and weight and increasing portability and simplicity of set up. A discussion of the design is presented in this chapter.

During development, main priority was to design a mechanism that would cover the required workspace and perform the required motions while *reducing the weight and size of the overall system.* In terms of size and weight, it is unfortunate that this design can become smaller and lighter. By using less common materials and less standardized cross-sectional areas, the overall weight and size could be altered favorably, but the improvement is limited, while this approach increases the cost significantly. For this reason, this optimization is not recommended. However, the achievement of this goal, has come with sacrifices on cost, standardized parts, and selection of the optimal transmission.

- The *electronic components* of the design are selected to significantly reduce size and weight. However, their cost is estimated to be higher than other possible solutions.
- The parts are designed to increase the compactness of the system. This led to the presence of *customized parts.* Overall, the number of customized parts increases manufacturing costs. Another approach can be to reduce the cost by using more standardized parts. For example, the beams in the RCM mechanism are curved to increase compactness, but straight beams can also be used. In the same way, parts with the same cross-section could be selected to reduce scrap after manufacturing. However, this approach increases the size and weight of the overall system.
- The design required the inclusion of many customized parts, that need to the go through at least one *manufacturing process.* This improves performance, reduces size and weight, but increases the likelihood of defects and overall cost.
- The *transmissions* selected for this design proved to be the most efficient choice in terms of size, weight, and compatibility with the motors. However, they can result in high costs.

Another important point to discuss is the behaviour of the robotic arm. The study of its motion has brought to light the *non-monotonic behaviour* of the RCM mechanism. A monotonic behaviour is one in which each output corresponds to a unique combination of inputs. This device is non-monotonic in the sense that there are multiple orientation solutions to reach the same point in space. This affects the control of the system and must be considered in the design. However, this characteristic can also be considered an advantage, as the system can increase the number of configurations to reach a position, thus increasing the likelihood of a more comfortable and safe configuration for assistants and patients during the surgery. This can lead to a specific pre-planning of the configuration for each procedure.

14.1 Limitations of the study and future works

Although great effort has been made in the construction and analysis of this system, the theoretical calculations and software simulations cannot be taken as final and self-evident. There are many other effects that have not been taken into account. In addition, some preliminary decisions set limitations that can be overcome with minor adjustments. In this chapter, the limitations of the study and future work will be discussed.

14.1.1 Performing a wider range of procedures

The robotic arm works for laparoscopic appendectomy, cholecystectomy, and inguinal hernia removal. This defined the required active working area, which was used to optimize the dimensions of the mechanisms. If other procedures are to be added, the RCM mechanism dimensions must be changed by performing the optimization again. This step is quick, but it must be taken into account in the software simulations. This is because there is no guarantee that the forces will still be sustainable. However, a quick redesign can be performed for each procedure using this design as a starting point.

14.1.2 Design of a control system: selection of sensors

The main focus of this project was the mechanical and electrical design. A major limitation of the design is the lack of a schematic control system. A deeper look into system control and the medical field is suggested and will go a long way in finalizing the design. Even though some sensors have been selected, the final selection will depend on the decision of the control system.

14.1.3 Material Study

One of the limitations of the study is the selection of the material and the manufacturing processes, without considering the impact that the second has on the mechanical properties of the first. In fact, the manufacturing process can lead to eventual defects, weakening and brittleness. Even if this factor is taken into account in the selection of the final manufacturing processes, it is advisable to verify it through experimentation. This is necessary to avoid risky situations and should be done especially for the curved beams. This is due to the selected manufacturing process, metal forming, which requires the material to undergo heating and cooling. This is more likely to result in different mechanical properties and inhomogenity. It is also proposed to test the frictional resistance of the pressure screws in the handles used to attach J_a3, Figure 49 with the chosen material. For this project, the pair of materials was selected from catalogs, but it is necessary to test the frictional resistance and optimize the material selection.

14.1.4 Transmission and motor study: Backdrivability

Another major limitation of the project is that it has not been demonstrated that the selected transmissions allow to backdrive the system under forces greater than 60 N. The manufacturer of the selected gearmotors was unable to provide an accurate value for backdrivability. For this reason, it is suggested to test the gearmotors. This can be done by purchasing the gearmotors and developing a simplified lever mechanism that simulates the forces applied by the final system. Finally, it is suggested to conduct a review of motors on a larger number of sites to make a better selection that can also optimize the cost of the overall system.

14.1.5 Sterility

In this project, a cover with a plastic drape was chosen because the instrument holder already has an interface for connecting the drape. However, the small dimensions of the robotic arm make it a candidate for full sterilization. In fact, its small dimensions allow it to be inserted directly into the sterilization chamber. This shortens the set up time and increases the protection of the electronic components. It is proposed to design an envelope of sterilizable material to cover the RCM mechanism.

14.1.6 Plan for instrument insertion and workspace alignment

A closer look at the alignment procedure can be taken and the second part of the alignment can be further specified. First, it is proposed to plan in detail the connection between the robotic arm and the instrument holder. In this project, it is assumed that the insertion of the instrument is done manually and the instrument holder is screwed to the end effector. However, it is possible to design the connection so that they are connected with a quick release mechanism. Thus, the instrument holder can be connected secondarily. This can improve the insertion and allows for safer and more precise alignment.
Aligning the working areas by manually moving $\theta 1$ and $\theta 2$, Figure 54, can also be counterintuitive and difficult to perform. However, there are actuators in the design that modify these two DOFs. Thus, it is possible to motorize this alignment without having to add additional components. This makes the process easier and more reliable because the system knows in advance where the end effector will be at the end of the alignment process.

15 Conclusion

This work addresses the modeling, design, partial prototype and experiments of a new robotic arm for laparoscopic appendectomy, gallbladder removal and inguinal hernia surgery. The main goal of the design was to design mechanically and electronically, a simple, lightweight, small robotic arm for laparoscopic cholecystectomy, appendectomy, and inguinal hernia surgery that can maneuver a laparoscopic instrument.

The proposed approach to achieve this goal included several phases, from the specification of requirements to a proposed complete mechanical and electrical design. There were three main phases that allowed to achieve the goal: a topological synthesis phase, a dimensional synthesis phase, an electronic and material synthesis phase. The first phase allowed to connect the requirements with the proposed solutions and strategies. The second phase applies the design theory for articulated spatial connections. The third phase connects the electrical and material requirements with solutions and concludes with the final design of the robotic arm.

The proposed design is based on the novel division of laparoscopic surgery into two sub-procedures: the active surgical motion performed by a remote center of motion center (RCM) mechanism, and the passive alignment of the remote center of rotation of the mechanism with the incision point, performed by a mechanism with 4 degrees of freedom (DOFs). By splitting these two operations, a smaller workspace is required for active surgical motion, so the overall size of the robotic arm can be reduced and a more compact, smaller robotic arm can be developed. To the best of the authors knowledge, there is no robotic arm on the market that divides the entire operation into these two phases. Two mechanisms have been developed, each focusing on one of the two sub-procedures.

The mechanism that focuses on the alignment procedure consists of 4 DOFs, three translation and one rotation. It is designed to minimize weight and size while maintaining mechanical integrity and meeting the required motion and workspace. However, the biggest advantage of the design is the simplicity of set up. Indeed, the mechanism is intuitive and simple, resembling the auxiliary devices that assistants set up during operations. An initial prototype of the alignment mechanism described in this article was fabricated, assembled, and systematically tested. Eight nonspecialist participants performed the alignment procedure after all steps were explained to them. The experiment showed good usability of the mechanism, a set up time of less than 2 minutes, and quick learning of the procedure. Participants were able to perform the procedure independently after reading the steps and observing the mechanism. Precise alignment showed a very short learning curve of 3 repetitions. However, it also showed the need to incorporate better feedback and indicators, such as lasers. Finally, the experiment showed that it was more likely that radial misalignment would be registered at the end of the procedure. It is believed that this is due to the definition of the steps and must be taken into account when defining the control of the robotic arm.

The mechanism responsible for the active surgical motion is a Remote Center of Motion (RCM) mechanism inspired by the theoretical spherical linkage. It consists of two revolute joints and one prismatic joint in series. Two curved beams are used to connect the joints. The geometrical parameters of the mechanism have been optimized. The result is two angles between the joints of 47.1° and 53.6° and a radius of 16.5 cm. Thanks to the preliminary decision to divide the two sub-processes, the mechanism has smaller dimensions than other spherical linkage mechanisms found in the literature.

Finally, the cooperation between the two mechanisms has been studied and two quick release mountings allow the RCM mechanism to be fixed on the alignment mechanism. In this way, the two mechanisms can be separated in a snap, reducing the overall size and improving the portability of the two. The weight and dimensions even meet European standards for portability.

In summary, the proposed robotic arm is suitable for laparoscopic appendectomy, gallbladder removal, and inguinal hernia surgery and has several advantages: it is smaller and lighter than commer-

cially available robotic arms, weighing less than 3 kg and measuring 318 mm x 241.4 mm x 35 mm and 385 mm x 178 mm x 101 mm, and it is portable as defined by the European standard. The modular design with a separation of the alignment mechanism and the operation mechanism has reduced the size of the overall system and its complexity. Overall, the robot arm has been shown to have a solid structure with several improvements in reducing size and weight.

References

[1] Alluminium online.

[2] Aluminium opmaat.

[3] Appendix removal (appendectomy) surgery patient information from sages.

[4] Beware the common bile duct: Surgical malpractice in gallbladder operations.

[5] Comhan holland.

[6] David scott company.

[7] Different types of electric motors.

[8] Electrocraft.

[9] Electrocraft: Brushless dc motors.

[10] Electrocraft: Gearmotors.

[11] Electrocraft: Lrpx32 brushless dc planetary gear motor.

[12] Electrocraft: universal drives.

[13] Engineering 360: Linear motors information.

[14] Engineers garage: Position sensor: Types of position sensor.

[15] Festo.

[16] Gallbladder removal surgery.

[17] Handy steel stocks.

[18] Hardware warehouse.

[19] Hernia repair.

[20] Industrial metal supply co.

[21] Inguinal hernia repair.

[22] Item.

[23] Kiwi electronics.

[24] Kondor blue mini quick release plate blue.

[25] Laparoscopic appendectomy.

[26] Laparoscopic appendectomy.

[27] Laparoscopic appendix removal surgery.

[28] Laparoscopic inguinal hernia repair.

[29] Linear dc-servomotors.

[30] Linear motors p01.

[31] Little bird electronics.

[32] Locks and clamps.

[33] Low-profile linear motors for the world's machines and robots.

[34] Mc master-carr.

[35] Measuring customer experience beyond nps.

[36] Metals for you.

[37] Mid central medical.

[38] Montanstahl: European normal channels.

[39] Pololu robotics electronics.

[40] Properties of ceramics: Mechanical, physical, electrical chemical properties.

[41] Quicklab® linear motor modules guides.

[42] Rextroth.

[43] Rs components.

[44] Skytron.

[45] Steris.

[46] Sus: The system usability scale.

[47] Types of gears.

[48] Universal medical.

[49] Wanted: An abdominal robot for same-day surgery.

[50] Webinar comparison of linear motors and other drive systems.

[51] Yellowstone surgery center: Laparoscopic appendectomy.

[52] Yoycart.

[53] Introduction to robot-assisted minimally invasive surgery (mis). *Paula Gomes, In Woodhead Publishing Series in Biomaterials, Medical Robotics*, pages 1–12, 2012.

[54] Nabeeha Ahmad, Ahmed A. Hussein, Lora Cavuoto, Mohamed Sharif, Jenna C. Allers, Nobuyuki Hinata, Basel Ahmad, Justen D. Kozlowski, Zishan Hashmi, Ann Bisantz, and Khurshid A. Guru. Ambulatory movements, team dynamics and interactions during robot-assisted surgery. *BJU International*, 118:132–139, 7 2016.

[55] Bob Kiaii Stuart A. Swinamer Reiza Rayman W. Douglas Boyd Alan H. Menkis, Kojiro Modera. Robotic surgery the first 100 cases: Where do we go from here? *The Heart of Surgery Forum*, 7, 1 2004.

[56] Ibrahim Alkatout, Hamid Salehiniya, and Leila Allahqoli. Assessment of the versius robotic surgical system in minimal access surgery: A systematic review. *Journal of Clinical Medicine*, 11:3754, 6 2022.

[57] Sujatha Alla. A statistical analysis of surgeons' preference on robot-assisted surgeries, 2019.

[58] Jenna C. Allers, Ahmed A. Hussein, Nabeeha Ahmad, Lora Cavuoto, Joseph F. Wing, Robin M. Hayes, Nobuyuki Hinata, Ann M. Bisantz, and Khurshid A. Guru. Evaluation and impact of workflow interruptions during robot-assisted surgery. *Urology*, 92:33–37, 6 2016.

[59] Maria S. Altieri, Jie Yang, Dana A. Telem, Jiawen Zhu, Caitlin Halbert, Mark Talamini, and Aurora D. Pryor. Robotic approaches may offer benefit in colorectal procedures, more controversial in other areas: a review of 168,248 cases. *Surgical Endoscopy*, 30:925–933, 3 2016.

[60] S. Ambardar, J. Cabot, V. Cekic, K. Baxter, T. D. Arnell, K. A. Forde, A. Nihalani, and R. L. Whelan. Abdominal wall dimensions and umbilical position vary widely with bmi and should be taken into account when choosing port locations. *Surgical Endoscopy*, 23:1995–2000, 2009.

[61] Balaiya Anitha, Karuppusamy Aravindhan, Sathasivam Sureshkumar, Manwar S Ali, Chellappa Vijayakumar, and Chinnakali Palanivel. The ideal size of mesh for open inguinal hernia repair: A morphometric study in patients with inguinal hernia. *Cureus*, 5 2018.

[62] Vigen Arakelian. Gravity compensation in robotics. *Advanced Robotics*, 30:79–96, 1 2016.

[63] Cédric Baradat, Vigen Arakelian, Sébastien Briot, Sylvain Guegan, Guegan Sylvain, C Baradat, V Arakelian, S Briot, and S Guegan. Design and prototyping of a new balancing mechanism for spatial parallel manipulators, 2008.

[64] William L Bargar, Andrk Bauer, and Martin Borner. Primary and revision total hip replacement using the robodoc@ system, 1998.

[65] R Berguer. New technology surgical technology and the ergonomics of laparoscopic instruments, 1998.

[66] Peter Berkelman and Ji Ma. A compact modular teleoperated robotic system for laparoscopic surgery. *International Journal of Robotics Research*, 28:1198–1215, 9 2009.

[67] Alessia De Biasi. Identification and deeper insight of the most emerging trend in minimally invasive surgery robotic systems, 2022.

[68] Ricardo Buettner, Alena Renner, and Anna Boos. A systematic literature review of research in the surgical field of medical robotics. pages 517–522. Institute of Electrical and Electronics Engineers Inc., 7 2020.

[69] David B. Camarillo, Thomas M. Krummel, and J. Kenneth Salisbury. Robotic technology in surgery: Past, present, and future. *American Journal of Surgery*, 188:2–15, 2004.

[70] Heather Carmichael, Anthony P. D'Andrea, Matthew Skancke, Vincent Obias, and Patricia Sylla. Feasibility of transanal total mesorectal excision (tatme) using the medrobotics flex® system. *Surgical Endoscopy*, 34:485–491, 1 2020.

[71] Shao Hui Chen, Zhao Ai Li, Rui Huang, and Hui Qin Xue. Robot-assisted versus conventional laparoscopic surgery for endometrial cancer staging: A meta-analysis, 8 2016.

[72] Samuel Chevailler. comparative study and selection criteria of linear motors, 2006.

[73] Ling Hui Chu, Wen Chun Chang, and Bor Ching Sheu. Comparison of the laparoscopic versus conventional open method for surgical staging of endometrial carcinoma. *Taiwanese Journal of Obstetrics and Gynecology*, 55:188–192, 4 2016.

[74] Roberto Cirocchi, Stefano Partelli, Stefano Trastulli, Andrea Coratti, Amilcare Parisi, and Massimo Falconi. A systematic review on robotic pancreaticoduodenectomy, 12 2013.

[75] Marco Controzzi, Christian Cipriani, and Maria Chiara Carrozza. Miniaturized non-backdrivable mechanism for robotic applications. *Mechanism and Machine Theory*, 10:1395–1406, 10 2010.

[76] F. Corcione, C. Esposito, D. Cuccurullo, A. Settembre, N. Miranda, F. Amato, F. Pirozzi, and P. Caiazzo. Advantages and limits of robot-assisted laparoscopic surgery: Preliminary experience. *Surgical Endoscopy and Other Interventional Techniques*, 19:117–119, 1 2005.

[77] J.A. Corrales, F.A. Candelas, and F. Torres. Hybrid tracking of human operators using imu/uwb data fusion by a kalman filter. *2008 3rd ACM/IEEE international conference on human–robot interaction (HRI)*, page 193–200, 2008.

[78] Yasukawa D, Aisu Y, and Hori T. World journal of gastrointestinal surgery world journal of gastrointestinal surgery opinion review crucial anatomy and technical cues for laparoscopic transabdominal preperitoneal repair: Advanced manipulation for groin hernias in adults 307. *World Journal of Gastrointestinal Surgery Contents Monthly*, 12:307–335, 2020.

[79] G. F. Dakin and M. Gagner. Comparison of laparoscopic skills performance between standard instruments and two surgical robotic systems. *Surgical Endoscopy and Other Interventional Techniques*, 17:574–579, 4 2003.

[80] Ibrahim Darwich, D. Stephan, M. Klöckner-Lang, M. Scheidt, R. Friedberg, and F. Willeke. A roadmap for robotic-assisted sigmoid resection in diverticular disease using a senhance™ surgical robotic system: results and technical aspects. *Journal of Robotic Surgery*, 14:297–304, 4 2020.

[81] Ara Darzi and Yaron Munz. The impact of minimally invasive surgical techniques, 2004.

[82] Biman Das and Yanqing Wang. Isometric pull-push strengths in workspace: 1. strength profiles. *International Journal of Occupational Safety and Ergonomics*, 10:43–58, 2004.

[83] Begos D.G. and Modlin I.M. Laparoscopic cholecystectomy: From gimmick to gold standard, journal of clinical gastroenterology. *Journal of Clinical Gastroenterology*, 19:325–330, 12 1994.

[84] Carlos Eduardo Díaz, Roemi Fernández, Manuel Armada, and Felipe De Jesús García Gutiérrez. State of the art in robots used in minimally invasive surgeries. natural orifice transluminal surgery (notes) as a particular case. *Industrial Robot*, 42:508–532, 10 2015.

[85] Kyung Jin Eoh, Dae Woo Lee, Ji Hyun Lee, Eun Ji Nam, Sang Wun Kim, and Young Tae Kim. Comparative survival outcome of robot-assisted staging surgery using three robotic arms versus open surgery for endometrial cancer. *Yonsei Medical Journal*, 62:68–74, 1 2021.

[86] George S. Ferzli and Abe Fingerhut. Trocar placement for laparoscopic abdominal procedures: A simple standardized method. *Journal of the American College of Surgeons*, 198:163–173, 2004.

[87] Rithvik Gambhir and Akshay Kumar Jha. Brushless dc motor: Construction and applications.

[88] Mostafa Hadavand, Alireza Mirbagheri, Saeed Behzadipour, and Farzam Farahmand. A novel remote center of motion mechanism for the force-reflective master robot of haptic tele-surgery systems. *International Journal of Medical Robotics and Computer Assisted Surgery*, 10:129–139, 2014.

[89] U. Hagn, M. Nickl, S. Jörg, G. Passig, T. Bahls, A. Nothhelfer, F. Hacker, L. Le-Tien, A. Albu-Schäffer, R. Konietschke, M. Grebenstein, R. Warpup, R. Haslinger, M. Frommberger, and G. Hirzinger. The dlr miro: A versatile lightweight robot for surgical applications. *Industrial Robot*, 35:324–336, 2008.

[90] Sang Hyup Han, Chang Moo Kang, Ho Kyoung Hwang, Dong Sup Yoon, and Woo Jung Lee. The yonsei experience of 104 laparoscopic pancreaticoduodenectomies: a propensity score-matched analysis with open pancreaticoduodenectomy. *Surgical Endoscopy*, 34:1658–1664, 4 2020.

[91] Eric J. Hanly and Mark A. Talamini. Robotic abdominal surgery. *American Journal of Surgery*, 188:19–26, 2004.

[92] Nasser Hashemnia and Behzad Asaei. Comparative study of using different electric motors in the electric vehicles. pages 1–5, 2008.

[93] Yutaka Hiroi and Akinori Ito. Influence of the size factor of a mobile robot moving toward a human on subjective acceptable distance, 10 2011.

[94] Johns Hopkins, K Gage Parr, and Mark A Talamini. Anesthetic implications of the addition of an operative robot for endoscopic surgery: A case report, 2002.

[95] Robert D Howe and Yoky Matsuoka. Robotics for surgery, 1999.

[96] Xiaobang Hu, Donna D. Ohnmeiss, and Isador H. Lieberman. Robotic-assisted pedicle screw placement: Lessons learned from the first 102 patients. *European Spine Journal*, 22:661–666, 3 2013.

[97] Tran Manh Hung, Tran Que Son, Tran Hieu Hoc, Tran Thanh Tung, Trieu Van Truong, Le Manh Cuong, and Vu Duy Kien. Long- and short-term survival following laparoscopic and open pancreaticoduodenectomy for patients with periampullary tumors in vietnam. *Annals of Medicine and Surgery*, 69, 9 2021.

[98] Frederick Huynh, Charles Jimenez Cruz, Ho Kyoung Hwang, Woo Jung Lee, and Chang Moo Kang. Minimally invasive (laparoscopic and robot-assisted) versus open approach for central pancreatectomies: a single-center experience. *Surgical Endoscopy*, 2021.

[99] B. Jaffray. Minimally invasive surgery, 5 2005.

[100] Jesse McKenney et al. John R. Goldblum, Laura W. Lamps. *Rosai and Ackerman's Surgical Pathology*, volume 2. 2017.

[101] Andreas M. Kaiser. Evolution and future of laparoscopic colorectal surgery. *World Journal of Gastroenterology*, 20:15119–15124, 11 2014.

[102] Sven Rainer Kantelhardt, Ramon Martinez, Stefan Baerwinkel, Ralf Burger, Alf Giese, and Veit Rohde. Perioperative course and accuracy of screw positioning in conventional, open robotic-guided and percutaneous robotic-guided, pedicle screw placement. *European Spine Journal*, 20:860–868, 6 2011.

[103] A J Karayiannakis, G G Makri, A Mantzioka, D Karousos, and G Karatzas. Postoperative pulmonary function after laparoscopic and open cholecystectomy, 1996.

[104] Peter Kazanzides, Gabor Fichtinger, Gregory D. Hager, Allison M. Okamura, Louis L. Whitcomb, and Russell H. Taylor. Surgical and interventional robotics - core concepts, technology, and design. *IEEE Robotics and Automation Magazine*, 15:122–130, 6 2008.

[105] Karl Khandalavala, Tim Shimon, Laura Flores, Priscila Rodrigues Armijo, and Dmitry Oleynikov. Emerging surgical robotic technology: A progression toward microbots, 1 2020.

[106] Kaushik Kumar and J. Paulo Davim. *Modern Manufacturing Processes*. 2020.

[107] Prabhat Kumar and B. Ravi. A comparative study of robots in laparoscopic surgeries. ICST, 7 2019.

[108] Chin-Hsing Kuo and Jian S Dai. Robotics for minimally invasive surgery: A historical review from the perspective of kinematics, 1 2009.

[109] Anthony R. Lanfranco, Andres E. Castellanos, Jaydev P. Desai, and William C. Meyers. Robotic surgery: A current perspective, 1 2004.

[110] Ho Kun Lee, Ka Eun Lee, Jiwon Ku, and Keun Ho Lee. Revo-i: The competitive korean surgical robot. *Gynecologic Robotic Surgery*, 2:45–52, 9 2021.

[111] J. Lee and S. Jung. Global position tracking control of an omni-directional mobile robot using fusion of a magnetic compass and encoders. In *2008 IEEE International Conference on Multisensor Fusion and Integration for Intelligent Systems*, pages 246–251, 2008.

[112] Pierre Letier, More Avraam, André Schiele, and A. Preumont. Survey of actuation technologies for body-grounded exoskeletons. 07 2006.

[113] Hongen Liao, Hirotaka Ishihara, Huy Hoang Tran, Ken Masamune, Ichiro Sakuma, and Takeyoshi Dohi. Fusion of laser guidance and 3-d autostereoscopic image overlay for precision-guided surgery. volume 5128 LNCS, pages 367–376, 2008.

[114] Jin Hong Lim, Woo Jung Lee, Seung Ho Choi, and Chang Moo Kang. Cholecystectomy using the revo-i robotic surgical system from korea: the first clinical study. *Updates in Surgery*, 73:1029–1035, 6 2021.

[115] Sally Kathryn Longmore, Ganesh Naik, and Gaetano D. Gargiulo. Laparoscopic robotic surgery: Current perspective and future directions. *Robotics*, 9, 6 2020.

[116] S C Low and L Phee. A review of master-slave robotic systems for surgery, 2006.

[117] Houston Lucas, Jamie Poston, Nathan Yocum, Zachary Carlson, and David Feil-Seifer. Too big to be mistreated? examining the role of robot size on perceptions of mistreatment. pages 1071–1076. Institute of Electrical and Electronics Engineers Inc., 11 2016.

[118] Mitchell J.H. Lum, Jacob Rosen, Mika N. Sinanan, and Blake Hannaford. Optimization of a spherical mechanism for a minimally invasive surgical robot: Theoretical and experimental approaches. *IEEE Transactions on Biomedical Engineering*, 53:1440–1445, 7 2006.

[119] M. Luo, E. Li, R. Guo, J. Liu, and Z. Liang. End-effector pose estimation in complex environments using complementary enhancement and adaptive fusion of multisensor. *Journal of Sensors*, 2021:1–18, 04 2021.

[120] M.J. Mack. Minimally invasive and robotic surgery. pages 568–72, 2 2001.

[121] Jacques Marescaux and Francesco Rubino. The zeus robotic system: Experimental and clinical applications, 2003.

[122] Rémi Merindol. Assemblage couche-par-couche de nano-composites bio-inspirés. 09 2014.

[123] J.F.M. Molenbroek. DINED - Anthropometric Database, 2018.

[124] Ahamed Muneef, Uday Kumbhar, Chellappa Vijayakumar, and Oseen Shaikh. A comparative study between single-incision laparoscopic appendicectomy using conventional instruments and glove-port (silacig) and conventional multiport laparoscopic appendicectomy (cmla). *Cureus*, 10 2020.

[125] Siamak Najarian and Elnaz Afshari. Evolutions and future directions of surgical robotics: A review. *International Journal of Clinical Medicine*, 03:75–82, 2012.

[126] Farr R. Nezhat and Ido Sirota. Perioperative outcomes of robotic assisted laparoscopic surgery versus conventional laparoscopy surgery for advanced-stage endometriosis. *Journal of the Society of Laparoendoscopic Surgeons*, 18, 2014.

[127] Tobias Ortmaier, Holger Weiss, and Volkmar Falk. Design requirements for a new robot for minimally invasive surgery, 2004.

[128] A. Passon, T. Schauer, and T. Seel. Inertial-robotic motion tracking in end-effector-based rehabilitation robots. *Front. Robot. AI*, 7:554639, November 2020.

[129] Jérôme Perret and Pierre Vercruysse. Advantages of mechanical backdrivability for medical applications of force control, 2014.

[130] Rodrigo Rodrigues Pessoa, Paul Maroni, Janet Kukreja, and Simon P. Kim. Comparative effectiveness of robotic and open radical prostatectomy, 5 2021.

[131] Alexandra Peteoaca, Andreea Istrate, Andrei Tanase, and Jacqueline Mocanu. A review of robotic surgery evolution, current applications and future prospects, 2 2018.

[132] Brian S. Peters, Priscila R. Armijo, Crystal Krause, Songita A. Choudhury, and Dmitry Oleynikov. Review of emerging surgical robotic technology, 4 2018.

[133] Marco Piccigallo, Umberto Scarfogliero, Claudio Quaglia, Gianluigi Petroni, Pietro Valdastri, Arianna Menciassi, and Paolo Dario. Design of a novel bimanual robotic system for single-port laparoscopy. *IEEE/ASME Transactions on Mechatronics*, 15:871–878, 12 2010.

[134] Vyas Prasad, Raja Fakhoury, Marc Remacle, and Georges Lawson. The medrobotics flex system – first use of a novel system for operating on three benign laryngeal cases. 06 2016.

[135] Pradeep P. Rao. Robotic surgery: new robots and finally some real competition! *World Journal of Urology*, 36:537–541, 4 2018.

[136] Jacob Rosen, Jeffrey D. Brown, Marco Barreca, Lily Chang, Blake Hannaford, and Mika Sinanan. The blue dragon - a system for monitoring the kinematics and the dynamics of endoscopic tools in minimally invasive surgery for objective laparoscopic skill assessment. volume 85, pages 412–418. IOS Press, 2002.

[137] Cesare Ruffolo, Alain Fiorot, Giulia Pagura, Michele Antoniutti, Marco Massani, Ezio Caratozzolo, Luca Bonariol, Francesco calia di pinto, and Nicolò Bassi. Acute appendicitis: What is the gold standard of treatment? *World journal of gastroenterology : WJG*, 19:8799–807, 12 2013.

[138] A.M. Sabatini. Quaternion-based extended kalman filter for determining orientation by inertial and magnetic sensing. *IEEE Transactions on Biomedical Engineering*, 53(7):1346–1356, 2006.

[139] D A Simon. Intra-operative position sensing and tracking devices.

[140] Levi Sutton. Auto-locking ball joint, 2015. US Patent US20170184149A1.

[141] Emma M. van der Schans, Marijn A.J. Hiep, Esther C.J. Consten, and Ivo A.M.J. Broeders. From da vinci si to da vinci xi: realistic times in draping and docking the robot. *Journal of Robotic Surgery*, 14:835–839, 12 2020.

[142] Joan L. Walker, Marion R. Piedmonte, Nick M. Spirtos, Scott M. Eisenkop, John B. Schlaerth, Robert S. Mannel, Richard Barakat, Michael L. Pearl, and Sudarshan K. Sharma. Recurrence and survival after random assignment to laparoscopy versus laparotomy for comprehensive surgical staging of uterine cancer: Gynecologic oncology group lap2 study. *Journal of Clinical Oncology*, 30:695–700, 3 2012.

[143] Qian Wan, Oliver Schoppe, Suvai Gunasekaran, Dónal Holland, Ellen Roche, Hye-Chun Hur, and Conor Walsh. Multifunctional laparoscopic trocar with built-in fascial closure and stabilization, 2006.

[144] Inneke Willekens, Els Peeters, Michel De Maeseneer, and Johan De Mey. The normal appendix on ct: Does size matter? *PLoS ONE*, 9, 5 2014.

[145] Jaehong Woo, Jong Tae Seo, and Byung Ju Yi. A static balancing method for variable payloads by combination of a counterweight and spring and its application as a surgical platform. *Applied Sciences (Switzerland)*, 9, 10 2019.

[146] Z. Wu and Y. Wu. Design of angular position and velocity observer for servo motors with reslovers. In *Proceedings of the 31st Chinese Control Conference*, pages 4350–4355, 01 2012.

[147] Binghong Xiong, Li Ma, Wei Huang, Qikang Zhao, Yong Cheng, and Jingshan Liu. Robotic versus laparoscopic total mesorectal excision for rectal cancer: a meta-analysis of eight studies. *Journal of Gastrointestinal Surgery*, 19:516–526, 3 2015.

[148] Shuang Xu, Minoru Yokoyama, and Tomoyuki Shimono. Back-drivability improvement of geared system based on disturbance observer and load-side disturbance observer. *IEEJ Journal of Industry Applications*, 9:475–485, 9 2020.

[149] W. Yang, A. Bajenov, and Y. Shen. Improving low-cost inertial-measurement-unit (imu)-based motion tracking accuracy for a biomorphic hyper-redundant snake robot. *Robot. Biomim. 4, 16*, 2017.

[150] Tsuneo Yoshikawa. Manipulability of robotic mechanisms.

[151] Matthew Zelhart and Andreas M. Kaiser. Robotic versus laparoscopic versus open colorectal surgery: towards defining criteria to the right choice, 1 2018.

[152] P. Zhang, J. Gu, E.E Milios, and P. Huynh. Navigation with imu/gps/digital compass with unscented kalman filter. *IEEE international conference mechatronics and automation*, 3:1497–15023, 2005.

16 Appendix A

Table 35: Quick overview of the linear motors [72]

Application	**Linear motor type**
Voice coil	• speed: very high • force: 160 N • accuracy: encoder dependent • cost: low • limitation: short travel
Force tube	• speed:4 m/s • force: 4800 N • accuracy: encoder dependent • cost: high • limitation: high profile
Stepper	• speed:25 to 2500 mm/s • force: 9 to 220 N • accuracy: 2 to 250 μm • cost: low • limitation: open loop, low stiffness, not efficient
Hybrid	• speed: 1.5 m/s • force: 800 N • accuracy: encoder dependent • cost: high • limitation: speed force characteristic

Table 36: Continue of Table 36 [72]

DC brush	• speed: 3.8 m/s • force: 1070 N • accuracy: encoder dependent • cost: moderate • limitation: contamination from brush wear, brush wear, arcing of brushes
AC induction	• speed: 6.85 m/s • force: 2225 N • accuracy: encoder dependent • cost: moderate • limitation: low duty cycle
Iron core AC Synchronous	• speed: 10 m/s • force: 11000 N • accuracy: encoder dependent • cost: high • limitation: exposed magnets can attract and hold ferrous objects
Ironless core AC Synchronous	• speed: 10 m/s • force: 2000 N • accuracy: encoder dependent • cost: high • limitation: exposed magnets can attract and hold ferrous objects. Needs liquid cooling for high force duty cycle

17 Appendix B

17.1 Attendance to a laparoscopic surgery

The day 15/06/2022, at 3pm, I have assisted a gallbladder removal minimum invasive surgery at the Hospital *Ospedale dei Castelli Romani, reparto di Chirurgia, surgery room 4*, Rome, Italy, for including practicalities and observations in my concept selection and discussion section. The main points that have been brought in light by this experience are:

- *Position of the Trocars*: the trocars are positioned by the assistants in base of the protocols and surgery that needs to be performed. The entrance angle of the trocar and the workspace depends on the surgery procedure. Additionally, each trocar for the same surgery has different entrance angle and workspace. In this procedure, 4 trocars where inserted. Two of them where used for passively hold the Gallbladder and the liver, and have a very small workspace. The same happen for the trocar used for the laparoscope, which is inserted just under the belly button with an angle of around 30 degrees. The active instrument is inserted in a trocar with an angle of 30 degrees and with an active workspace of a conic shape with opening of almost 15 degrees each side.

- *External workspace of the trocar*: the length of the trocar inserted in the abdominal cavity depends on the procedure and on the trocar's position and function. In the assisted procedure, the different trocars had different lengths outside the abdominal cavity. The longer length of trocar that was staying out of the patient was around 6 cm. This means that the hard head of the trocar that was staying out was making a large motion with respect to the incision point, do to the rotation around it.

- *Incision point*: the incision point, during the procedure, keeps slightly bleeding. The assistants repetitively clean around the incision point. Additionally, at the end of the procedure, the instruments are used on the wall of the incision point, while the trocar is being removed. This is done for curing the damage caused by the trocar in the skin.

- *Set up of the existing technologies*: for the ball bladder some feet holders were set up after the patient was asleep. The set up of the feet holders was done by the use of sliding joints fixed with pressure screws. The technology is quite familiar to the assistants.

- *Surgical table*: the main interesting part of the surgical table for this project is the lateral rail, Figure 156. This rail is already present in the surgical tables, and allows the set up of adds such as the feet holder discussed previously, arm holders, thighs holders and so on. This rail runs on the longitudinal side of the bed, and allows to insert any slider that can be fixed through a pressure screw. Usually, there are already extra structure near the limbs of the patients, but not at the height of the abdominal cavity.

Finally, some insights were gained by asking some questions at the assistant experts:

- *Global positioning design*: the assistants present in the operating room were asked what they thought about the set up designs, mainly the three cylindrical joints one and the trocar radial one. Most of them agreed on saying that the first seems more intuitive and comfortable for them to set up, since it resembles the set up of the already existing adds on.

- *Incision point*: additionally, they suggested to leave the incision point free of constraint.The incision point is usually reached in case of emergency. This is why, while observing the design 4 and 5, they suggested the 4 to be safer and better for the procedure.

Figure 156: Surgical bed [45]

18 Appendix C

18.1 System for rotational motion

For the design 5, systems that allow the rotation of the two rings must be selected. The rotation should happen in a ring with an opening that can satisfy the dimensions required.
The possible solutions are listed below and compare.

- *Belt drives: Electric motors + belts*: an option for achieving this motion is to connect an electric motor to a timing belt, and have the belt running over the ring. In this application, toothed belts should be selected, for achieving the required accurate drive or speed. They can be used for long centre distance, absorbing shocks and vibrations. They do not require lubricants and are not affected by dirt and dust, while being very quite. The main disadvantages of this system is the fact that friction belts are prone to slip, due to stretching after use and need to be adjusted. Additionally, they are easily damaged by heat. They have a shorter life and need more space as compared to gear drive, and they have low power transmitting capacity. They have high friction loss, therefore lower transmission and less efficiency. They require periodic inspections and maintenance.

- *Gear drives: Electric motors + gears*: In these drives, different types of gears are used for different purposes. However, worm gears are highly not backdrivable, for this reason they are left out of the possible solution.
  In general, gear drivers are non-slip drivers, are mechanically strong, deliver high transmission efficiency, and are more compact compared to the belt drivers. Additionally, they have a much grater life expectancy than belt drives. However, they are not ideal for large velocities, they increase the overall weight of the system, and they have no flexibility. They, also, require regular lubrication, they do not isolate from shock and vibration, and they are noisy in the operation.

- *Piezoelectric motors*: they are based on the piezoelectric effect, that is the ability of certain materials to generate an electric change in response to the applied mechanical stress. These motors works on this principle, only in reverse. A voltage is applied to the piezoelectric element of an elastic body, stator, which expands and contracts, creating a motion in the rotor. These motors best fit the design, because they have compact size: they are small, thin and lightweight. Additionally, they present a good efficiency, can produce high torque, leaving aside the need of transmission. They, also, have a good holding torque, that means the motor does not move if powered off, increasing the hold in place stability. They are highly controllable, and they have high response, all with an overall low cost. Finally, they do not generate magnetic field. However, they use high frequency power supply and it is necessary to suppress heat while functioning. Finally, they come in small dimensions, and it is necessary to check if they can reach the required dimensions.

- *Frameless torque motors*: Called also direct drive units, they are permanent-magnet direct drive motors that rotate along an axis. These motors can be used wherever a rotary movement is required and offer numerous advantages over conventional servo drives. The two main characteristics are a three phase stator and a permanent magnet rotor which consists out of a minimum of 4 poles. Their advantages are to have hollow shaft, direct drive due to the fact that they have high torque and, thus, do not need gearbox, high precision and response, thin rotor and low inertia. Additionally, their diameter has a big range, from 19 to 790 mm. They have a compact design, a simplified machine structure, they produce less noise and need less maintenance. Moreover, the direct connection to the load increases torsional stiffness.

After this overview, a preliminary decision of the most suitable motor is taken, leaving the decision between frameless torque motors and piezoelectric motors. The decision between the two is taken after the dimensioning of the system and the calculations of required torque and velocity.

19 Appendix D

19.1 Forward Kinematics RCM mechanism

```
%% forward kinematics
%% forward kinematics
clc
clear all
syms a1 a2 R ;
syms t1 t2 d a b x bo;
syms px py pz;

% create a numerical or symbolic DH parameter
DH=[ t1      a1       R-R*cos(a1);            %frame2
     t2      a2       R-R*cos(a2);            %frame3
     0       0        d];                     %frame4


H01=BuildTw([0;0;0],[0;0;0]);
H12=BuildTw([-R*sin(a1)*sin(t1);+R*sin(a1)*cos(t1);R-R*cos(a1)],[a1;0;t1]);
H23=BuildTw([-R*sin(a2)*sin(t2);+R*sin(a2)*cos(t2);R-R*cos(a2)],[a2;0;t2]);
H34=BuildTw([0;0;d],[0;0;0]);



H02=H01*H12;
H03=H02*H23;
H04=H02*H23*H34;
A04=H04*[0;0;0;1];
%A04=simplify(A04)
A04=simplify(A04)

function Tws=BuildTw(pos,angle)

x=angle(1);
y=angle(2);
z=angle(3);

rotx=[1          0           0
      0          cos(x)     -sin(x)
      0          sin(x)      cos(x)]; %rotational matrix when rotation around x

roty=[cos(y)     0           sin(y)
      0          1           0
     -sin(y)     0           cos(y)]; %rotational matrix when rotation around y

rotz=[cos(z)    -sin(z)          0
      sin(z)     cos(z)          0
      0          0               1];  %rotational matrix when rotation around z

rot=rotz*roty*rotx;    %final rotational matrix
Tws=[rot pos;0 0 0 1]; %construction of homogeneous matrix
end
```

19.2 Jacobian matrix RCM mechamism

```
R01=H01(1:3,1:3);
 R12=H12(1:3,1:3);
 R02=R01.'*R12.';
 R23=H23(1:3,1:3);
 R13=R12.'*R23.';
 R03=R02*R23.';
 V=[0;0;1];

the_J = jacobian([A04(1) A04(2) A04(3)],[t1 t2 d])

 J21=R03.'*V;
 J22=simplify(R23.'*V);
 J23=V;

 J=[the_J;
    J21 J22 J23]

Jw=J(4:5,1:2)
simplify(sqrt(det(Jw*Jw.')))
```

19.3 Inverse kinematics

```
%% inverse kinematics

%% new inverse
su=subs(A04(3),cos(t2),x);
cost2sol=solve(su==pz,x)

new=subs(A04,sin(t1),a);
neww=solve(new(1)==px,a);
new=subs(new,a,neww);
new=simplify(subs(new,cos(t1),b));
cost1sol=simplify(solve(new(2)==py,b))
sint1sol=simplify(subs(neww,cos(t1),cost1sol))
```

20 Appendix E

In this section the angles the three procedures are defined. The dimensioning is done referring to the blue points and the black dark line sketched on the figures.

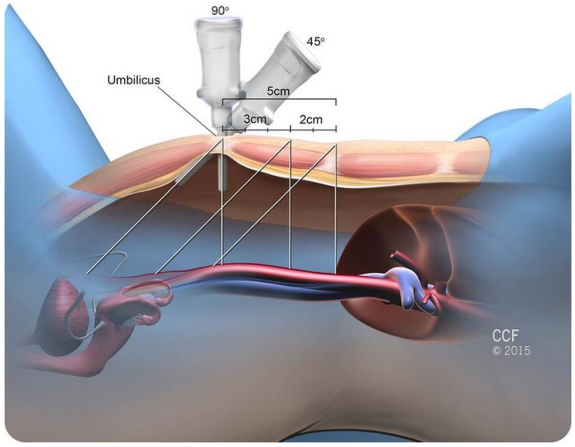

Figure 157: Position of primary trocars for gallbladder removal [4]

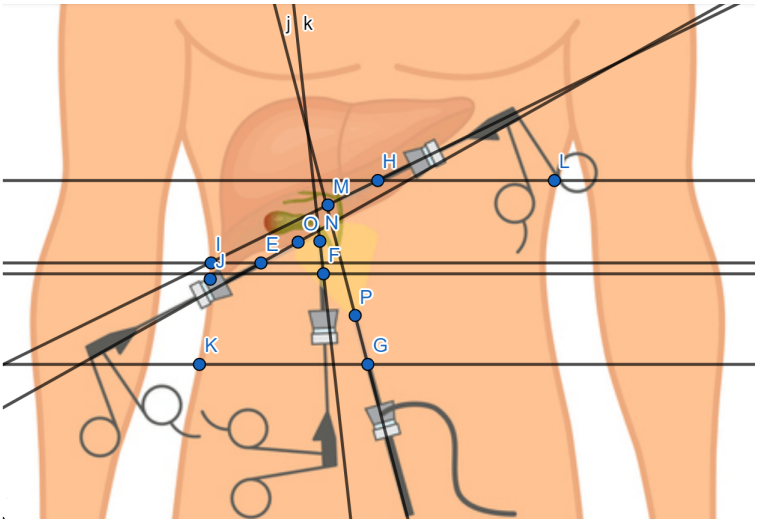

Figure 158: Position of trocars for gallbladder removal [4]

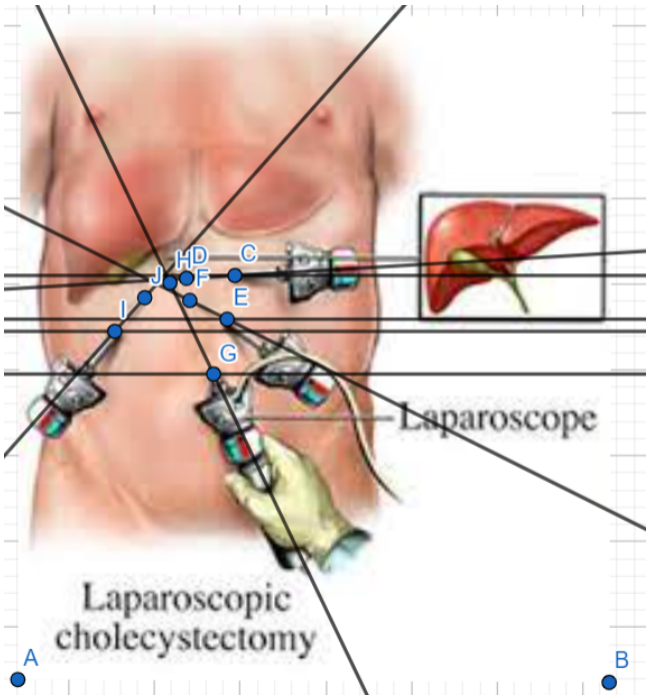

Figure 159: Position of trocars for gallbladder removal [16]

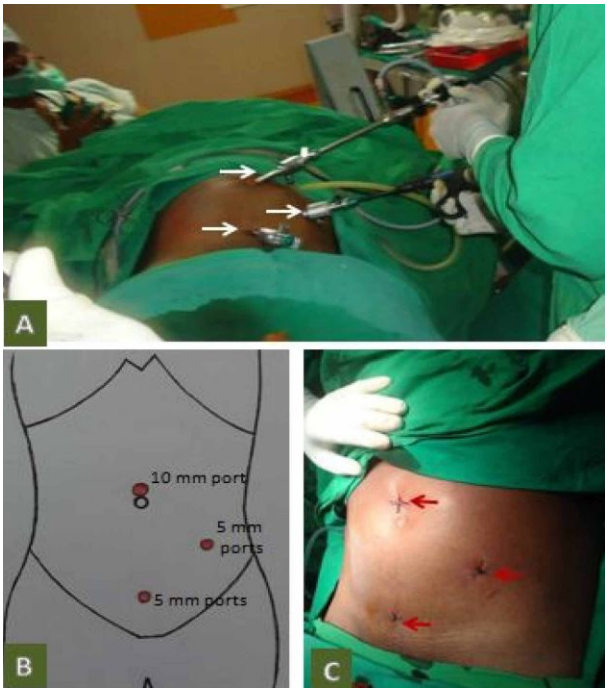

Figure 160: Position of trocars for appendectomy [124]

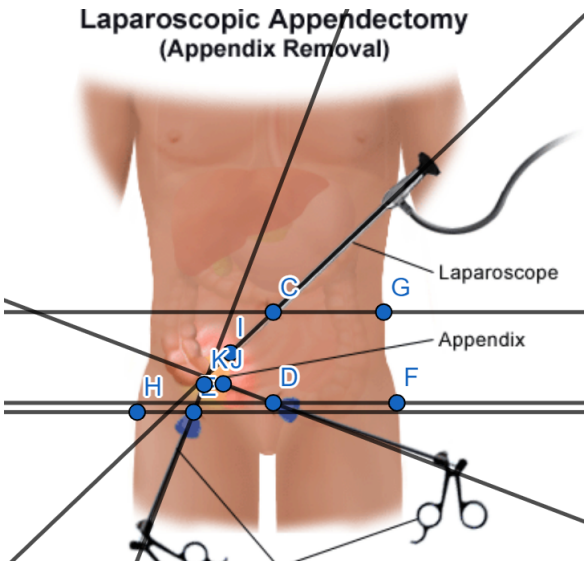

Figure 161: Position of trocars for appendectomy [25]

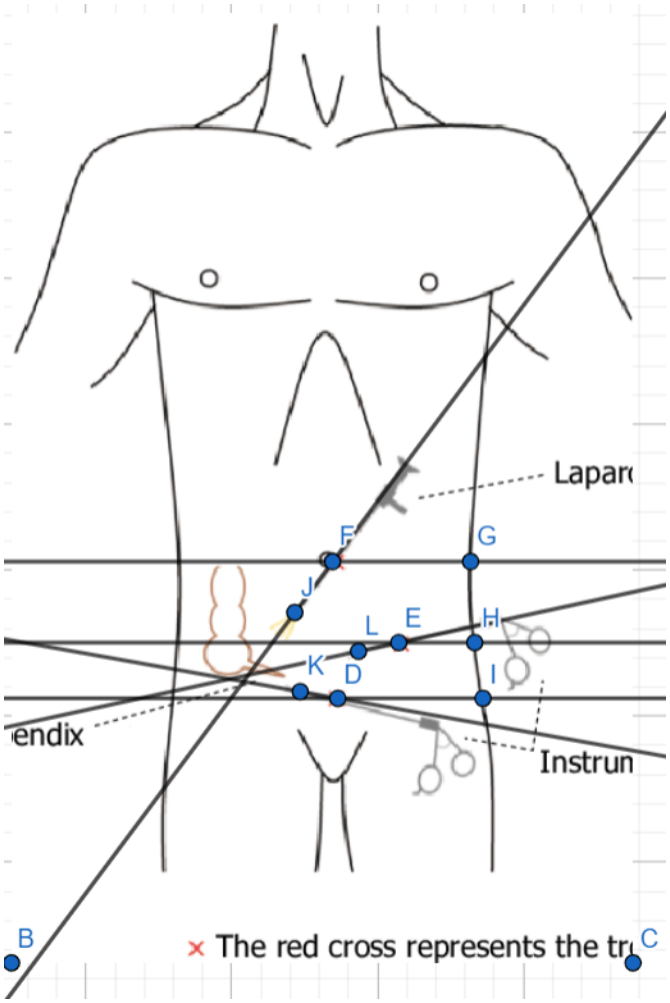

Figure 162: Position of trocars for appendectomy [137]

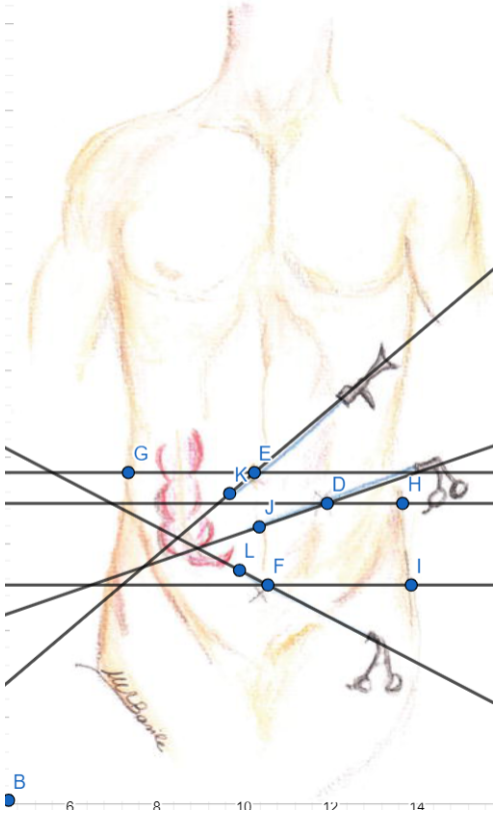

Figure 163: Position of trocars for appendectomy [26]

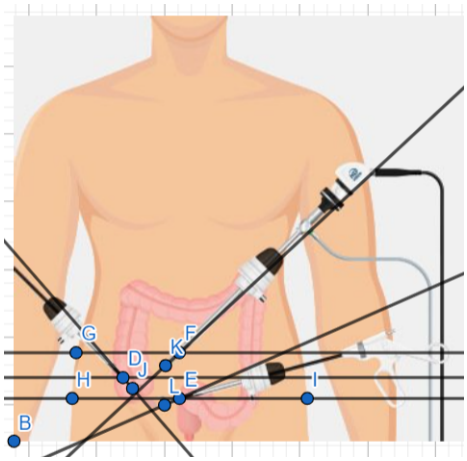

Figure 164: Position of trocars for appendectomy [27]

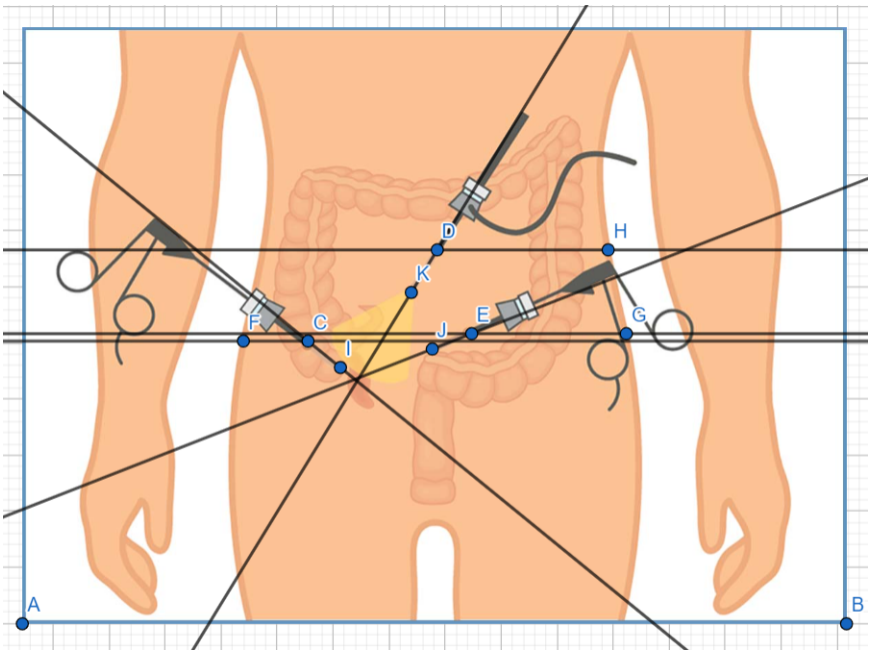

Figure 165: Position of trocars for appendectomy [51]

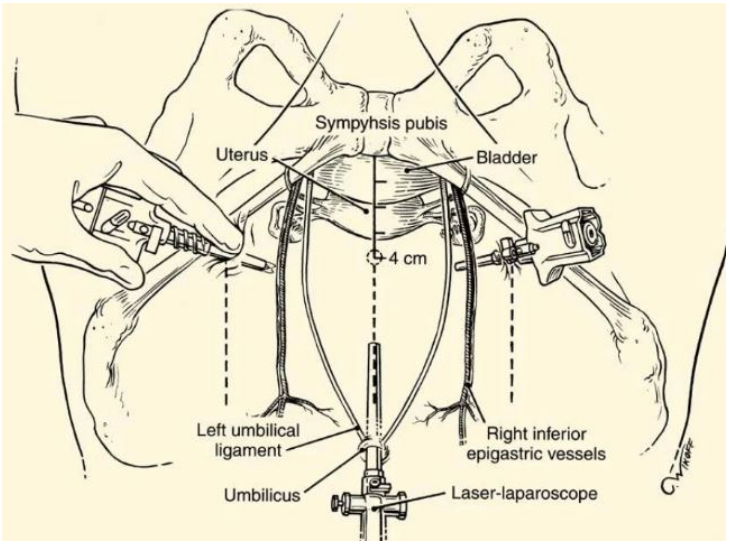

Figure 166: Position of trocars for inguinal hernia surgery [78]

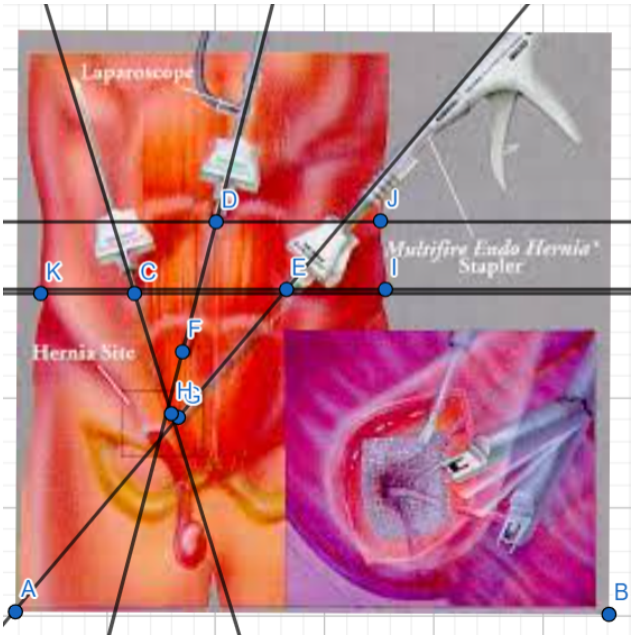

Figure 167: Position of trocars for inguinal hernia surgery [28]

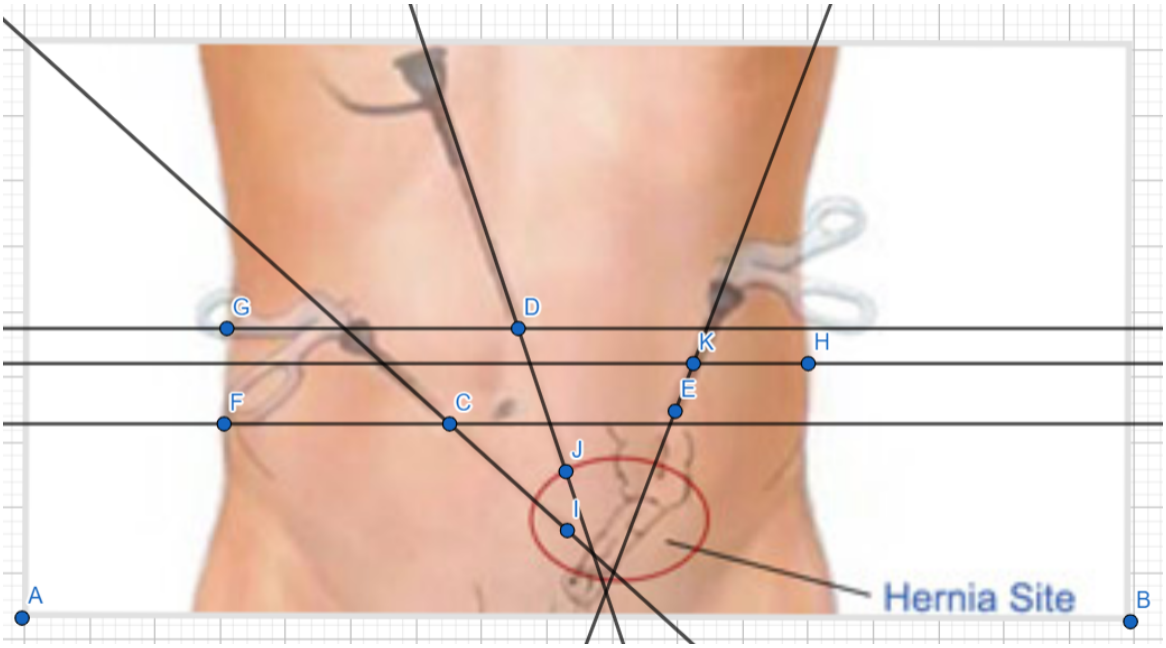

Figure 168: Position of trocars for inguinal hernia surgery [21]

21 Appendix F

The following code permits to calculate and visualize the forward kinematics and the inverse kinematics of the RCM mechanism.

```
%% possible position of worspaces
clear all
clc
syms t1 t2 a1 a2 t1 t2 d a b x d
syms  px py pz
a1n=deg2rad(49.7207);
a2n=deg2rad(25.8175);
R=18;

H01=BuildTw([0;0;0],[0;0;0]);
H12=BuildTw([-R*sin(a1)*sin(t1);+R*sin(a1)*cos(t1);R-R*cos(a1)],[a1;0;t1]);
H23=BuildTw([-R*sin(a2)*sin(t2);+R*sin(a2)*cos(t2);R-R*cos(a2)],[a2;0;t2]);
H34=BuildTw([0;0;d],[0;0;0]);
H02=H01*H12;
H03=H02*H23;
H04=H02*H23*H34;
A04=H04*[0;0;0;1];


%% next step for forward
XE_MLF = matlabFunction(A04(1),'Vars',[a1 a2 t1 t2 d]);
YE_MLF = matlabFunction(A04(2),'Vars',[a1 a2 t1 t2 d]);
ZE_MLF = matlabFunction(A04(3),'Vars',[a1 a2 t1 t2 d]);

%% visualize forward kinematics
t1_degs_row = linspace(-90,90,100);
t2_degs_row = linspace(-180,180,100);
d_value= linspace(0,10,100);
[tt1_degs,tt2_degs] = meshgrid(t1_degs_row,t2_degs_row);
tt1_rads = deg2rad(tt1_degs);
tt2_rads = deg2rad(tt2_degs);

for i=0:1
X_mat = XE_MLF(a1n,a2n,tt1_rads,tt2_rads, 0);
Y_mat = YE_MLF(a1n,a2n,tt1_rads,tt2_rads, 0);
Z_mat = ZE_MLF(a1n,a2n,tt1_rads,tt2_rads, 0);
figure(1)
plot3(Z_mat,X_mat,Y_mat)
plot3(18,0,0,'*')
title("motion");
xlabel('z axis');
ylabel('x axis');
zlabel('y axis')
hold on
figure(2)
plot(Z_mat,Y_mat)
title("motion");
xlabel('z axis');
ylabel('y axis');
hold on
figure(3)
plot(X_mat,Y_mat)
```

```
title("motion");
xlabel('x axis');
ylabel('y axis');
hold on
figure(4)
plot(Z_mat,X_mat)
title("motion");
xlabel('z axis');
ylabel('x axis');
hold on
i=i+1;
end

plot_XY_given_theta_2dof(tt1_degs,tt2_degs,X_mat,Y_mat,(a1n+a2n))
plot_XZ_given_theta_2dof(tt1_degs,tt2_degs,X_mat,Z_mat,(a1n+a2n))



%% function for creating homogeneous matrices
function Tws=BuildTw(pos,angle)

x=angle(1);
y=angle(2);
z=angle(3);

rotz=[cos(z)    -sin(z)     0
      sin(z)     cos(z)     0
      0          0          1];
roty=[cos(y)     0          sin(y)
      0          1          0
    -sin(y)    0           cos(y)];
rotx=[1          0          0
      0         cos(x)     -sin(x)
      0         sin(x)     cos(x)];
rot=rotz*roty*rotx;
Tws=[rot pos;0 0 0 1];
end


%% plot forward kinematics
function plot_XY_given_theta_2dof(theta_1_mat_degs,theta_2_mat_degs,...
 X_mat,Y_mat,a_cmax)

xlab_str = '\theta_1 (degs)';
ylab_str = '\theta_2 (degs)';
figure;
hax(1) = subplot(1,2,1);
 contourf(theta_1_mat_degs, theta_2_mat_degs, X_mat);
 caxis(hax(1), [-30 30]);
 colormap(gca,'jet'); colorbar
 xlabel(xlab_str, 'Interpreter', 'tex');
 ylabel(ylab_str, 'Interpreter', 'tex');
 title(hax(1), 'X_E', 'Interpreter', 'tex')
hax(2) = subplot(1,2,2);
 contourf(theta_1_mat_degs, theta_2_mat_degs, Y_mat);
 caxis(hax(1), [-30 10]);
```

```
 colormap(gca,'jet'); colorbar
 xlabel(xlab_str, 'Interpreter', 'tex');
 ylabel(ylab_str, 'Interpreter', 'tex');
 title(hax(2), 'Y_E', 'Interpreter', 'tex')
end
function plot_XZ_given_theta_2dof(theta_1_mat_degs,theta_2_mat_degs,...
 X_mat,Z_mat,a_cmax)

xlab_str = '\theta_1 (degs)';
ylab_str = '\theta_2 (degs)';
figure;
hax(1) = subplot(1,2,1);
 contourf(theta_1_mat_degs, theta_2_mat_degs, X_mat);
 caxis(hax(1), [-30 30]);
 colormap(gca,'jet'); colorbar
 xlabel(xlab_str, 'Interpreter', 'tex');
 ylabel(ylab_str, 'Interpreter', 'tex');
 title(hax(1), 'X_E', 'Interpreter', 'tex')
 hax(2) = subplot(1,2,2);
 contourf(theta_1_mat_degs, theta_2_mat_degs, Z_mat);
 caxis(hax(1), [0 30]);
 colormap(gca,'jet'); colorbar
 xlabel(xlab_str, 'Interpreter', 'tex');
 ylabel(ylab_str, 'Interpreter', 'tex');
 title(hax(2), 'Z_E', 'Interpreter', 'tex')
end
```

22 Appendix G

In this appendix, the results of the simulation for calculating where the workspace can lay are reported. This simulation is performed for some initial angle decided from the *Step 2* of the alignment procedure.

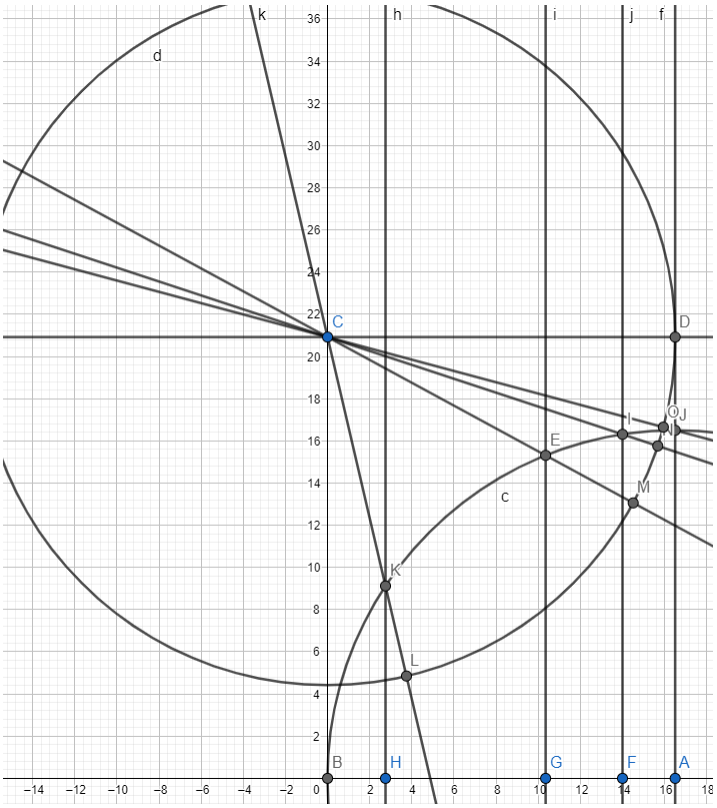

Figure 169: GeoGebra used for calculating the motion for step 2 and 3 in the alignment procedure for Gall Bladder removal

The value found are used for running a simulation and understand what are the possible angle of the workspace inclination with respect to the horizontal. The found graphs are reported below. The simulation is performed using the forward kinematics and the values of pre-alignment found.

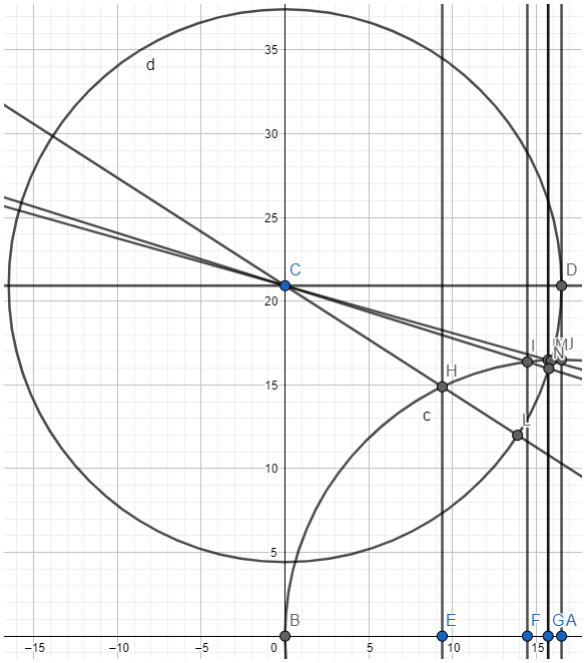

Figure 170: GeoGebra used for calculating the motion for step 2 and 3 in the alignment procedure for Appendectomy configuration 1

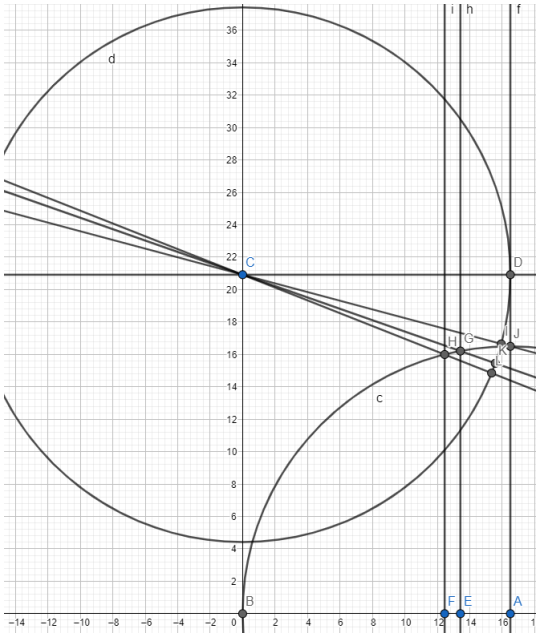

Figure 171: GeoGebra used for calculating the motion for step 2 and 3 in the alignment procedure for Appendectomy configuration 2

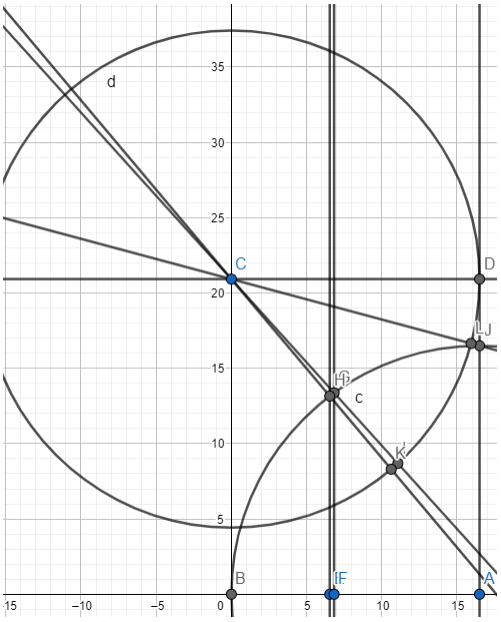

Figure 172: GeoGebra used for calculating the motion for step 2 and 3 in the alignment procedure for Inguinal hernia surgery

23 Appendix H

The following code permits to display the forward kinematics and the simulation for validating the position of the workspace's axis.

```
%% possible position of worspaces
clear all
clc
syms t1 t2 a1 a2 t1 t2 d a b x d
syms nx ny nz ox oy oz ax ay az px py pz
a1n=deg2rad(53.6);
a2n=deg2rad(47.1);

%d=0;
R=16.5;

H01=BuildTw([0;0;0],[0;0;0]);
H12=BuildTw([-R*sin(a1)*sin(t1);+R*sin(a1)*cos(t1);R-R*cos(a1)],[a1;0;t1]);
H23=BuildTw([-R*sin(a2)*sin(t2);+R*sin(a2)*cos(t2);R-R*cos(a2)],[a2;0;t2]);

H34=BuildTw([0;0;d],[0;0;0]);
H02=H01*H12;
H03=H02*H23;
H04=H02*H23*H34;
A04=H04*[0;0;0;1];
%% next step for forward
XE_MLF = matlabFunction(A04(1),'Vars',[a1 a2 t1 t2 d]);
YE_MLF = matlabFunction(A04(2),'Vars',[a1 a2 t1 t2 d]);
ZE_MLF = matlabFunction(A04(3),'Vars',[a1 a2 t1 t2 d]);

%% visualize forward kinematics
t1_degs_row = linspace(-90,90,100);
t2_degs_row = linspace(-150,150,100);
d_value= linspace(0,10,100);
[tt1_degs,tt2_degs] = meshgrid(t1_degs_row,t2_degs_row);
tt1_rads = deg2rad(tt1_degs);
tt2_rads = deg2rad(tt2_degs);
for i=0:1
X_mat = XE_MLF(a1n,a2n,tt1_rads,tt2_rads, 0);


Y_mat = YE_MLF(a1n,a2n,tt1_rads,tt2_rads, 0);


Z_mat = ZE_MLF(a1n,a2n,tt1_rads,tt2_rads, 0);

figure(1)
plot3(Z_mat,X_mat,Y_mat)

title("motion");
xlabel('z axis');
ylabel('x axis');
zlabel('y axis')
hold on
r = 16;
[X,Y,Z] = cylinder(r);
h=40;
```

```
Z(1,:)=h;
surf(X+16.5,Z-20,Y-16,'FaceColor','magenta')
hold on
figure(2)
plot(Z_mat,Y_mat)
title("motion");
xlabel('z axis');
ylabel('y axis');
angles = linspace(pi/2, 3*pi/2, 500);
radius = 16;
CenterX = 16.5;
CenterY = 0;
x = radius * cos(angles) + CenterX;
y = radius * sin(angles) + CenterY;
plot(x, y, 'b-', 'LineWidth', 2);
hold on;
plot(CenterX, CenterY, 'k+', 'LineWidth', 3, 'MarkerSize', 14);
grid on;
hold on
figure(3)
plot(X_mat,Y_mat)
title("motion");
xlabel('x axis');
ylabel('y axis');
hold on
figure(4)
plot(Z_mat,X_mat)
title("motion");
xlabel('z axis');
ylabel('x axis');
end
plot_XY_given_theta_2dof(tt1_degs,tt2_degs,X_mat,Y_mat,(a1n+a2n))
plot_XZ_given_theta_2dof(tt1_degs,tt2_degs,X_mat,Z_mat,(a1n+a2n))

%% next step for inverse
XE_MLF = matlabFunction(A04(1),'Vars',[a1 a2 t1 t2]);
YE_MLF = matlabFunction(A04(2),'Vars',[a1 a2 t1 t2]);
ZE_MLF = matlabFunction(A04(3),'Vars',[a1 a2 t1 t2]);
%% find inverse kinematics
su=subs(A04(3),cos(t2),x);
cost2sol=solve(su==pz,x);
sint2sol=sqrt(1+cost2sol.^2);
THETA2=atan2(sint2sol,cost2sol);
THETA2=subs(THETA2,[a1,a2],[a1n,a2n]);
new=subs(A04,sin(t1),a);
neww=solve(new(2)==py,a);
new=subs(new,a,neww);
new=simplify(subs(new,cos(t1),b));
cost1sol=simplify(solve(new(1)==px,b));
sint1sol=simplify(subs(neww,cos(t1),cost1sol));
sint1sol=subs(sint1sol,t2,THETA2);
cost1sol=subs(cost1sol,t2,THETA2);
THETA1=atan2(sint1sol,cost1sol);
THETA1=subs(THETA1,[a1,a2],[a1n,a2n]);
TH1_MLF = matlabFunction(THETA1,'Vars',[px py pz]);
TH2_MLF = matlabFunction(THETA2,'Vars',[px py pz]);
```

```
%% try one
[zmat,xmat] = meshgrid(3.7966:0.1:19.6766,-7.94:0.1:7.94);
ymat=16.213;
tmp_th1_mat = TH1_MLF(xmat,ymat,zmat);
tmp_th1_mat = rad2deg(tmp_th1_mat);
tmp_th2_mat = TH2_MLF(xmat,ymat,zmat);
tmp_th2_mat = rad2deg(tmp_th2_mat);

th1_mat = NaN(size(tmp_th1_mat));
th2_mat = NaN(size(tmp_th2_mat));

tf_mat = imag(tmp_th1_mat) == 0;
th1_mat(tf_mat) = real(tmp_th1_mat(tf_mat));

tf_mat = imag(tmp_th2_mat) == 0;
th2_mat(tf_mat) = real(tmp_th2_mat(tf_mat));

plot_theta_given_XZ_2dof(xmat,zmat,th1_mat,th2_mat)

%% new two
[ymat,zmat] = meshgrid(3.7966:0.1:19.6766,-7.94:0.1:7.94);
xmat=16.213;
tmp_th1_mat = TH1_MLF(xmat,ymat,zmat);
tmp_th1_mat = rad2deg(tmp_th1_mat);
tmp_th2_mat = TH2_MLF(xmat,ymat,zmat);
tmp_th2_mat = rad2deg(tmp_th2_mat);

th1_mat = NaN(size(tmp_th1_mat));
th2_mat = NaN(size(tmp_th2_mat));

tf_mat = imag(tmp_th1_mat) == 0;
th1_mat(tf_mat) = real(tmp_th1_mat(tf_mat));

tf_mat = imag(tmp_th2_mat) == 0;
th2_mat(tf_mat) = real(tmp_th2_mat(tf_mat));
plot_theta_given_ZY_2dof(zmat,ymat,th1_mat,th2_mat)

%% new three
[xmat,ymat] = meshgrid(3.7966:0.1:19.6766,-7.94:0.1:7.94);
zmat=13.2;
tmp_th1_mat = TH1_MLF(xmat,ymat,zmat);
tmp_th1_mat = rad2deg(tmp_th1_mat);
tmp_th2_mat = TH2_MLF(xmat,ymat,zmat);
tmp_th2_mat=tmp_th2_mat *ones (size(xmat));
tmp_th2_mat = rad2deg(tmp_th2_mat);

th1_mat = NaN(size(tmp_th1_mat));
th2_mat = NaN(size(tmp_th2_mat));

tf_mat = imag(tmp_th1_mat) == 0;
th1_mat(tf_mat) = real(tmp_th1_mat(tf_mat));

tf_mat = imag(tmp_th2_mat) == 0;
th2_mat(tf_mat) = real(tmp_th2_mat(tf_mat));
plot_theta_given_XY_2dof(xmat,ymat,th1_mat,th2_mat)
```

```
%% trying to do all
[xmat,ymat,zmat] = meshgrid(-15:0.2:15,0:0.1:15,0:0.1:15);
zmat=13.2;
tmp_th1_mat = TH1_MLF(xmat,ymat,zmat);
tmp_th1_mat = rad2deg(tmp_th1_mat);
tmp_th2_mat = TH2_MLF(xmat,ymat,zmat);
tmp_th2_mat=tmp_th2_mat *ones (size(xmat));
tmp_th2_mat = rad2deg(tmp_th2_mat);

th1_mat = NaN(size(tmp_th1_mat));
th2_mat = NaN(size(tmp_th2_mat));

tf_mat = imag(tmp_th1_mat) == 0;
th1_mat(tf_mat) = real(tmp_th1_mat(tf_mat));

tf_mat = imag(tmp_th2_mat) == 0;
th2_mat(tf_mat) = real(tmp_th2_mat(tf_mat));
plot_theta_given_XY_2dof(xmat,ymat,th1_mat,th2_mat)
%% Jacobian
the_J = jacobian([A04(1) A04(2) A04(3)],[t1 t2])
%% function for creating homogeneous matrices

function Tws=BuildTw(pos,angle)

x=angle(1);
y=angle(2);
z=angle(3);

rotz=[cos(z)    -sin(z)     0
      sin(z)    cos(z)      0
      0         0           1];
roty=[cos(y)    0           sin(y)
      0         1           0
    -sin(y)   0           cos(y)];
rotx=[1         0           0
     0          cos(x)      -sin(x)
     0          sin(x)      cos(x)];
rot=rotz*roty*rotx;
Tws=[rot pos;0 0 0 1];
end
%% plot forward kinematics
function plot_XY_given_theta_2dof(theta_1_mat_degs,theta_2_mat_degs,...
 X_mat,Y_mat,a_cmax)

xlab_str = '\theta_1 (degs)';
ylab_str = '\theta_2 (degs)';
figure;
hax(1) = subplot(1,2,1);
 contourf(theta_1_mat_degs, theta_2_mat_degs, X_mat);
 caxis(hax(1), [-30 30]);
 colormap(gca,'jet'); colorbar
 xlabel(xlab_str, 'Interpreter', 'tex');
 ylabel(ylab_str, 'Interpreter', 'tex');
 title(hax(1), 'X_E', 'Interpreter', 'tex')
hax(2) = subplot(1,2,2);
 contourf(theta_1_mat_degs, theta_2_mat_degs, Y_mat);
```

```
 caxis(hax(2), [-18 18]);
 colormap(gca,'jet'); colorbar
 xlabel(xlab_str, 'Interpreter', 'tex');
 ylabel(ylab_str, 'Interpreter', 'tex');
 title(hax(2), 'Y_E', 'Interpreter', 'tex')
end
function plot_XZ_given_theta_2dof(theta_1_mat_degs,theta_2_mat_degs,...
 X_mat,Z_mat,a_cmax)

xlab_str = '\theta_1 (degs)';
ylab_str = '\theta_2 (degs)';
figure;
hax(1) = subplot(1,2,1);
 contourf(theta_1_mat_degs, theta_2_mat_degs, X_mat);
 caxis(hax(1), [-30 30]);
 colormap(gca,'jet'); colorbar
 xlabel(xlab_str, 'Interpreter', 'tex');
 ylabel(ylab_str, 'Interpreter', 'tex');
 title(hax(1), 'X_E', 'Interpreter', 'tex')
 hax(2) = subplot(1,2,2);
 contourf(theta_1_mat_degs, theta_2_mat_degs, Z_mat);
 caxis(hax(2), [0 20]);
 colormap(gca,'jet'); colorbar
 xlabel(xlab_str, 'Interpreter', 'tex');
 ylabel(ylab_str, 'Interpreter', 'tex');
 title(hax(2), 'Z_E', 'Interpreter', 'tex')
end


%% plot inverse kinematics
function plot_theta_given_XZ_2dof(X_mat,Y_mat,theta_1_mat_degs,...
                                  theta_2_mat_degs)

xlab_str = 'X (m)';
ylab_str = 'Z (m)';

figure;
hax(1) = subplot(1,2,1);
   contourf(X_mat, Y_mat, theta_1_mat_degs);
      caxis(hax(1), [-180 180]);
      colormap(gca,'jet'); colorbar
      xlabel(xlab_str, 'Interpreter', 'tex');
      ylabel(ylab_str, 'Interpreter', 'tex');
      title(hax(1), '\theta_1', 'Interpreter', 'tex')
      axis('equal')
hax(2) = subplot(1,2,2);
   contourf(X_mat, Y_mat, theta_2_mat_degs);
      caxis(hax(2), [-180 180]);
      colormap(gca,'jet'); colorbar
      xlabel(xlab_str, 'Interpreter', 'tex');
      ylabel(ylab_str, 'Interpreter', 'tex');
      title(hax(2), '\theta_2', 'Interpreter', 'tex')
      axis('equal')

end
function plot_theta_given_ZY_2dof(X_mat,Y_mat,theta_1_mat_degs,...
```

```
                                    theta_2_mat_degs)

xlab_str = 'Z (m)';
ylab_str = 'Y (m)';

figure;
hax(1) = subplot(1,2,1);
   contourf(X_mat, Y_mat, theta_1_mat_degs);
      caxis(hax(1), [-180 180]);
      colormap(gca,'jet'); colorbar
      xlabel(xlab_str, 'Interpreter', 'tex');
      ylabel(ylab_str, 'Interpreter', 'tex');
      title(hax(1), '\theta_1', 'Interpreter', 'tex')
      axis('equal')
hax(2) = subplot(1,2,2);
   contourf(X_mat, Y_mat, theta_2_mat_degs);
      caxis(hax(2), [-180 180]);
      colormap(gca,'jet'); colorbar
      xlabel(xlab_str, 'Interpreter', 'tex');
      ylabel(ylab_str, 'Interpreter', 'tex');
      title(hax(2), '\theta_2', 'Interpreter', 'tex')
      axis('equal')

end
function plot_theta_given_XY_2dof(X_mat,Y_mat,theta_1_mat_degs,...
                                    theta_2_mat_degs)

xlab_str = 'X (m)';
ylab_str = 'Y (m)';

figure;
hax(1) = subplot(1,2,1);
   contourf(X_mat, Y_mat, theta_1_mat_degs);
      caxis(hax(1), [-180 180]);
      colormap(gca,'jet'); colorbar
      xlabel(xlab_str, 'Interpreter', 'tex');
      ylabel(ylab_str, 'Interpreter', 'tex');
      title(hax(1), '\theta_1', 'Interpreter', 'tex')
      axis('equal')
hax(2) = subplot(1,2,2);
   contourf(X_mat, Y_mat, theta_2_mat_degs);
      caxis(hax(2), [-180 180]);
      colormap(gca,'jet'); colorbar
      xlabel(xlab_str, 'Interpreter', 'tex');
      ylabel(ylab_str, 'Interpreter', 'tex');
      title(hax(2), '\theta_2', 'Interpreter', 'tex')
      axis('equal')

end
```

Additionally, all the planes are displayed for each incision point with the following code.

```
%% possible position of worspaces
clear all
close all
clc
syms t1 t2 a1 a2 t1 t2 d a b x d xv yv zv
syms nx ny nz ox oy oz ax ay az px py pz
```

```
a1n=deg2rad(53.6);
a2n=deg2rad(47.1);

%d=1;
R=16.5;
%angle= 47.8691; dist=-6.31853 ; %%Inguinal hernia 2
 angle=49.8958; dist=-6.34755; %%Inguinal hernia 1
%angle= 19.3401; dist=-2.2774; %%Appendectomy 2 2
%angle=21.5825; dist=-3.11131; %%Appendectomy 2 1
%angle=15.7894; dist=-0.19; %%Appendectomy 1 3
%angle= 17.455; dist=-1.3420; %%Appendectomy 1 2
%angle=32.7585; dist=-5.34606; %%Appendectomy 1 1
%angle=15; dist=0.058179; %% gall bladder 4 %%Appendectomy 2 3 %% Inguinal hernia 3
%angle=18.228; dist=-1.76033; %% gall bladder 3
%angle=28.455; dist=-4.727806; %%gall bladder 2
%angle=76.88; dist=-4.38436; %% gall bladder 1



H01=BuildTw([0;16.5+4.42;0],[deg2rad(angle);0;0]);
H12=BuildTw([-R*sin(a1)*sin(t1);+R*sin(a1)*cos(t1);R-R*cos(a1)+dist],[a1;0;t1]);
H23=BuildTw([-R*sin(a2)*sin(t2);+R*sin(a2)*cos(t2);R-R*cos(a2)],[a2;0;t2]);

H34=BuildTw([0;0;d],[0;0;0]);
H02=H01*H12;
H03=H02*H23;
H04=H02*H23*H34;
A04=H04*[0;0;0;1];
%% next step for forward
XE_MLF = matlabFunction(A04(1),'Vars',[a1 a2 t1 t2 d]);
YE_MLF = matlabFunction(A04(2),'Vars',[a1 a2 t1 t2 d]);
ZE_MLF = matlabFunction(A04(3),'Vars',[a1 a2 t1 t2 d]);

%% visualize forward kinematics
t1_degs_row = linspace(-90,90,100);
t2_degs_row = linspace(-180,180,100);

[tt1_degs,tt2_degs] = meshgrid(t1_degs_row,t2_degs_row);
tt1_rads = deg2rad(tt1_degs);
tt2_rads = deg2rad(tt2_degs);
for i=0:1
X_mat = XE_MLF(a1n,a2n,tt1_rads,tt2_rads, 0);


Y_mat = YE_MLF(a1n,a2n,tt1_rads,tt2_rads, 0);


Z_mat = ZE_MLF(a1n,a2n,tt1_rads,tt2_rads, 0);


figure(1)
plot3(Z_mat,X_mat,Y_mat)
title("motion");
xlabel('z axis');
ylabel('x axis');
zlabel('y axis')
```

```
hold on
r = 16;
[X,Y,Z] = cylinder(r);
h=40;
Z(1,:)=h;
surf(X+16.5,Z-20,Y,'FaceColor','magenta')
[y,x] = meshgrid(-50:15:50);
z = zeros(size(y));
%mesh(x,y,z)
hold on
%anglex=-87.274;%% gall bladder 2
%anglex=52.001;%% gall bladder 1
%anglex=51.653;%% gall bladder 3
%anglex=60.884;%% gall bladder 4
%anglex=-88.238;%% appendectomy 1 1
%anglex=74.357-90;%% appendectomy 1 2
%anglex=35.256;%% appendectomy 1 3
%anglex=-47.272;%% appendectomy 2 1
%anglex=90-10.548;%% appendectomy 2 2
%anglex=+22.276-90;%% appendectomy 2 3
anglex=90-3.271;%% hernia 1
%anglex=-55.838;%% hernia 2
%anglex=28.616-90;%% hernia 3
Rp1=BuildTw([0;0;0],[0;deg2rad(angle);0]);


for i2=1:size(x)
    for j=1:size(x)
v = Rp1*[x(i2,j); y(i2,j); z(i2,j); 1];
xn(i2,j)=v(1);
yn(i2,j)=v(2);
zn(i2,j)=v(3)+16.5+4.42;
    end
end
mesh(xn,yn,zn)
hold on
Rp1=BuildTw([0;0;0],[pi/2;0;0]);


for i2=1:size(x)
    for j=1:size(x)
v = Rp1*[x(i2,j); y(i2,j); z(i2,j); 1];
x1(i2,j)=v(1);
y1(i2,j)=v(2);
z1(i2,j)=v(3)+16.5+4.42;
    end
end
%mesh(x1,y1,z1)
hold on

Rp1=BuildTw([0;0;0],[0;0;deg2rad(anglex)]);
for i2=1:size(x1)
    for j=1:size(x1)
v = Rp1*[x1(i2,j); y1(i2,j); z1(i2,j); 1];
xn(i2,j)=v(1)+16.5*cos(deg2rad(angle))+dist*cos(deg2rad(angle));
yn(i2,j)=v(2);
```

```
zn(i2,j)=v(3);
j+1;
    end
i2+1;

end
mesh(xn,yn,zn)
hold on
figure(2)
plot(Z_mat,Y_mat)
title("motion");
xlabel('z axis');
ylabel('y axis');
angles = linspace(pi/2, 3*pi/2, 500);
radius = 16.5;
CenterX = 16.5;
CenterY = 0;
x = radius * cos(angles) + CenterX;
y = radius * sin(angles) + CenterY;
plot(x, y, 'b-', 'LineWidth', 2);
hold on;
plot(CenterX, CenterY, 'k+', 'LineWidth', 3, 'MarkerSize', 14);
grid on;
hold on
figure(3)
plot(X_mat,Y_mat)
title("motion");
xlabel('x axis');
ylabel('y axis');
hold on
figure(4)
plot(Z_mat,X_mat)
hold on
title("motion");
xlabel('z axis');
ylabel('x axis');


i=i+1;
end
plot_XY_given_theta_2dof(tt1_degs,tt2_degs,X_mat,Y_mat,(a1n+a2n))
plot_XZ_given_theta_2dof(tt1_degs,tt2_degs,X_mat,Z_mat,(a1n+a2n))


%% function for creating homogeneous matrices
function Tws=BuildTw(pos,angle)

x=angle(1);
y=angle(2);
z=angle(3);

rotz=[cos(z)    -sin(z)     0
      sin(z)    cos(z)      0
      0         0           1];
roty=[cos(y)    0           sin(y)
      0         1           0
```

```
    -sin(y)    0            cos(y)];
rotx=[1          0            0
      0          cos(x)      -sin(x)
      0          sin(x)       cos(x)];
rot=rotz*roty*rotx;
Tws=[rot pos;0 0 0 1];
end
%% plot forward kinematics
function plot_XY_given_theta_2dof(theta_1_mat_degs,theta_2_mat_degs,...
 X_mat,Y_mat,a_cmax)

xlab_str = '\theta_1 (degs)';
ylab_str = '\theta_2 (degs)';
figure;
hax(1) = subplot(1,2,1);
 contourf(theta_1_mat_degs, theta_2_mat_degs, X_mat);
 caxis(hax(1), [-30 30]);
 colormap(gca,'jet'); colorbar
 xlabel(xlab_str, 'Interpreter', 'tex');
 ylabel(ylab_str, 'Interpreter', 'tex');
 title(hax(1), 'X_E', 'Interpreter', 'tex')
hax(2) = subplot(1,2,2);
 contourf(theta_1_mat_degs, theta_2_mat_degs, Y_mat);
 caxis(hax(2), [-18 18]);
 colormap(gca,'jet'); colorbar
 xlabel(xlab_str, 'Interpreter', 'tex');
 ylabel(ylab_str, 'Interpreter', 'tex');
 title(hax(2), 'Y_E', 'Interpreter', 'tex')
end
function plot_XZ_given_theta_2dof(theta_1_mat_degs,theta_2_mat_degs,...
 X_mat,Z_mat,a_cmax)

xlab_str = '\theta_1 (degs)';
ylab_str = '\theta_2 (degs)';
figure;
hax(1) = subplot(1,2,1);
 contourf(theta_1_mat_degs, theta_2_mat_degs, X_mat);
 caxis(hax(1), [-30 30]);
 colormap(gca,'jet'); colorbar
 xlabel(xlab_str, 'Interpreter', 'tex');
 ylabel(ylab_str, 'Interpreter', 'tex');
 title(hax(1), 'X_E', 'Interpreter', 'tex')
 hax(2) = subplot(1,2,2);
 contourf(theta_1_mat_degs, theta_2_mat_degs, Z_mat);
 caxis(hax(2), [0 16]);
 colormap(gca,'jet'); colorbar
 xlabel(xlab_str, 'Interpreter', 'tex');
 ylabel(ylab_str, 'Interpreter', 'tex');
 title(hax(2), 'Z_E', 'Interpreter', 'tex')
end


%% plot inverse kinematics
function plot_theta_given_XZ_2dof(X_mat,Y_mat,theta_1_mat_degs,...
                                  theta_2_mat_degs)
```

```
xlab_str = 'X (m)';
ylab_str = 'Z (m)';

figure;
hax(1) = subplot(1,2,1);
   contourf(X_mat, Y_mat, theta_1_mat_degs);
      caxis(hax(1), [-180 180]);
      colormap(gca,'jet'); colorbar
      xlabel(xlab_str, 'Interpreter', 'tex');
      ylabel(ylab_str, 'Interpreter', 'tex');
      title(hax(1), '\theta_1', 'Interpreter', 'tex')
      axis('equal')
hax(2) = subplot(1,2,2);
   contourf(X_mat, Y_mat, theta_2_mat_degs);
      caxis(hax(2), [-180 180]);
      colormap(gca,'jet'); colorbar
      xlabel(xlab_str, 'Interpreter', 'tex');
      ylabel(ylab_str, 'Interpreter', 'tex');
      title(hax(2), '\theta_2', 'Interpreter', 'tex')
      axis('equal')

end
function plot_theta_given_ZY_2dof(X_mat,Y_mat,theta_1_mat_degs,...
                                  theta_2_mat_degs)

xlab_str = 'Z (m)';
ylab_str = 'Y (m)';

figure;
hax(1) = subplot(1,2,1);
   contourf(X_mat, Y_mat, theta_1_mat_degs);
      caxis(hax(1), [-180 180]);
      colormap(gca,'jet'); colorbar
      xlabel(xlab_str, 'Interpreter', 'tex');
      ylabel(ylab_str, 'Interpreter', 'tex');
      title(hax(1), '\theta_1', 'Interpreter', 'tex')
      axis('equal')
hax(2) = subplot(1,2,2);
   contourf(X_mat, Y_mat, theta_2_mat_degs);
      caxis(hax(2), [-180 180]);
      colormap(gca,'jet'); colorbar
      xlabel(xlab_str, 'Interpreter', 'tex');
      ylabel(ylab_str, 'Interpreter', 'tex');
      title(hax(2), '\theta_2', 'Interpreter', 'tex')
      axis('equal')

end
function plot_theta_given_XY_2dof(X_mat,Y_mat,theta_1_mat_degs,...
                                  theta_2_mat_degs)

xlab_str = 'X (m)';
ylab_str = 'Y (m)';

figure;
hax(1) = subplot(1,2,1);
   contourf(X_mat, Y_mat, theta_1_mat_degs);
```

```
        caxis(hax(1), [-180 180]);
        colormap(gca,'jet'); colorbar
        xlabel(xlab_str, 'Interpreter', 'tex');
        ylabel(ylab_str, 'Interpreter', 'tex');
        title(hax(1), '\theta_1', 'Interpreter', 'tex')
        axis('equal')
hax(2) = subplot(1,2,2);
    contourf(X_mat, Y_mat, theta_2_mat_degs);
        caxis(hax(2), [-180 180]);
        colormap(gca,'jet'); colorbar
        xlabel(xlab_str, 'Interpreter', 'tex');
        ylabel(ylab_str, 'Interpreter', 'tex');
        title(hax(2), '\theta_2', 'Interpreter', 'tex')
        axis('equal')

end
```

24 Appendix I

The following code permits to calculate the optimized dimensions of cross section area for the beams of the RCM mechanism.

```
clear all
clc
syms t1
%E=190000; %steel N/mm^2
E=69000; % al
a1=deg2rad(53.6);
a2=deg2rad(47.1);
h=49.2; %mm distance between the com motor and beam
R1=165; %mm radius
w=0.336*9.81; %joint motor 2 weight
v=0.206*9.81; %linear stage weight
u=1*9.81; %instrument plus instrument actuator weight
b=35; %mm base of the cross section area
%objective=@(x) (x(1)+x(2))/pi();
objective=@(x) 0.8*x(1)+0.2*x(2);
%objective=@(x) (1/sin(x(1)));
x0=[0,0];

A=[];
b=[];
Aeq=[];
beq=[];
ceq=[];
lb=[2, 1];
ub=[50, 5];
% nonlinear constraints
nonlincon = @nlcon;


x=ga(objective,2,A,b,Aeq,beq,lb,ub,@nlcon,options);
% show final objective
disp(['Final Objective: ' num2str(objective(x))])

% print solution
disp('Solution')
disp(['x1 = ' num2str(x(1))])
disp(['x2 = ' num2str(x(2))])


area= (b-2*x(2))*x(2) + x(1)*x(2)*2; %u shape
%area= 2*(32-2*x(2))*x(2) + x(1)*x(2)*2; %rectangle


Smod= 32*x(1).^2/6 - ((32-x(2))*(x(1)-2*x(2).^2))/(6*x(1));
M1=-w/cos(pi-a1)*h;
M2=(v+u)*(R1+R1*cos(pi-a1-a2));
stress=(M1+M2)/Smod;

den=0.0027; %al g/mm3
%den=0.00785; %steel g/mm3
massle=area*den;
function [c,ceq] = nlcon(x)
```

```
%E=190000; %steel N/mm^2
E=69000; % al
a1=deg2rad(53.6);
a2=deg2rad(47.1);
h=49.2; %mm distance between the com motor and beam
R1=165; %mm radius
w=0.336*9.81; %joint motor 2 weight
v=0.206*9.81; %linear stage weight
u=1*9.81; %instrument plus instrument actuator weight
b=32; %mm base of the cross section area
%inertia of rectangular cross section
%I= (b*x(1).^3)/12 - ((b-2*x(2))*(x(1)-2*x(2)).^3)/12;
%inertia of u shaped cross section
I= ((b-2*x(2))*x(2).^3)/3 + 2*((x(2))*(x(1)).^3)/3;
c1=((v+u)*R1.^3)/ (E*I) *((a1+a2)*(0.5+cos(pi-a1-a2).^2)+0.75*sin(2*(pi-a1-a2)))
+(((w*h))*(R1+x(1)).^2)/ (E*I) *((a1)*(0.5+cos(pi-a1).^2)+0.75*sin(2*(pi-a1)))-0.355;
c2=-x(1)+2*x(2);
c=[c1, c2];
ceq=[];
end
```

25 Appendix J

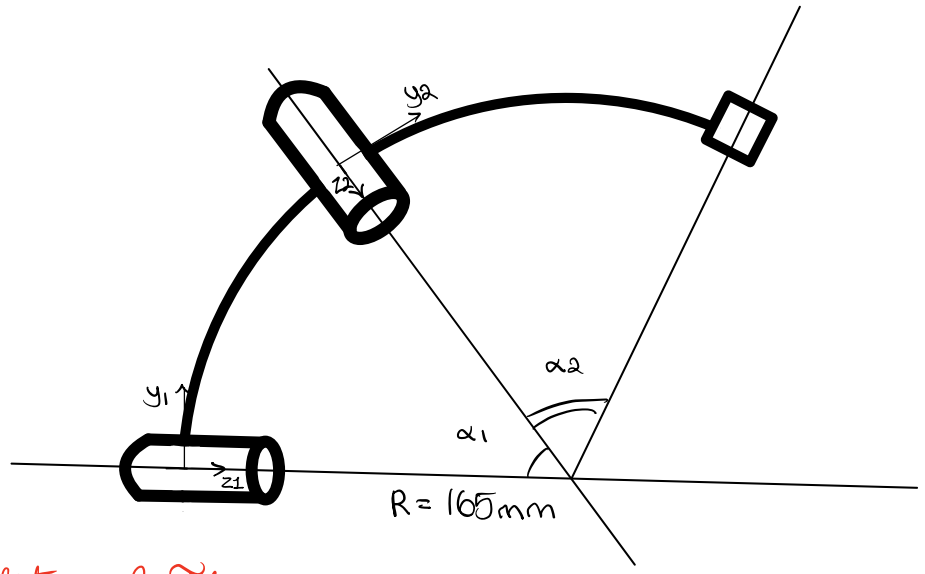

Calculation of T1

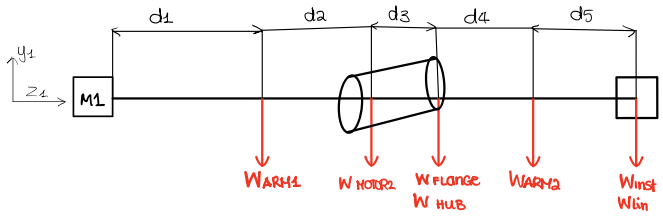

: configuration max Torque

CoM :

ARM1 : $z_L = 24.97\,mm$, $y_L = 75.64\,mm$

ARM2 : $z_L = 18.80\,mm$, $y_L = 66.02\,mm$

MOTOR : $z_L = 49.5\,mm$

d_1 : center of mass of arm1 : z_L

$d_1 + d_2 + d_3$: Length of arm1 · $(R - R \cdot \cos(\alpha_1))$

$d_1 + d_2$: lenght of arm1 · $(R - R\cos(\alpha_1))$ − center of mass MOTOR $z_L \cdot \cos(\alpha_1)$

d_4 : center of mass of arm2$_x$ · $\cos(\alpha_1)$ + center of mass of arm2$_y$ · $\sin(\alpha_1)$

$d_1 + d_2 + d_3 + d_4 + d_5$: $R + R \cdot \cos(\alpha_1 + \alpha_2)$

$a = d_1 = 24.97\,mm$

$b = d_1 + d_2 = 46.027\,mm$

$c = d_1 + d_2 + d_3 = 67.085\,mm$

$d = d_1 + d_2 + d_3 + d_4 = 121.39\,mm$

$e = d_1 + d_2 + d_3 + d_4 + d_5 = 195.634\,mm$

MASS:

$m_{ARM1} = 502.09\,g$ $\quad m_{MOTOR2} = 336\,g$ $\quad m_{INST} = 1000\,g$

$m_{ARM2} = 190.41\,g$ $\quad m_{(flange+hub)} = 32.2\,g$ $\quad m_{lin} = 206\,g$

$W = m \cdot 9.81\ m/s^2$

TORQUE

$$\tau_1 = W_{ARM1} \cdot a + W_{MOTOR2} \cdot b + W_{(flange+hub)} \cdot c + $$
$$+ W_{ARM2} \cdot d + W_{lin} \cdot e + W_{INST} \cdot e$$

$$\boxed{\tau_1 = 2.837158\ Nm}$$

Calculation of τ_2

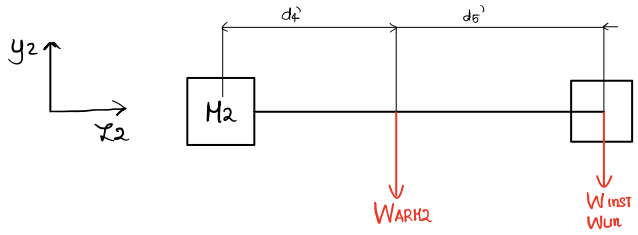

d_4' : center of mass of arm2 along x_L

$d_4' + d_5'$: length of arm2 along x_2 : $R - R \cdot \cos(\alpha_2)$

$$\begin{cases} f = d_4' = 18.80\,mm \\ g = d_4' + d_5' = 52.681\,mm \end{cases}$$

$$\tau_2 = W_{ARM2} \cdot f + W_{INST} \cdot g + W_{lin} \cdot g$$

$$\boxed{\tau_2 = 0.65836\,Nm}$$

26 Appendix K

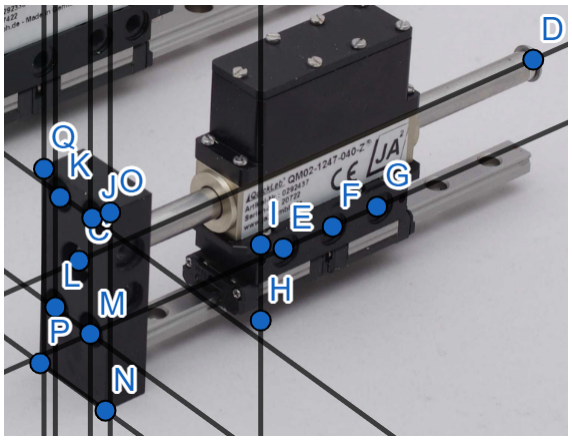

Figure 173: Dimension of the hole pattern in the linear actuator [41]

Known dimensions:

- **ON**: 57 mm
- **NP**: 30 mm
- **LD**: 59.6 mm

Calculated dimensions:

- **LM=KJ**: 16 mm
- **MJ=KL**: 33 mm
- **HI**: 22 mm
- **EF=FG**: 6.5 mm

27 Appendix L

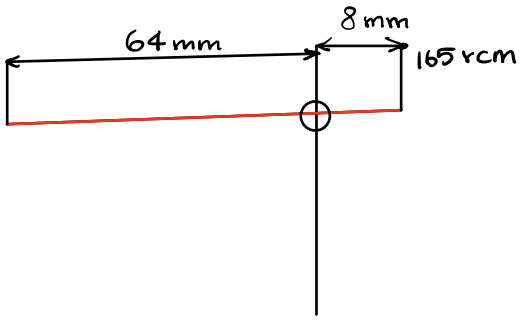

tot = 72 mm

— : slider

197.3 RCM + 17.5 cos = 214.8 dist

(214.8 − 165) mm = 49.8 mm

49.8 mm − 8 mm = 41.8 mm

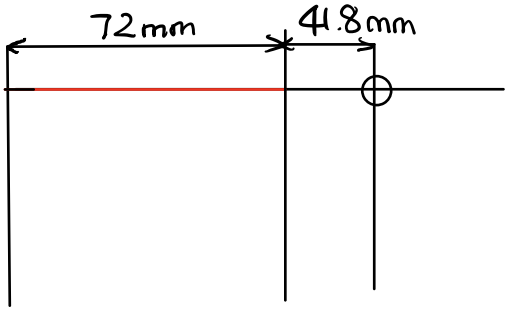

need to add and consider the slider mechanical limitation → 9 mm in front, 52 mm back

72 mm + 63 mm = 135 mm

41.8 mm − 9 mm = 31.8 mm

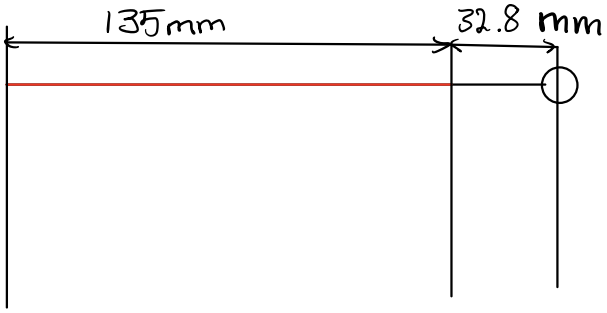

- Thickness of Revolute Joint = 14 mm

(32.8 + 7) mm = 39.8 mm → 40 mm

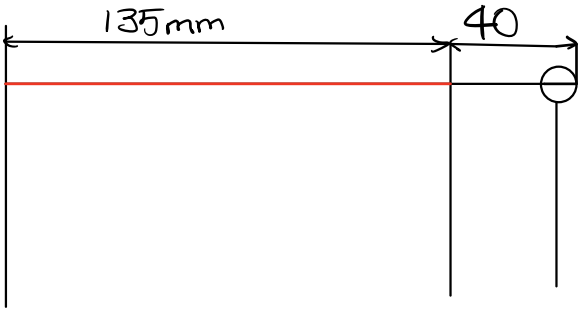

28 Appendix M

28.1 Procedure for alignment of the mechanism: steps for the experiment

Step to be followed for the alignment:

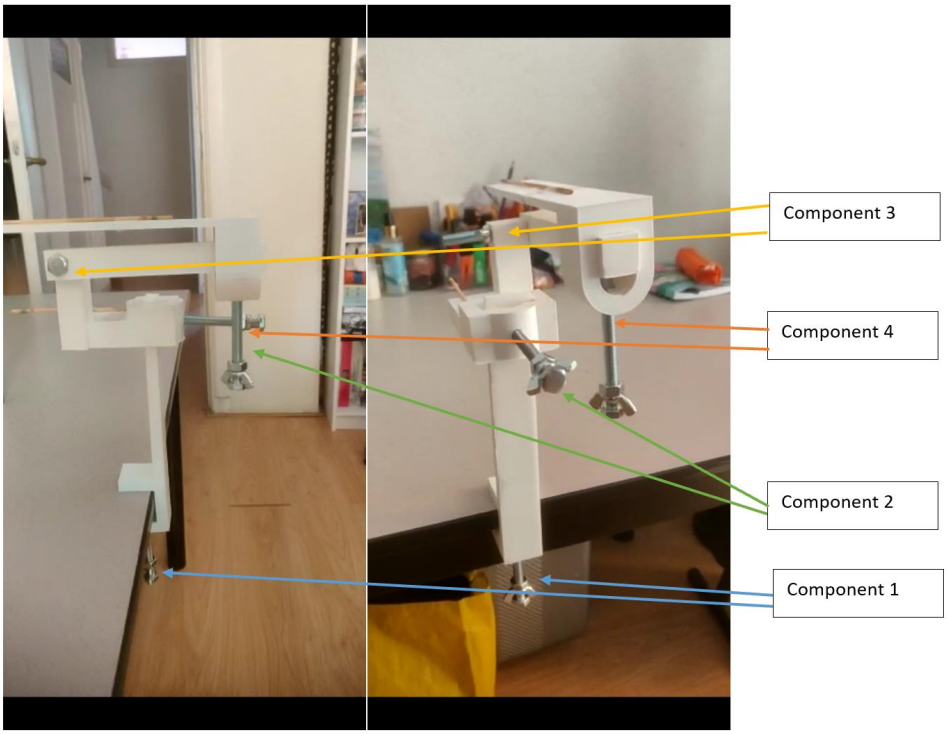

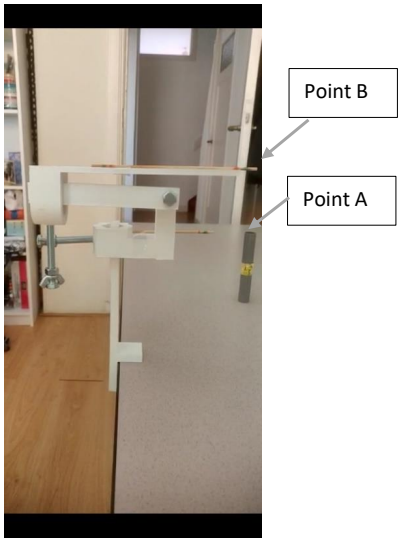

GOAL: align Point A and Point B following the steps explained below.

1. Align the plane 1 of the system with the point A as shown in figure 1. To do so you have to unscrew and slide the component 1 (circle in the photo). Once done, screw component 1 back.

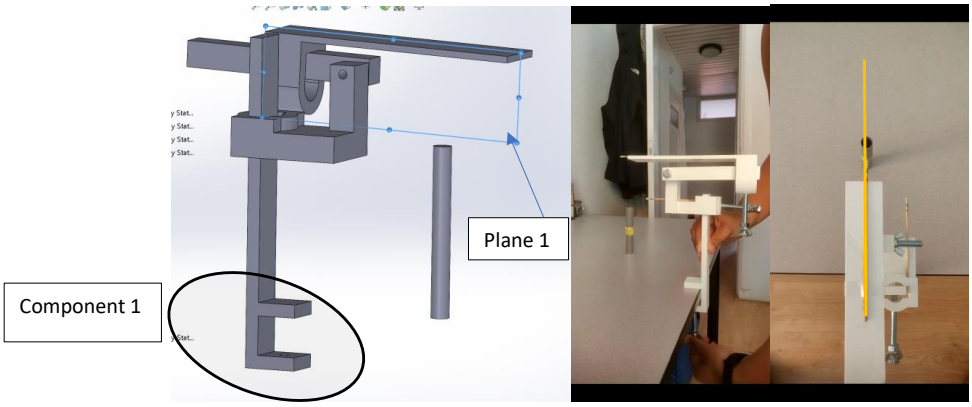

2. Align the plane 2 of the system with the point A as shown in figure 2. To do so, you have to unscrew and slide the component 2 (circle in the photo). Once done, screw component 2 back.

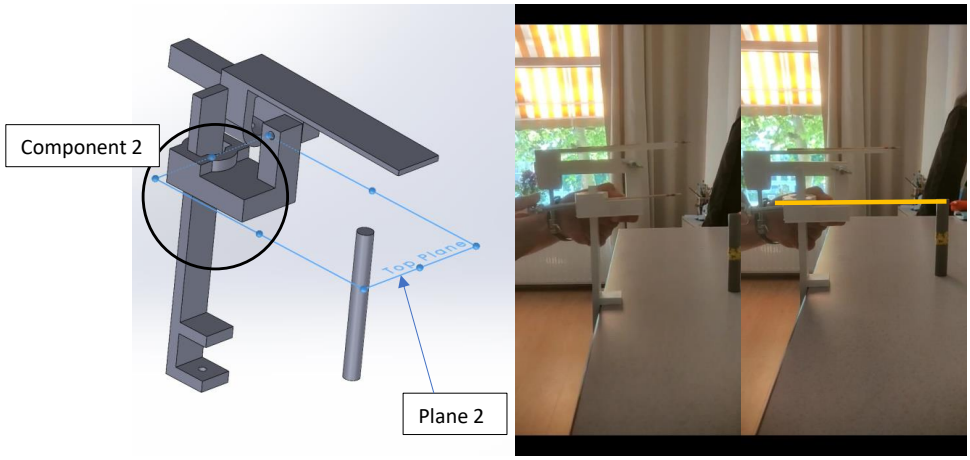

3. Align the plane 3 of the system with the point A as shown in figure 3. To do so, you have to unscrew the component 3 and rotate bar 3 (circles in the photo). Once done, screw component 3 back.

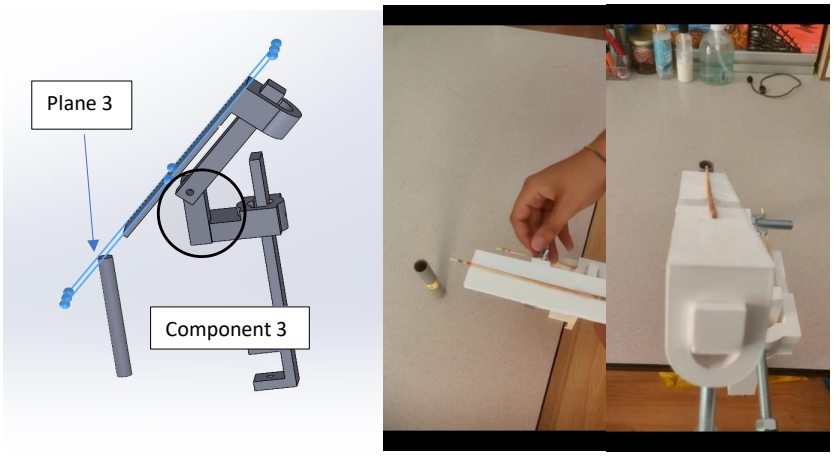

4. Align the point with the point A as shown in figure 4. To do so, you have to unscrew and slide the component 4 (circle in the photo). Once done, screw component 4 back.

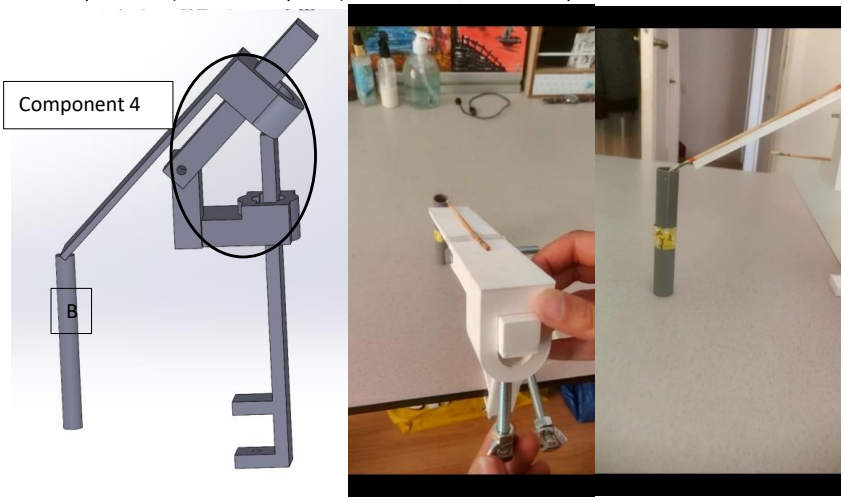

FINAL SETUP